Characterisation of Distinct Inhibitory Interneuron Populations in the Spinal Dorsal Horn

Robert Ganley

MRes Biomedical Sciences (University of Glasgow)

BSc (Hons) Biomedical Sciences (University of Lancaster)

October 2015

Submitted in fulfilment of the requirements for the Degree of Doctor of Philosophy

Institute of Neuroscience and Psychology

College of Medical, Veterinary and Life Sciences

University of Glasgow

Summary

The dorsal horn of the spinal cord is the first node in the somatosensory pathway, and is an area essential for controlling the flow of sensory information sent to the brain. Interneurons constitute the vast majority of neurons in this area, and between 25-40% of those in laminae I-III are inhibitory. These inhibitory interneurons are critical for normal somatosensation, for example, by suppressing pain in the absence of noxious stimuli. Interneurons of the dorsal horn are poorly understood due to their morphological and functional diversity, and this is a major factor limiting our understanding of the neuronal circuitry of the dorsal horn.

In order to better understand sensory processing in the dorsal horn it is first necessary to characterise the neurons in this area, and to determine the neuronal circuits in which they are integrated. To address this issue, two separate and non-overlapping populations of inhibitory interneurons in the dorsal horn were thoroughly characterised in terms of their morphological and physiological properties. To achieve this, whole-cell recordings were taken from neurons labelled with green fluorescent protein (GFP) under the control of the Prion promoter (PrP) and the neuropeptide Y (NPY) promoter in spinal cord slices from mice. The recording electrodes contained Neurobiotin, which filled the cells during recording and was revealed with fluorescent molecules, enabling three-dimensional reconstruction of cell bodies and dendrites and axons of neurons. Slices containing these labelled neurons were then resectioned for immunocytochemical reactions to determine their neurochemical content and their synaptic inputs and outputs.

This study demonstrated that both PrP- and NPY-GFP cells were morphologically heterogeneous although neither group contained islet cells, which are a distinct morphological class of interneuron. PrP- and NPY-GFP cells in lamina II could not be distinguished from each other by using hierarchical cluster analysis with measures of somatodendritic morphology. This suggests that morphological properties may not be useful in distinguishing these populations of interneurons. The vast majority of PrP- and NPY-GFP cells either displayed tonic or initial burst firing of action potentials. However, these groups of cells showed significant differences in some of their active and passive membrane properties, such as membrane resistance, spike frequency adaptation and mV drop in action potential height. When hierarchical cluster analysis was used to group these cells in lamina II based on physiological parameters, PrP- and NPY-GFP cells could be

distinguished with some accuracy. This suggests that some physiological differences may exist between these two groups.

Within the PrP-GFP group there was a subset that included lamina I among its synaptic outputs, and these cells could provide inhibition to the projection neurons located in this lamina, since GFP boutons from this mouse line can form synapses with giant cells and neurokinin-1 receptor (NK1r)-expressing lamina I neurons. Some PrP-GFP cells showed immunoreactivity for neuronal nitric oxide synthase (nNOS) or galanin, and these two groups had slight morphological differences, which included their laminar location and the spread of their processes. Several experimental approaches, such as electrophysiological, pharmacological and anatomical techniques, indicated that PrP-GFP cells received input from many different types of primary afferent fibre, including peptidergic and non-peptidergic C-afferents, as well as low-threshold mechanosensory fibres. Taken together these findings establish the PrP-GFP cells as a much more functionally heterogeneous group than previously reported.

NPY-GFP cells were located in laminae II and III, but were preferentially found in lamina III. The lamina III cells had dendrites with a greater dorsoventral extent than the lamina II cells, and this extent was seen be more dorsal from the soma than ventral. Many NPY-GFP cells received synaptic input from C-fibres, and a subset of those tested lacked TRPV1. Since the TRPV1-lacking C-fibres mostly correspond to the non-peptidergic C-fibres, including non-peptidergic nociceptors and C-low threshold mechanoreceptors, this suggests that NPY-GFP cells could receive input from these fibres. Dorsal root stimulation experiments showed that labelled NPY-GFP cells with somata located in lamina III often received synaptic input from unmyelinated C-fibres, and NPY-expressing neurons in lamina III could respond to noxious mechanical stimuli. A select group of NPY-GFP cells were seen to innervate putative anterolateral tract (ALT) neurons located in lamina III, which could be identified by their dense innervation by bundles of axons containing either NPY or calcitonin gene related peptide (CGRP).

Taken together these data suggest that the PrP- and NPY-GFP neurons are distinct populations based on their primary afferent input and post-synaptic targets, and that more than one functional population exists within each of these groups. Despite their many differences, morphological parameters do not appear to be useful in distinguishing the PrP- and NPY-GFP cells, or detecting different functional populations within these groups. The

PrP-GFP cells are more morphologically heterogeneous than previous reports suggested, and due to similar features with cells that require the transcription factor Bhlhb5 to develop, they may include a population that are involved in suppressing itch-related signals. NPY-GFP cells could play a role in limiting the spread and intensity of noxious stimuli due to their input from C-fibres, and a small subset of these could inhibit ALT neurons in lamina III. These results further support the view that different neurochemical populations of inhibitory neurons have distinct functional roles, and also highlight the complexity of the neuronal circuitry in the superficial dorsal horn.

Acknowledgements

First and foremost, I would like to thank my supervisor Professor Andrew Todd, without whom this PhD project would not have been possible. I am incredibly fortunate and privileged to have had such a dedicated and thoughtful supervisor, whose hard work and guidance have ensured that this project was a success. I would also like to thank Drs Noboru Iwagaki and Allen Dickie for their huge contribution to the electrophysiology data used in this project, but especially for their time, effort and patience to teach me how to perform the electrophysiology experiments myself, for which I am truly grateful.

I would like to extend my thanks to Drs Erika Polgár, Najma Baseer, and Zilli Huma who taught me the immunocytochemistry and microscopy techniques used in this project, and for supporting me throughout my time in the lab. I cannot express enough gratitude to Mrs Christine Watt and Mr Robert Kerr whose technical support and help have been invaluable. I thank Drs David Hughes and John Riddell for their advice and assistance during this project, as my project assessor and co-supervisor.

It has been a great pleasure to have worked alongside all members of the Spinal Cord Group during my time here in the lab. In particular I would like to thank post-doctoral research assistants Maria Gutierrez-Mecinas, Patricia del-Rio, Anne Bannatyne, and Kieran Boyle; and fellow students Andrew Bell, Marami Binti Mustapa, and Judit Mészáros who have made my time here all the more enjoyable.

I also thank the BBSRC for funding this PhD, and the MRes that preceded it.

I will finally thank my parents for their continuous love, support and encouragement.

Declaration

I declare that the work presented in this thesis is my own work, except where explicit reference is made. Drs Noboru Iwagaki and Allen Dickie performed the vast majoriy of the electrophysiology experiments, and Dr Erika Polgár performed the quantification of the NPY-GFP cells that were NPY-expressing, presented in section 4.2.1. Animals used for noxious pinch stimulation in section 4.2.5 were used in a previous study (Smith et al., 2015), and these stimulation experiments were performed by Dr David Hughes. This degree has not been submitted in any previous application for any other degree in the University of Glasgow or any other institution.

Robert Ganley
October 2015

List of Abbreviations

AAV	adeno-associated virus
ALT	anterolateral tract
A-LTMR	A low threshold mechanoreceptor
BAC	bacterial artificial chromosome
Bhlhb5	basic helix-loop-helix b5
BNP	B natriuretic polypeptide
B5-I	bhlhb5-dependent inhibitory
CCI	chronic construction injury
CFA	complete Freund's adjuvant
CGRP	calcitonin gene related peptide
C-LTMR	C low threshold mechanoreceptor
Cre	cre recombinase
CTb	cholera toxin subunit B
CVLM	caudal ventrolateral medulla
DAB	3, 3' diaminobenzidine
DREADD	designer receptors exclusively activated by designer drugs
DRG	dorsal root ganglion
eEPSC	evoked excitatory post synaptic current
ER	oestrogen receptor
ERK	extracellular regulated kinase
GABA	γ-aminobutyric acid
GFP	green fluorescent protein
GlyT2	glycine transporter 2
GRP	gastrin releasing peptide
HRP	horseradish peroxidase
IB4	*Bandeiraea simplifica* Isolectin B4
LDA	linear discriminant analysis
LI	lamina I
LII	lamina II
LIII	lamina III
LPb	lateral parabrachial area
LTMR	low threshold mechanoreceptor
LTP	long term potentiation

mEPSC	miniature excitatory post synaptic current
MrgprA3	mas related G protein coupled receptor A3
MrgprD	mas-related G protein coupled receptor D
NF200	neurofilament 200
NKA	neurokinin A
NK1r	neurokinin 1 receptor
NMDA	N-methyl-D-aspartate receptor
nNOS	neuronal nitric oxide synthase
Nmb	neuromedin B
NPY	neuropeptide Y
NTS	nucleus of the solitary tract
PAG	periaqueductal grey matter
PB	phosphate buffer
PBS	phosphate-buffered saline
PCA	principal component analysis
pERK	phosphorylated extracellular regulated kinase
PKCγ	protein kinase Cγ
PPD	preprodynorphin
PrP	prion promoter
PSDC	post-synaptic dorsal column
RA	rapidly adapting
Ret	receptor tyrosine kinase
SA	slowly adapting
SCT	spino-cervicothalamic tract
sEPSC	spontaneous excitatory post-synaptic current
sst_{2A}	Somatostatin receptor 2A
TH	tyrosine hydroxylase
trkA	receptor tyrosine kinase A
TRPA1	transient receptor potential receptor ankyrin 1
TRPM8	transient receptor potential receptor melastatin 8
TRPV1	transient receptor potential receptor vanilloid 1
TTX	tetrodotoxin
VGAT	vesicular GABA transporter
VGluT	vesicular glutamate transporter

Table of contents

List of Figures

List of tables

1 Introduction

The spinal cord is part of the central nervous system located in the vertebral column, and is continuous with the brainstem and higher brain centres. The spinal cord can be divided broadly into the grey and white matter. The white matter consists of ascending and descending myelinated axonal tracts that project to and from the brain. The grey matter contains the cell bodies, dendrites, and unmyelinated axons from many types of neurons. The spinal grey matter is a symmetrical H shape that surrounds a central canal, and this H shape varies depending on its rostrocaudal position. The spinal grey matter can be divided into 10 laminae according to histological criteria, such as cell size and packing density of neurons. This scheme was first devised by Bror Rexed to describe the cytoarchitecure of the cat spinal cord (Rexed, 1952), and it was later shown to apply to many species of mammals, including the rat and macaque (Molander et al., 1984, 1989; Ralston, 1979, 1982).

The spinal dorsal horn contains projection neurons that send signals from the spinal cord to regions of the brain. This region also contains the terminals of descending input from brainstem regions, including the nucleus raphe magnus and the locus coeruleus, which modulate signal processing in the dorsal horn through volume transmission of monoamines. It is also the termination zone for primary afferent fibres that conduct signals from peripheral tissues to the dorsal horn. However, the vast majority of the cells in this region are local interneurons that process incoming signals. These interneurons possess axons and dendrites that remain within the spinal dorsal horn, and are therefore only involved in local signal processing. The role of the interneurons is to regulate the output of the projection neurons thus controlling the information that is sent to the brain (Todd, 2010; West et al., 2015). This enables the nervous system to limit a sensation to the duration of a stimulus, to discriminate between several sensory modalities, and to locate the stimulus precisely to the correct somatotopic region (Sandkühler, 2009). These main components will be described in further detail and particular attention will be given to the interneurons of the dorsal horn, as these are the main subject of this study.

1.1 **Primary afferent fibres**

Primary afferent fibres conduct signals to the spinal cord. Morphologically they are pseudo-unipolar neurons, with their cell bodies contained within the dorsal root ganglia (DRG). The axons of these cells bifurcate into central and peripheral branches; the peripheral branches terminate in their target tissue and the central branches project to the

central nervous system. These afferent fibres are sensitive to various types of stimuli, depending on the tissue type innervated by the peripheral terminals, and the ion channels and receptors that these terminals express. The organisation of the central terminals of primary afferents in the dorsal horn is related to sensory modality, with low threshold cutaneous mechanosensory fibres terminating in the deep dorsal horn, and nociceptive fibres terminating in the superficial dorsal horn (Todd, 2010). All primary afferent fibres use glutamate as their fast transmitter, and therefore have an excitatory effect on their synaptic targets. They also express vesicular glutamate transporters (VGluTs) in their central terminals, which are responsible for packaging glutamate into synaptic vesicles. These include VGluT1, VGluT2 and VGluT3, which are expressed in different types of primary afferents. For example VGluT1 is expressed in the central terminals of low threshold mechanoreceptors (LTMRs) in laminae IIi-VI, whereas VGluT2 is expressed at low levels in many unmyelinated fibres (Todd et al., 2003a). More recently VGluT3 was shown to be expressed in primary afferents that are unmyelinated and transmit mechanosensory information that is thought to underlie pleasurable touch (see below)(Seal et al., 2009). Therefore there appears to be a largely non-redundant expression of these VGluTs.

Primary afferent fibres can be classified by the diameter of their axons and whether or not they are myelinated. Both of these features affect the conduction velocity of action potentials and the maximum firing frequency for these cells. They have been classified as slow conducting unmyelinated C-fibres, thinly myelinated Aδ fibres, and large myelinated Aβ fibres. The C-fibres generally transmit nociceptive and pruritic (itch related) information, although there are some low threshold C-fibres (C-LTMRs) that respond to non-painful stimuli and express VGluT3 (see above)(Abraira and Ginty, 2013; Li et al., 2011; Seal et al., 2009). Thinly myelinated Aδ fibres conduct impulses faster than C-fibres and normally conduct nociceptive signals, but some innervate down hairs and encode mechanosensory information (Light and Perl, 1979). The thickly myelinated Aβ fibres generally transmit innocuous mechanosensory information and terminate in laminae IIi-VI, but Aβ nociceptors have also been identified (Djouhri and Lawson, 2004). Evidently there is no definite rule for primary afferent fibre size, myelination and modality, although clear patterns do exist. Further details on these types of afferents are as follows.

1.1.1 **Aβ fibres**

Except for the proprioceptive afferents, the Aβ fibres are the largest and fastest conducting primary afferent fibres type. They are thickly myelinated, have a larger diameter and a rapid conduction velocity above 10 m/s in the mouse (Koltzenburg et al., 1997). The majority of Aβ fibres are LTMRs and can be broadly divided into two groups; these are rapidly adapting (RA) fibres and slowly adapting (SA) fibres. This refers to the response of these fibres to skin indentation; the RA fibres will only discharge action potentials during the onset and offset of skin indentation, whereas the SA fibres will fire throughout the stimulus. This feature is related to the mechanosensory end organ with which the peripheral branch is associated; SA fibres are associated with Merkel cells and Ruffini endings, and RA fibres are associated with Pacinian and Meissner corpuscles (Abraira and Ginty, 2013). The combination of activities from these different fibres enables our ability to detect and distinguish a wide range of tactile sensations.

The central branches from Aβ fibres terminate in the deeper dorsal horn between laminae IIi – VI. The Aβ fibres that arise from distal skin regions terminate in the medial part of the cord, whereas the fibres innervating proximal regions terminate in the lateral region of the dorsal horn, which demonstrates somatotopic organisation at this first stage in sensory transduction (Brown et al., 1991). Upon entering the spinal cord these fibres immediately bifurcate giving rise to rostrally and caudally directed branches. Collaterals from these branches then enter the dorsal horn where they arborise and form synapses with dorsal horn neurons. Occasionally the rostral branch will extend directly through the dorsal column and into the dorsal column nuclei, providing a more direct route to the brain from the periphery (Brown and Fyffe, 1981).

It has been possible to see the central projections of identified RA and SA Aβ fibres in the mouse using an *ex vivo* somatosensory preparation of dorsal skin, peripheral nerve, DRG and spinal cord (Woodbury and Koerber, 2007; Woodbury et al., 2001). Intracellular recording of DRG neurons and labelling them with Neurobiotin allows their responses to maintained low threshold mechanical stimulation to be determined and their central axons to be labelled. The RA fibres terminate in deeper laminae and exhibit a flame shaped arborisation pattern, with the SA fibres giving rise to dorsally and a ventrally directed components that can innervate both deeper and more superficial laminae (Woodbury and Koerber, 2007; Woodbury et al., 2001).

Even though virtually all Aβ fibres are LTMRs there have been reports of nociceptive fibres with conduction velocities in the Aβ range (Djouhri and Lawson, 2004). Other reports show Aβ nociceptors recorded and labelled in the *ex vivo* preparation of skin/nerve/DRG/spinal cord, which conduct impulses with a conduction velocity of Aβ fibres and have central terminals also present in superficial laminae where nociceptive fibres terminate (Woodbury et al., 2008). Furthermore the action potentials generated in these afferents were broad and inflected on the falling phase of the spike, which is strongly suggestive of nociceptors, and the central branches were reminiscent of flame-shaped arbors, where the parent branch projects deep but turns back and arborises dorsally (Djouhri et al., 1998; Koerber et al., 1988; Scheibel and Scheibel, 1968).

1.1.2 **Aδ fibres**

The Aδ fibres are thinly myelinated and many of these fibres are nociceptive and are responsible for fast sharp pain. However, some are non-nociceptive and innervate down hair follicles on hairy skin (Light and Perl, 1979). The central terminals of these fibres can extend through laminae I-V, although the nociceptive fibres mainly terminate in lamina I, IIo and V, whereas the D-hair afferents terminate in lamina IIi and III. This distinct central termination pattern between mechanical nociceptors and low threshold mechanoreceptors was shown by recording the responses from these different sensory fibres and subsequently labelling their axons with horseradish peroxidise (HRP). The nociceptive Aδ fibres can project in the Lissauers tract or the dorsal columns, whereas the LTMRs only projected in the dorsal columns, and in three quarters of cases in the cat the nociceptive Aδ fibres projected 1 or 2 segments rostrally from the root entry zone (Traub and Mendell, 1988).

Many previous studies of myelinated fibres have used nerve injection of cholera subunit toxin B (Ctb) to label axons (Shehab and Hughes, 2011). The Aδ fibres can be difficult to study using this approach, as injection of Ctb into a peripheral nerve to stain myelinated fibres also labels the thickly myelinated Aβ fibres. Although not much is known about the synaptic targets of the Aδ fibres, a recent study has shown that they innervate projection neurons in lamina I labelled from the lateral parabrachial area (LPb). These Ctb labelled Aδ afferents preferentially innervate the projection neurons that do not express the neurokinin 1 receptor (NK1r) and these Ctb labelled terminals were virtually all non-peptidergic (Baseer et al., 2014). The density of contacts onto projection neurons was also assessed, and NK1r-lacking projection cells received a higher contact density from Aδ fibres than the NK1r-expressing projection cells. However, it has been demonstrated that

silent Aδ input onto NK1r neurons can be unmasked in a model of inflammatory pain, and this effect is mediated through N-methyl-D-aspartate (NMDA) receptors (Torsney, 2011).

1.1.3 **C-fibres**

The unmyelinated C-fibres transmit nociceptive and/or pruritoceptive signals to the spinal cord, and can be divided into several classes according to their neurochemical content and function. Peptidergic C-fibres contain various peptides including calcitonin gene related protein (CGRP), substance P/neurokinin A (NKA), somatostatin and galanin (Gibson et al., 1984; Hökfelt et al., 1975, 1976, 1987). The non-peptidergic C-nociceptors do not contain such peptides and are often identified by the binding of the isolectin B4 (IB4), or by the expression of certain receptors. For example the mas-related G protein coupled receptors (Mrgprs) are found to be exclusively expressed in this sub-population of C-fibres, with Mrgprd found to be coexpressed in 75% of IB4 binding C-fibres (Zylka et al., 2005). All nociceptive C-fibres require the receptor tyrosine kinase trkA and nerve growth factor (NGF) signalling for survival. However, whereas the peptidergic C-fibres continue to express the trkA receptor into maturity, the non-peptidergic C-nociceptors downregulate this receptor and upregulate another receptor tyrosine kinase called Ret (2004). As the expression of Mrgprd is a more selective marker for non-peptidergic C-nociceptors than IB4 binding, and other non-nociceptive C-fibres are also non-peptidergic and express IB4, the non-peptidergic C-nociceptors will be referred to as C^{Mrgprd} fibres henceforth. Unmyelinated afferents account for 80% of cutaneous primary afferent fibres, and are therefore much more numerous than the Aβ and Aδ fibres described above (Lynn, 1984). However, they have a much smaller receptive field than myelinated afferents, and thus more fibres are required to innervate a given area of skin.

Peptidergic C-fibres and C^{Mrgprd} fibres appear to be functionally and anatomically distinct, with their central terminals being present in adjacent laminae in the dorsal horn. Peptidergic C-fibres terminate in laminae I and IIo, whereas non-peptidergic C-fibres terminate within a narrow band between lamina IIo and IIi, with little overlap with peptidergic C-fibres (Zylka et al., 2005). Peripherally, the peptidergic C-fibres innervate the viscera, joints and skin, whereas the non-peptidergic C-fibres mostly terminate in the superficial layers of the epidermis (Taylor et al., 2009). The IB4 binding and peptidergic C-fibres are differentially affected by several nerve injury models. During this pain state in the rat, the IB4 binding is transiently lost in the affected side of the spinal cord, whereas the CGPR immunoreactivity is maintained at a normal level (Bailey and Ribeiro-da-Silva,

2006). This study indicated that a loss of non-peptidergic C-fibres as opposed to a loss of IB4 binding was responsible, because the number of type I glomeruli in the ipsilateral dorsal horn was also reduced in these animals, which originate from non-peptidergic C-fibres (see below)(Ribeiro-Da-Silva et al., 1986). The modality of these fibres has been shown to be somewhat distinct. Using genetic models of conditional ablation in mice, TRPV1 expressing fibres (the majority of which are peptidergic C-fibres) were shown to be required for thermal nociception without affecting mechanonociception, whereas non-peptidergic Mrgprd expressing fibres were required for the full expression of mechano-nociception with no alteration in thermo-nociception (Cavanaugh et al., 2009, 2011). This is likely due to the central processing of these fibres as the C^{Mrgprd} fibres are seen to respond to both thermal and mechanical noxious stimuli in the *ex vivo* skin/nerve/DRG/spinal cord somatosensory preparation (Rau et al., 2009). The C^{Mrgprd} fibres have also been implicated in some forms of itch, as Mrgprd is the receptor for the pruritogen β-alanine and the peripheral terminals of these fibres are in superficial skin, which is consistent with the sensation of itch only being perceived in the surface of the skin (Ross, 2011; Shinohara et al., 2004; Zylka et al., 2005). This β-alanine induced itch has been shown to be Mrgprd dependent, and separate from histamine dependent itch (Liu et al., 2012a).

A third group of C-fibres exist that do not respond to noxious stimuli, and these are known as the C-LTMRs (Zotterman, 1939). These were originally believed to be involved in ticklish sensations, but recently they have been associated with pleasant touch sensation in humans (Löken et al., 2009). C-LTMRs express the vesicular glutamate transporter 3 (VGluT3) and the enzyme tyrosine hydroxylase (TH), both of which have been used to specifically label them (Li et al., 2011; Seal et al., 2009). In terms of their physiological properties they are slow conducting, and respond to mechanical stimuli with adaptation in firing frequency of action potentials, and also respond to gentle cooling but not heating. The action potentials are inflected on the falling phase which is consistent with them being C-fibres. The central terminals of these fibres are mainly located in lamina IIi, and the peripheral terminals are associated with hair follicles as lanceolate endings. These fibres are only found on hairy skin in mice, and therefore their central terminals are restricted to the lateral two thirds of the dorsal horn. These C-LTMRs are molecularly distinct from the peptidergic and C^{Mrgprd} fibres, although Seal *et al* (2009) found a minority of C-LTMRs displayed IB4 binding in DRG neurons (2009). However, using TH-cre mice to label C-

LTMRs found no co-localisation of IB4 binding in labelled cells, but most C-LTMRs were labelled with c-Ret (>90%)(Li et al., 2011).

The TRPM8 channel is activated by cooling and menthol, and is responsible for cold sensation *in vivo*, since mice lacking this channel have defects in behavioural responses to cold stimuli (Dhaka et al., 2007). Although a lack of TRPM8 resulted in loss of sensitivity to unpleasant cold sensation, these animals had normal responses to sub-zero nociceptive cold stimuli. Unmyelinated C-fibres that express TRPM8 and are sensitive to innocuous cooling represent a distinct subset of sensory neurons, and are entirely separate from the C fibre nociceptors (Dhaka et al., 2008). Farnesylated enhanced GFP (EGFPf) was used to label the membranes of TRPM8 expressing cells with GFP, and hence allow the axons and axon terminals of these fibres to be visualised. This study showed that these fibres project to lamina I and they respond to innocuous cooling as well as the TRPM8 agonist menthol. Surprisingly, the incidence of DRG neurons that expressed both EGFPf and TRPV1 increased from 12 to 20% during CFA induced inflammation (Dhaka et al., 2008). Other physiological studies have identified non-nociceptive C-fibres that responded exclusively to cooling sensations, which agrees with the findings of this study (Hensel, 1981). In the trigeminal ganglia it is found that approximately one-quarter of TRPM8 expressing neurons also co-express the peptidergic markers CGRP and substance P (Kim et al., 2014). However, it is found that a higher proportion of neurons express TRPM8 mRNA in the TG than in the DRG (35% vs 22%), and almost half of myelinated afferents immunoreactive for neurofilament 200 (NF200) were TRPM8 positive in the DRG (Kobayashi et al., 2005). This suggests that TRPM8 is not restricted to cooling fibres but may be expressed by other afferents. However, this study found TRPM8 mRNA was colocalised with trkA, a marker of peptidergic neurons in the DRG, suggesting that at least some of these cells belong to a subset of peptidergic C-fibres (Snider and McMahon, 1998).

C-fibres are also seen in structures known as synaptic glomeruli, which are the structures involved in GABAergic pre-synaptic inhibition. Two types of synaptic glomeruli have been identified based on differences in morphological appearance when viewed by transmission electron microscopy. Type I glomeruli are dark, contain dense spherical vesicles of varying size and display an indented contour, whereas type II glomeruli are translucent, larger, have a lower vesicle density and a regular contour (Ribeiro-da-Silva and Coimbra, 1982). Type I glomeruli are seen to originate from unmyelinated afferents, because topical application of capsaicin in neonates is seen to selectively damage the type I

glomeruli (Lawson and Nickels, 1980; Ribeiro-da-Silva and Coimbra, 1984). Furthermore, these unmyelinated afferents that form glomerular structures are IB4-binding and are concentrated in lamina II, strongly suggesting that they are from C^{Mrgprd} fibres (Gerke and Plenderleith, 2004).

Controversy has surrounded the transmission of itch signals to the spinal cord. One theory suggests that there are labelled lines that are responsible for the transmission of itch signals and that these are separate from fibres that transmit other sensory modalities. Another theory suggests that the combination of afferent fibre activation is responsible for the perception of itch, and these populations of fibres may overlap with afferents that transmit other sensory modalities (Ross, 2011). This ambiguity is due to similarities in the populations of primary afferent fibre transmitting both pain and itch signals, raising the question of how these sensations are perceived as different. Recently a population of C-fibres that express MrgprA3 have been shown to be specifically involved in the transmission of itch but not pain (Han et al., 2012). These fibres were seen to terminate in superficial skin layers, respond to multiple pruritogens, and their ablation was shown to reduce responses to itch without affecting pain responsiveness. Interestingly this group of sensory neurons belong to a small population of cells that are both IB4 binding and express CGRP, but it was noted that these cells expressed a lower level of CGRP than surrounding profiles (Han et al., 2012).

B-type natriuretic peptide (BNP) has also been associated with the transmission of itch signals in the spinal cord, and this is seen to be contained in primary afferent fibres (Mishra and Hoon, 2013). BNP was co-localised with TRPV1 in DRG neurons, which suggest that these afferents are a subpopulation of peptidergic nociceptors. Animals without BNP showed reduced responses to injection of multiple pruritogens but performed normally in behavioural tests of thermal, touch and proprioceptive stimuli. Interestingly, all DRG neurons that expressed BNP were also immunoreactive for MrgprA3, and over 70% of MrgprA3 expressing cells contained BNP (Mishra and Hoon, 2013). This suggests that the $MrgprA3^{+}/BNP^{+}$ fibres represent a unique subset of unmyelinated nociceptors that transmit itch signals to the spinal cord. A summary of the molecular markers that are found in the different types of unmyelinated fibres is displayed in Figure 1-2.

Unmyelinated C fibres

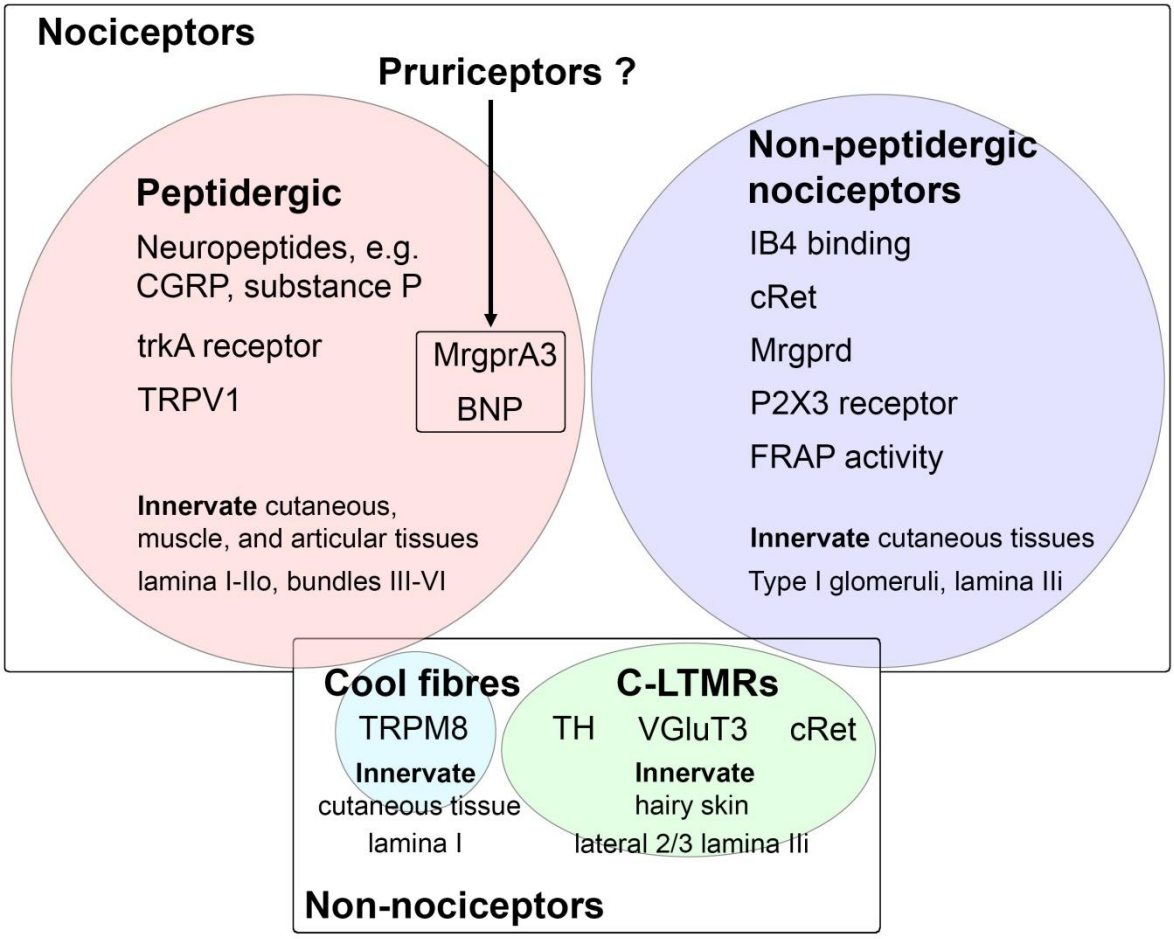

Figure 1-1 Molecular markers, and peripheral and central terminals of unmyelinated C-fibres.

Diagram summarising the different types of unmyelinated C-fibres that are known to innervate the dorsal horn and the markers that they express. The majority of unmyelinated fibres are nociceptive, and these can be broadly divided into peptidergic and non-peptidergic C-nociceptors based on their expression of neuropeptides. These groups have different termination zones in peripheral tissues and in the central nervous system. Non-nociceptive C-fibres include C-LTMRs that respond to low-threshold mechanical stimuli, and cool fibres that respond to innocuous cooling. There is some overlap in the expression of markers between these different types of fibres. Co-localisation of the C-LTMR marker VGluT3 and IB4 binding is occasionally observed in DRG neurons (7% of VGluT3-IR neurons); TG neurons express CGRP and substance P in approximately 25% of those that express TRPM8; some DRG afferents that express low levels of CGRP can also bind IB4 (Han et al., 2012; Kim et al., 2014; Seal et al., 2009). MrgprA3 expressing cells belong to the small subset of DRG neurons that express low levels of CGRP and bind IB4, and these also express the peptide BNP (70% of MrgprA3 expressing neurons), which is required for normal transmission of itch signals (Han et al., 2012; Mishra and Hoon, 2013). Therefore these afferents may be a distinct population that transmit itch-related signals to the spinal cord from the periphery. Diagram is not to scale, CGRP = calcitonin gene related peptide, C-LTMR = C low-threshold mechanoreceptor, DRG = dorsal root ganglia, TG = trigeminal ganglia, trkA = tyrosine kinase A, TRPV1 = transient receptor potential vanilloid 1, MrgprA3 = mas-related G protein coupled receptor A3, BNP = b-type natriuretic peptide, IB4 = isolectin B4, Ret = receptor tyrosine kinase, P2X3 = purinergic P2X3 receptor, FRAP = fluoride resistant acid phosphatase, TRMPM8 = transient receptor potential melastatin 8, TH = tyrosine hydroxylase, VGluT3 = vesicular glutamate transporter

1.2 **Projection neurons**

The projection neurons of the dorsal spinal cord are the output from this region to various structures in the brainstem. Most of the current knowledge of projection neurons and their targets are from retrograde tracing studies, mainly performed in the rat. The three main ascending tracts to the brain are the anterolateral tract (ALT), the post-synaptic dorsal column (PSDC) pathway, and the spino-cervicothalamic tract (SCT). Since the ALT is involved in relaying nociceptive information to the brain, and ALT neurons are the most abundant projection neuron in laminae I-III, this study will mainly focus on this pathway.

The projection neurons are found throughout the dorsal horn except in lamina II. Projection neurons in lamina I and many in laminae III-IV contribute to the ALT, which transmits signals related to pain behaviours. Although lamina I projection neurons have dendritic trees that are restricted to this lamina, the ALT neurons in laminae III-IV have dendrites that extend dorsally into lamina II. In the rat, ALT neurons in laminae III-IV are NK1r-expressing, and are densely innervated by GABAergic NPY-containing boutons, which allows them to be distinguished from PSDC neurons in this area (Polgár et al., 1999a). Although these lamina III ALT neurons do not express the NK1r in the mouse, they can still be identified by their dense innervation by intermingled bundles of CGRP-expressing and NPY-expressing boutons (Cameron et al., 2015). The vast majority of projection neurons project to contralateral brainstem regions and thalamic nuclei, although some of these cells project bilaterally (Spike et al., 2003). These brain regions include the lateral parabrachial area (LPb), the caudal ventrolateral medulla (CVLM) the periaqueductal grey matter (PAG), and the nucleus of the solitary tract (NTS) as well as the thalamus. Many ALT neurons of the dorsal horn project to multiple brainstem regions, such as the CVLM and LPb in the rat (Spike et al., 2003). The lamina I ALT neurons have been categorised morphologically into three groups; these are fusiform, multipolar, and pyramidal (Zhang et al., 1996). Fusiform cells have a bipolar soma and two primary dendrites, multipolar cells have variable soma morphology with multiple dendrites, and pyramidal cells are distinguished by their pyramid shaped soma. Some studies have correlated these morphological properties with the function of cells, for example, Han *et al* (1998) reported that fusiform cells were nociceptive specific, pyramidal cells only responded to innocuous cooling and multipolar cells were either polymodal or nociceptive specific in the cat. However, studies in the rat have shown that these morphological types of neuron in lamina

I do not differ in their expression of NK1r, or their responses to noxious thermal stimuli (Todd et al., 2002, 2005). Despite this finding, it was found that multipolar projection neurons in lamina I did show a higher proportion of cells that responded to noxious cold stimuli, when compared to fusiform and pyramidal cells (Todd et al., 2005).

Many of these ALT cells can be identified by the expression of the NK1r, which is the receptor for substance P and is found on approximately 80% of the projection neurons in lamina I (Marshall et al., 1996; Todd et al., 2000). In the rat 45% of neurons in lamina I express NK1r, and these include interneurons as well as projection neurons, since only 5-10% of cells in this lamina are projection neurons (Spike et al., 2003). Although some interneurons in lamina I also express NK1r, it has been shown that the NK1r immunoreactivity in these cells is much lower and their somata are significantly smaller than those of NK1r expressing projection neurons (Al-Ghamdi et al., 2009). Consequently, only very sensitive techniques would be able to activate or detect these cells. Furthermore the NK1r expressing projection cells of the ALT are required for nociception, as their ablation by intrathecal injection of substance P-saporin reduces nocifensive behaviour in rats, as well as reduced mechanical and thermal hyperalgesia (Mantyh et al., 1997; Nichols et al., 1999). They are also reported to be a site for long term potentiation (LTP) and contribute to altered pain states (West et al., 2015). In two papers from the Sandkühler group it was shown that LTP could be induced between C-fibres and NK1r-expressing ALT neurons, and this could provide a mechanism for some forms of hyperalgesia (Ikeda et al., 2003, 2006). LTP was induced between C-fibres and NK1r-expressing ALT neurons labelled from the LPb in response to high frequency stimulation (100 Hz), and could also be induced by low frequency stimulation (2 Hz) for 2 minutes in cells projecting to the PAG, similar to what would be seen in the case of inflammation. Furthermore, this LTP was blocked by NMDA antagonists, and is further evidence that C-fibre mediated activity dependent plasticity in the dorsal horn requires NMDA receptors (Dickenson and Sullivan, 1987; Ikeda et al., 2006).

These same NK1r-expressing projection neurons are also seen to be under tonic inhibitory control. An excitatory polysynaptic pathway activated by innocuous mechanosensory fibres is unmasked by blocking glycinergic and GABAergic inhibition in slices of rat spinal cord, and this can activate NK1r expressing projection neurons that would normally only respond to nociceptive stimuli (Torsney and MacDermott, 2006). Monosynaptic Aδ input to these cells was increased during complete Freund's adjuvant (CFA) mediated

inflammation, which was shown to be mediated through NMDA channels that are normally silent (see above)(Torsney, 2011).

Another anatomically distinct type of projection neuron has been identified in lamina I, distinguished by its dense input from inhibitory axonal boutons that express vesicular GABA transporter (VGAT) and VGluT2-expressing boutons originating from local interneurons (Polgár et al., 2008; Puskár et al., 2001). These cells have been termed giant cells, which resemble large multipolar lamina I neurons and do not express the NK1r. Although rare, these projection cells likely play a role in nociception, as they express the activity dependent marker c-fos in response to noxious stimuli. They are also selectively innervated by nNOS-expressing inhibitory boutons, identified by their immunoreactivity to nNOS and VGAT (nNOS+/VGAT+). Many of these nNOS+/VGAT+ boutons are lost in the bhlhb5$^{-/-}$ mouse, in which a subset of inhibitory interneurons fails to develop that require the basic helix loop helix b5 (bhlhb5) transcription factor for development (see section 1.3.1.4 below)(Baseer, 2014; Ross et al., 2010). Despite this selective loss of nNOS-expressing inhibitory boutons, the proportion of nNOS-/VGAT+ boutons increases suggesting that there is some compensation for the loss of inhibitory input to giant cells in these mice.

Although there are inevitably some anatomical differences between the mouse and rat, these are likely to be subtle and may involve differences in expression of neurochemicals and receptors in projection neurons as opposed to the brain regions they innervate. It is seen that there are fewer lamina I NK1r immunoreactive cells in the mouse than in the rat (Polgár et al., 2013). Also the lamina III ALT neurons express NK1r in the rat but this receptor is absent or expressed at very low levels in the mouse (Cameron et al., 2015). This report also identified the same population of giant cells in the mouse, which could be retrogradely labelled from the LPb. Unlike the case for rat, the giant cells in the mouse could not always be labelled from the LPb (32% of cells) and sometimes expressed the NK1r (36%) (Cameron et al., 2015). Interestingly, all of the giant cells that could be retrogradely labelled form the LPb expressed NK1r.

1.3 **Interneurons of the dorsal horn**

Incoming signals from primary afferents are processed by local interneuron populations to control the flow of information from the spinal cord to higher brain centres. The

interneurons can be broadly divided into excitatory and inhibitory interneurons, with excitatory interneurons using glutamate as their fast transmitter, and inhibitory interneurons using GABA and/or glycine. The vast majority of neurons in laminae I-III are interneurons, with virtually all lamina II cells being interneurons. Between 25-40% of the neurons in laminae I-III are GABA containing inhibitory interneurons, and a subpopulation of these are enriched with glycine, which is thought to act as a co-transmitter (Todd and Sullivan, 1990). Although inhibitory neurons that only use glycine as their fast inhibitory transmitter are present in other regions of the central nervous system, this is never seen in laminae I-III of the spinal dorsal horn. However, purely glycinergic synapses have also been identified in the dorsal horn (Yasaka et al., 2007). These purely glycinergic synapses are presumably due to either, cells that only contain glycine as a fast transmitter that originate from outside the dorsal horn, or the lack of $GABA_A$ receptors in the post-synaptic cell, since these receptors would be required for a synaptic response to GABA (Todd, 2010). A higher proportion of inhibitory cells in lamina III are enriched with glycine than in laminae I and II, in the rat these are 9, 14, and 30% of neurons in laminae I, II and III respectively (Todd and Sullivan, 1990). Inhibitory interneurons are important in suppressing pain signals from the periphery, as it is seen that blocking inhibition at the spinal level with intrathecal bicuculine or strychnine results in enhanced pain sensitivity, and pain in response to innocuous stimuli in rats (Sherman and Loomis, 1994; Yaksh, 1989).

There is currently no reliable method for detecting glutamate directly in the somata of excitatory interneurons using immunocytochemistry. This is partly due to the difficulty generating antibodies against glutamate, and the fact that glutamate is also present in proteins in all cells. However, it is assumed that all local neurons that do not contain GABA and are not enriched with glycine are excitatory interneurons. It is also possible to detect vesicular glutamate transporters in the axonal boutons of excitatory cells, allowing confirmation of their excitatory phenotype (Maxwell et al., 2007; Yasaka et al., 2010). By using *in situ* hybridisation, it is possible to confirm whether a cell expresses the VGluT2 transcript and would therefore be excitatory, and unlike immunostaining for VGluT2, the cell bodies are also labelled (Landry et al., 2004; Oliveira et al., 2003). Glycine can be detected in the cell bodies by immunocytochemistry even thought this is also a common amino acid, since antibodies have been raised against glutaraldehyde conjugated versions of these antigens (Pow and Crook, 1993). For this reason, glycine can only be detected using these antibodies in glutaraldehyde fixed tissues

1.3.1 Classification of dorsal horn interneurons

The superficial dorsal horn is a difficult region to study due to the density and heterogeneity of its constituent neurons. The study of dorsal horn circuitry is further complicated by the lack of a comprehensive classification scheme for interneurons, with the most commonly accepted schemes classifying cells based on their somatodendritic morphology alone or in combination with action potential firing patterns (Grudt and Perl, 2002; Prescott and De Koninck, 2002; Yasaka et al., 2007, 2010). Identifying and characterising populations of interneurons that perform the same functions is therefore an important step towards understanding the organisation of the spinal dorsal horn.

1.3.1.1 Morphology

There are many ways of classifying interneurons in this region; these include using electrophysiological properties, cell morphology, the expression of neurochemical markers and the developmental expression of transcription factors as parameters for defining cells. The most commonly accepted scheme, which was devised by Grudt and Perl (2002) uses somatodendritic morphology and action potential firing pattern to identify different classes of interneurons. The four main morphological classes identified in this study are islet, central, radial, and vertical cells, and the central cells can be divided into two groups based on firing pattern. The islet cells have a large dendritic rostrocaudal extent (>400 μm) and an axon that arborises within the dendritic tree (Yasaka et al., 2007). Central cells are elongated in the rostrocaudal axis, but are smaller than the islet cells (<400 μm) and possess an axon that extends beyond the dendritic tree. Radial cells are smaller than central cells and have short dendrites emanating in all directions from the soma. Vertical cells have dendrites that project ventrally. Examples of these morphological classes are illustrated in Figure 1-2, and each of these classes will now be discussed in greater detail.

Vertical cells have a distinct morphological appearance, and correspond to the stalked cells first identified in the cat (Gobel, 1975; Gobel et al., 1980). Although most vertical cells are excitatory (Yasaka et al., 2010), there are several examples of inhibitory vertical cells that either express VGAT or are labelled by eGFP in the GIN mouse, which labels a subset of inhibitory interneurons with GFP (see below) (Heinke et al., 2004; Maxwell et al., 2007). The vertical cells that express VGAT are generally smaller, and possess a less extensive dendritic tree than the excitatory vertical cells (Yasaka et al., 2010). This suggests that there may be distinct populations of vertical cells that are involved in different functions. In paired recording experiments with subsequent morphological identification, some

vertical cells provide excitatory input to lamina I projection neurons, which were identified by retrograde labelling from the rostral thoracic cord (Lu and Perl, 2005). Paired recording experiments have also demonstrated vertical cells can receive excitatory input from transient central cells, and inhibitory input from a population of interneurons that express GFP from the Prion promoter (PrP) (Lu and Perl, 2005; Zheng et al., 2010). Dorsal root stimulation experiments indicate that vertical cells can receive monosynaptic input from Aδ and C-fibres (Yasaka et al., 2007). Recent evidence suggests that vertical cells could also receive Aβ input from LTMRs, indicated by VGluT1-immunoreactive contacts onto dendritic spines of Neurobiotin-labelled vertical cells, with many of these VGluT1-expressing boutons co-expressing Ctb following sciatic nerve injection of Ctb (Yasaka et al., 2014). This Ctb injection method reliably labels myelinated fibres at the site of injection and confirms that many of these VGluT1 inputs originate from myelinated LTMRs (Shehab and Hughes, 2011).

The radial cells are the only morphological type that is consistently reported to be excitatory interneurons (Yasaka et al., 2010). They have dendrites that radiate in all directions when the spinal cord is viewed in the sagittal plane, and these are flattened in the mediolateral axis (Grudt and Perl, 2002). Yasaka *et al* (2007) used quantitative criteria of dendrites to distinguish these cells. The criteria included a ratio of dendritic rostrocaudal to dorsoventral extent (RC:DV) of less than 3.5, and a ratio of dendritic ventral extent to dorsal extent SV/SD of less than 3.5. Dorsal root stimulation experiments showed radial cells receive monosynaptic input from C and Aδ fibres, as well as frequently receiving multiple IPSCs from myelinated and unmyelinated primary afferents (Yasaka et al., 2007). In addition, Yasaka *et al* (2007) demonstrated the majority of IPSCs evoked in radial cells had variable latencies and were typically more sensitive to strychnine than bicuculine, indicating that these inhibitory synapses were glycine dominant. They typically display a high frequency of spontaneous EPSCs (sEPSCs) and sIPSCs, suggesting they receive synapses from many excitatory and inhibitory cells(Grudt and Perl, 2002; Yasaka et al., 2007). The action potential firing pattern of these cells is delayed from the onset of current injection, and the discharge pattern of action potentials is irregular throughout the current injection (Grudt and Perl, 2002).

Islet cells are the largest of the four main morphological classes, with a dendritic rostrocaudal extent of over 400 μm (Yasaka et al., 2007). They are also limited in their dorsoventral extent, and Yasaka *et al* (2007) defined these cells as having a dendritic

RC:DV ratio of less than 3.5. The islet cells were one of the first morphological cell types identified in the cat trigeminal nucleus, and were described as having a dendritic tree and axonal arbor restricted to the substantia gelatinosa (Gobel, 1975). Islet cells are also seen to possess an axon that arborises within the volume of the dendritic tree, whereas the similarly shaped but smaller central cells, had an axon that extended well beyond the dendritic tree (Grudt and Perl, 2002; Yasaka et al., 2007). Dorsal root stimulation experiments show that the eEPSCs of islet cells typically have much greater amplitude than EPSCs evoked in other morphological cell types (Grudt and Perl, 2002). Furthermore, these monosynaptic EPSCs were only evoked from C-fibres, indicating these cells only receive monosynaptic input from unmyelinated afferents (Yasaka et al., 2007).

Central cells, which have been also been termed small islet cells (Todd and McKenzie, 1989), have rostrocaudally oriented dendritic trees and axonal arbors (Grudt and Perl, 2002). As mentioned above, central cells differ from islet cells as they have a dendritic rostrocaudal extent of less than 400 μm, and an axon that extends beyond the dendritic tree and often into adjacent laminae. Grudt and Perl (2002) divided the central cells into two groups, those that discharged action potentials throughout a suprathreshold depolarising current pulse, and those that only discharged action potentials at the onset of the current pulse. These were termed tonic central and transient central cells respectively. Central cells can be excitatory or inhibitory, and Yasaka *et al* (2010) found these were in approximately equal proportions.

Schemes that use morphological classes are somewhat effective, as islet cells are found to be inhibitory, and radial and most vertical cells are excitatory (Grudt and Perl, 2002; Maxwell et al., 2007; Yasaka et al., 2007, 2010). However, around 20% of interneurons do not fit into any of the four classes, and are termed unclassified. Furthermore, there are many cells that display intermediate forms of these main cell types, and there is often difficulty in assigning them to one of the four main morphological classes. Central cells also display variable firing properties in response to injection of suprathreshold square current pulses, and are described as tonic central or transient central cells depending on whether they fire action potentials throughout the current pulse or only at the start (Grudt and Perl, 2002). This indicates that there is considerable heterogeneity within these groups.

Mice expressing fluorescent proteins under the control of various promoters have been generated to label specific populations of cells. This use of transgenic animals has been

utilised to study subsets of inhibitory (glycinergic and GABAergic) and excitatory (glutamatergic) interneurons, in mice in which GFP is expressed from different promoters. For instance, the GlyT2, GAD67 and VGluT2 promoters have been used to label glycinergic, GABAergic and glutamatergic interneurons respectively (Heinke et al., 2004; Punnakkal et al., 2014; Zeilhofer et al., 2005). GFP expression can be used for purely anatomical studies and to target specific cell populations for whole cell recordings. These studies were used to investigate the physiological and morphological properties of these cells. Other populations of cells defined by their expression of neurochemical markers can be labelled by using GFP expression under the control of various promoters. For example, parvalbumin-expressing cells have been targeted for whole cell recordings using a mouse in which GFP is expressed under the control of the parvalbumin promoter (Hughes et al., 2012).

Morphology of a subset of inhibitory cells was investigated by Heinke *et al* to test whether there were shared properties between these cells that differed from the other neurons in lamina II. Whole-cell recordings were taken from mice in which enhanced GFP is expressed under control of the GAD67 promoter, termed the GIN mouse (Oliva et al., 2000), in order to label a subset of GABAergic local interneurons. In the GIN mouse approximately 35% of the GABAergic neurons in the superficial dorsal horn were labelled with GFP (Heinke et al., 2004). In the GIN mouse, the morphological classes of of GFP expressing cells were mostly islet (62%), and the remainder were either vertical (14%) or unclassified.

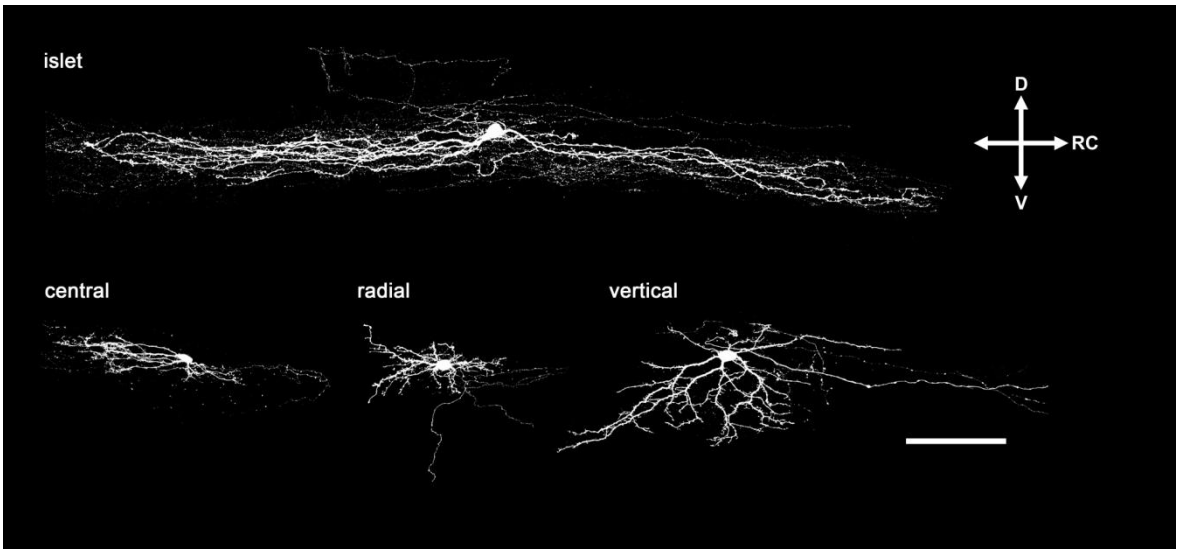
islet
D
RC
V
central
radial
vertical

Figure 1-2 Morphological classes of lamina II interneurons in the dorsal spinal cord. Examples of cells from each of the four main morphological classes of lamina II interneuron described by Grudt and Perl (2002). Islet cells have an extensive rostrocaudal spread and limited dorsoventral extent. Central cells are similar to islet cells in terms of shape, although they are less extensive in the rostrocaudal axis. Radial cells have short-projecting dendrites that radiate in all directions from the cell soma, and vertical cells have a dorsally located soma with dendrites that project ventrally. All of the displayed morphological classes are flattened in the mediolateral axis. Scale bar = 100 μm, D = dorsal, V = ventral, RC = rostrocaudal. Modified from Todd (2010)

1.3.1.2 Action potential firing properties

Other schemes have used action potential firing pattern and membrane properties as criteria for classifying cells. Many different firing patterns have been observed in response to suprathreshold depolarising current steps, and these include tonic, initial bursting, single spike, delayed, gap and reluctant firing (Heinke et al., 2004; Ruscheweyh and Sandkühler, 2002; Yasaka et al., 2010). During tonic firing, action potentials are discharged throughout the suprathreshold current step, and with initial bursting firing, action potentials are only discharged at the onset of current injection. Only one or two action potentials are generated at the onset of current injection for single spike firing neurons, presumably due to inactivation of voltage gated currents shortly after membrane depolarisation. Delayed firing neurons have a characteristic gap between the onset of current injection before the first action potential is discharged, and this gap becomes shorter with increased depolarising current steps. Gap firing neurons have a long interval between the first and second action potential, followed by continuous, regular firing of action potentials. Reluctant or non-firing cells do not discharge action potentials in response to depolarising current injection. Other action potential firing patterns are also observed, such as phasic bursting firing, in which action potentials fire throughout the current injection but with irregular intervals between spikes (Ruscheweyh and Sandkühler, 2002). This same group identified a separate group of burst firing cells, in which the onset of depolarisation induced a burst of action potentials followed by tonic firing with regular inter-spike intervals (Ruscheweyh et al., 2004).

These criteria for classifying neurons based on firing pattern have also been applied to cells in different laminae. In lamina I of the spinal cord, four different cell classes could be distinguished based on these criteria; these were tonic, phasic, delayed onset and single spiking firing patterns (Prescott and De Koninck, 2002). These patterns of action potential firing was found to be correlated with intrinsic membrane properties of the cells, and these groups could be distinguished by cluster analysis using three measurements of active membrane properties from these cells. The authors predicted that these different cell types would be related to their function within the dorsal horn circuitry, with single spiking and phasic cells acting as coincidence detectors based on their ability to follow high frequency stimulus trains, and tonic and delayed onset cells acting as integrators due to their response following the summation of synaptic inputs.

Particular action potential firing patterns are more often associated with inhibitory or excitatory interneurons in lamina II (Yasaka et al., 2010). It is thought that tonic and initial burst firing patterns are associated with inhibitory interneurons. However, these are not definitive criteria, since excitatory neurons can also exhibit these firing patterns, and a recent study of a subset of excitatory interneurons that transiently expressed VGluT3 showed the majority of these cells displayed tonic or initial burst firing (Peirs et al., 2015). It has also been shown that firing pattern can change depending on the voltage across the cell membrane, where cells with tonic firing became gap or delayed firing when they were hyperpolarised to between-65 and-85 mV (Yasaka et al., 2010). This is likely due to an A-type potassium current that is responsible for gap and delayed firing patterns, which become inactivated at more depolarised membrane potentials (Ruscheweyh et al., 2004). This is supported by Yasaka et al (2010) who showed that cells with delayed or gap firing patterns could become tonic firing when held at a membrane potential between -50 and -65 mV.

Patterns of action potential firing are seen to differ between unidentified interneurons and projection neurons in lamina I (Ruscheweyh et al., 2004). This study demonstrated that projection neurons labelled from the LPb predominantly displayed gap firing in response to suprathreshold depolarising current injection, whereas spino-PAG neurons showed gap or bursting firing. A random selection of unidentified neurons in lamina I showed a range of firing patterns, including tonic, delayed and phasic bursting firing patterns, which were rarely seen in the spino-parabrachial and spino-PAG neurons. This study confirmed that there are differences between cell type and action potential firing pattern, which can be related to the function of the cell.

1.3.1.3 Expression of developmental markers

Developmental expression of transcription factors determines the fate and function of interneurons in the dorsal horn. Between embryonic days 11.5 and 13.5 most dorsal horn interneurons express the transcription factor Lbx1, and these cells can be divided into those that express the transcription factors Pax2 or Tlx3 (Gross et al., 2002). Tlx3 acts to antagonise the effects of Lbx1, and as a result neurons develop an excitatory phenotype; in the absence of Tlx3 the cells develop as inhibitory interneurons which are marked by Pax2 and Lbx1 expression (Cheng et al., 2004). In contrast Ptf1a is required for expression of Pax2 and acts to suppress Tlx3, which results in cells with an inhibitory phenotype (Glasgow et al., 2005). Tlx3 expression is largely undetected in the spinal cords of adult

animals at post-natal day 16.5, but the inhibitory cell marker Pax2 is still present in the adult dorsal horn and can be used to identify these cells (Xu et al., 2013). However, excitatory cells can be labelled with a reporter protein through the developmental expression of Tlx3, which can be marked by using a cross between $Tlx3^{Cre}$ mice and a reporter line (Peirs et al., 2015; Xu et al., 2013).

Although Pax2 and Tlx3 can broadly distinguish excitatory from inhibitory neurons, other transcription factors that are expressed during development can also be used to define more restricted cell populations. A study of the deep dorsal horn identified 9 populations based on the combinatorial expression of transcription factors, including 4 excitatory groups and 5 inhibitory groups (Del Barrio et al., 2013). Multiple transcription factors including Lbx1, RORβ, MafB, and c-Maf were found in both excitatory and inhibitory populations. It is likely that a combination of transcription factors would be used as opposed to a single factor, as no single factor was found to define any of the populations in this study. The authors reasoned that since all the transcription factors used in the study were previously shown to regulate cell fate specification in the spinal cord, the resulting scheme would identify functionally relevant classes in the dorsal horn.

A recent genome-wide study of inhibitory neurons in mice lacking the transcription factors Ptf1a and Ascl1, revealed other genes that may be useful markers in defining inhibitory interneurons of the dorsal horn (Wildner et al., 2013). The inhibitory interneurons of the dorsal horn develop in two phases of neurogenesis. The Ptf1a gene is required for the development of all dorsal horn inhibitory interneurons, and Ascl1 is required only for late born (Ascl1 dependent) inhibitory interneurons (Glasgow et al., 2005; Wildner et al., 2006). The gene expression profile was studied in mice lacking these transcription factors, and candidate genes for early and late born inhibitory interneurons were identified. From these genes, spatially restricted populations were identified using the Allen brain atlas and their restricted expression was confirmed by *in situ* hybridisation. The genes Tfap2b, Rorb, Kcnip2 and pDyn were identified as spatially non-overlapping and ideal candidates for markers of distinct inhibitory interneuron populations.

These methods of characterising cells have the advantage of being able to objectively find markers for cells that would otherwise be unknown. They also enable the generation of genetically modified animals to allow the study of these cells, unlike morphologically defined cells, or cells with a particular firing pattern. However, the expression level of

some genes might be incidental and unrelated to the function of the cell, and therefore caution should be taken when identifying new markers for cells.

1.3.1.4 Neurochemical classification of interneurons

Neurochemistry is suggested to provide an alternative and potentially useful method of classifying cells (Todd, 2010). Certain neurochemical markers are found in non-overlapping neuronal populations, and others are found exclusively in excitatory or inhibitory cells. This section will discuss the distribution of different neurochemical markers in populations of dorsal horn interneurons, and will describe recent evidence that suggest neurochemically defined populations include functionally distinct groups of cells.

Inhibitory Interneurons

The expression of peptides, calcium binding proteins and other molecules has proved to be a useful way of classifying inhibitory cells in the superficial dorsal horn. In the rat, neuropeptide Y (NPY) parvalbumin, nNOS, and galanin are expressed in largely non-overlapping populations of inhibitory interneurons, and these account for over half of all inhibitory cells in the superficial dorsal horn (Sardella et al., 2011a). The somatostatin receptor sst_{2A} is also restricted to inhibitory cells, and this receptor is present on approximately half of all inhibitory interneurons of the dorsal horn (Polgár et al., 2013a, 2013b; Todd et al., 1998). In the mouse this restricted expression of sst_{2A} receptor on inhibitory interneurons is the same (Polgár et al., 2013). Interestingly, the nNOS- and galanin-expressing inhibitory interneurons belong to the half of inhibitory interneurons that express the sst_{2A} receptor, and the parvalbumin- and NPY-expressing cells broadly do not. However, a minority of NPY expressing cells do express the sst_{2A} receptor (Polgár et al., 2013b). Although nNOS-immunoreactivity is seen in excitatory as well inhibitory interneurons, sst_{2A}-expression is found on virtually all inhibitory nNOS cells and can be used to distinguish them from excitatory nNOS cells (Polgár et al., 2013b). In the mouse this pattern of expression for NPY, parvalbumin, nNOS and galanin is broadly the same. However, there are some subtle differences, such as a larger proportion of cells that express both nNOS and galanin (Iwagaki et al., 2013). As hyperpolarisation of inhibitory cells by somatostatin through the sst_{2A} receptor is an inhibitory effect on inhibitory neurons, its effect is likely pro-nociceptive or pro-pruritic due to inhibition of inhibitory circuits (Yasaka et al., 2010).

There appear to be functional differences between these neurochemical groups, since parvalbumin cells are rarely seen to phosphorylate ERK in response to a variety of noxious stimuli (Polgár et al., 2013b). The phosphorylation of ERK is a marker of neuronal activity, and this finding suggests the parvalbumin cells are not responsive to noxious stimuli. Conversely the galanin- and NPY- expressing cells often phosphorylated ERK in response to chemical, thermal and mechanical noxious stimuli. Inhibitory nNOS cells rarely phosphorylated ERK in response to pinch, heat, capsaicin or formalin, but some cells did respond to heat and formalin stimulation by expressing c-fos (another marker of neuronal activity). However, inhibitory nNOS cells did not respond to capsaicin injection, which is surprising since the heat sensitive channel TRPV1 is also activated by capsaicin, and so it would be expected that the same cells would respond to both heat and capsaicin (Caterina et al., 1997). Polgár *et al* (2013b) suggested that their upregulation of c-fos could be through an alternative pERK-independent pathway. It is also possible that the inhibitory nNOS cells are activated by heat stimuli through nociceptors that lack TRPV1, such as C polymodal afferents that are heat activated even in mice that do not express the TRPV1 receptor (Woodbury et al., 2004).

The synaptic targets of inhibitory interneurons also appear to be related to their neurochemical properties. For example, NPY-expressing cells in the dorsal horn provide numerous axonal boutons to the dense bundles of NPY-containing boutons surrounding NK1r expressing lamina III projection neurons (Polgár et al., 1999a). Another study showed that PKCγ-expressing interneurons in lamina II and giant lamina I cells are also included among their post-synaptic targets (Polgár et al., 2011). However, the NPY-expressing boutons that are in contact with giant cells are at a lower percentage than the general population of inhibitory boutons in lamina I. Therefore the giant cells do not appear to be targeted selectively by NPY-expressing cells. This same study also demonstrated differences between the populations of NPY-expressing boutons that innervated the NK1r-expressing lamina III projection neurons and PKCγ-expressing lamina II cells in terms of their size and NPY immunoreactivity. The boutons that contacted the NK1r-expressing lamina III projection neurons were larger and had stronger NPY-immunoreactivity than the axonal boutons that innervated the PKCγ expressing interneurons; these are therefore predicted to belong to separate populations of NPY-expressing cells. The post-synaptic targets of parvalbumin-immunoreactive inhibitory cells of lamina IIi and III include central axon terminals of low-threshold mechanosensory fibres (Hughes et al., 2012). The parvalbumin-expressing cells also receive axodendritic contacts

from the same population of sensory fibres. Due to their input from mechanosensory fibres and outputs onto mechanosensory fibres, it was suggested that the parvalbumin-expressing cells play a role in processing tactile information, and a disruption in these cells could result in tactile allodynia.

Inhibitory interneurons that express nNOS are also selective in their post-synaptic targets, and as mentioned previously, these include the giant cells in lamina I (see section 1.2 above)(Puskár et al., 2001). These inhibitory nNOS boutons were confirmed as synaptic, if they apposed post-synaptic gephyrin puncta. Inhibitory nNOS-expressing boutons provide synaptic input to NK1r-expressing neurons in lamina I, which are likely to be projection neurons (Al-Ghamdi et al., 2009). However, nNOS-containing boutons were only present at 3% of gephyrin puncta on NK1r-expressing cells. Since 13% of inhibitory boutons in lamina I are nNOS containing (Sardella et al., 2011a), nNOS-containing inhibitory boutons are likely underrepresented among the inhibitory inputs to NK1r-expressing cells.

The expression of the opioid dynorphin appears to be selective among these neurochemical populations. Dynorphin is expressed in both inhibitory and excitatory neurons in laminae I – II, but it is found to be present in around 95% of galanin-expressing cells, which are inhibitory (Sardella et al., 2011b). By measuring gene expression levels in Ptf1a mutant mice, in which inhibitory dorsal horn interneurons do not develop, there was almost no dynorphin mRNA present in the dorsal horn at embryonic day 18 (Bröhl et al., 2008). This suggests that most dynorphin is restricted to inhibitory cells in the dorsal horn. Although dynorphin is found in some excitatory neurons and boutons in the superficial dorsal horn, the expression of dynorphin is a distinguishing feature of galanin-expressing inhibitory interneurons. A recent study has suggested that dynorphin-expressing interneurons are involved in gating mechanical pain (Duan et al., 2014). Mice in which dynorphin expressing cells were ablated showed normal responses to heat or cold stimuli, but showed mechanical allodynia. However, the cells ablated in this study will have included cells that express dynorphin transiently during development, as well as those that are excitatory

interneurons. Nevertheless, this group of dynorphin expressing cells is likely to include one or more groups involved in suppressing mechanical allodynia under normal conditions.

Certain interneuron populations in the superficial dorsal horn have been associated with the suppression of itch by scratching (Ross et al., 2010). Mice in which the transcription factor bhlhb5 is knocked out are found to lack a population of dorsal horn neurons, and these are mostly inhibitory interneurons. This mouse model develops pathological chronic itch and this was shown to be due to a loss of the inhibitory interneurons that required the expression of the transcription factor bhlhb5 for survival (Kardon et al., 2014; Ross et al., 2010). This population of inhibitory interneurons, referred to as the B5-I neurons, account for two thirds of the cells in this region that express the sst_{2A} receptor. This study also demonstrated that galanin- and nNOS- expressing inhibitory interneurons are among the inhibitory populations missing in the bhlhb5 knockout mice, which are required for the normal suppression of itch (Kardon et al., 2014). This study showed that κ-opioid receptor agonists can suppress itch response to injection of several pruritogens and the dry skin model, and the endogenous κ-opioid receptor agonist dynorphin is expressed by the B5-I neurons that are galanin-immunoreactive. Although spinal κ-opioid receptor agonists affects the response to itch, there is likely a GABA/glycine mediated component involved as well, since wild type and $PPD^{-/-}$ mice showed similar itch responses to intradermal pruritogen injection.

Transgenic mice have been generated in an attempt to label specific populations of interneurons, which may show functional homogeneity and consistent features. These mice were generated from a construct of the Prion promoter and GFP, which was allowed to randomly integrate into the mouse genome (van den Pol et al., 2002). In one mouse line the combination of the promoter and integration site led to the selective expression in a small subset of GFP in lamina II interneurons, called the PrP-GFP cells. These cells were subsequently reported to be a homogeneous population of inhibitory interneurons with central cell morphology (Hantman et al., 2004). They were also reported to receive monosynaptic C fibre input exclusively, and fire tonically in response to suprathreshold current injection. This suggests that the PrP-GFP cells represent a functionally homogeneous population of cells. More recently, it has been shown that these cells belong to neurochemically defined populations, with PrP-GFP cells either expressing galanin and/or nNOS (Iwagaki et al., 2013). Results from this study also showed that PrP-GFP cells invariably express the sst_{2A} receptor, and that all PrP-GFP cells respond to

somatostatin by hyperpolarisation, and this is mediated through activation of GIRK channels.

Excitatory Interneurons

The neurochemical content of excitatory interneurons has also been studied. These cells express the vesicular glutamate transporter VGluT2 in their axonal boutons at higher levels than in primary afferents, which allows the axonal boutons of these neurons to be distinguished from each other (Todd et al., 2003a). Several neuropeptides, such as neurotensin, neurokinin B, gastrin releasing peptide (GRP) and somatostatin have been identified in excitatory interneurons in the dorsal horn, and may be used to identify distinct populations of excitatory interneurons (Gutierrez-Mecinas et al., 2014; Polgár et al., 2006; Proudlock et al., 1993). This section will discuss what is known about excitatory interneurons that express certain neurochemical markers, and behavioural phenotypes that have been associated with excitatory interneurons.

The precursor to neurokinin B, preprotachykinin B, was detected exclusively in VGluT2 expressing axonal boutons in the dorsal horn, and therefore is restricted to excitatory interneurons (Polgár et al., 2006). Neurons immunoreactive for preprotachykinin are located at the lamina II/III border, with fewer preprotachykinin-immunoreactive cell bodies located in laminae I and IIo. This report also showed that preprotachykinin B is co-localised in neurons with other neurochemicals, such as PKCγ, somatostatin, and calbindin. Although dynorphin is found in inhibitory cells that express galanin, there is also a population of excitatory cells that are immunoreactive for preprodynorphin, the precursor of dynorphin (Marvizón et al., 2009, Sardella et al., 2011). Dynorphin is also expressed in projection neurons and some peptidergic C-fibres (Marvizón et al., 2009; Standaert et al., 1986).

GRP and its receptor GRPR have been associated with the perception of itch (Sun and Chen, 2007; Sun et al., 2009), and some excitatory interneurons are found to express GRP (Gutierrez-Mecinas et al., 2014). The GRP expressing interneurons are predicted to be located in laminae I-II of the dorsal horn, based on the location of eGFP in the GRP-EGFP mouse. However, GRP is also reported to be contained in some unmyelinated afferent fibres (Liu et al., 2012b; Sun and Chen, 2007), and there is controversy as to whether this expression of GRP in primary afferent fibres is genuine. Recent studies in the mouse have found that there is no GRP expression in DRG neurons, and suggest that the previous

reports may have used antibodies that cross react with other antigens, such as substance P and neuromedin B (Nmb) (Fleming et al., 2012; Gutierrez-Mecinas et al., 2014; Solorzano et al., 2015). Among the boutons derived from excitatory interneurons, somatostatin in co-expressed in approximately 70% of GRP-expressing boutons (Gutierrez-Mecinas et al., 2014). In contrast, it is highly likely that GRP is not present in PKCγ-expressing interneurons, since GRP-EGFP neurons were rarely co-localised with PKCγ.

The receptor for GRP (GRPR) is also involved in normal itch sensation, with mice deficient for the GRPR showing reduced itch behaviours but unaltered pain behaviour (Sun and Chen, 2007). In a follow up study, ablation of GRPR-expressing cells with intrathecal bombesin-saporin reduced behavioural responses to intradermal pruritogen injections without affecting normal pain behaviour (Sun et al., 2009). Furthermore, ablation of GRPR-expressing cells was not seen to reduce the number of dynorphin, PKCγ, neurotensin, or NK1r expressing cells in lamina I, suggesting that these markers are not co-expressed.

Somatostatin-expressing neurons are located in laminae I-II, and are rarely observed in lamina III (Proudlock et al., 1993). These somatostatin-expressing cells located in superficial laminae are never seen to express GABA or glycine, although some somatostatin-expressing cells in deeper laminae are inhibitory. Somatostatin is likely to be expressed by many different types of excitatory interneurons, since it is co-expressed with many other neurochemical markers found in neurons, such as GRP, PKCγ and Met-enkephalin (Gutierrez-Mecinas et al., 2014; Polgár et al., 1999b; Todd and Spike, 1992). A recent study by Duan *et al* (2014) suggests that the somatostatin expressing interneurons are required for the transmission of mechanical pain, but were not involved in innocuous touch sensation. This study used a complex intersectional strategy using several transgenes to specifically label and ablate the somatostatin-expressing interneurons in the dorsal horn. The somatostatin expressing cells are likely a heterogeneous population that does not have a single role in processing sensory information, as demonstrated by the multiple types of afferent input to these cells in the dorsal root stimulation recordings in this report. However, it is likely that this group does include one of more populations of cells that are required for mechanical nociception.

In a study of excitatory dorsal horn neurons that transiently express VGluT3, it was shown that these cells are required for mechanical hypersensitivity, and this is supposedly one of

the first components in a polysynaptic pathway linking LTMRs to nociceptive NK1r projection neurons in lamina I (Peirs et al., 2015). Using several transgenic lines to specifically remove VGluT3 from neurons in the dorsal horn it was shown that mechanical pain failed to develop in response to the spared nerve injury model, 3% carageenan injection and the Randall Selitto test. This study suggested that VGluT3-expressing excitatory interneurons were part of a circuit responsible for mechanical allodynia. The results from this study also associated calretinin-expressing excitatory interneurons with allodynia in response to inflammation, and PKCγ-expressing excitatory interneurons with allodynia in response to neuropathic pain. In support of this suggestion, another report investigating mechanical allodynia in the medullary dorsal horn of rats also showed PKCγ-expressing interneurons were involved in allodynia (Miraucourt et al., 2007). In this report intracisternal strychnine induced dynamic allodynia, and PKCγ-expressing cells were included among those that expressed c-fos in response to light brushing following intracisternal strychnine. It was also shown that inhibition of PKCγ reduced the allodynia score and the number of c-fos reactive cells in response to intracisternal strychnine and light brushing. The authors concluded that PKCγ-expressing neurons were part of a circuit that was normally inhibited by glycine, and blockade of this glycinergic inhibition resulted in allodynia. Conversely, the authors concluded that inhibition of the PKCγ-expressing interneurons reduced allodynia.

1.4 Using cluster analysis to classify interneurons

Classifying cells in the central nervous system has largely relied on morphological criteria from as early as the first anatomical studies of Golgi-stained tissue by Ramon y Cajal (1909).The huge variability in the shape and size between neurons, together with consistent features of certain cells suggested that morphological differences were important in defining neurons with distinct functional roles in the central nervous system. Historically this was one of the only possible methods to characterise neurons. There are now many ways that groups of cells can be classified, although it is not yet certain how important these methods of classification are in defining functionally related groups of cells. Therefore an approach that includes all of these features should be used to: a) assess how important each of these features are in defining cells that have the same functional role and b) determine whether some of these features are related to each other.

In principle, cluster analysis is a way of classifying objects (neurons in the context of this project) into particular groups, such that the objects within a group are more closely related to each other than to those in different groups. What is defined as a group or class is dependent on the operator, and how much tolerance is placed on the classification process. In other words, how many differences can be tolerated between objects within the same group? With no tolerance each cell would belong in its own group, and with complete tolerance all cells would be within a single group. The cluster analysis can only categorise objects based on variables measured by the operator, so the selection of variable is important in determining which objects are seen as related. Without prior knowledge of what will be important in classifying objects it seems that the most objective way would be to measure as many variables as possible and cluster objects based on these measures. However, a large number of variables will introduce noise into the dataset, and the presence of outliers in some variables will influence the clustering process. There may also be redundancy in some of the measures if they are strongly correlated, for example different measures of size such as surface area and volume will be correlated. However, there are methods to reduce the dimensionality and redundancy of the data whilst maintaining the variance in the dataset. This is important as it greatly simplifies a large and often complicated datasets, as well as providing a more accurate way of representing the dataset than the original parameters.

1.4.1 Principal component analysis (PCA)

Principal component analysis (PCA) is a method of reducing the dimensionality of a dataset while maintaining as much of the variability as possible. This is useful when there are a large number of variables and if there are some variables that are correlated with each other. PCA removes this redundancy, as the principle for the analysis is to maintain as much of the variance in the dataset as possible. It also makes the dataset easier to visualise, as two or three dimensional data can be represented graphically.

The theory behind PCA relies on the dataset being represented as a matrix, with rows representing objects and columns representing variables. This matrix can be used to identify eigenvectors, also known as principal components. Eigenvectors are the vectors through the dataset where the variation is greatest, and each is associated with an eigenvalue. The larger the eigenvalue is the more variance is retained from the original dataset. The number of possible eigenvectors from a matrix is equal to its dimensionality,

i.e. how many variables it has. This means in a dataset with 50 variables, there would be 50 possible eigenvectors.

Initially, as many principal components as variables will be extracted from the dataset, and since the purpose of PCA is to reduce the dimensionality of the dataset, the number of principal components to keep must first be determined. Therefore the number of principal components to be retained needs to be decided by the operator. There are many ways to decide how many principal components to extract. For example when the eigenvalue associated with the eigenvector is greater than 1, the eigenvector represents more of the variability than the original variables, which all have an initial eigenvalue of 1 when the data is standardised. Therefore one strategy would be to retain all components with an eigenvalue greater than 1. An alternative strategy is to retain as many components as necessary to account for a certain percentage of the total variability in the dataset. For example, if only 70% of the variability in the dataset was required, then only the number of principal components that account for 70% of the total variability in the dataset would be retained. Another strategy is to use a scree plot of the eigenvectors to decide how many principal components to retain. A scree plot is a graph of the eigenvalues associated with each eigenvector, plotted in descending order of size. Using the point at which the scree plot levels off can also be used to determine the number of eigenvectors to retain and can be used when many of the eigenvectors have eigenvalues greater than 1 (Cattell, 1966).

Other methods of dimension-reduction exist, such as linear discriminant analysis (LDA). This is similar to PCA, except that instead of simply trying to maximise the variance retained from the original dataset, LDA will also try to maximise the difference between groups. This is achieved by maximising the variance between groups and minimising the variance within groups when reducing the dimensionality of a dataset. Therefore the vectors generated by LDA will allow the separation of different groups to be maximised. Although this appears to be a superior method of dimension-reduction it can only be achieved when different groups are already known to the operator, and it is therefore not entirely objective. This is known as a supervised method of classification, as it relies on group allocation that is provided by the operator, and not just the raw data provided in the dataset. However, it has been used in a number of studies in the dorsal horn to confirm that groups of supposedly distinct neurons can be distinguished, which support the original allocation made by the authors .

1.4.2 Clustering methods and measures of distance between objects

The difference between objects is measured as Euclidian distance, which is the theoretical distance between objects in a multidimensional space and is calculated by the Pythagorean theory $a^2 + b^2 + c^2 + ... = n^2$ where n is the dimensionality of the dataset. Other measures of distance between objects exist, such as Cosine, and Pearson's correlation, although the most widely used and easily understood measure is Euclidian distance or squared Euclidian distance. There are different types of cluster analysis and linkage rules, which are the methods by which objects are grouped together. As this is such a vast subject, I will only focus on the most commonly used methods, and the methods that will be used in this study.

The choice of clustering algorithm can influence the outcome of the analysis. The two main types of cluster analysis are K-means and hierarchical cluster analysis. The former categorises the objects into a pre-determined number of clusters chosen by the operator, and reassigns the objects iteratively until none of the objects move between the groups. The latter treats all objects as their own cluster, and progressively joins the two closest objects until all objects are clustered together. K-means clustering is useful if the number of clusters to expect from the data is known, although in many instances this is not the case. Hierarchical clustering is useful if the relationship between the objects and the number of groups is not known. Both of these methods will always produce clusters regardless of the objects given to be analysed, and so the clusters formed may not be informative. An advantage of K-means clustering over hierarchical clustering is reassignment can happen at the later stages of the clustering, whereas objects stay linked from the initial stages of the clustering in hierarchical cluster analysis. This can provide better global optimisation for the clustering procedure. This is also an example of supervised classification, since the data labels (groups) are already provided by the operator.

The unweighted pair group method using arithmetic averages (UPGMA) is the simplest and easiest to understand clustering algorithm. Briefly, at the first stage of clustering the two closest objects are combined into a group, the centre of this group is the average of these two values. This central value is the new value given to this group, and if subsequent objects are included, the average is recalculated. The distance between two clusters is the difference between the averaged values for all objects in each cluster. This is repeated until

all objects are clustered together, and this data is used to construct a dendrogram giving the distance at which objects and clusters joined together.

The most widely used clustering algorithm in the field of biology is Ward's method, in which the clustering is done to minimise the square of the distance between all objects within a group at each stage of the clustering procedure (Ward, 1963). This value is called the variance or the sum of squares, and at each stage many calculations are made to determine how this value will change with the addition of another object to that group, or the merging of two groups. The value that will result in the smallest increase in variance is the next step that is chosen. Again this procedure is repeated iteratively until all objects are clustered together, and the distances at which these objects combine are plotted as a dendrogram. A summary of cluster analysis methods and linkage rules can be found in Romesburg (2004).

1.4.3 Cluster analysis and PCA as tools for defining neuronal populations

Cluster analysis has been used successfully to categorise cells in several different regions of the central nervous system, and many of these have used morphological parameters as their measure of similarity between cells. In the superficial dorsal horn there is a large diversity of morphological shapes, and it has been difficult to classify cells of this region in terms of their morphology. Studies that have used cluster analysis to categorise cells in this region have used measures of active membrane properties, and measures of somatodendritic morphology to cluster cells into different categories (Prescott and De Koninck, 2002; Yasaka et al., 2007). However, in some examples a small number of variables were used, making the clustering process dependent on few features of the cell and largely dependent on the choice of variables by the operator. These groupings do show that it is possible to distinguish pre-determined groups of cells based on chosen parameters, or that it is possible to use this method to identify criteria that are useful in determining these classes.

Morphological analyses by Yasaka *et al* (2007) were able to distinguish between the four main morphological classes of dorsal horn interneuron by using four different measures of somatodendritic morphology. These measures included dendritic rostrocaudal extent (RC), distance from soma to most dorsal point of the dendritic tree (SD), the distance from the centre of the soma to the most ventral point of the dendritic tree minus SD (SV-SD), and

the rostrocaudal to dorsoventral ratio of dendritic extent (RC:DV). Virtually all cells that were assigned these classes by visual inspection could be distinguished based on these four measures with K-means cluster analysis, LDA, and hierarchical cluster analysis. Although this was an impressive use of these analytical techniques, and the only attempt so far to quantify these morphological classes, this was not a truly objective method as it only confirmed that these different cell shapes could be distinguished on a select number of measures of the dendritic tree. However, this did generate useful criteria to distinguish these morphological types in a way that is not purely subjective. For example, islet cells were defined as having a rostrocaudal extent of over 400 μm, or between 300-400 μm with an axon that arborises within the volume of the dendritic tree (Yasaka et al., 2007).

Cluster analysis has also been used to classify interneurons in other regions of the central nervous system, such as the neocortex (McGarry et al., 2010). It was possible to objectively distinguish 3 different types of somatostatin expressing interneurons in the neocortex using cluster analysis, and these same groups were found using morphological and physiological parameters separately (McGarry et al., 2010). This involved the targeted recording of GFP positive cells in GIN mice, which also label a subset of somatostatin-expressing cells in the cortex with GFP, with microelectrodes containing Neurobiotin to fill their somata, dendrites and axon (Oliva et al., 2000). In this study hierarchical, K-means cluster analysis and PCA were all used and distinguished the same 3 groups, which highlighted the reliability of the groups produced.

Gene expression levels can also be used as a basis for cell classification, determined using RNA sequencing data. Recently, Usoskin *et al* (2015) used iterative PCA to identify 11 different types of primary afferent fibres. These belonged to four main groups that matched those previously identified by molecular markers and physiological characterisation of conduction velocity (Cameron et al., 1986; Cavanaugh et al., 2009; Koerber and Mendell, 1988; Li et al., 2011; Snider and McMahon, 1998; Zotterman, 1939). These groups included myelinated fibres, peptidergic and non-peptidergic unmyelinated nociceptors and C-LTMRs. By identifying population-specific genes that had an abundant and selective expression, the authors were able to find selective markers for each of the groups they identified. This is important work as it provides a means of genetically manipulating these populations, such as using targeted ablation or activation by optogenetic techniques to better understand their connectivity and function *in vivo*.

The advantage of PCA and cluster analysis is that the chosen parameters can include any property of the cell that is measurable, and can include multiple parameters. This means the number of possible ways to categorise cells is limitless, provided there is a way of measuring the feature of interest.

1.5 Aims of the project

Although several attempts have been made in the past to classify interneurons in the dorsal horn, there is currently no universally accepted classification scheme that includes all neurons. This is one of the main limitations in understanding the neuronal circuitry of the dorsal horn, and many of the currently used schemes do not provide information on the functions of the different classes. The overall aim of this project was to test the validity of using morphological parameters to classify interneurons in the dorsal horn. To do this, two non-overlapping and neurochemically distinct populations of inhibitory interneurons were characterised, the PrP-GFP and the NPY-GFP cells. These mouse lines label interneurons with GFP under the control of the Prion promoter and the NPY promoter respectively. Other specific questions related to each of these cell populations are as follows.

1. The PrP-GFP inhibitory interneurons of lamina II are a well characterised cell population that are believed to be a homogeneous populations in terms of their morphological parameters, primary afferent input and role in the dorsal horn microcircuitry (Hantman et al., 2004; Zheng et al., 2010). Previous work suggests that they belong to a population of cells that express nNOS and/or galanin and the sst_{2A} receptor (Iwagaki et al., 2013). Earlier work on nNOS-expressing dorsal horn interneurons suggests that they are in fact morphologically heterogeneous (Valtschanoff et al., 1992a). Since the PrP-GFP cells include nNOS-expressing cells these observations are at odds with one another, unless only one morphological type of nNOS-expressing cell is labelled in the PrP-GFP mouse. To resolve this, one aim of the project was to perform detailed morphological analysis on these PrP-GFP cells to see whether they constitute a morphologically homogeneous group of cells.

2. Inhibitory interneurons that express nNOS are found to receive primary afferent input from synapses in type II glomeruli, which are mostly formed by low-threshold mechanosensory fibres (Bernardi et al., 1995; Ribeiro-da-Silva and

Coimbra, 1982). The PrP-GFP cells, which include this inhibitory nNOS population, are only reported to receive afferent input from unmyelinated C-fibres. Therefore an aim of this project was to determine whether there is evidence of input from low-threshold primary afferents to the PrP-GFP cells. Another aim was to determine whether certain subtypes of C-fibres provide the input to the PrP-GFP cells.

3. The NPY-expressing interneurons of the spinal dorsal horn are seen to contact several populations of neuron in the dorsal horn, including lamina III ALT neurons, and PKCγ-expressing interneurons (Polgár et al., 2011). However, the synaptic inputs, physiological properties and morphological appearance of these cells are unknown. In order to study these cells we used whole-cell recordings with Neurobiotin-filled pipettes to study the membrane properties of cells labelled with GFP from the NPY promoter (NPY-GFP cells), and subsequently investigate their morphological properties. Sections that contained filled dendrites from these cells were then immunoreacted to test whether they received contacts from primary afferent fibres, such as LTMRs that expressed VGluT1.

4. Bundles of NPY-expressing axons densely innervate projection neurons of the ALT in lamina III. These projection neurons can be identified in the mouse by the dense input they receive from axonal boutons containing GGRP and NPY onto their somata and proximal dendrites (Cameron et al., 2015). Little is known about the source of this NPY, although it is assumed to arise from a population of local inhibitory interneurons that have larger axonal boutons and express higher levels of NPY than other NPY-expressing cells (Polgár et al., 2011). This raises some questions; is the source of NPY bundles from few or many cells, how often do the axons of NPY-expressing cells contribute to these bundles, and are there any other distinguishing features of these cells. To investigate this, sections of labelled NPY-GFP cells that contain axon were immunostained for NPY and CGRP.

5. Morphological criteria have been frequently used to distinguish populations of cells in the dorsal horn, although the relevance of interneuron morphology to function is unresolved. Therefore we used PrP-GFP and NPY-GFP cells which represent two

genetically distinct non-overlapping populations of inhibitory interneurons to determine whether morphology could distinguish these two populations.

2 Materials and methods

2.1 **Animals used**

NPY-GFP mice:

The animals used in this study are from the same mouse line generated by van den Pol *et al* (2009). This group generated mice to produce GFP in NPY-expressing cells using a BAC vector containing the gene for humanised Renilla GFP (hrGFP) under the control of the NPY promoter (van den Pol et al., 2009). This GFP is derived from the fluorescent protein of the sea pansy *Renilla reniformis*, and is codon corrected to enable expression in mammalian cells (Kirsch et al., 2003). The animals used for whole-cell recording experiments were all heterozygous for the GFP expressing allele, and GFP-expressing mice were crossed with C57Bl/6 wild type animals. GFP expression in the offspring was confirmed by visualising GFP fluorescence in the P3-P4 animals, since this could be seen through the skin of mice at this age.

PrP-GFP mice:

Transgenic mice were generated by random site integration of a transgene, in which GFP was expressed under the control of the prion promoter (van den Pol et al., 2002). A line of these mice was found to express GFP in a subset of lamina II inhibitory interneurons, which have been characterised in several previous reports (Hantman and Perl, 2005; Hantman et al., 2004; Iwagaki et al., 2013; Zheng et al., 2010). These mice were crossed with Swiss Webster mice, and homozygous animals were used for all experiments.

All experiments were approved by the Ethical Review Process Applications Panel of the University of Glasgow and were performed in accordance with the UK Animals Scientific Procedures Act 1986.

2.2 **Slice preparation and electrophysiology**

The spinal lumbar enlargement of young adult animals (4-6 weeks old) was removed under isofluorane anaesthesia (1-3%) into ice cold dissection solution (in mM: NaCl 0, KCl 1.8, KH_2PO_4 1.2, $CaCl_2$ 0.5, $MgCl_2$ 7, $NaHCO_3$ 26, glucose 15, sucrose 254, oxygenated with 95% O_2, 5% CO_2). Mice were killed by decapitation following removal of the spinal cord. The lumbar spinal cord was prepared for cutting by carefully removing the meningeal layers and dorsal and ventral roots in a Petri dish containing oxygenated ice-cold dissection solution. Parasagittal slices (300-600 µm) were taken from the lumbar enlargement with a

vibrating blade microtome (Microm HM 650V, Fisher Scientific, Loughborough, UK). Alternatively, for the preservation of longer dorsal roots another method of dissection was used. Mice were anaesthetised and killed by decapitation, and the vertebral column was quickly removed. The spinal cord was dissected from the ventral side of the vertebral column in oxygenated ice-cold dissecting solution. The ventral roots, most dorsal roots and the meningeal layers were carefully removed, while preserving the L4 and L5 dorsal roots. The cord was then embedded in 3% low melting point agar in order to take parasagittal slices (300-600µm) with dorsal roots attached. All slices were equilibrated for 1 hour in recording solution (in mM: NaCl 125.8, KCl 3.0, NaH_2PO_4 1.2, $CaCl_2$ 2.4, $MgCl_2$ 1.3, $NaHCO_3$ 26.0, glucose 15.0, oxygenated with 95% O_2, 5% CO_2) at room temperature prior to recording. Slices were then transferred to the recording chamber where they were continuously perfused with oxygenated recording solution at room temperature (flow rate approximately 2 ml/min).

Cells were targeted for whole-cell patch-clamp recording using glass microelectrodes with a tip resistance 4-6 MΩ. Microelectrodes were pulled from thin, or thick wall glass capillaries using a horizontal puller (Sutter instrument, Novato, CA, USA). These microelectrodes were filled with internal solution (in mM potassium gluconate 120, KCl 20, $MgCl_2$ 2, Na_2ATP 2, NaGTP 0.5, Hepes 20, EGTA 0.5) and 0.2% Neurobiotin was included to label the recorded cells. In some dorsal root stimulation experiments a caesium-based internal solution was used that also contained Neurobiotin (in mM: Cs-methylsulfonate 120, Na-methylsulfonate 10, EGTA 10, $CaCl_2$ 1, HEPES 10, QX-314-Cl 5, Mg_2-ATP 2, and 0.2% Neurobiotin). The inclusion of caesium and QX-314-Cl inhibited the voltage-activated sodium and potassium currents of the recorded cells respectively and hence prevented action potential firing of these cells during dorsal root stimulation experiments. Patch-clamp signals were amplified and filtered with a Multiclamp 700B amplifier (4 kHz low-pass Bessel filter) and sampled at 10 kHz using a digidata 1440A (Molecular Devices). In voltage clamp, brief 100 ms sub-threshold voltage steps were used to determine the resting membrane potential (-70 to -50 mV in 2.5mV increments). Using a line of best fit from a voltage (x axis) against current (y axis) graph, the gradient of this line could be calculated. This value indicated the conductance of the cell (G = I/V). The reciprocal of the conductance is resistance (i.e. R = 1/G), and so the reciprocal of the gradient for the I/V line gives a value for input resistance. The point at which the line crosses the voltage axis at 0 pA is the resting membrane potential as this is the point at which no current is being injected into the cell. Cells were excluded from further analysis

of physiological properties if they had a resting membrane potential greater than -30 mV. In current-clamp mode the firing pattern was assessed in response to injection of suprathreshold depolarising current steps (1 s each). Cells were held at around -60mV with continuous bias current injection before the step protocol was started. For the majority of the voltage-clamp recordings, cells were held at -60 mV. Analysis of passive and active membrane properties was performed offline using pClamp 10 software.

2.2.1 Dorsal root stimulation experiments

In experiments to determine primary afferent input to cells, the dorsal root was drawn into a suction electrode prior to whole-cell recordings. Once the whole-cell configuration was achieved, cells were voltage clamped at -70 mV and the dorsal root was stimulated at increasing intensities using an ISO-Flex stimulus isolator (A.M.P.I. Intracel) in order to determine the types of afferent fibre generating the eEPSCs. The stimulation intensities were 25 μA for Aβ fibres, 100 μA for Aδ fibres and 0.5-1 mA for C-fibres (Dickie and Torsney, 2014; Torsney, 2011; Torsney and MacDermott, 2006). If there was no monosynaptic response at all following stimulation of the dorsal root at 1 mA, the stimulation intensity was increased to 3 and 5 mA to confirm the lack of monosynaptic input to the cell, and to detect polysynaptic responses. The dorsal roots were stimulated 3 times at a low frequency of 0.05 Hz to identify types of afferent input by conduction velocity, and 20 times at a higher frequency to determine whether the response was monosynaptic or polysynaptic. These higher frequency stimuli were delivered at 20 Hz for Aβ fibres, 2 Hz for Aδ fibres and 1 Hz for C-fibres (Dickie and Torsney, 2014; Torsney, 2011; Torsney and MacDermott, 2006). The absence of synaptic failures and a latency variability of less than 2 ms were used as criteria for monosynaptic response for A fibres. For C fibre responses, the lack of synaptic failures alone was used to confirm the response as monosynaptic, since the C-fibres have a slower conduction velocity and hence a greater variability in latency from stimulation to response. Also, there is evidence of C fibre slowing in response to repeated stimulation, and therefore changes in latency may reflect this C fibre slowing

2.2.2 mEPSC analysis in response to TRP channel agonists

To determine whether the afferents that provided monosynaptic input to recorded cells expressed TRPV1 or TRPM8 channels, miniature excitatory post-synaptic currents (mEPSCs) were recorded in the presence and absence of various TRP channel agonists.

Cells were recorded in the presence of tetradotoxin (TTX, 0.5 µM), bicuculine (10 µM) and strychnine (5 µM) to prevent action potential firing and inhibitory input to these cells. After a 5 minute control recording period, drugs were applied via 3-way stopcocks without a change in the perfusion rate, and a 5 minute recording was taken in the presence of drugs, following a 5 minute period to allow the drugs to wash in. The drugs applied were 2 µM capsaicin (TRPV1 agonist) 10 µM icilin (TRPM8 and TRPA1 agonist), and 10 µM icilin together with 5 µM A967079 (selective TRPA1 antagonist). The mEPSC frequency was analysed offline using Mini-analysis software (Synaptosoft), and significant responses to drug application were determined by the Kolmogorov-Smirnov test ($p < 0.05$). Drugs were supplied by Tocris Bioscience (TTX, icilin, and A967079) or by Sigma Aldrich (1(S),9(R)-(-)-Bicuculline methiodide, strychnine hydrochloride and capsaicin). For experiments in which there was application of icilin, the temperature of the recording chamber was raised to 32°C, because many TRPM8 channels would be active at room temperature, and hence a TRPM8 response may be masked due to constitutive TRPM8 activation (McKemy et al., 2002).

2.2.3 Capsaicin sensitivity of monosynaptic C-fibre input to NPY-GFP cells

The sensitivity of monosynaptic C fibre input to NPY-GFP cells was tested during some dorsal root stimulation experiments. This sample included 6 monosynaptic C fibre eEPSCs from 4 NPY-GFP cells, since 2 of the tested cells received 2 separate C fibre components that could be distinguished, due to their different latencies from stimulus to response. EPSCs were evoked at 0.05Hz by 1 mA stimulation of the dorsal root for 10 minutes in recording solution, and for 10 minutes in the presence of capsaicin (2 µM). To determine the sensitivity of C fibre inputs to capsaicin, the peak amplitude of the EPSCs evoked during the final 3 minutes of the control recording and the final 3 minutes of the capsaicin application were compared using the Wilcoxon matched-pairs signed rank test.

2.3 Tissue processing and imaging

After completion of cell recordings slices were fixed overnight in 4% formaldehyde dissolved in 0.1 M phosphate buffer (PB). Following fixation, tissues were rinsed three times for 10 minutes each in phosphate-buffered saline that contained 0.3 M NaCl (referred to as PBS henceforth) and incubated in Avidin-Rhodamine (1:1000; Jackson ImmunoResearch, West Grove, PA) overnight at 4°C. All antibodies were diluted in PBS,

which contained 0.3% Triton X-100 to enhance antibody penetration. Slices were mounted in anti-fade medium on microscope slides within a 270 µm thick agar window, to ensure that the coverslip would rest flat on the slice and to prevent compression of the slice by the objective lens of the microscope.

Slices were scanned on a Zeiss LSM 710 confocal microscope equipped with Argon multiline, 405 nm diode, 561 nm solid state and 633 nm HeNe lasers. Confocal scans were either taken through a 5x, 10x and 20x dry lens, as well as a 40x and 63x oil immersion lenses (numerical apertures were 1.3 for the 40x objective and 1.4 for the 63x objective) and the pin hole was set to one Airy unit in order to exclude out of focus light.

To resection parasagittal spinal cord slices, the tissues were flat embedded in 3% agar dissolved in distilled water. These embedded spinal cord slices were kept at 4°C for at least 10 minutes to allow the agar to set before sectioning. A block containing the spinal cord was cut from the agar and the bottom right corner of the agar was removed so that the slices cut from the block could be mounted in the correct orientation. In most cases the agar remained attached to the spinal cord sections during tissue processing and immunocytochemical reactions, allowing sections to be mounted in the correct orientation Sections were taken from this block at 60 µm thickness with a vibrating blade microtome (Leica VT 1200, Leica Microsystems Ltd Milton Keynes, UK) and were mounted in anti-fade medium. Sections were kept in serial order with a consistent orientation on microscope slides, and were stored at -20°C.

Certain sections taken from these slices were used for immunocytochemical reactions, and these will be discussed in detail later (see section 2.5 below). All of the immunocytochemical reactions performed in this study followed the same basic principles and protocol. Briefly, 60 µm sections were rinsed three times for 10 minutes each before they were incubated in primary antibodies. Sections were incubated for three days at 4°C in primary antibody, and were rinsed three times for 10 minutes in PBS before secondary antibodies were added. Sections were incubated overnight at 4°C in species specific secondary antibodies, which were conjugated to fluorescent proteins to allow their detection by confocal microscopy. Again, sections were rinsed three times for 10 minutes each in PBS before they were mounted onto microscope slides in anti-fade medium. All sections were mounted in the correct orientation, as judged by the shape of the agar surrounding the section, and stored at -20°C.

All images produced in this work were produced using Adobe Photoshop CS6 or Adobe Illustrator, and were produced from .tif files exported from Zen 2010.

2.4 Reconstruction and analysis of neurons

Initially, the slices were scanned with the confocal microscope before they were resectioned. This was to allow most of the cell to be visualised, and enable the sections that contained processes from the cells to be aligned correctly following sectioning of the slice. Cells reconstructions were excluded from morphological analysis if their dendrites were very short beaded and appeared to have been truncated. Cells were also excluded if their processes appeared to be cut very near to where they had left the cell soma, since it was possible that a large amount of processes would be missing from the cell reconstructions of these cells. However, this was rarely observed and it is likely that many cells with large parts of their dendritic tree and axonal arbor cut would be unhealthy and not recorded or recovered following recording.

Confocal image stacks with 0.5 µm z-spacing were acquired through the 63x lens using the 561 nm laser to reveal the neuronal morphology of recorded cells. Several image stacks were taken to visualise the entire axonal and dendritic tree of the cell. The depth from which satisfactory images of the cell could be obtained was scanned, and this was often sufficient to allow visualisation of the deepest projecting processes. However, in some cases the deepest processes could not be seen clearly through the thickness of the slice. In all cases the presence of GFP was confirmed in the cell bodies. To locate the cells in slices, tile scans of the whole slice were taken with the 561 nm laser and darkfield illumination through the 5x objective and this was used as a guide when determining the laminar location of the cell. All images were saved as Zeiss .lsm 5 files and were acquired and viewed using Zen 2010 software.

Image stacks were combined in Neurolucida 11 software (MBF Bioscience) by matching areas of image overlap and z-depth. These combined images were used as templates for cell reconstruction by Neurolucida's manual neuron tracing function, and cell reconstructions were saved as a Neurolucida .DAT files. Axons were easily distinguished from dendrites as they were much thinner and did not taper with increasing distance from the cell soma. In addition the presence of spines indicated that a process was dendritic. Axons also had varicosities, which were seen as irregularly spaced swellings along the

process. These varicosities were represented in reconstructions as a single point from which diameter could be determined, and this was used as a measure of varicosity size. Parameters for each neuron were obtained from the Neurolucida Explorer output, or were calculated by using results from the Neurolucida Explorer output. A list of all the parameters measured is included in the Appendix.

All slices from which cells were recorded were sectioned at 60 µm. For some cells this allowed deeper projecting processes to be seen, and these were scanned in a similar manner to that described above. These scans were used as templates for reconstruction in Neurolucida, and were added to the original cell reconstructions. This ensured the complete dendritic and axonal arbors were included in each cell reconstruction. The cell containing sections were reserved for immunocytochemical reactions (see below section 2.5). The first section that did not contain any part of the cell was reacted to reveal PKCγ to determine laminar boundaries (Figure 2-1), since a PKCγ-immunoreactive plexus delineates the IIo-IIi and IIi-III borders (Lu et al., 2013; Polgár et al., 2007). Originally this reaction also included antibodies against NK1r to delineate lamina I. However, due to the variability of NK1r staining in immersion fixed tissue following recording experiments, this method was not used to determine lamina I. Instead, this lamina was defined as the area 20µm below the white matter, since the NK1r-immunoreactive area appears to be uniform in thickness in transverse sections from mouse spinal cord.

Tile scans of the section immunoreacted for PKCγ were scanned with the 5x objective, and more detailed scans were taken from the area of the filled cell with the 10x and 20x objectives using darkfield illumination to identify lamina II and the immunoreactive PKCγ plexus. The sections that contained the cell somata were scanned with 5x and 20x objectives to locate the position and orientation of the filled cell. The tile scans of these sections were opened in Neurolucida software, and the orientation was adjusted to allow the sections to be aligned as accurately as possible. The laminar boundaries were drawn using the immunoreacted section. The border between the white and grey matter, and a parallel line 20µm below this were used to delineate lamina I, and the immunoreactive PKCγ plexus was used to draw the IIo/IIi and IIi/III borders. Although there are PKCγ-immunoreactive cells present in lamina III and lamina IIo, the dense immunoreactive plexus allows a reliable boundary to be drawn between laminae IIi and III, and between laminae IIi and IIo. This immunoreactive PKCγ band is often used as a marker for lamina IIi (Polgár et al., 1999b). The cell reconstruction was positioned within these laminar

boundaries and rotated to best fit the orientation of the cell in the section. A flowchart of the reconstruction procedure is summarised in Figure 2-1.

In order to measure the overall orientation of dendrites and axons of reconstructed cells, polar histograms were generated to measure the length of processes that lay in a particular direction. This involved projecting the cell onto the plane of section and measuring the total length of processes that lay within a specific range of angles. These polar histograms measure the orientation of a process as opposed to its position relative to the soma, and therefore part of a process that changes direction will be included in a different range of angles. These polar histograms were divided into 8 bins (ranges of angles) and the rostrocaudal bins were added together to give a single value for rostrocaudal length, and the dorsoventral bins were pooled to give a single value of dorsoventral length. With reference to Figure 2-2, the angles for rostrocaudal length are between 315° - 45° and 135° - 225°, and the angles between 45° - 135° and 225° - 315° are taken to be dorsoventral length.

Since many PrP-GFP cells projected their axons into lamina I, and it was seen that numerous GFP-expressing axonal boutons from the PrP-GFP mouse form synapses with projection neurons in lamina I (Ganley et al., 2015), the PrP-GFP cell reconstructions were divided into cells that innervated lamina I and those that did not. Most reconstructed PrP-GFP cells had at least some of their axon present in lamina I, and many of these only contributed a few axonal boutons to this lamina. More stringent criteria were used to define lamina I innervating cells. Since the axonal boutons are the source of synaptic output, this was used as criteria for defining a lamina I innervating cell. Approximately one third of the reconstructed PrP-GFP cells had an axon with between 10 and 20 boutons in lamina I, and the number of cells with over 20 boutons in lamina I decreased sharply as the bouton number increased. Cells with twenty boutons present in lamina I were therefore defined as lamina I innervating cells, since it was more likely that a cell with 20 boutons in lamina I would innervate projection neurons than a cell with 10 boutons.

Table 2-1 Table of antibodies used in this study

Antibody	Species	Dilution	Source
CGRP	Guinea pig	1:10000	Penninsula
Galanin	Rabbit	1:1000	Bachem
nNOS	Sheep	1:2000	Gift from PC Emson
NPY	Rabbit	1:1000	Sigma
pERK	Mouse	1:500	Santa Cruz Biotechnology
PKCγ	Guinea pig	1:500	Gift from M Watanabe
VGluT1	Guinea pig	1:1000	Millipore
VGluT1	Rabbit	1:1000	Synaptic systems

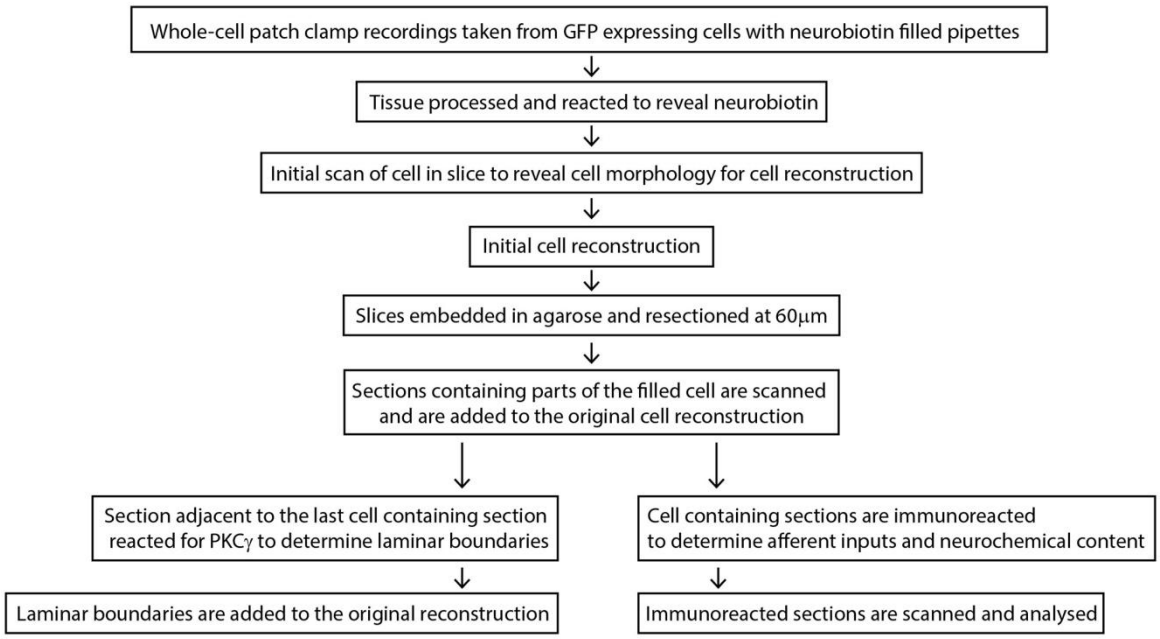

Figure 2-1 Flowchart of the cell labelling and reconstruction process

Flowchart summarises the process of single cell labelling, tissue processing, and immunoreactions for the labelled tissue. Note that the sections that do not contain the cell are used to determine the laminar boundaries, whereas the cell containing sections are used to determine neurochemical phenotype and pre-synaptic inputs by immunocytochemistry

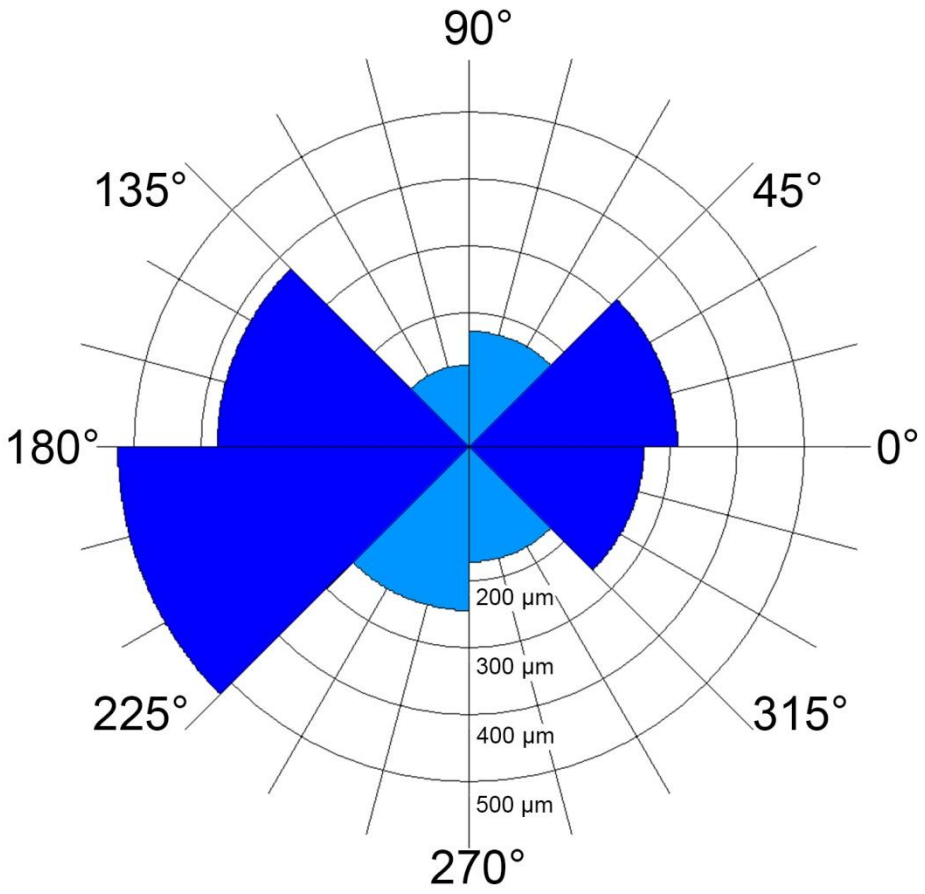
90°
135°
45°
180°
0°
225°
315°
270°
200 µm
300 µm
400 µm
500 µm

Figure 2-2 Example of a polar histogram for the dendritic tree of a cell

The polar histograms are generated to show the lengths of dendritic tree that lie within a certain range of angles. A two-dimensional projection of the cell reconstruction is produced, and the length of processes that are oriented within ranges of angles are measured and binned. The number of bins chosen was eight. The lengths of dendritic trees are divided into octants, and the dark blue segments indicate the rostrocaudal oriented processes. The lighter blue octants represent the lengths of dendrites that have a dorsoventral orientation. The concentric circles indicate the length of dendritic tree present within each octant. Length of process within angles 315° - 45° and 135° - 225° are pooled together and are defined as rostrocaudal length, whereas the length of process 45° - 135° and 225° - 315° are taken as the total dorsoventral length of a cell. This same process is used for the axon to define rostrocaudal and dorsoventral length

2.5 Immunocytochemistry of recorded cells

All of the primary antibodies used in this work are summarised in Table 2-1, which also states the concentration of each antibody used. Each of the primary antibodies is known to bind specifically to its antigen, and details on antibody characterisation are given later (see section 2.8 below). Sections were rinsed three times with PBS before antibodies were added, and sections were incubated or at least 3 days at 4°C in primary antibody. Primary antibodies were revealed by species specific secondary antibodies, all of which were raised in donkey. Secondary antibodies were conjugated to the fluorescent molecules Rhodamine-Red, Alexa 488, Pacific Blue, or Alexa 647. All antibodies were diluted in PBS that also contained 0.3% Triton X-100 to improve the penetration of antibodies.

2.5.1 Determining the presence of galanin or nNOS in the axonal boutons of PrP-GFP cells

Sections from slices that contained axon and axonal boutons of filled PrP-GFP cells were selected for immunocytochemical reactions. These were tested for the presence of nNOS and/or galanin, which were previously shown to be present in PrP-GFP cells (Iwagaki et al., 2013). Some of these sections also contained other parts of the cell, such as the cell soma and dendrites. These sections were immunoreacted with a sheep antibody against nNOS and a rabbit antibody against galanin. These were revealed with Alexa 647 and Pacific Blue conjugated antibodies raised against goat and rabbit antibodies respectively. Image stacks with 0.5 μm z-spacing were taken from these immunoreacted sections through the 63x oil immersion lens to reveal the cell processes and determine whether they contained nNOS or galanin. A cell was defined as positive for these neurochemicals if either there were 5 or more clearly immunoreactive axonal boutons, or a stretch of dendrite was immunoreactive for nNOS or galanin.

2.5.2 Contacts from A-LTMRs onto dendritic spines of PrP-GFP and NPY-GFP cells

Sections of cells that contained dendrites with spines were immunoreacted for VGluT1 as this is expressed in the majority of A-LTMRs in laminae IIi-V (Todd et al., 2003a). Sections were selected from PrP-GFP cells that had an axon that innervated lamina I and therefore were likely to inhibit projection neurons, and also from cells that responded to

capsaicin (determined by mEPSC analysis, see 2.2.2) and therefore received input from TRPV1-expressing primary afferents. Image stacks of these reacted sections were scanned through a 63x oil immersion lens with 0.5 µm z-spacing, and overlapping image stacks were taken to capture the entire dendritic tree in the section. Counting the contacts from VGluT1-immunoreactive boutons onto dendritic spines was performed using Neurolucida software. The area ventral to and including lamina IIi was outlined based on the area of dense VGluT1 immunoreactivity. Once this area was defined, the channel that revealed VGluT1 was switched off, and the dendritic trees and spines within the section were reconstructed. The total number of spines within laminae IIi-III was counted for the dendritic tree within the section, and the number of spines contacting a VGluT1 immunoreactive bouton was counted when the channel for VGluT1 was switched back on.

2.5.3 Determining output of NPY-GFP cells and presence of NPY in axonal boutons

To determine whether the filled NPY-GFP cells contained detectable NPY in their axonal boutons and whether the axon of NPY-GFP cells targeted the ALT neurons in lamina III, sections containing axons of filled NPY-GFP cells were reacted with a rabbit antibody against NPY and a guinea pig antibody against CGRP. These antibodies were revealed with secondary antibodies conjugated to fluorescent molecules Alexa 647 and Pacific blue respectively. This strategy was chosen as bundles of CGRP-expressing and NPY-expressing boutons densely innervate the cell bodies and dendrites of ALT neurons in lamina III, allowing them to be visualised without the need for brain injection of retrograde tracers (Cameron et al., 2015). This immunoreaction also allowed the presence of NPY to be determined in the axonal boutons. A cell was defined as containing NPY if its axon had 5 or more axonal boutons with detectable levels of NPY. Immunoreacted sections were scanned through the 63x oil immersion lens with 0.5 µm z-spacing, and many overlapping image stacks were taken to include all of the filled axon that was present in the section.

2.6 Noxious mechanical stimulation of mice

Many recorded NPY-GFP neurons with their somata found in lamina III received monosynaptic input from C-fibres, many of which are known to transmit nociceptive information (Cavanaugh et al., 2009, 2011). All tested C-fibres were insensitive to capsaicin, which indicated they did not express TRPV1 and were therefore unlikely to be peptidergic nociceptors. This meant it was likely that non-peptidergic nociceptors, which

are likely mechanonociceptors, or C-LTMRs were providing this input (Cavanaugh et al., 2009; Li et al., 2011). However, in these experiments it was not possible to determine the type of C fibre providing this monosynaptic input to NPY-GFP cells. To test whether the C fibre input these cells received was from C mechanonociceptors, mice were stimulated by a noxious mechanical stimulus, and the activity of NPY-expressing cells in lamina III were assessed.

Three male C57Bl/6J mice weighing 17 g each were stimulated unilaterally with noxious mechanical pinch to the hindpaw. Originally this was to assess the response of calretinin-immunoreactive cells to noxious mechanical stimulation (Smith et al., 2015), but this tissue was also used in the present report. Briefly, mice were initially anaesthetised with isofluorane and maintained under anaesthesia by intraperitoneal injection of 10% urethane. Folds of glabrous skin above the tarsus were pinched at ten different locations with watchmaker's forceps (5 s each), and mice were transcardially perfused with fixative 5 minutes after the final stimulus. These stimulation experiments were performed by Dr David Hughes.

Tissues from these mice were immunoreacted with antibodies against pERK to identify the activated cells, NPY to identify NPY-expressing cells, and PKCγ to identify the lamina II/III border, as this is the ventral boundary of the PKCγ-immunoreactive plexus (Polgár et al., 2007). These primary antibodies were revealed with secondary antibodies conjugated to rhodamine, Alexa 488, and Pacific Blue respectively for pERK, NPY and PKCγ primary antibodies. Image stacks with 1 µm z-spacing were taken from immunoreacted tissue through the 40x lens, with 0.7x digital zoom. Overlapping image stacks were taken to include the entire dorsal horn ipsilateral to the stimulated hindlimb.

Image stacks were analysed using Neurolucida software. Firstly, lamina III was defined using the channel that revealed PKCγ to draw the lamina II/III border, and a parallel line 100 µm ventral to this was taken to be the lamina III/IV border. The dense immunoreactive PKCγ band clearly indicated the border between laminae IIi and III, although there were occasional PKCγ-immunoreactive cell somata and dendrites in adjacent laminae, which has been reported previously (Polgár et al., 1999b). Once this region was defined, the NPY and PKCγ channels were switched off, and the cells with detectable pERK were outlined. Once all pERK positive cells in lamina III were counted, the NPY channel was revealed and each pERK cell was inspected for the presence of detectable NPY-immunoreactivity.

This cell counting method indicated the number of pERK positive cells in lamina III that were NPY-expressing.

2.7 **Perfusion fixation**

Perfusion fixation and analysis of perfusion fixed tissue from NPY-GFP mice was performed by Dr Erika Polgár

To assess the relationship between NPY-expressing and GFP positive cells in the NPY-GFP mouse, spinal cord tissue form NPY-GFP mice was perfusion fixed and used for analysis. Three mice were injected with 50 mg pentobarbitone to induce deep anaesthesia. Animals were pinned to the dissecting board by the upper limbs, and the thoracic cavity was exposed. When the heart could be seen clearly, the perfusion needle was inserted into the left ventricle and the right atrium was cut. The mice were perfused with a small volume of Ringer's solution to clear all the blood from the circulatory system before perfusion of the fixative. Mice were perfused with 250 ml 4% freshly depolymerised formaldehyde diluted in 0.1 M phosphate buffer. After perfusion the lumbar spinal cord was dissected from the vertebral column and the dura and pia mater were carefully removed. The lumbar spinal cord was segmented and removed, using the dorsal roots to identify the different segments. Spinal cord segments were post-fixed in the same fixative overnight at 4°C.

2.8 **Antibody characterisation**

The antibodies used in this study have been previously characterised and are shown to give specific staining for the antigens that they target. The galanin antibody staining can be prevented by pre-incubating the antibody in galanin, demonstrating its specificity for galanin (Simmons et al., 1995). The nNOS antibody was also prevented by incubation with nNOS, and it labelled a band of 155 kDa in Western blots taken from the rat hypothalamus extracts, which corresponds to the molecular weight of nNOS (Herbison et al., 1996). NPY antiserum that has been incubated with NPY is no longer able to stain specific structures in the superficial dorsal horn, where NPY immunoreactivity is normally present (Rowan et al., 1993). The guinea pig and rabbit VGlutT1 and VGluT2 antibodies have been characterised, and the rabbit and guinea pig antibodies stain identical structures (Todd et al., 2003). The rabbit VGluT1 antiserum is raised against the C terminal region of the protein expressed in a glutathione-S-transferase (GST) fusion protein, and recognises a

band of 60 kDa in purified synaptic vesicles; the VGluT2 antiserum recognises a protein band of 65 kDa in these purified vesicles (Takamori et al., 2001). The binding of these antibodies to their targets can be blocked by preincubation with their corresponding protein, but not by preincubation with the other (Takamori et al., 2001). The CGRP antibody is able to detect both α and β form of the peptide (manufacture's specification). The PKCγ antibody is raised against the 14 C terminal amino acids of the mouse PKCγ protein and detects a band of 75 kDa in protein extracts from wild type mice, which is absent in protein extracts from PKCγ knockout mice (Yoshida et al., 2006). The pERK monoclonal antibody recognises both ERK 1 and ERK 2 that are phosphorylated on two amino acid residues (Thr202 and Tyr204) and has been used successfully in other studies (Polgár et al., 2013b).

2.9 **Cluster analysis**

Morphological parameters were either measured directly from, or were calculated from results generated by, Neurolucida explorer. The parameters were recorded in a spreadsheet, with each row representing a different cell and each column representing a parameter. Passive and active membrane properties of cells were also measured during the whole-cell recordings and used for cluster analysis. In some experiments TTX, bicuculine, and strychnine had been applied to the recording chamber before the active membrane properties could be determined, and therefore not all cells with reconstructed morphology had physiological parameters available. Similarly, not all cells that had physiological parameters measured were recovered for morphological analysis. PCA was performed on a standardised dataset of z-scores, calculated as each value minus the parameter mean divided by the standard deviation $((x-\mu)/\delta)$. All morphological and physiological parameters can be found in the Appendix.

PCA was used to reduce the dimensionality of the dataset, since many parameters may be related to one other and this introduces redundancy in the classification procedure. The number of principal components retained was determined as the point at which the eigenvalues reached a plateau on a scree plot of eigenvalues plotted against principal components, with principal components arranged from highest to lowest eigenvalue along the x axis (Cattell, 1966). Each dataset was then transformed using the appropriate number of principal components before hierarchical clustering. In some instances a plot of the first two principal components was used to generate a scatterplot to see how similar two or

more groups were. To rescale a dataset in terms of its principal components, matrices of the standardised dataset and the retained principal components were multiplied together.

Hierarchical clustering was performed using squared Euclidian distance as a measure of similarity, and Ward's method was used as the linkage rule for clustering. This is an agglomerative clustering algorithm, which places objects into groups based on Euclidian distance, starting with n clusters of size 1 until there is only one cluster of size n. Objects within the same cluster are more closely related than objects between clusters. Principal component analysis and cluster analysis were performed using SPSS statistical software (IBM) and the rescaling of each dataset in terms of its principal components was performed in Microsoft Excel, using the matrix multiplication function. A flowchart summarising this procedure for cluster analysis is shown in Figure 2-3.

Several datasets were used for principal component analysis and cluster analysis. These included datasets of morphological parameters and physiological parameters. This was done for PrP-GFP cells, for NPY-GFP cells and for both PrP-GFP and NPY-GFP cells. In some experiments a subset of a group was used, for example only those PrP-GFP cells that had identifiable neurochemistry. Each time a different dataset was used, principal component analysis was repeated and the principal components retained were used to reduce the dimensionality of that particular dataset. If the dataset contained a variable that had no variance, this variable was not included in the principal component analysis or the cluster analysis. In some experiments, cluster analysis was used to determine whether cells with a particular neurochemical or anatomical feature could be distinguished.

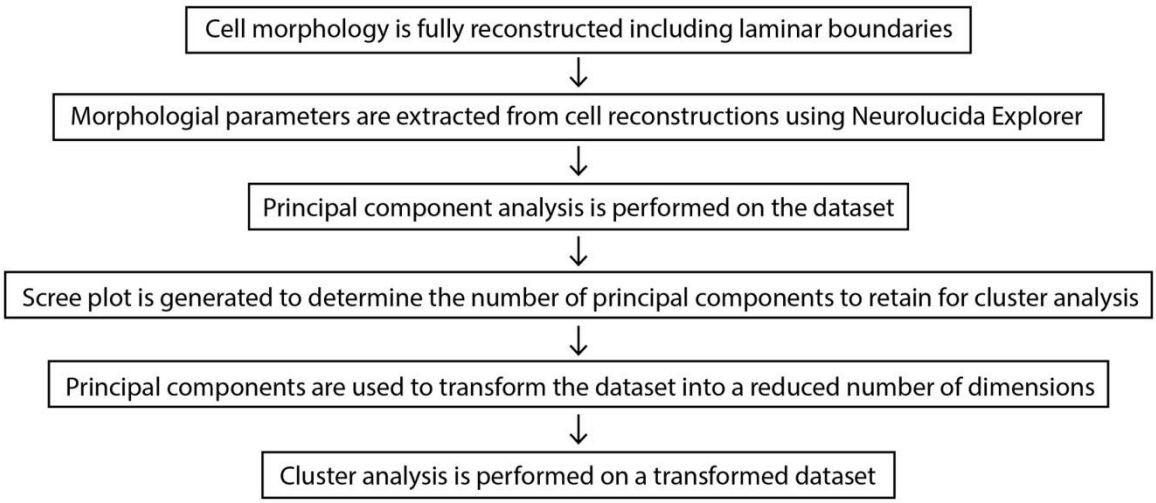

Figure 2-3 Flowchart summarising the cluster analysis procedure

Flowchart summarising the use of the data extracted from reconstructed neurons or physiological data acquired during the electrophysiology experiments for cluster analysis. Hierarchical cluster analysis was performed on a dataset that was reduced in dimensionality using principal component analysis (PCA). Morphological and physiological parameters used for cluster analysis are described in the appendix

2.10 **Statistics**

A change in the distribution in the mEPSC inter-event intervals was assessed using the Kolmogorov-Smirnov test. The increase in mEPSC frequency before and after drug application was determined as significant by Student's paired t-test, and differences in morphological properties were assessed using Student's unpaired t-test assuming unequal variances. As spine density was not a normally distributed property, comparisons were made using the Mann-Whitney U test. Peak amplitude of eEPSCs before and after capsaicin application was compared using Wilcoxon matched-pairs signed rank test. Student's paired t-test was used for comparing dorsal and ventral dendrite extent for the lamina II and lamina III NPY-GFP cells, since the comparison was from different measures in the same cell. Significance was taken as $p < 0.05$ for all statistical tests.

3 Electrophysiological data

The vast majority of the electrophysiological experiments and analyses discussed in this and the following chapter were performed by Drs Noboru Iwagaki, Allen Dickie and Kieran Boyle.

3.1 Physiological properties of PrP-GFP cells

3.1.1 Membrane properties of PrP-GFP cells

Fourteen physiological properties were measured from each cell for hierarchical cluster analysis. These included both passive and active membrane properties. The results of hierarchical cluster analysis using these physiological properties will be reported in the following chapter and details of these measurements are listed in the appendix. To determine the resting membrane potential and input resistance, the voltage was stepped to different subthreshold values (-70 to -50 mV in 2.5 mV increments) to establish a current-voltage (I-V) relationship. From 138 PrP-GFP cells the average resting membrane potential was -53.7 ± 0.9 mV and the average input resistance was 1034.3 ± 61.3 MΩ.

3.1.2 Action potential firing pattern

In total, membrane properties from 138 PrP-GFP cells were recorded from the superficial dorsal horn. Of these 87 were recovered for complete morphological reconstruction and their morphological properties will be discussed in the following chapter. The action potential firing properties of PrP-GFP cells were assessed with suprathreshold square current pulses. The majority of these cells had a tonic firing pattern, in which action potentials were generated throughout the current injection (n = 95), with a maximum firing frequency of 28.1 ± 1.0 Hz (Figure 3-1 a). The second most common firing pattern was initial bursting (n = 18), in which cells only generated action potentials at the start of the depolarising step. Some cells did not generate action potentials in response to depolarising current steps, and these were termed reluctant cells (n = 12). A minority of cells only generated one or two action potentials at the onset of current injection, and these were termed single spiking cells (n = 9). Other common firing patterns that are seen in dorsal horn neurons such as delayed firing or gap firing were never seen in these cells. These data are summarised below (Figure 3-1 b)

3.1.3 Dorsal root input to PrP-GFP cells

To determine which primary afferents provided input to PrP-GFP cells, dorsal root stimulation experiments were performed on parasagittal slices of lumbar spinal cord with intact dorsal roots. Twenty nine PrP-GFP cells were targeted for whole-cell recording and EPSCs were evoked by stimulating the dorsal root in 17 cells. The stimulation intensities used were 25 µA for Aβ fibres, 100 µA for Aδ fibres and 500 µA and 1 mA for C-fibres, and were delivered to the dorsal root via a suction electrode. To determine whether there were any additional polysynaptic inputs from C-fibres, the stimulation intensity was increased to 3 mA and 5 mA, but no further synaptic input was detected in any cells at these intensities. This input was confirmed as monosynaptic if evoked EPSCs (eEPSCs) could follow a particular stimulation frequency 20 times without any synaptic failures (Nakatsuka et al., 2000). Initially the stimulation frequency was 0.02 Hz when testing all fibre types and this frequency was increased to 20 Hz for Aβ fibres, 2 Hz for Aδ fibres and 1 Hz for C-fibres when testing for synaptic failures.

From the 17 cells that responded to dorsal root stimulation, 7 received monosynaptic C fibre input and one of these also received monosynaptic Aδ input (Figure 3-2 a and b). In 5 out of 7 cells that received monosynaptic C fibre input, additional polysynaptic input was seen from Aβ (1), Aδ (3), and C (1) fibres. The other cells (10/17) only received polysynaptic evoked EPSCs (eEPSCs), and these were from Aβ (1), Aδ (1) C (4), and both C and Aδ (4) fibres. The example traces show PrP-GFP cells that receive monosynaptic C fibre input only and monosynaptic input from both C and Aδ fibres (Figure 3-2).

3.1.4 PrP-GFP cell responses to capsaicin and icilin

To determine monosynaptic inputs to PrP-GFP cells, we recorded the frequency of mEPSCs before and after the application of the TRPV1 and TRPM8 agonists' capsaicin and icilin. These experiments test whether the pre-synaptic terminals providing input to the PrP-GFP cells express TRPV1 or TRPM8 channels. Opening the channels on pre-synaptic terminals will cause depolarisation and hence an increase in release probability of synaptic vesicles. The post-synaptic effects of this vesicle release is a miniature EPSC (mEPSC), which is a rapid small inward current followed by a longer decay time. An increase in vesicle release will result in an increase in the frequency of these mEPSCs. In both control and test conditions the drugs TTX (0.5 µM) bicuculine (10 µM) and strychnine (5 µM) were present in the recording solution to prevent action potential firing and to block

inhibitory GABAergic and glycinergic input to the cells. Cells were voltage clamped at -60mV and a 5 minute recording period was taken for control conditions. Five minutes was also given for the drugs to wash into the slice, and a 5 minute trace was then taken during the application of drugs. This inter-event interval between mEPSCs was compared for control conditions and during drug application; a significant change in the inter-event intervals for mEPSCs was taken as $p < 0.05$ by the Kolmogorov-Smirnov test. A significant change in the distribution of the mEPSC inter-event intervals is indicative of cells receiving monosynaptic input from axon terminals that express the channels activated by the drug.

Thirteen out of 16 cells responded to capsaicin (2 μM) (Kolmogorov Smirnov test, $p < 0.05$) with the average frequency of mEPSCs increasing 16 fold during application (13.2 ± 7.9 events/min before capsaicin to 215.8 ± 54.3 events/min after capsaicin) (Figure 3-3). This increase in frequency was seen as significant using Student's paired t-test ($p < 0.01$). No inward current or change in the amplitude of mEPSCs was seen in cells tested, which indicates TRPV1 was not expressed by the PrP-GFP cells themselves. These results demonstrate that most PrP-GFP cells receive direct synaptic input from TRPV1-expressing primary afferent fibres.

For icilin experiments, the temperature of the recording chamber was increased to 32°C because TRPM8 channels are likely to be already active at room temperatures < 27°C (McKemy et al., 2002). This increase in recording temperature caused an increase in baseline mEPSC frequency similar to previous reports for mouse superficial dorsal horn neurons (Graham et al., 2008). Icilin (20 μM) was applied and produced a significant decrease in the inter-event intervals of mEPSCs in 14 out of 24 cells. When icilin-responsive cells were pooled together, a doubling in mEPSC frequency was observed during icilin application (35.0 ± 7.3 to 68.6 ± 12.0 events/min) and this was seen to be significant (Student's paired t-test, $p < 0.01$). Icilin is also an agonist of TRPA1 channels at higher concentrations, but is apparently selective for TRPM8 at lower concentrations of 3 – 10 μM (Wrigley et al., 2009). This study estimated the EC_{50} for icilin is 1.1 μM for TRPM8 channels, and is 74 μM for TRPA1 channels. It is possible that the concentration of icilin used in the present study (20 μM) could also activate TRPA1 channels. To show that this increase in mEPSC frequency was due to TRPM8 channel activity, some icilin experiments were performed in the presence of a TRPA1 channel antagonist (A967079). The bath application of icilin still caused a significant decrease in inter-event intervals in 5

out of 10 cells in the presence of this TRPA1 antagonist (Kolmogorov Smirnov test, $p < 0.05$), and the average mEPSC frequency of the responsive cells was 1.4 fold higher in the presence of icilin than in control conditions (64.0 ± 23.8 to 92.0 ± 32.9 events/min; Student's paired t-test, $p < 0.05$). Again no increase in inward current or increase in mEPSC amplitude was seen during application of icilin, suggesting that TRPM8 channels are not expressed post-synaptically. These data indicate that around half of the PrP-GFP cells can also receive direct synaptic input from TRPM8 expressing afferents. Further populations could not be identified within the responsive and non-responsive cells, since the baseline frequency of mEPSCs was highly variable between different cells.

To test whether the same cell received direct synaptic input from TRPM8 and TRPV1 expressing afferents, six of the experiments tested PrP-GFP cells for responses to both icilin and capsaicin. In these experiments the bath temperature was again raised to 32°C so the effects of icilin could be observed. A recovery period of 10 minutes was given following icilin application to allow the mEPSC frequency to return to baseline frequency before capsaicin was applied. In 2 cells there was an increase in mEPSC frequency in response to both icilin and capsaicin application, seen as a significant reduction in inter-event intervals. In all six of these experiments the cells responded to capsaicin. This demonstrates that the PrP-GFP cells can receive input from both TRPM8 and TRPV1 expressing primary afferents.

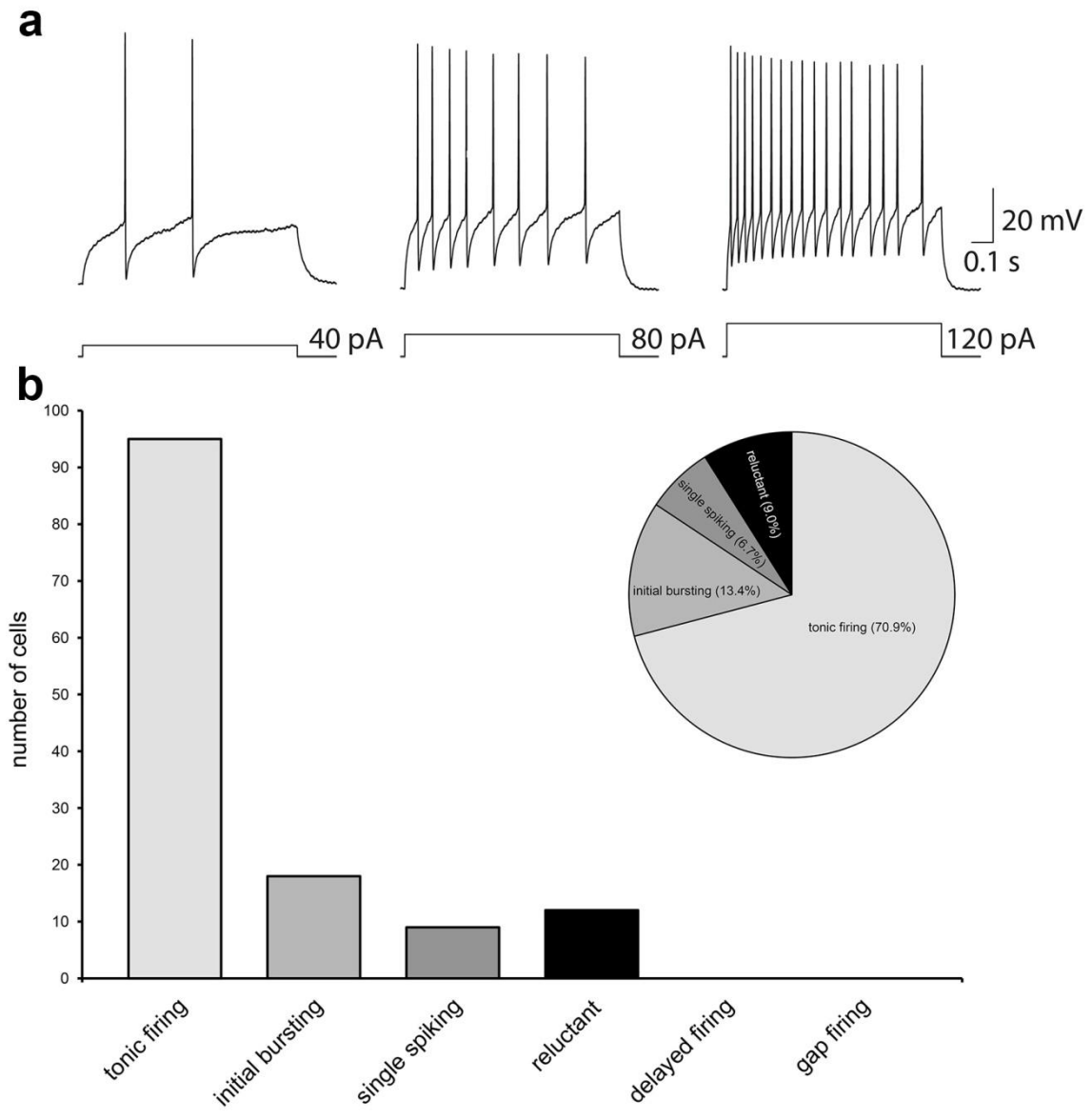
a
20 mV
0.1 s
40 pA
80 pA
120 pA
b
number of cells
100
90
80
70
60
50
40
30
20
10
0
tonic firing
initial bursting
single spiking
reluctant
delayed firing
gap firing
reluctant (9.0%)
single spiking (6.7%)
initial bursting (13.4%)
tonic firing (70.9%)

Figure 3-1 Action potential firing patterns of recorded PrP-GFP cells

a shows an example of trace from a tonic firing cell, the frequency of firing increases with increased current injection. **b**, bar chart showing the number of PrP-GFP cells that exhibited different action potential firing patterns when challenged with a 1s suprathreshold current injection. Inset show a pie chart of this data indicating the percentage of all cells tested that exhibited a particular action potential firing pattern. Note that delayed and gap firing are never observed for these cells.

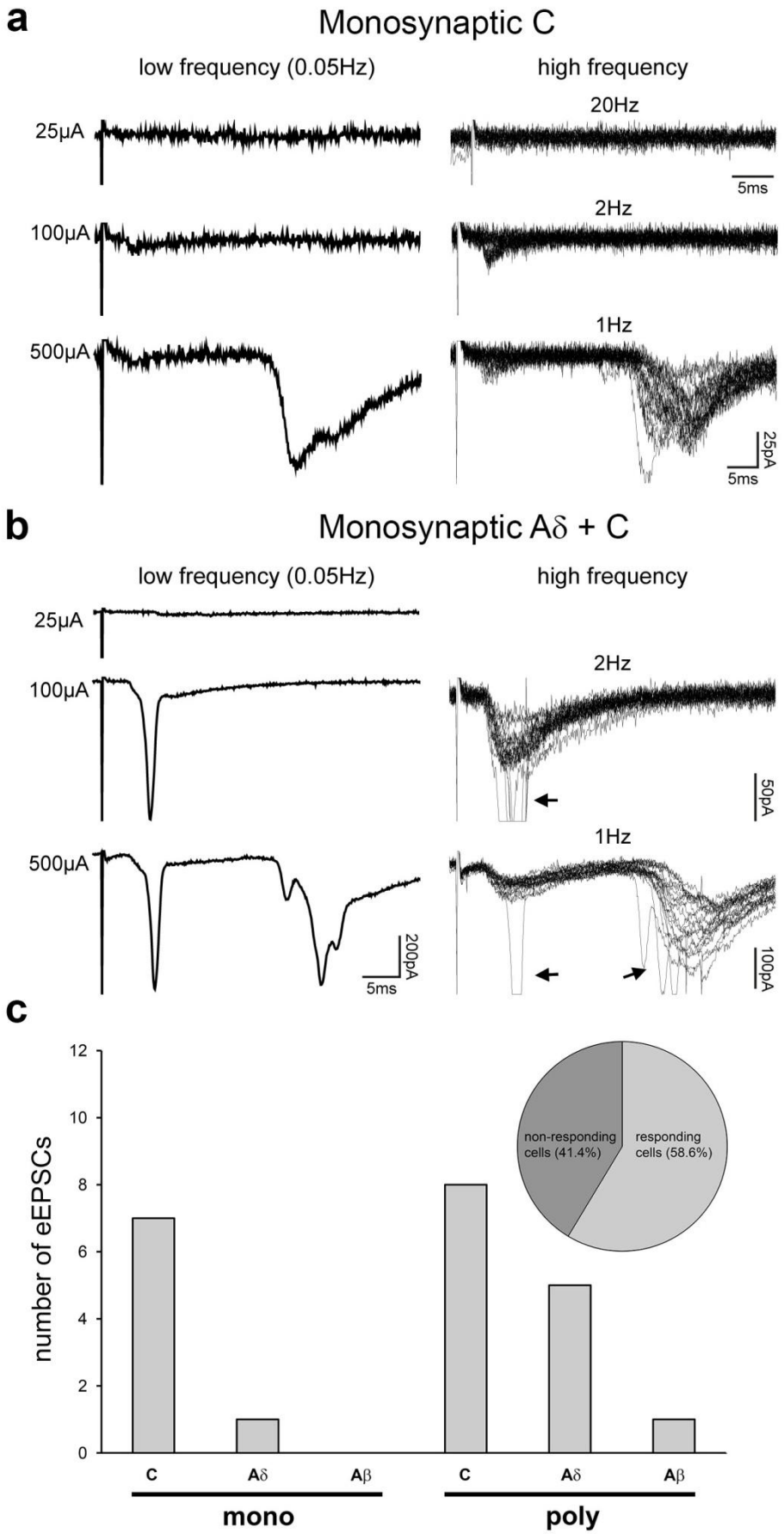
a
Monosynaptic C
low frequency (0.05Hz)
high frequency
25μA
100μA
500μA
20Hz
2Hz
1Hz
5ms
25pA
5ms
b
Monosynaptic Aδ + C
low frequency (0.05Hz)
high frequency
25μA
100μA
500μA
2Hz
1Hz
50pA
200pA
5ms
100pA
c
number of eEPSCs
12
10
8
6
4
2
0
non-responding cells (41.4%)
responding cells (58.6%)
C
Aδ
Aβ
C
Aδ
Aβ
mono
poly

Figure 3-2 Examples of dorsal root input to PrP-GFP cells

a: Whole-cell recording showing monosynaptic evoked EPSCs (eEPSCs) from C-fibres. The response is only seen when the dorsal root is stimulated at C fibre strength (500 μA) and does not fail in response to high frequency stimulation (1 Hz). **b**: An example of a whole-cell recording showing a cell receiving monosynaptic input from both Aδ and C-fibres. The response to Aδ fibres has a shorter latency and is evoked by lower stimulation intensity (100 μA) than the C fibre response. Neither of these eEPSCs fails in response to high frequency stimulation (Aδ = 2Hz, C = 1Hz). Note that the responses in this example are strong enough to initiate action potential firing in this cell as seen by the large inward sodium currents evoked during the eEPSCs when stimulated at high frequencies, indicated by arrows. Panels on the left are averages of three traces stimulated at a low frequency of 0.05 Hz, and panels on the right show 20 superimposed traces from high frequency stimulation of the dorsal root (Aβ = 20 Hz, Aδ = 2 Hz, and C = 1 Hz). **c** shows a bar chart summarising all the eEPSCs generated by dorsal root stimulation for the PrP-GFP cells that responded, the pie chart gives the percentages of the tested cells that responded.

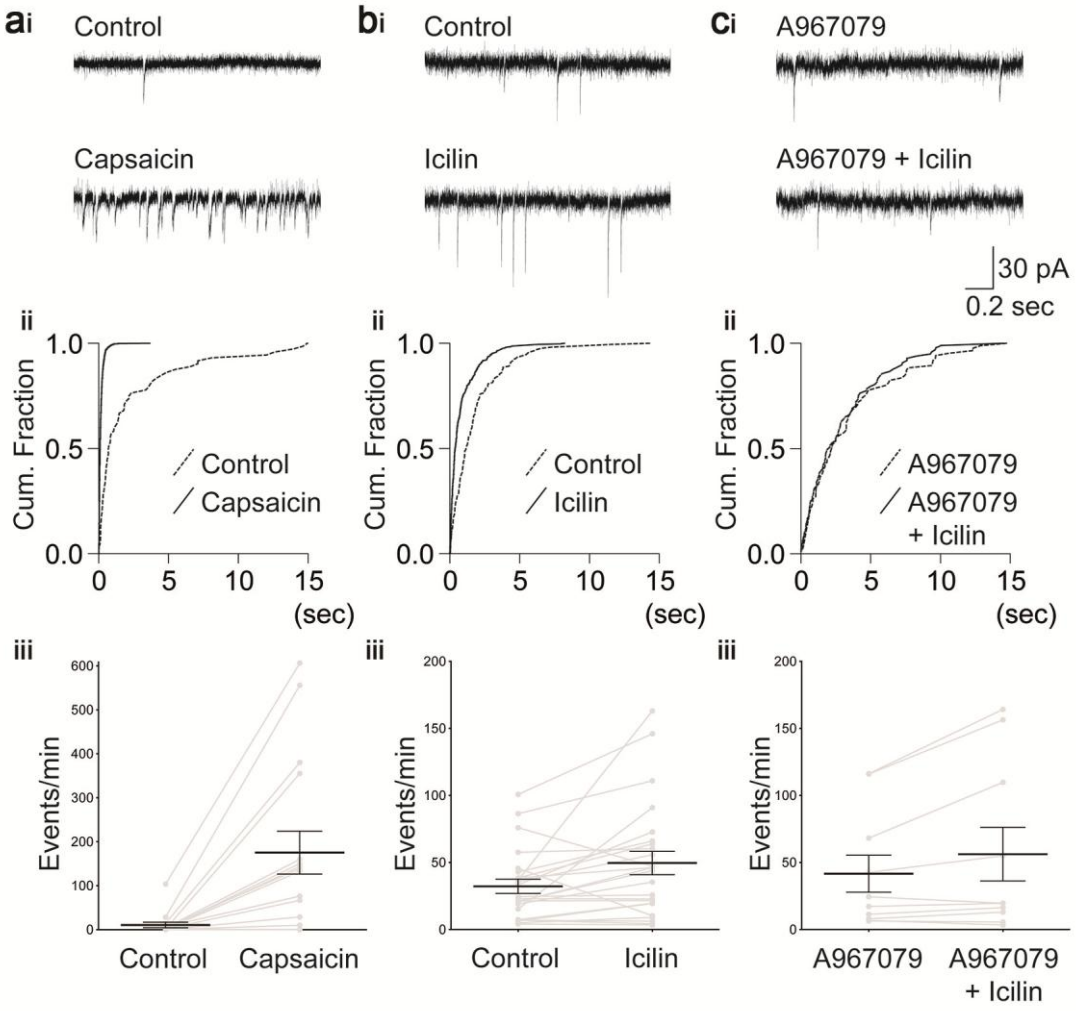
ai
Control
Capsaicin
bi
Control
Icilin
ci
A967079
A967079 + Icilin
30 pA
0.2 sec
ii
Cum. Fraction
1.0
0.5
0.0
0
5
10
15
(sec)
Control
Capsaicin
Control
Icilin
A967079
A967079
+ Icilin
iii
Events/min
600
500
400
300
200
100
0
150
50
Control
Capsaicin
Control
Icilin
A967079
A967079
+ Icilin

Figure 3-3 Responses of PrP-GFP cells to bath application of TRP channel agonists capsaicin and icilin

a: Response of cells to application of 2 µM capsaicin **i)** Raw trace of a cell responding to bath application of capsaicin by increasing the frequency of mEPSCs; **ii)** cumulative response plot showing the change in the distribution of inter event intervals before and after capsaicin application ($p < 0.05$, Kolmogorov-Smirnov test); **iii)** chart summarising the mEPSC frequency before and during capsaicin application in all experiments with the mean ± S.E.M for all data highlighted. A 16-fold increase in mEPSC frequency was observed for the 13/16 cells that responded to capsaicin ($p < 0.01$, Student's paired t-test). **b**: Response of cells to application of 20 µM icilin. **i)** Raw trace showing an increase in the number of mEPSCs after icilin application; **ii)** cumulative frequency plot from the example trace showing a significant decrease in inter event intervals ($p < 0.05$, Kolmogorov-Smirnov test); **iii)** chart shows the mEPSC frequency before and during the application of icilin for all experiments, and the mean ± S.E.M are indicated for all data. The pooled data from the 8/12 cells that responded significantly ($p < 0.05$, Kolmogorov-Smirnov test) showed a significant 2-fold increase in mEPSC frequency on average ($p < 0.05$, Student's paired t-test). **c**: Cells that responded to 20 µM icilin in the presence of a TRPA1 antagonist (5 µM A967079). **i)** An example trace of a cell before and after the application of icilin in the presence of a TRPA1 antagonist; **ii)** the cumulative frequency plot from the cell whose example trace is illustrated, note that there is no change in the distribution in the inter event intervals; **iii)** chart summarising all experiments measuring the frequency of mEPSCs in the presence of TRPA1 antagonist A967079 before and during the application of icilin. This chart displays the mean ± S.E.M for all data. The 5/10 cells that did respond significantly to icilin in the presence of A967079 ($p < 0.05$, Kolmogorov-Smirnov test) showed a 1.4-fold increase in mEPSC frequency, which was seen as significant ($p < 0.05$, Student's paired t-test).

3.2 Physiological properties of NPY-GFP cells

3.2.1 Membrane properties of NPY-GFP cells

In total, 96 NPY-GFP cells were targeted for whole-cell recordings. The resting membrane potential and input resistance was determined for each cell in the same manner as described for the PrP-GFP cells. The average resting membrane potential was -51.1 ± 1.0 mV and the average input resistance was 1433.6 ± 79.8 MΩ for these recorded cells. The same 14 physiological parameters were measured for cluster analysis, and these will be reported in the following chapter.

3.2.2 Action potential firing pattern

Similar to the PrP-GFP cells, most of the NPY-GFP cells displayed a tonic firing pattern (81/96) or an initial bursting firing pattern (8/96). The remaining cells were single spiking (7/96), and only discharged one or two action potential at the start of the depolarising step. Reluctant, gap firing and delayed firing patterns, which are indicative of an A-type potassium current associated with excitatory neurons, were never seen in these cells (Yasaka et al., 2010). These results are summarised in Figure 3-4 c

3.2.3 Dorsal root input to NPY-GFP cells

Dorsal root input was assessed in the NPY-GFP cells in the same manner as for the PrP-GFP cells, using the same stimulation protocol and the same criteria for identifying inputs. Altogether 39 NPY-GFP cells were tested for dorsal root input and EPSCs were evoked in 15 of these cells (38.5%). Eleven of these had monosynaptic C fibre input (73.3%), and 4 only received polysynaptic inputs from C-fibres. Examples of monosynaptic C fibre input are shown in Figure 3-5 a and b. Of the 11 cells that received monosynaptic C fibre input, 8 were seen to receive additional input. One of these additional inputs was monosynaptic Aδ, 2 were polysynaptic C fibre, 2 were polysynaptic Aβ, while 3 cells received both polysynaptic Aδ and Aβ input. In 2 cases, there were 2 monosynaptic C fibre EPSCs evoked in the same cell Figure 3-5 a, which had different latencies that could be distinguished. These data are summarised in Figure 3-5 c.

3.2.4 **NPY-GFP cell responses to capsaicin and icilin**

To test whether NPY-GFP cells received input from TRP channel-expressing primary afferent fibres, the frequency of mEPSCs were assessed in response to application of different TRP channel agonists. NPY-GFP cells were targeted for whole-cell recordings, and frequency of mEPSCs were measured before and 5 minutes after application of the TRPV1 and TRPM8 agonists capsaicin and icilin. For the experiments where the effects of icilin were tested, the bath temperature was again raised to 32°C to ensure that TRPM8 would not be active during the control recording. Most NPY-GFP cells did not respond to TRP agonists, as shown by a change in the distribution of inter event intervals by the Kolmogorov-Smirnov test (Figure 3-6). Only 2/12 of cells tested showed a significant increase in mEPSC frequency in response to capsaicin, and these significant increases were from 3.8 to 22.8 events per minute and 3.8 to 85 events per minute. None of the 8 cells tested responded to icilin.

The sensitivity of dorsal root evoked C fibre EPSCs to capsaicin was also assessed. Six monosynaptic eEPSCs evoked at C fibre strength from 4 NPY-GFP cells were tested for capsaicin sensitivity. Two of these cells had 2 separate C fibre components which were distinguishable and could be assessed independently. No differences were observed between the amplitude of these 6 responses before or during capsaicin application.

Taken together this suggests that although these cells receive input from C-fibres that do not commonly express TRPV1 or TRPM8, and are therefore unlikely to originate from peptidergic C-fibres or innocuous cooling fibres (Cavanaugh et al., 2011; Dhaka et al., 2008).

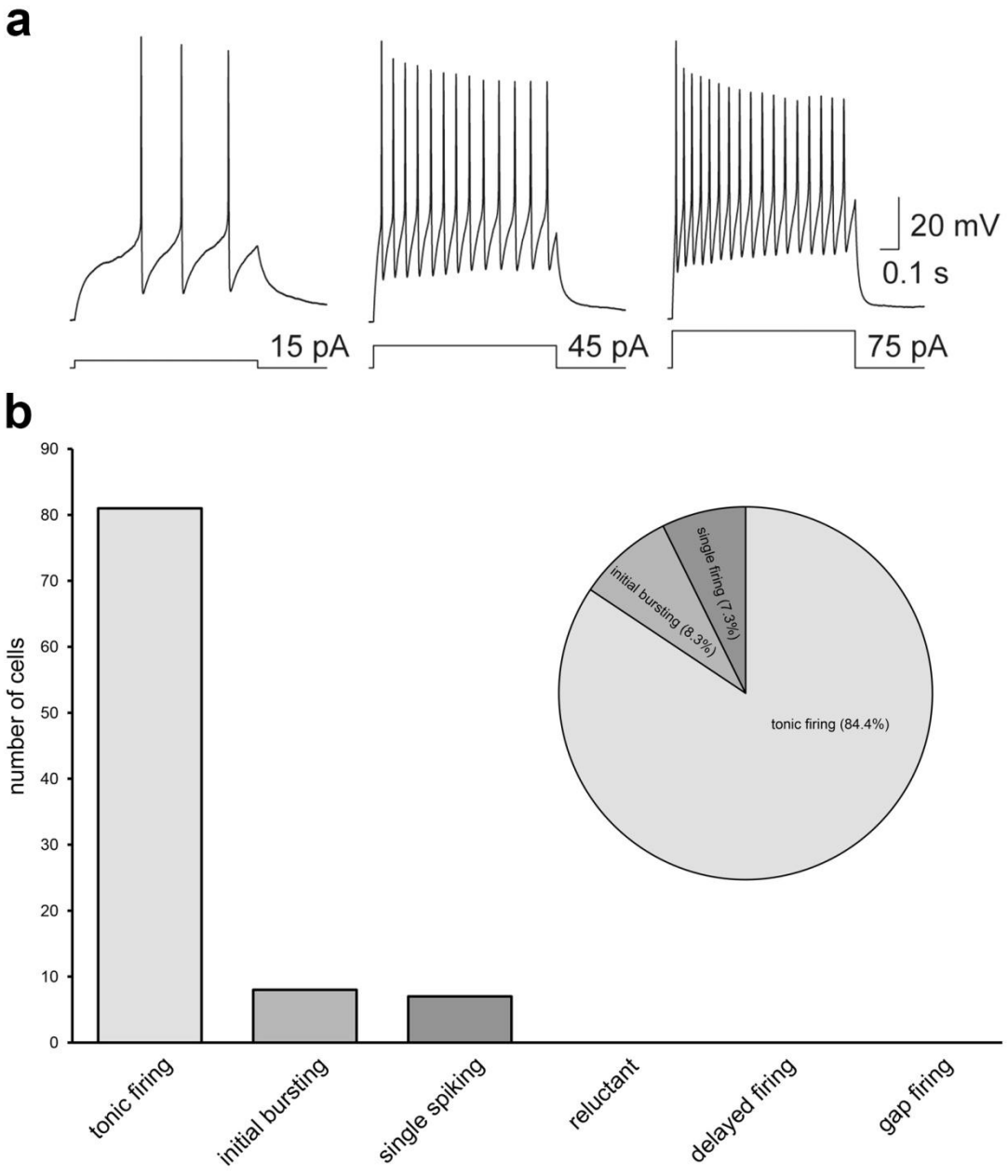
a
20 mV
0.1 s
15 pA
45 pA
75 pA
b
number of cells
90
80
70
60
50
40
30
20
10
0
tonic firing
initial bursting
single spiking
reluctant
delayed firing
gap firing
single firing (7.3%)
initial bursting (8.3%)
tonic firing (84.4%)

Figure 3-4 Action potential firing patterns in NPY-GFP cells

a, shows an example trace from a cell that displays tonic firing, and discharges action potential at a higher frequency with greater current injection. **b**, is a bar chart showing the number of NPY-GFP cells that exhibit a particular firing pattern, note that the vast majority of cells have a tonic firing pattern and no cells have a delayed, gap, or reluctant firing pattern. The inset displays this information as a pie chart and indicates the percentages of cells that show these firing patterns.

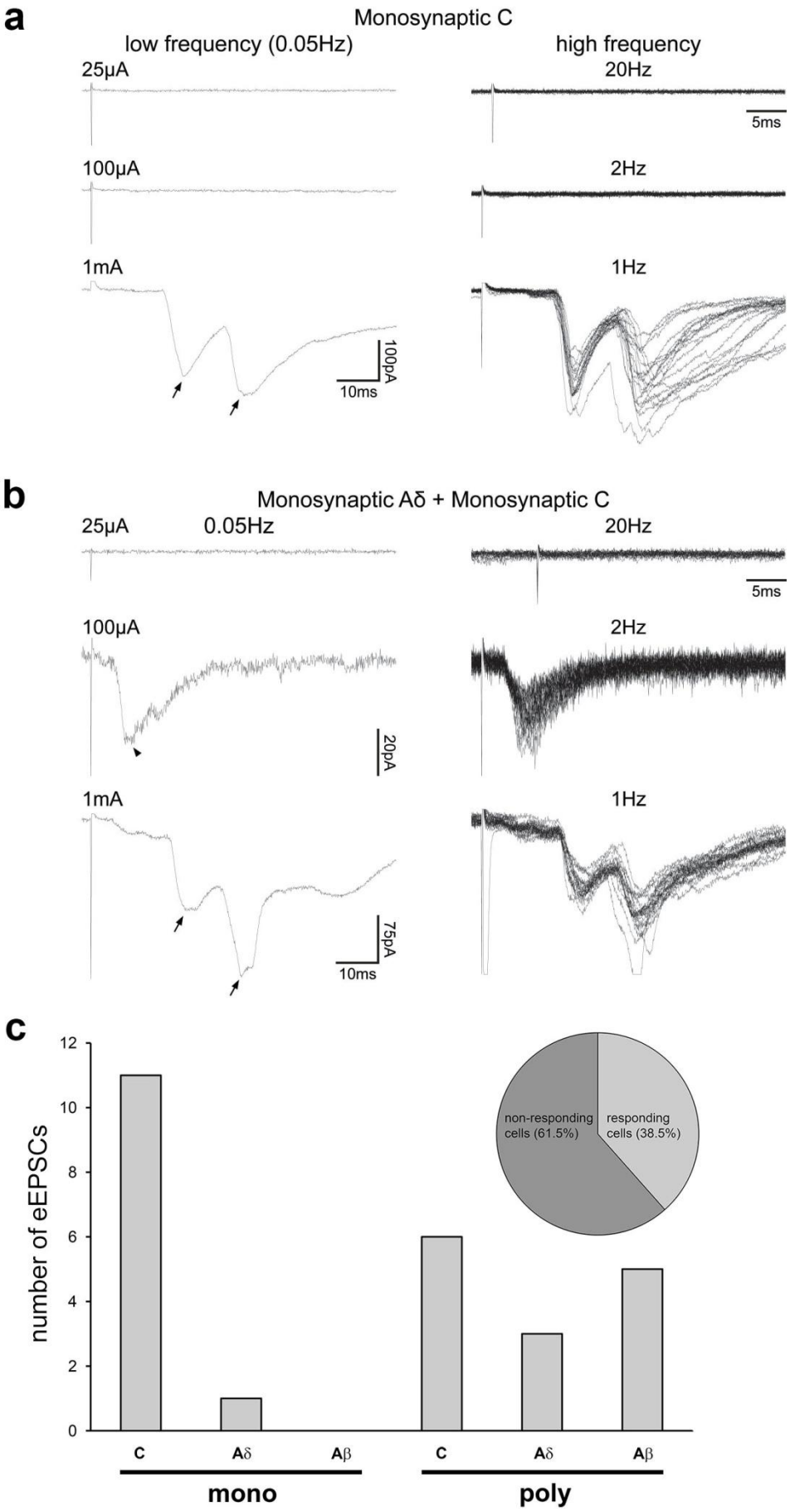
a
Monosynaptic C
low frequency (0.05Hz)
high frequency
25μA
20Hz
5ms
100μA
2Hz
1mA
1Hz
100pA
10ms
b
Monosynaptic Aδ + Monosynaptic C
25μA
0.05Hz
20Hz
5ms
100μA
2Hz
20pA
1mA
1Hz
75pA
10ms
c
number of eEPSCs
non-responding cells (61.5%)
responding cells (38.5%)
C
Aδ
Aβ
mono
poly

Figure 3-5 Primary afferent input to NPY-GFP cells determined by dorsal root stimulation experiments

a shows an example of a trace from a cell that receives monosynaptic C fibre input from dorsal root stimulation at 500 μA. Note that this trace has two distinct components evoked from stimulation at C fibre strength and both of these are monosynaptic, indicated by the lack of failures at high frequency stimulation of the dorsal root (1 Hz). **b** shows an example from a cell with monosynaptic input from Aδ and C-fibres. The response from Aδ fibres is shown at a stimulation intensity of 100 μA and there are no synaptic failures when stimulated at a higher frequency of 2 Hz. The C fibre component is evoked by stimulating the root at 500 μA and is able to follow high frequency stimulation without failure. Panels on the left show an averaged trace from three sweeps at a low frequency (0.05 Hz), and panels on the right show superimposed traces from 20 sweeps at high frequency stimulation of the dorsal root (Aβ = 20 Hz, Aδ = 2 Hz, and C = 1Hz). **c** is a bar chart summarising the eEPSCs generated in NPY-GFP cells by dorsal root stimulation. The pie chart illustrates the percentage of cells that responded to stimulation of the dorsal root.

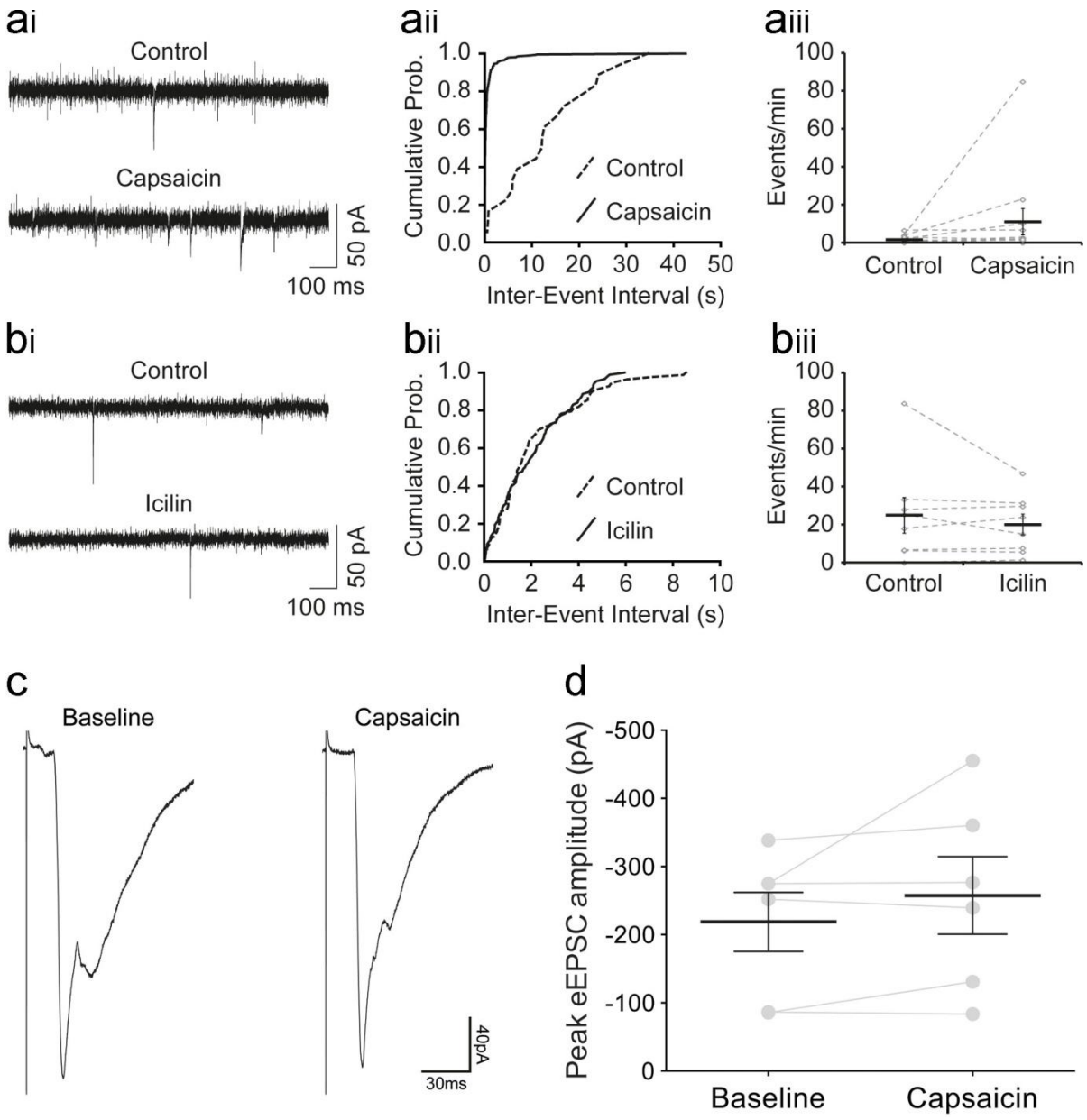
ai
Control
Capsaicin
50 pA
100 ms
aii
Cumulative Prob.
1.0
0.8
0.6
0.4
0.2
0.0
0 10 20 30 40 50
Inter-Event Interval (s)
Control
Capsaicin
aiii
Events/min
100
80
60
40
20
0
Control
Capsaicin
bi
Control
Icilin
50 pA
100 ms
bii
Cumulative Prob.
1.0
0.8
0.6
0.4
0.2
0.0
0 2 4 6 8 10
Inter-Event Interval (s)
Control
Icilin
biii
Events/min
100
80
60
40
20
0
Control
Icilin
c
Baseline
Capsaicin
40pA
30ms
d
Peak eEPSC amplitude (pA)
-500
-400
-300
-200
-100
0
Baseline
Capsaicin

Figure 3-6 Responses of NPY-GFP cells to bath application of TRP channel agonists capsaicin and icilin

ai shows an example trace where bath application of 2 μM capsaicin increased the frequency of mEPSCs, aii illustrates the change in distribution of inter event intervals before and after the application of capsaicin, and corresponds to the trace in **ai**. The shift of the distribution to the left during the capsaicin treatment indicates a reduction in the inter-event intervals (time between mEPSCs) and hence an increase in mEPSC frequency. **aiii** summarises the frequency of mEPSCs in NPY-GFP cells before and after capsaicin application, with the mean ± S.E.M displayed on the chart. Only 2/12 of these showed a significant change in the distribution of inter event intervals determined by the Kolmogorov-Smirnov test ($p < 0.05$). **bi** illustrates an example trace of an NPY-GFP cell before and during icilin application. **bii** shows the cumulative frequency plot of the distribution of inter event intervals before and during application of icilin for the trace shown in bi. The distribution appears to be the unaffected by application of icilin in this example. **biii** summarises the change in mEPSC frequency before and during the application of icilin for all NPY-GFP cells tested, with the mean ± S.E.M highlighted. None of the cells tested show a significant change in their distribution of inter-event intervals, which was tested using the Kolmogorov-Smirnov test. **c** show an example of a C fibre evoked response to dorsal root stimulation before and during capsaicin application. In this example the amplitude of the eEPSC is unaffected by the application of capsaicin. **d** summarises the amplitude of all C fibre eEPSCs tested with capsaicin, none of which are altered by capsaicin application determined using the Wilcoxon paired signed rank test.

3.3 Comparison of physiological parameters between cells that were recovered for morphological reconstruction and those that were not

In order to assess whether there was a systematic difference in physiological parameters measured between cells that were recovered for morphological reconstruction following recording and those that were not, the 14 physiological parameters were compared between PrP-GFP cells that were recovered for morphological reconstruction and those that were not. A similar comparison was performed between successfully filled NPY-GFP cells and those that were not. Certain action potential properties, such as height, width, rise and fall were seen to differ significantly between these groups for both PrP-GFP and NPY-GFP cells ($p < 0.05$, Student's t-test). However, passive membrane properties such as resting membrane potential, and most other active membrane properties were not seen to differ. Nevertheless, to avoid any systematic bias, only physiological parameters for cells that were recovered for morphology were used in the results chapter of this study. See sections 4.1.3, 4.1.6, and 4.3.2 for comparisons of physiological parameters between different groups of cells.

4 Results

4.1 PrP-GFP cells

4.1.1 Morphological features of recorded neurons

Eighty seven PrP-GFP cells from 53 animals were successfully filled with Neurobiotin and reconstructed for morphological analysis. The dendritic trees of six of these cells were extremely small and appeared to have been truncated. Therefore these cells were excluded from analysis of dendritic trees. Examples of these cell reconstructions are shown in Figure 4-1 and Figure 4-2. The 87 cells recovered for morphological reconstruction were from 82 different slice preparations, with a maximum of two cells per slice. These cells were sufficiently far apart to be distinguished during the cell reconstruction processes.

The PrP-GFP cell bodies were mostly found in lamina II (n = 70) but a minority were located in lamina III (n = 17). However, these were only seen in the dorsal region of lamina III. Dendrites were present in lamina II in all cases, and in 7 cases they also projected into lamina I. In most cases (48/81) dendrites were also found in lamina III, and in 3 cases these were present between laminae I-III. The axon was always present within lamina II and in virtually all cases the axon entered adjacent laminae (84/87). In 53 cells some of the axon was found in lamina I, and in the vast majority of cells (74/87) the axon also entered lamina III (data summarised in Table 4-1).

The PrP-GFP cells displayed a variety of shapes and sizes, but they generally appeared to be elongated in the rostrocaudal axis for both dendrites and axons. To measure the orientation of dendrites and axon for each cell, polar histograms were generated (Figure 4-3 b). To generate a polar histogram, the cell is projected onto the plane of section and the total length of process that projects within a certain range of angles is measured. All of the rostrocaudal segments were added together to give a single value for rostrocaudal length, and the dorsoventral segments were pooled to give a value for dorsoventral length. These measures give the direction in which dendritic trees and axonal arbors project overall, and these measurements are not skewed by a single process extending much further than the rest of the cell, which was seen in some instances (see Figure 4-1 c and e and Figure 4-2 c and d for examples). The scatter plot of rostrocaudal length against dorsoventral length shows that these cells do indeed have a general rostrocaudal orientation for both dendrites and axons (Figure 4-3 cii and dii). PrP-GFP cells showed a huge range in total process

length for both dendrites and axons, which are indicated by adding the rostrocaudal and dorsoventral components from each point together (Figure 4-3 cii and dii).

To compare these cells with similar populations described previously, the dendritic rostrocaudal and dorsoventral spread of each cell was measured. This gives a measure of how far the dendritic trees of cells extends in each axis, and these are criteria used by (Yasaka et al., 2007) to determine morphological classes. Central and islet cells were defined as having a ratio of rostrocaudal:dorsoventral dendritic spread (RC:DV spread) greater than 3.5, with central cells having a rostrocaudal spread less than 400 µm. Although this was measured for the rat and there are undoubtedly scaling differences between the mouse and the rat, there are currently no reports quantifying measures of different morphological classes of interneuron in the mouse dorsal horn. Nevertheless, these dimensions are used to give an indication of the category these cells would belong to according to this scheme. Contrary to what was reported previously by Hantman *et al* (2004) the PrP-GFP cells rarely fit the criteria for central cells, with few cells exhibiting a RC:DV spread greater than 3.5. (Figure 4-3 ci). The majority of these reconstructed cells would be unclassified according to the morphological classification scheme devised by Grudt and Perl, as they had somatodendritic shapes that were uncharacterised, or displayed morphological properties that were an intermediate of two different classes (examples shown in Figure 4-1 and Figure 4-2). Although PrP-GFP cells had a variety of somatodendritic shapes they were never islet cells, and none of them had a dendritic rostrocaudal spread greater than 400 µm (Figure 4-3 ci). In virtually all cases the axon extended further than the dendritic tree, which can be seen by comparing values for spread between axon and dendrite Figure 4-3 ci and di). As described previously, measures of axonal extent can be skewed by a single process extending far beyond the rest of the axonal arbors of a cell. Examples of this can be seen in the chart in Figure 4-3 ci, where some data points are outliers from the majority of the data.

The spine density of PrP-GFP cells was also highly variable (range = 0.9 – 16.3 spines/100 µm dendrite; mean = 6.8 spines/100 µm) (Figure 4-4). A major site for excitatory transmission is though the dendritic spines of neurons. To determine whether the excitatory input to the PrP-GFP cells was correlated with dendritic spine number, a scatterplot of spine number versus baseline mEPSC frequency recorded at room temperature was plotted (Figure 4-4). Only cells recorded at room temperature were included since previous studies have shown that the physiological properties and

excitability of cells recorded from spinal cord slices can vary with temperature (Graham et al., 2008). These data were only available for a subset of cells where pharmacological experiments were performed and complete dendritic morphology was recovered following these experiments. The spine number was strongly correlated with the baseline mEPSC frequency and indicates that part of the excitatory input to these cells is through dendritic spines ($R_s = 0.84$, $p < 0.001$; Spearman's rank order correlation test). Although this does not exclude the possibility of synaptic input onto the dendritic shafts of these cells, it does indicate that excitatory input to these cells is correlated with the number of dendritic spines.

Table 4-1 Distribution of dendritic and axonal processes of Neurobiotin-filled PrP-GFP cells

Laminae	Dendritic tree	Axonal arbor
I-II	4 (5)	10 (11)
I-III	3 (4)	43 (49)
II	29 (36)	3 (3)
II-III	45 (56)	31 (36)
Total	**81**	**87**

Number of cells with the distribution of their dendritic tree and axonal arbor present in different laminae, between laminae I-III. Number in parentheses refers to the percentage of all cells with a particular process distribution

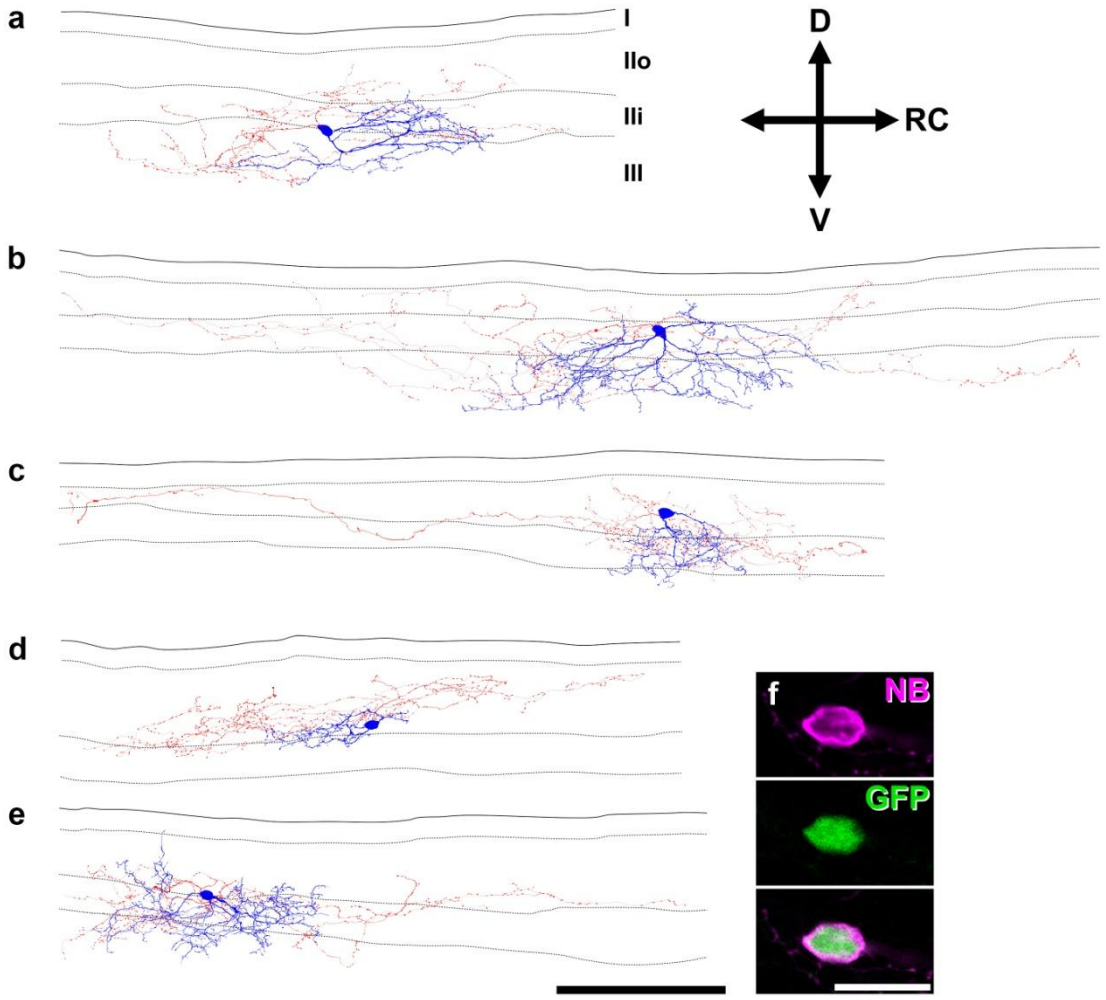
a
I
IIo
IIi
III
D
RC
V
b
c
d
e
f
NB
GFP

Figure 4-1 Neuronal morphology of PrP-GFP neurons that did not innervate lamina I Examples of five cell reconstructions from representative Neurobiotin-filled PrP-GFP cells that did not appear to innervate lamina I **(a-e)**. Dendrites and somata are displayed in blue, and axons are shown in red; laminar boundaries are labelled in **a,** and this same scheme is used for all cells. **f** illustrates a single optical section through the cell soma shown in **e** and demonstrates the presence of GFP in the soma. Neurobiotin is displayed as magenta and GFP is green in this image. Scale bar is 100µm in **a-e** and 20µm in **f,** GFP = green fluorescent protein, NB = Neurobiotin.

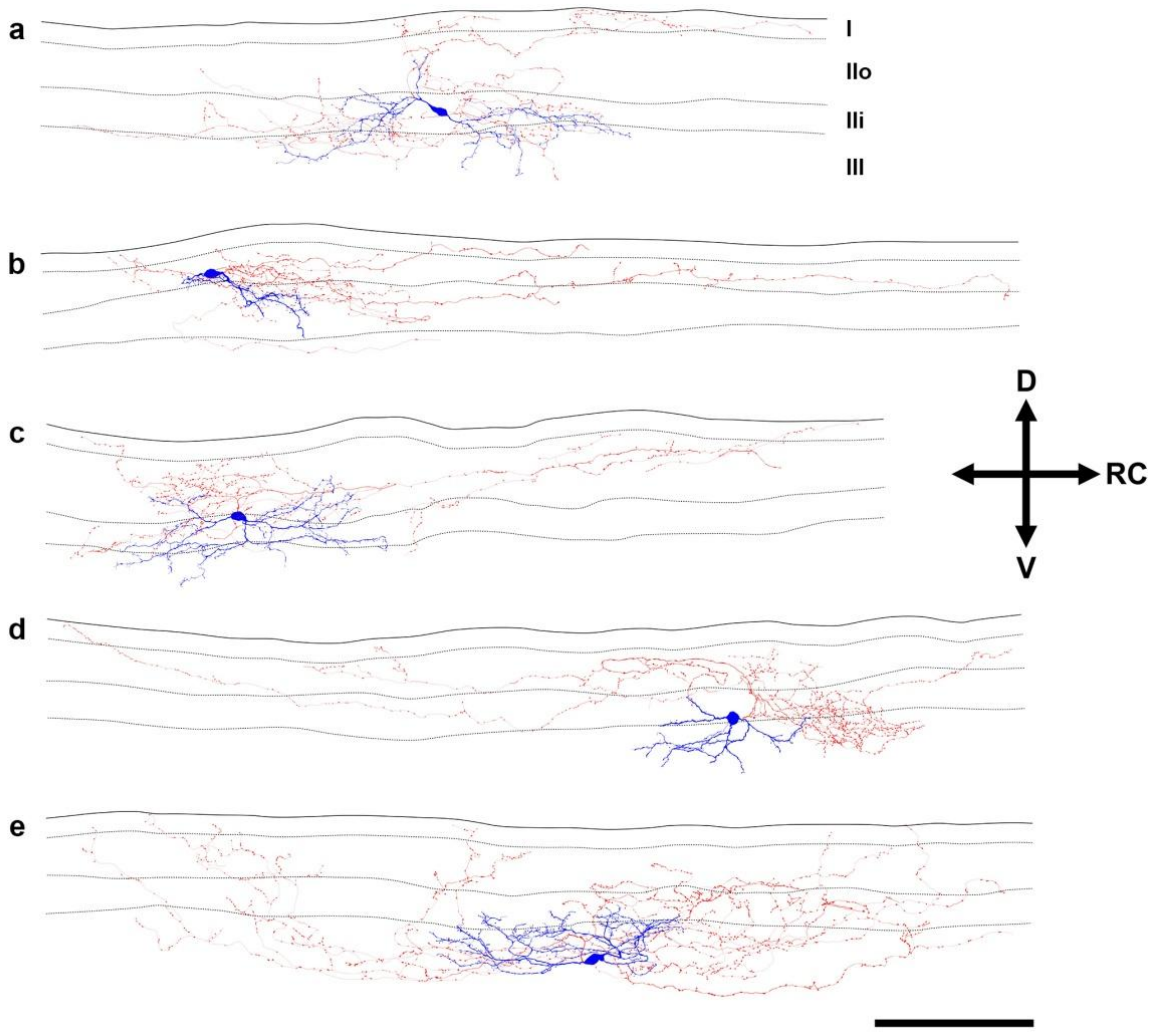
a
b
c
d
e
I
IIo
IIi
III
D
RC
V

Figure 4-2 PrP-GFP neurons that project their axon into lamina I

Examples of five PrP-GFP neuronal reconstructions of cells that innervate lamina I of the spinal cord (a-e). These cells all contained an axon that had 20 or more axonal boutons present in lamina I. Somata and dendrites are displayed in blue and axons are shown in red; laminar boundaries are labelled in **a,** and this same scheme is used for all cells. Inset shows the orientation of the cells in the parasagittal plane. D = dorsal, V = ventral, RC = rostrocaudal Scale bar is 100µm in **a-e**.

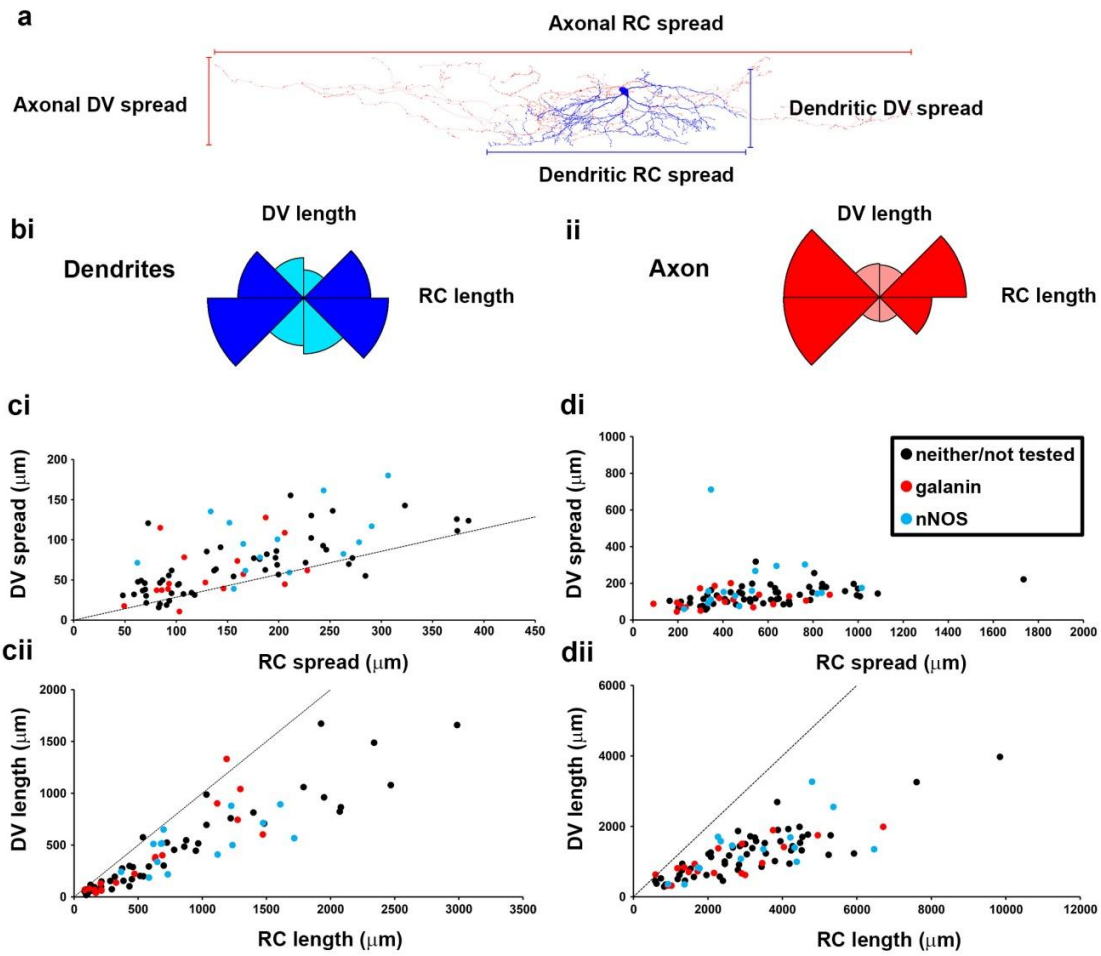
a
Axonal RC spread
Axonal DV spread
Dendritic DV spread
Dendritic RC spread
bi
Dendrites
DV length
RC length
ii
Axon
DV length
RC length
ci
DV spread (μm)
RC spread (μm)
di
DV spread (μm)
RC spread (μm)
neither/not tested
galanin
nNOS
cii
DV length (μm)
RC length (μm)
dii
DV length (μm)
RC length (μm)

Figure 4-3 Morphological characterisation of PrP-GFP neurons

a, Diagram explaining the measurement of rostrocaudal (RC) and dorsoventral (DV) spread in processes from a cell illustrated in Figure 4-1 b. **b,** Example polar histograms from the same cell for dendrites and axon, measuring the total length of process projecting in a particular direction, RC length is calculated from the sum of the darker octants and DV length is the sum of the remaining lighter coloured octants. **ci** Scatterplot showing RC spread plotted against DV spread for dendrites, a line of y = x/3.5 is included since a RC:DV ratio of 3.5 was used as a determining feature of central cells of the rat spinal cord in Yasaka *et al* 2007. **cii** is a scatterplot of RC length against DV length for dendrites and a line of y = x is included. **di** and **dii** are similar scatterplots to **ci** and **cii** except axonal measures are used instead of dendritic measures.

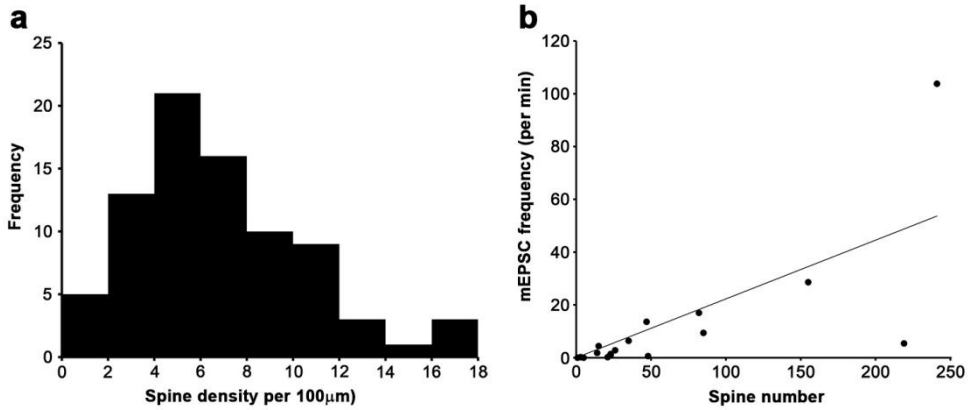
a
Frequency
Spine density per 100μm)
b
mEPSC frequency (per min)
Spine number

Figure 4-4 Spine density and correlation between spine number and synaptic inputs for PrP-GFP neurons

a, Frequency histogram showing the spine density per 100 μm of dendrite for PrP-GFP neurons, illustrating the large variability in spine density. **b,** A plot of spine number versus mEPSC frequency from whole-cell recordings of PrP-GFP cells taken at room temperature, there is a strong positive correlation between spine number and mEPSC frequency (Spearman's rank order correlation test, $p < 0.001$).

4.1.2 Post synaptic targets of PrP-GFP cells

Approximately one third (30/87) of the filled cells had an axon that entered lamina I and gave rise to considerable synaptic input to this lamina (>20 axonal boutons) (see Figure 4-2 for examples). These cells are of particular interest as GFP positive boutons from PrP-GFP animals are seen to provide input to various projection cells in lamina I, including NK1r-expressing projection neurons and giant cells, which are delineated by VGluT2 and VGAT boutons (Puskár et al., 2001; Ganley et al., 2015). Therefore it is likely that filled cells with an axon in lamina I include projection neurons among their post-synaptic targets. However, the axons from these PrP-GFP cells were never found exclusively in lamina I, and therefore these cells must also have post-synaptic targets in other laminae. Since projection neurons are rarely ever found in lamina II and the majority of the axons of the PrP-GFP cells are located in lamina II, this suggests that other interneurons are the main target of these cells. Examples of interneurons that are innervated by PrP-GFP cells have been reported previously (Zheng et al., 2010). Only a minority of cells have over 20 of their axonal boutons in lamina I, and the vast majority of the GFP boutons in contact with giant cells are from the nNOS-expressing subset (Ganley et al., 2015). Both of these features are only seen in around a third of all PrP-GFP cells; since cells only expressing nNOS represent 35% of the PrP-GFP cells and 34% of the recorded PrP-GFP cells (30/87) have an axon with over 20 boutons in lamina I. This suggests that these features are selective for a group of PrP-GFP cells, and these groups likely overlap somewhat. Taken together this suggests that the cells in contact with the projection neurons may represent a distinct subset of the PrP-GFP cells.

4.1.3 Using hierarchical cluster analysis to distinguish PrP-GFP cells that innervate lamina I from other PrP-GFP cells

Since the PrP-GFP cells could be divided into those that provided considerable input to lamina I and those that did not, they were likely to have different post-synaptic targets and could therefore have distinct functional roles in the dorsal horn microcircuitry. Since many recent studies have attempted to correlate somatodendritic morphology with function, this was tested on these cells using measures of somatodendritic morphology (Grudt and Perl, 2002; Yasaka et al., 2007, 2010). Hierarchical cluster analysis was performed on PrP-GFP cells that innervated lamina I (n = 30) and those that did not (n = 48) using 55 measures of somatodendritic morphology (see appendix). Many measurements were taken to ensure the clustering procedure was objective, and not due to a few select measures defined by the

operator. PCA was performed on a standardised dataset of z-scores of the morphological parameters, and the dimensionality of this dataset was reduced to 5 principal components, which maintained 63% of the original variance. These were chosen as the point where the eigenvalues reach a plateau on a scree plot of principal components (Figure 4-5 a). Hierarchical clustering using Ward's method did not separate PrP-GFP cells that innervated lamina I into distinct clusters from those that did not (Figure 4-5 b). This suggests that the two groups cannot be distinguished using these measures of somatodendritic morphology.

This same method of hierarchical cluster analysis with PCA was used to determine whether physiological parameters could be used to objectively distinguish the PrP-GFP cells that innervate lamina I from those that did not. This analysis only included those cells recorded at room temperature, (see electrophysiology data chapter, sections 3.1.4 and 3.2.4). This is because it is highly likely that the recorded physiological properties of cells will be affected by higher recording temperature (Graham et al., 2008). It was assumed that ion channel kinetics and the movement of ions in solutions would be altered at different temperatures, and therefore it would be inappropriate to include these cells together in the analysis. This hierarchical cluster analysis included 15 PrP-GFP cells that innervated lamina I and 22 PrP-GFP cells that did not innervate lamina I. Four principal components were identified that accounted for 78% of the original variance in the dataset, which again was determined from the point at which a scree plot reached a plateau (Figure 4-6 a). This hierarchical clustering failed to distinguish the two groups, and cells from both groups were found in the same clusters (Figure 4-6 b). This indicates that these physiological parameters are also insufficient for separating these cells into distinct groups.

When morphological and physiological parameters were combined for hierarchical cluster analysis of the 15 lamina I innervating PrP-GFP cells and the other 22 PrP-GFP cells, this also failed to separate cells into distinct groups. Five principal components were identified which accounted for 64% of the original variance of the dataset, and this was used to rescale a standardised dataset of z-scores for all parameters. Taken together this suggests that except for having an axon present in lamina I, these cells that innervate lamina I projection neurons are similar to other PrP-GFP cells and would be indistinguishable in terms of other parameters.

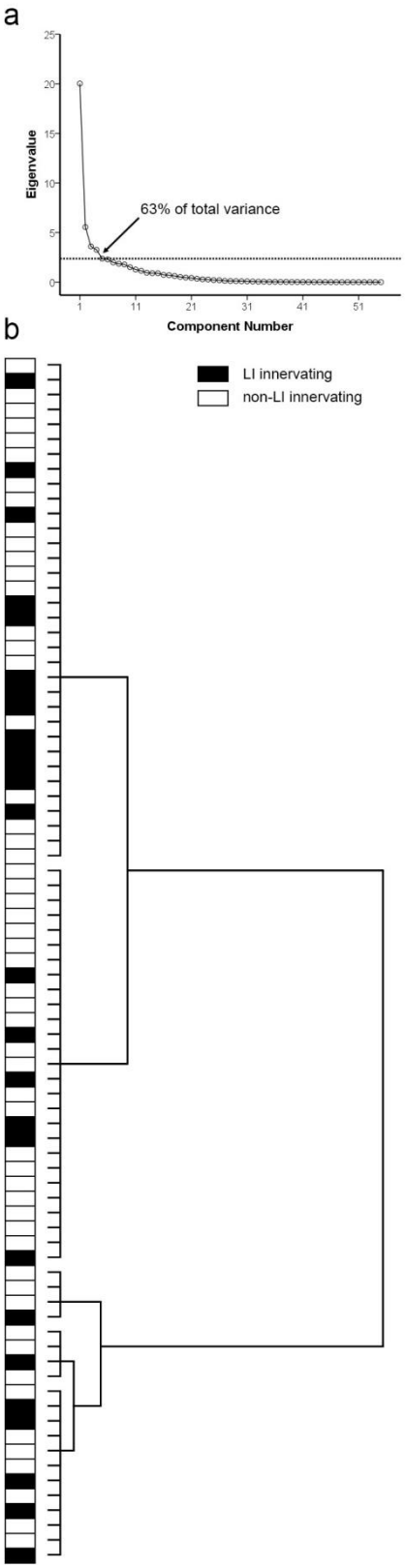
a
Eigenvalue
25
20
15
10
5
0
63% of total variance
1
11
21
31
41
51
Component Number
b
LI innervating
non-LI innervating

Figure 4-5 PrP-GFP cells that provide input to lamina I cannot be distinguished from other PrP-GFP cells based on somatodendritic morphology

a, Scree plot of principal components and their associated eigenvalues, dashed line indicates the point at which the plot reaches a plateau and determines the number of components retained for analysis. **b,** Dendrogram showing hierarchical clustering of PrP-GFP cells. Note that lamina I innervating cells are interspersed with those cells that do not innervate lamina I, and do not form distinct clusters.

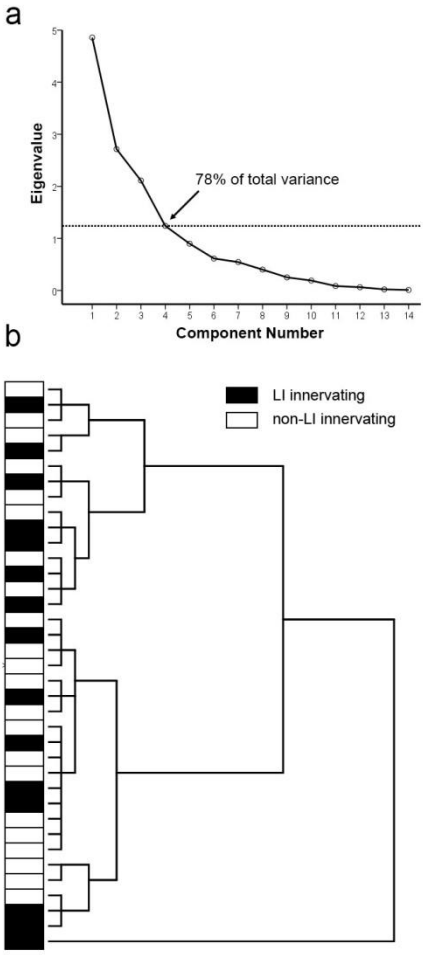
a
Eigenvalue
78% of total variance
Component Number
b
LI innervating
non-LI innervating

Figure 4-6 lamina I innervating PrP-GFP cells are not distinguishable from other PrP-GFP cells based on physiological parameters and cluster analysis

a, Scree plot generated from a dataset of parameters of active and passive membrane properties from cells that innervated lamina I and those that did not. The dashed line indicates where the plot was seen to reach a plateau by visual inspection, and this represents the number of principal components retained for hierarchical cluster analysis. **b,** Dendrogram showing the hierarchical clustering of PrP-GFP cells that innervated lamina I and those that did not using the first 4 principal components from the dataset. This method does not appear to separate the lamina I-innervating PrP-GFP cells from the non-lamina I-innervating cells into different groups

4.1.4 Effects of recording temperature on physiological membrane properties of PrP-GFP cells

To confirm that cells recorded at different temperatures would have differences in their physiological parameters 117 PrP-GFP cells that were recorded at room temperature and 34 PrP-GFP cells that were recorded at 32°C bath temperature were analysed with hierarchical cluster analysis using physiological parameters. PCA identified 5 principal components from a scree plot that accounted for 80% of the total variance (Figure 4-8 a). As predicted, the elevated bath temperature altered the membrane properties recorded, and this can be seen by the separation of these cells from those recorded at room temperature (Figure 4-8 bi). Complete separation was not achieved with 9 cells recorded at 32°C being included in other clusters, and 2 cells recorded at room temperature were clustered together with cells recorded at a higher bath temperature. Nevertheless, these groups of cells appeared to be genuinely distinct from one another, and incorrect assignment was probably a reflection of the variation in the dataset. This is also illustrated in the scatterplot of the first 2 principal components, where the cells recorded at room temperature are largely non-overlapping with those recorded at a higher temperature (Figure 4-8 bii). This minimal overlap in the scatterplot is likely correlated with the imperfect assignment of cells in the hierarchical cluster analysis. This confirms that the exclusion of cells recorded at a higher temperature from cluster analysis of physiological parameters was appropriate.

a

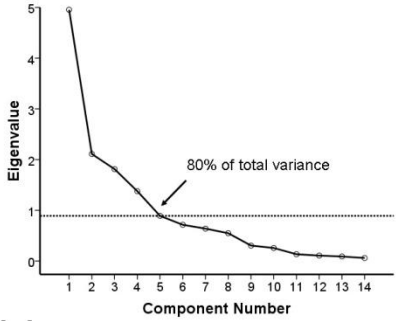
Eigenvalue
Component Number
80% of total variance
0
1
2
3
4
5
1 2 3 4 5 6 7 8 9 10 11 12 13 14

bi

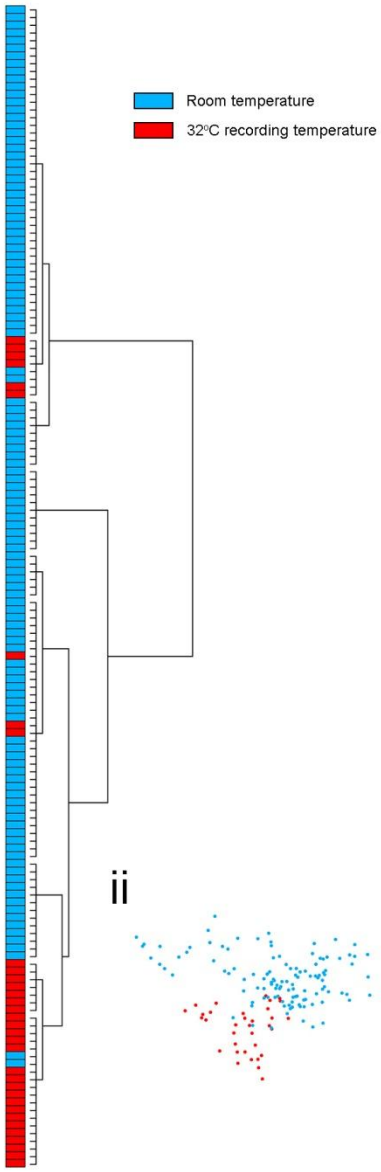
Room temperature
32°C recording temperature

ii

Figure 4-7 Recording temperature affects the physiological properties measured for cluster analysis

a Scree plot to determine the number of principal components to retain for hierarchical cluster analysis. This is generated from a dataset of physiological parameter for PrP-GFP cells recorded at room temperature or at an elevated temperature of 32°C. Five principal components are chosen as this is the point where the chart appears to plateau and this retains 80% of the variance of the original dataset. **bi** Dendrogram showing hierarchical clustering of PrP-GFP cells recorded at different temperatures based on the first 5 principal components of the dataset of physiological parameters. These different groups are largely separated with some misallocation of cells. **ii** A scatterplot of the first two principal components for PrP-GFP cells recorded at different temperatures. Cells appear to be separated in this plot and suggest that physiological parameters are different between cells recorded at different temperatures

4.1.5 Neurochemical features of recorded neurons

Following morphological reconstruction of the dendrites and axons from Neurobiotin-filled cells, the slices of spinal cord were resectioned at 60 µm and sections that contained the axon were immunostained for nNOS and galanin to determine the neurochemical phenotype of each cell. Galanin was only seen to be present in the axonal boutons of certain cells and had a granular appearance, whereas nNOS could be detected in both the axon and dendrites of immunoreactive cells and had a continuous appearance that filled processes (Figure 4-8 and Figure 4-9). This difference in appearance is because galanin is stored in dense core vesicles, whereas nNOS is present as a cytoplasmic protein and is free to diffuse into all parts of the cell (Valtschanoff et al., 1992b; Zhang et al., 1995). From 72 Neurobiotin-filled PrP-GFP cells tested only 15 were immunoreactive for nNOS and 18 were galanin-immunoreactive. The remaining 33 cells did not have detectable levels of nNOS or galanin in their axonal boutons, or detectable levels of nNOS in their somata and dendrites. Furthermore no cells were seen to express both galanin and nNOS, which coexists in 35% of PrP-GFP cells (Iwagaki et al., 2013). This is likely due to the contents of the cell being diluted by the intracellular solution of the recording electrode during the whole-cell recording, and hence only those cells with an initially high level of galanin or nNOS will have detectable levels remaining after a recording.

Since a subset of recorded PrP-GFP cells could be classified as containing nNOS or galanin, it was possible to see whether there were any morphological differences between these two groups (graphs in Figure 4-3 distinguish nNOS and galanin cells). It was found that the dendritic trees of nNOS-containing cells had a significantly greater spread in all axes than those of the galanin-containing cells, although the dendritic length did not differ significantly in any of these axes (table 4-2). This suggests that the nNOS-containing cells project their dendrites over a larger area than the galanin-containing cells, but do not significantly differ in total dendritic length. The axonal projections were also found to extend significantly further in nNOS cells in the dorsoventral and mediolateral axes, but this was not found for the total length of axon extending in these axes. Although morphological differences were found between these neurochemical groups, their shapes did not appear to be different and the measures that differed were associated with scale. In other words, the processes from the nNOS cells extended further than those of the galanin cells in all axes, and therefore these groups would not appear to have different shapes.

These groups therefore would not be distinguished using the Grudt and Perl classification scheme of lamina II neurons.

To compensate for variations in thickness of the superficial dorsal horn between slices, the soma location was expressed as a percentage of the distance from the dorsal white matter to the lamina II/III border. The lamina II/III border was taken to be 100% and values greater than this were assigned to cells that were located in lamina III, with values between 0 and 100% indicating a soma within laminae I and II. The nNOS-containing cells were found to be significantly more ventral than the galanin-containing cells, and the mean values for these were 83 and 61% respectively (unpaired t-test, $p < 0.05$) (table 4-2). This is in agreement with previous findings that galanin-expressing PrP-GFP cells are on average more dorsally located than the nNOS-expressing PrP-GFP cells (Iwagaki et al., 2013).

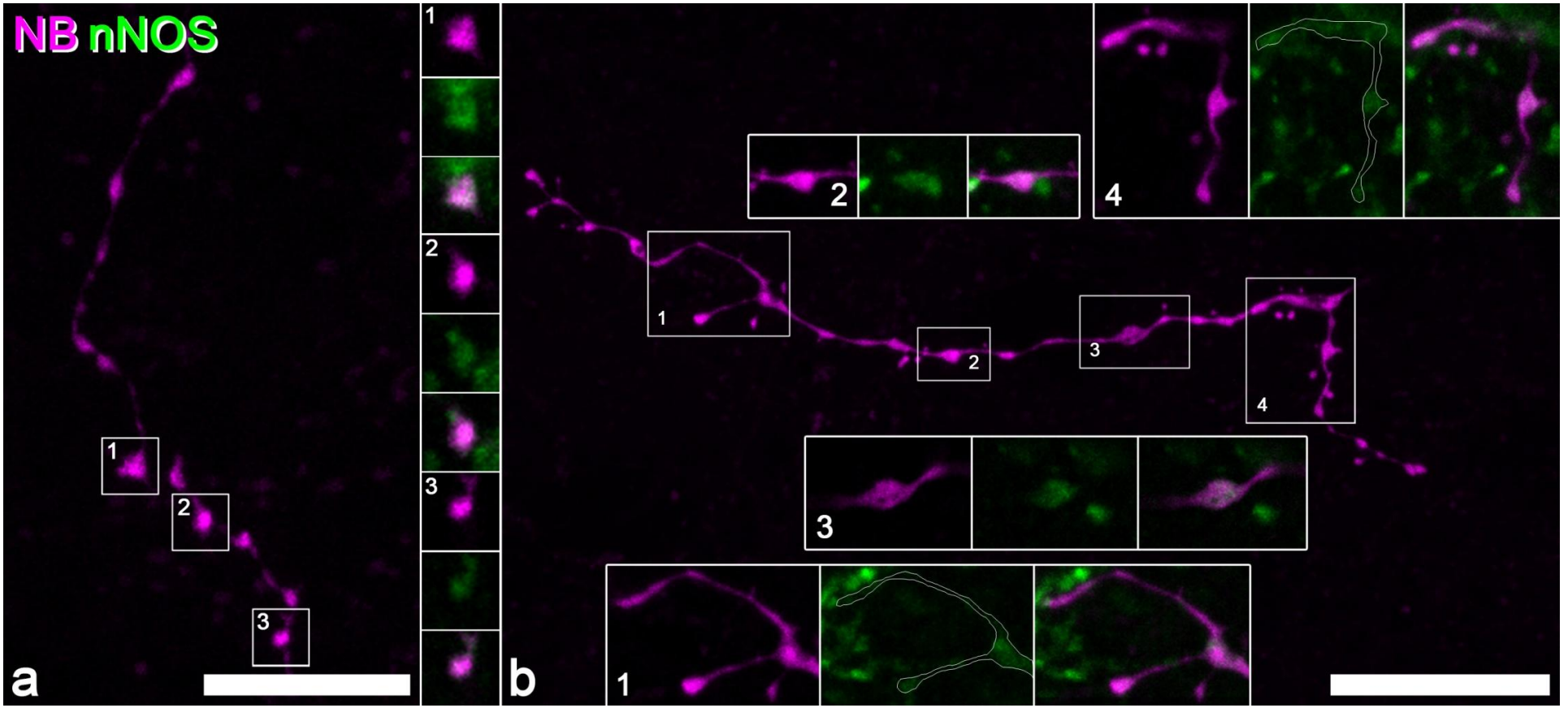
NB nNOS
a
b
1
2
3
4

Figure 4-8 Detectable levels of nNOS in the axon and dendrites of PrP-GFP neurons confirmed by immunocytochemistry

a, Example of a Neurobiotin-filled axon from a PrP-GFP cell that contains nNOS in its axonal boutons, shown as a projection of eight optical sections (0.5 µm z-spacing). Insets 1-3 are enlarged images of regions highlighted in the figure and are single optical sections **b,** Example of a stretch of dendrite from a PrP-GFP cell, shown as a projection of 21 optical sections (0.5 µm z-spacing). Insets 1-4 show that certain regions of dendrite contain detectable levels of nNOS due to its presence in the cell cytoplasm (insets 1 and 3 are projections of 3 images and insets 2 and 4 are single optical sections). Scale bar in **a** is 10 µm and is 20 µm in **b.**

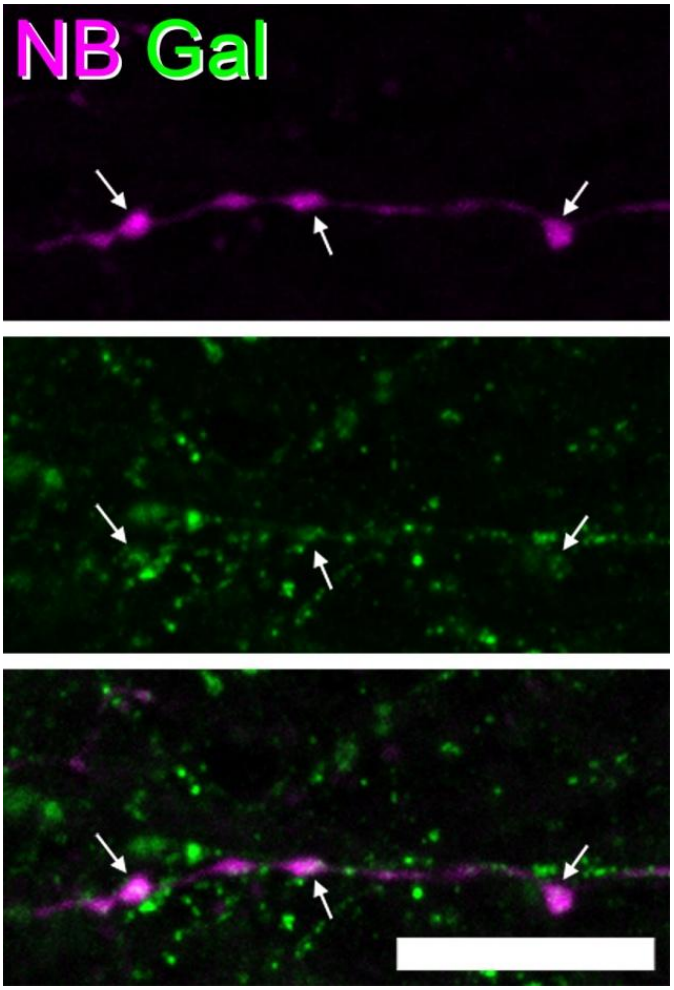
NB Gal

Figure 4-9 Galanin presence in PrP-GFP axons

An example of an axon from a Neurobiotin-filled PrP-GFP neuron that contains galanin in its axonal boutons, which are indicated by arrows. Images are projections of 4 optical sections (0.5 µm z-spacing) and the scale bar is 10 µm.

Table 4-2 Comparison of morphological parameters between nNOS- and galanin-expressing PrP-GFP cells

	Measure	Galanin	nNOS	P Value
Soma	Soma Depth (%)	61 ± 16	83 ± 42	0.023*
Dendrites	RC spread (µm)	133 ± 54	201 ± 69	0.0053**
	DV spread (µm)	59 ± 34	100 ± 40	0.0048**
	ML spread (µm)	37 ± 21	58 ± 21	0.010*
	RC length (µm)	629 ± 489	957 ± 431	0.063
	DV length (µm)	411 ± 402	510 ± 223	0.43
	RC:DV ratio	1.97 ± 0.90	2.03 ± 0.79	0.86
	Spine density (per 100 µm)	5.2 ± 2.3	7.4 ± 4.3	0.085
Axon	RC spread (µm)	423 ± 217	538 ± 230	0.152
	DV spread (µm)	110 ± 44	199 ± 160	0.0308*
	ML spread (µm)	65 ± 24	105 ± 65	0.037*
	Bouton density (per 100 µm)	11.4 ± 3.1	11.1 ± 2.5	0.69
	Axon length (µm)	3584 ± 2039	4675 ± 2183	0.15
	RC length (µm)	2560 ± 1590	3265 ± 1611	0.21
	DV length (µm)	1008 ± 518	1386 ± 762	0.10
	RC:DV ratio	2.6 ± 1.0	2.6 ± 1.0	0.97

Measurements of soma position, dendritic length and axonal length, and values are compared between nNOS- and galanin-expressing cells using unpaired Students t-test. In all cases the mean ± standard deviation are shown. Measurements that show a significant difference are highlighted in yellow, significance is taken at $p < 0.05$ (*) and 0.01 (**)

4.1.6 **Distinguishing galanin from nNOS expressing PrP-GFP cells**

There were many statistically significant morphological differences between nNOS- and galanin-expressing PrP-GFP neurons, and it could be possible to distinguish them objectively based on morphological parameters. To test this, cluster analysis was performed on PrP-GFP cells for which complete morphological data and neurochemical phenotype were available; this sample included 16 galanin- and 14 nNOS-expressing cells. From 108 morphological parameters 10 principal components were identified which accounted for 78% of the variance in the dataset, and these were selected by visual inspection of a scree plot of eigenvalues where the gradient reached a plateau (Figure 4-10 a). The dataset was then rescaled in terms of these 10 principal components, and hierarchical cluster analysis was performed on this dimension-reduced dataset. Although perfect separation of nNOS from galanin cells was not possible, the cluster analysis could broadly separate these two groups of cells in terms of morphological parameters (Figure 4-10 b). This indicates that there is a notable difference between these cells in terms of morphological features.

It was not possible to perform cluster analysis on these groups of cells using physiological membrane properties, as there were too few examples of cells for which neurochemistry was confirmed for cluster analysis to be performed reliably (10 nNOS and 8 galanin). Some cells had drugs applied which prevented their active membrane properties from being measured, and others were recorded at a higher bath temperature that would alter their membrane properties. This meant that it would be inappropriate to group cells together that were recorded at different temperatures (see section 4.1.4 above). Although cluster analysis could not be performed on such a small sample of cells, it was possible to compare the measured physiological parameters between these two groups. These comparisons demonstrated that nNOS-expressing PrP-GFP cells differed from galanin expressing cells in several action potential properties, such as action potential height, width and fall ($p < 0.05$ for action potential width, $p < 0.01$ for action potential height and fall; Student's unpaired t-test). These values are summarised in Table 4-3 and show nNOS cells have greater action potential height, smaller action potential width, and a more rapid repolarisation. This suggests that the nNOS cells have taller thinner action potentials than the galanin-expressing cells. The value for input resistance also differed significantly between nNOS and galanin cells with galanin cells having a higher input resistance (galanin = 1142 ± 714 MΩ, nNOS = 632 ± 262 MΩ; $p < 0.05$).

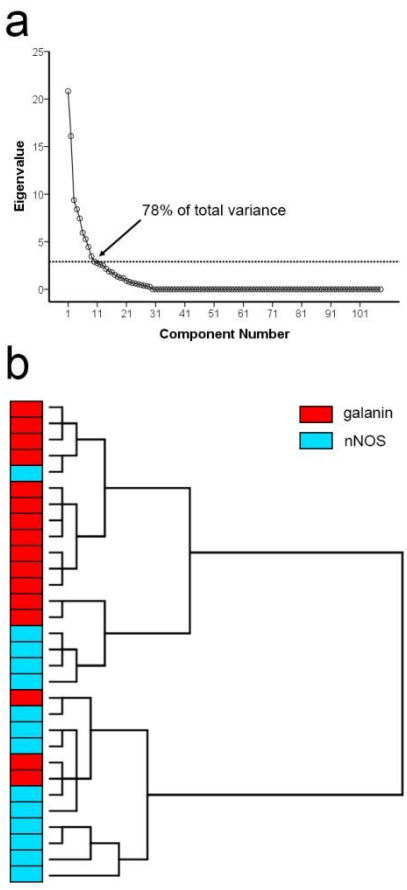
a
Eigenvalue
25
20
15
10
5
0
78% of total variance
1
11
21
31
41
51
61
71
81
91
101
Component Number
b
galanin
nNOS

Figure 4-10 Distinguishing nNOS and galanin expressing PrP-GFP cells using hierarchical cluster analysis

ai, Scree plot of principal components identifies 10 principal components based on the point where the gradient of the plot begins to plateau. **b,** Dendrogram generated from hierarchical clustering of cell morphological data rescaled in terms of the first 10 identified principal components. Cells that were seen to contain nNOS and galanin can be broadly distinguished from each other based on morphological parameters. However, misallocation of cells is seen in 6 cases. Blue = nNOS-expressing and red = galanin-expressing cells.

Table 4-3 Passive and active membrane properties in galanin- and nNOS-expressing PrP-GFP cells

Physiological parameter	Galanin	nNOS	p-value
IV slope (nS)	1.2 ± 0.7 [a]	1.8 ± 0.6	0.068
Input resistance (MΩ)	1142 ± 714 [a]	632 ± 262	0.048*
Resting membrane potential (mV)	-54.9 ± 11.0 [a]	58.3 ± 10.3	0.485
Rheobase current (pA)	22.9 ± 12.6	34.2 ± 13.6	0.090
Latency to first action potential (ms)	258 ± 132	279 ± 129	0.738
Action potential threshold (mV)	-30.6 ± 3.0	-33.0 ± 3.5	0.132
Action potential height (mV)	46.6 ± 8.0	59.4 ± 10.1	0.010**
Afterhyperpolarisation (mV)	25.4 ± 3.7	28.5 ± 4.0	0.107
Action potential width (ms)	4.0 ± 0.7	2.8 ± 1.4	0.049*
Action potential rise (mV/ms)	50.6 ± 12.4	83.6 ± 49.3	0.085
Action potential fall (mV/ms)	-27.8 ± 7.6	-50.5 ± 21.6	0.012*
Maximum firing frequency (Hz)	22.1 ± 6.0	25.2 ± 6.3	0.315
Spike frequency adaptation	0.56 ± 0.10	0.51 ± 0.18	0.438
Drop in action potential height (mV)	9.2 ± 10.8	8.3 ± 8.1	0.846

Comparisons of different membrane properties between PrP-GFP cells that were confirmed as nNOS or galanin expressing. nNOS n = 10, galanin n = 8, for values indicated with [a] galanin n = 10. Measurements showing a significant difference are highlighted in yellow, significance is taken at $p < 0.05$ (*) and $p < 0.01$ (**) using Student's unpaired t-test

4.1.7 **Inputs and outputs of PrP-GFP cells**

In the previous chapter (electrophysiology data, section 3.1.4) it was reported that PrP-GFP cells received monosynaptic input from TRPV1- and TRPM8-expressing C-fibres, and that C-fibre input could be recorded from dorsal root stimulation experiments. However, in these experiments only one example of monosynaptic input from myelinated fibres was recorded. To assess anatomically whether PrP-GFP cells received inputs from myelinated afferent fibres, 60 µm sections that contained part of the dendritic tree were immunoreacted for VGluT1, and contacts onto dendritic spines were counted. The majority of VGluT1 immunoreactivity in laminae IIi – III is from myelinated LTMRs, and these are non-nociceptive afferent fibres (Todd et al., 2003a). Only contacts onto dendritic spines were counted as these are major sites of excitatory input to cells and are therefore more likely to be synaptic than contacts onto dendritic shafts. This is supported by the finding that spine number is strongly correlated with the mEPSC frequency in these cells (Figure 4-4). Only VGluT1 boutons in laminae IIi – III was counted, as VGluT1-IR boutons found dorsal to lamina IIi are more likely to originate from sources other than LTMRs, such as descending input from the forebrain (Todd et al., 2003)

All six tested cells received contacts from VGluT1-expressing axonal boutons onto dendritic spines. Five of these cells possessed an axon that entered lamina I, and two cells responded to capsaicin during pharmacological experiments (see electrophysiology chapter section 3.1.4 for details). One of these cells both possessed an axon that entered lamina I and responded to capsaicin (illustrated in Figure 4-11). For all cells tested between 26-93 spines within laminae IIi and III were counted (the counts for the individual cells are displayed in table 4-3). For the lamina I-innervating cells between 7-31 contacts from VGluT1-immunoreactive boutons were identified, and this represented 14-39% of spines counted in laminae IIi and III (example shown in Figure 4-12). For the capsaicin responsive cells 12 and 10 contacts from VGluT1-immunoreactive boutons onto dendritic spines were counted, and this represented 15 and 39% of counted spines (table 4-3). This suggests that these PrP-GFP cells with dendrites present in laminae IIi-III receive input from LTMRs. It also suggests convergence of primary afferents with different sensory modalities onto the same cell, since cells that receive input from capsaicin sensitive fibres are also innervated by LTMRs. In addition it suggests there could be feed forward inhibition to projection neurons from LTMRs, because cells that project their axons into lamina I also receive contacts from VGluT1-immunoreactive mechanosensory fibres.

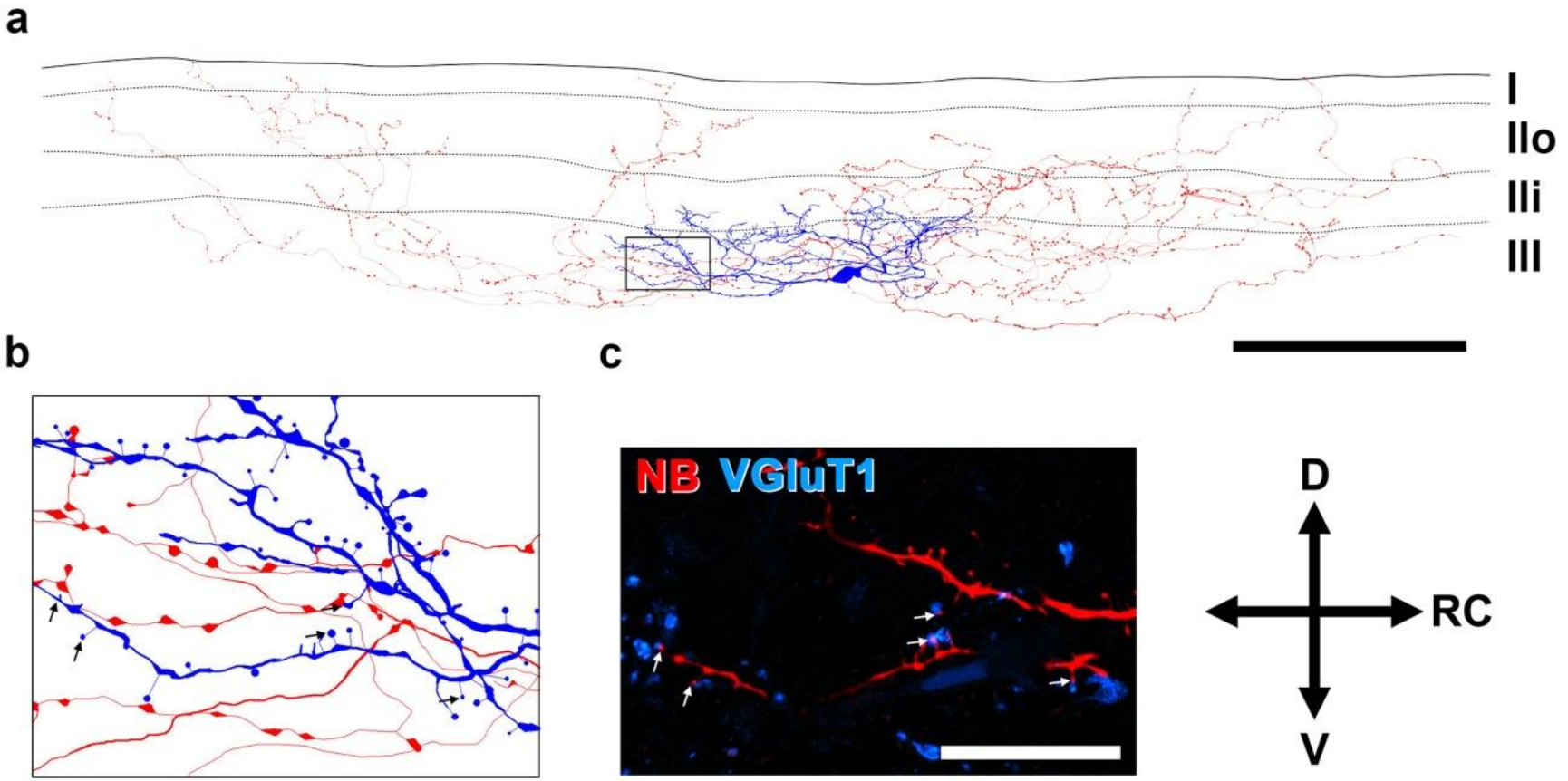
a
I
IIo
IIi
III
b
c
NB VGluT1
D
RC
V

Figure 4-11 VGluT1-IR inputs from low threshold mechanoreceptors to a capsaicin responsive PrP-GFP cell

a, Cell reconstruction of a cell that both projects its axon into lamina I and responds to bath application of capsaicin. **b,** Enlargement of the boxed region in **a** showing an area of dendrites with dendritic spines. **c,** Immunostaining for VGluT1 demonstrates that dendritic spines from the Neurobiotin-filled PrP-GFP cell receives contacts from VGluT1-IR boutons, which are likely to originate from low threshold mechanosensory fibres. Arrows in b and c indicate spines that are contacted by VGluT1-IR boutons. Image in **c** is a projection of 4 optical slices (0.5 µm z-spacing).

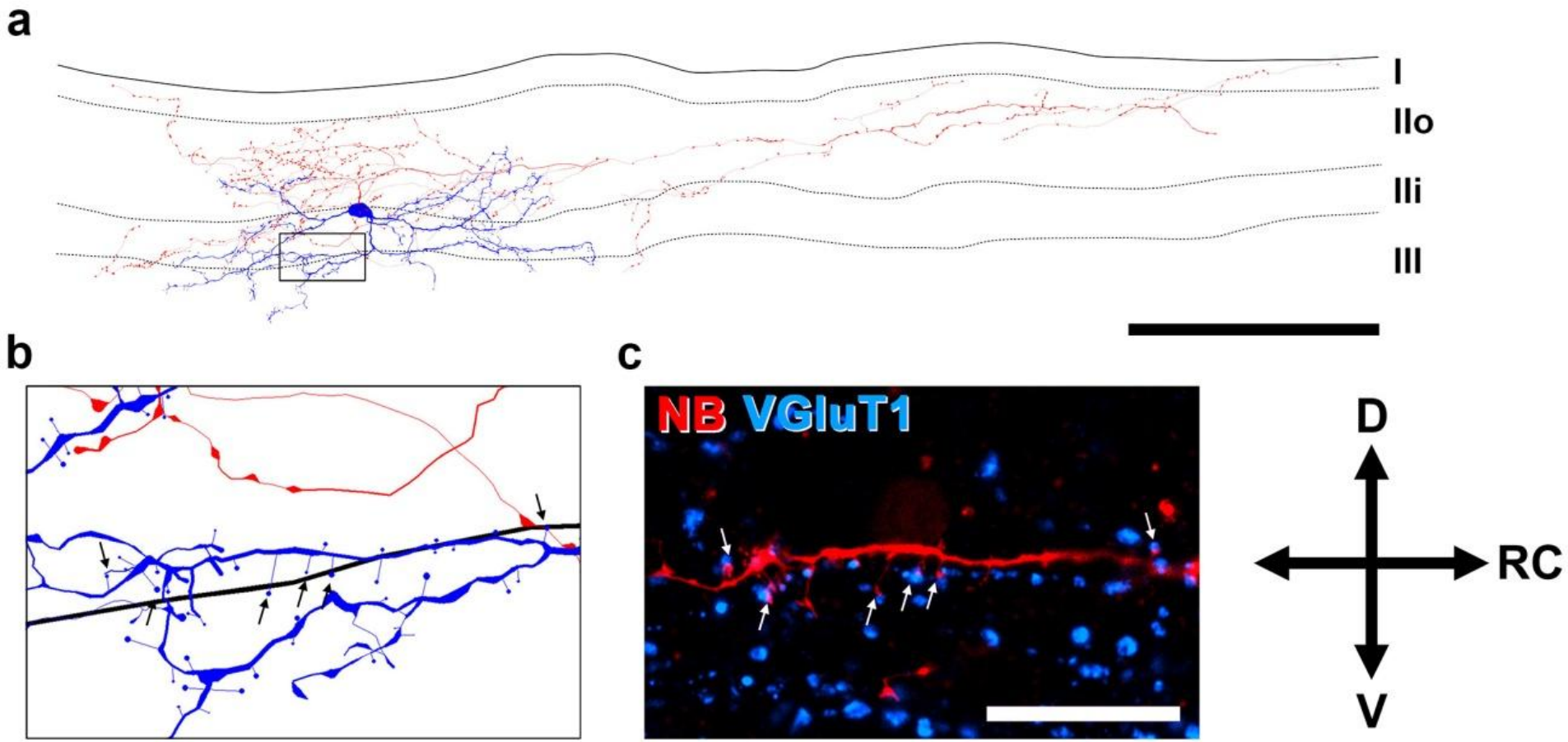
a
I
IIo
IIi
III
b
c
NB VGluT1
D
RC
V

Figure 4-12 VGluT1-IR boutons from low threshold mechanoreceptors contacting spines of a filled PrP-GFP cell that innervates lamina I

a, Cell reconstruction of a cell that projects its axon into lamina I, which contains 20 or more axonal boutons in this lamina. **b,** Enlargement of the boxed region in **a** showing a stretch of dendrite and dendritic spines. **c,** Immunostaining for VGluT1 shows contacts between Neurobiotin-filled dendritic spines and VGluT1-IR boutons from low threshold mechanosensory fibres. Arrows in b and c indicate spines that are contacted by VGluT1-IR boutons. Image in **c** is a projection of 4 optical slices (0.5 µm z-spacing), scale bar in **a** is 100 µm and 20 µm in **c**.

Table 4-4 VGluT1 input onto dendritic spines of Neurobiotin-filled PrP-GFP cells

Over 20 axonal boutons in lamina I	Responsive to capsaicin	Spines counted	Spines with contact from VGluT1-IR boutons
Yes		89	31 (35)
Yes		93	25 (27)
Yes		50	7 (14)
Yes		66	16 (24)
	Yes	82	12 (15)
Yes	Yes	26	10 (39)

Table showing the counts of dendritic spines contacted by VGluT1-IR boutons in individual PrP-GFP cells. Number in parentheses refers to the percentage of contacts from spines counted

4.2 NPY-GFP cells

4.2.1 Morphological features of NPY-GFP cells

The relationship between expression of NPY and GFP in the NPY-GFP mouse was assessed to see whether this mouse line reliably labelled the NPY-expressing interneurons in the dorsal horn (Table 4-1). In the NPY-GFP mouse, GFP-expressing cells were immunoreactive for NPY in 85.1% of cases, and this was similar for superficial laminae and those in lamina III. The expression of GFP preferentially labelled the NPY-immunoreactive cells in lamina III (81.5%) and the cells in superficial laminae were not as frequently labelled (33.4%). Therefore the NPY-GFP cells that are targeted for whole-cell recording are more likely to be located in lamina III as these are more frequently labelled with GFP (A.J. Todd and E. Polgár unpublished data).

From the NPY-GFP experiments, 65 cells from 41 animals were successfully filled with Neurobiotin and could be reconstructed for morphological analysis. Similar to the PrP-GFP cells, the dendritic trees of some of the NPY-GFP cells appeared to be truncated and displayed very short and beaded dendrites. Seven cells exhibited this and were discarded from analysis of dendritic tree morphology but were included in analysis of axonal arbors. Analysis of dendritic trees was possible for the remaining 58 cells. The 65 NPY-GFP cells successfully reconstructed for analysis were from 58 different slices, with a maximum of three cells recovered in a slice. Again, these cells were sufficiently far apart to be reconstructed without any difficulty determining which processes belonged to which cell.

The dendrites of reconstructed cells displayed a variety of morphological shapes and sizes. However, these cells were never seen to have islet morphology, which is the only morphological cell type consistently found to have an inhibitory phenotype (Grudt and Perl, 2002; Yasaka et al., 2007). Approximately two thirds of NPY-GFP cells were located in lamina III (42) and the rest of the cells had their cell bodies in lamina II (23). The dendritic trees of these cells were found in laminae I-III, with the vast majority of cells having dendritic trees that were present in both laminae II and III (41/58) (Table 4-6). Some cells had dendrites only present in lamina III (10), and fewer had dendrites that were restricted to lamina II (3). No filled NPY-GFP dendritic trees were found exclusively in

lamina I, but 4 cells had some of their dendritic tree present in lamina I and in 3 of these cases the dendrites spread between laminae I-III.

Axonal arbors of NPY-GFP cells were similarly distributed with over three quarters of these being present in both laminae II and III (50/65). Cells were never found to have an axon restricted to lamina II, but in 4 cases cells had an axon found exclusively in lamina III. Eleven NPY-GFP cells had an axon present in lamina I and in 10 of these cases the axon was found to extend between laminae I-III. The distribution of filled NPY-GFP processes is summarised in Table 4-6 and examples are shown in Figure 4-13 and Figure 4-14.

The mean spread of dendrites in rostrocaudal, dorsoventral and mediolateral axes for NPY-GFP cells were 166, 90, and 50 µm respectively. In general the cells were found to have their dendrites extended in the rostrocaudal axis relative to the other axes, and the majority of the dendritic trees were flattened in the mediolateral axis. A similar pattern was seen for the axon of these cells, with the axonal arbors of NPY-GFP cells being extended in the rostrocaudal axis (mean = 390 µm) and flattened in the mediolateral axis (mean = 69 µm). The mean dorsoventral spread for the axons of these cells was 145 µm, and these data for dendritic and axonal spread are summarised in Table 4-7. In some of the cell reconstructions there was a notable dorsoventral spread of axons and dendrites, as opposed to the general rostrocaudal spread seen in the PrP-GFP and other NPY-GFP cells (Figure 4-14).

Since the superficial dorsal horn (laminae I-II) and the deep dorsal horn (III-VI) are the termination sites for nociceptive and non-nociceptive afferent fibres respectively, the cells present in these different laminae are likely to belong to different functional populations. Furthermore the Grudt and Perl classification scheme only included cells in lamina II and may not apply to cells in deeper laminae for which much less is known. The organisation of the deep dorsal horn appears different to that of superficial layers, and it was possible that there were morphological or physiological differences between cells present in different laminae. To test this possibility the NPY-GFP cells were divided into two groups, those with cell bodies located in lamina II and those with cell bodies in lamina III.

The total length of dendritic tree was similar between NPY-GFP cells in lamina II (22) and lamina III (36) (mean values 1296 and 1311 µm respectively). The dendritic extent in the different axes was compared, and the spread in the rostrocaudal and mediolateral axes was

not significantly different (Table 4-7). The mean values for dorsoventral spread of the dendritic trees for lamina II and lamina III cells were 68 and 101 µm respectively, and these were seen to be significantly different ($p < 0.01$, t test). When the total lengths projecting in the rostrocaudal and dorsoventral axes were compared between lamina II and lamina III cells no significant differences were observed. This suggests that the dendrites of these cells differ in extent in the dorsoventral axis but the length of dendrite that projects in this axis is the same between these groups.

Some NPY-GFP cells received monosynaptic C fibre input from dorsal root stimulation experiments (see electrophysiology chapter, section 3.2.3). Nociceptive C-fibres terminate in laminae I-II where they contact projection neurons or local interneurons (Todd, 2010). Of the 15 cells that received eEPSCs, 11 were monosynaptic C fibre input. Eight of these 11 cells were recovered for morphological analysis and it was possible to determine their soma location; 2 were located in lamina IIi and 6 were located in lamina III (examples Figure 4-13 d and Figure 4-14 c). This was unexpected as the vast majority of unmyelinated fibres terminate dorsal to lamina III, where many of the NPY-GFP cell bodies are located. Therefore the dendritic morphology of these lamina III cells was inspected more closely. All of those cells that were located in lamina III and received monosynaptic C fibre input had a dendritic tree that projected into lamina II, an area where many C-fibres terminate.

Since the dorsoventral extent of dendrites was greater for NPY-GFP cells with somata located in lamina III, and some cells that received monosynaptic input from C-fibres in this lamina had dorsally projecting dendrites C-fibres, it was predicted that a feature of lamina III NPY-GFP cells is that they have dorsally projecting dendrites (examples in Figure 4-14 a, c – f). To test this possibility, the dorsal and ventral extents of dendrites from the centre of the cell bodies were measured. These are the distances from the midpoint of the cell soma to the most dorsal or most ventral point of the dendritic tree. In lamina III cells the mean dorsal and ventral extents were 63 and 36 µm respectively, and these were significantly different ($p < 0.01$, Student's paired t-test). The same comparison between dorsal and ventral dendritic extent was performed for lamina II cells. The dorsal and ventral extents were 38 and 32 µm respectively, which were not seen to be significantly different

Axonal measures were also compared between NPY-GFP cells with somata located in lamina II and lamina III. The mean total lengths of axon for lamina II and lamina III cells

were 5270 and 4778 µm respectively, and these were not seen to differ significantly. The axonal spread of lamina II and lamina III NPY-GFP cells were compared for all axes. Axonal extents in the rostrocaudal and mediolateral axes were similar for lamina II and lamina III cells. However, the mean values for lamina II and lamina III cells were 125 and 158 µm respectively for dorsoventral extent, and these were significantly different ($p < 0.01$, t test). It was observed in the cell reconstructions that some cells had axons that were more extended in the dorsoventral axis, and some of these are illustrated in Figure 4-14 (note that most examples of cells in this figure have their somata located in lamina III). This feature was of interest since NPY-expressing boutons that contact ALT neurons in lamina III often have dorsoventrally directed intervaricose portions, and this is seen in both mice and rats (Cameron et al., 2015; Polgár et al., 2011). Therefore it would be expected that the NPY-expressing cells that innervate lamina III ALT neurons would have axons that were extended in the dorsoventral axis.

Table 4-5 Expression of NPY in GFP positive cells in the NPY-GFP mouse

	All cells	LI-II cells	LIII cells
GFP cells counted	45.3 (39-52)	16.3 (15-17)	29 (22-37)
NPY expressing cells counted	71.3 (55-85)	39.3 (32-49)	32 (23-37)
Cells counted that express both GFP and NPY	38.7 (33-46)	12.7 (11-14)	26 (19-33)
% GFP cells that express NPY	85.1 (82-89)	77.9 (65-87)	89.5 (86-93)
% NPY expressing cells that also express GFP	54.7 (50-60)	33.4 .(27-44)	81.5 (70-92)

Number of cells counted or percentages of cells are displayed in the table. Values are the mean cell counts for 3 mice, and the ranges are indicated in parentheses.

Table 4-6 Laminar distribution of NPY-GFP processes from recorded cells

Laminar location of processes	Dendritic tree	Axonal arbor
I-III	3 (5)	10 (15)
I-II	1 (2)	1 (2)
II	3 (5)	0 (0)
II-III	41 (71)	50 (77)
III	10 (18)	4 (6)
Total	**58**	**65**

Laminar location of the axon and dendrites from filled NPY-GFP cells from laminae I-III. The number in parentheses refers to the percentage of all cells for which dendrites or axons are filled

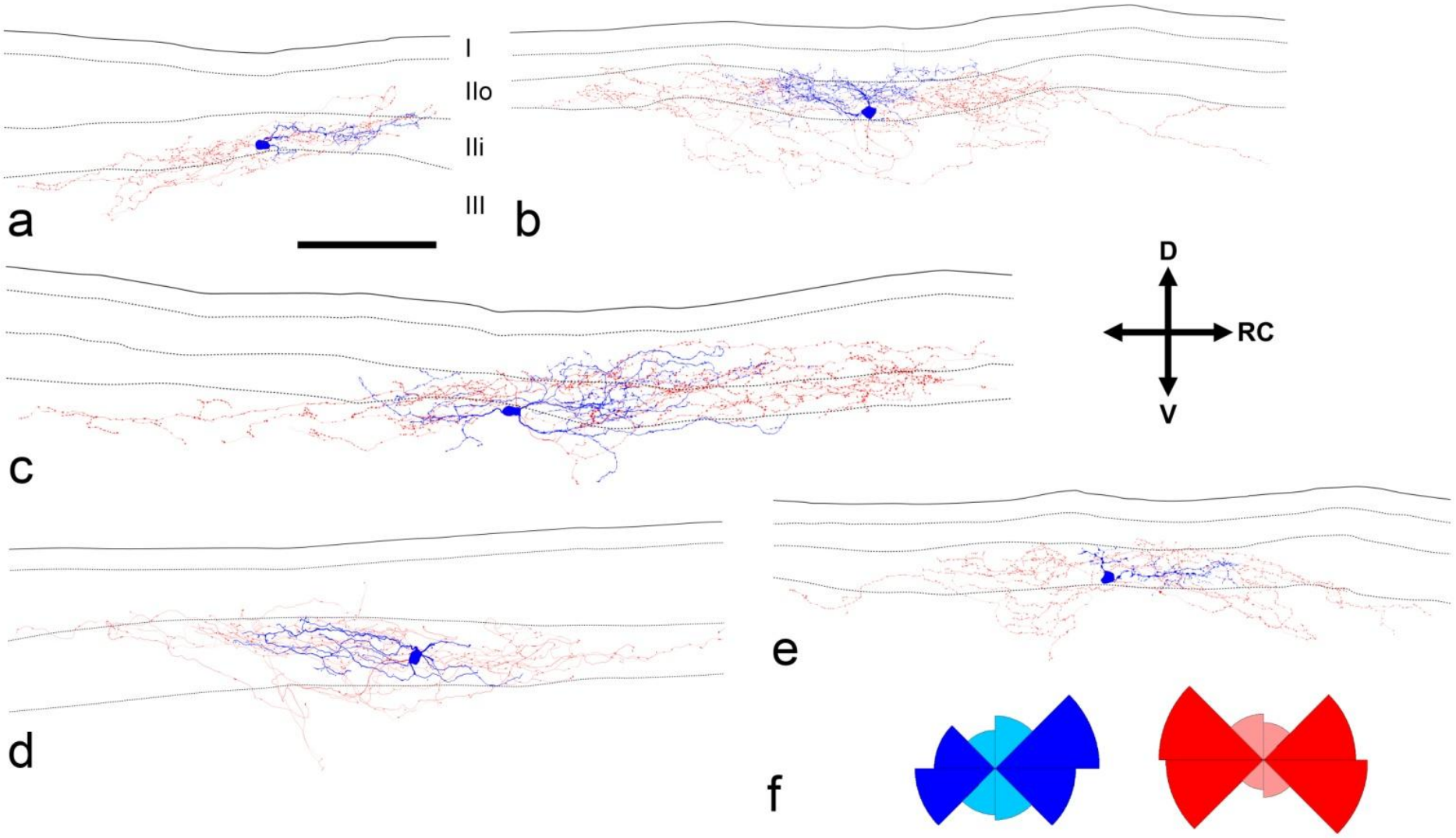
I
IIo
IIi
III
a
b
c
d
e
f
D
RC
V

Figure 4-13 Examples of NPY-GFP cells elongated in the rostrocaudal axis

a-e, examples of reconstructed NPY-GFP cells. Dendrites and cell bodies are shown in blue and axons are shown in red. Laminar boundaries for all cell reconstructions are the same as displayed in **a**; the solid line represents the border between the white and grey matter, and the dashed lines indicate the laminar boundaries between I, IIo, IIi, and III. **f,** polar histograms of the dendrites and axons from the cell reconstruction shown in **e** are shown in blue and red respectively (not to scale), darker shades highlight the rostrocaudal component and are greater for both axons and dendrites. Scale bar in a-e = 100 μm, D = dorsal, V = ventral, RC = rostrocaudal.

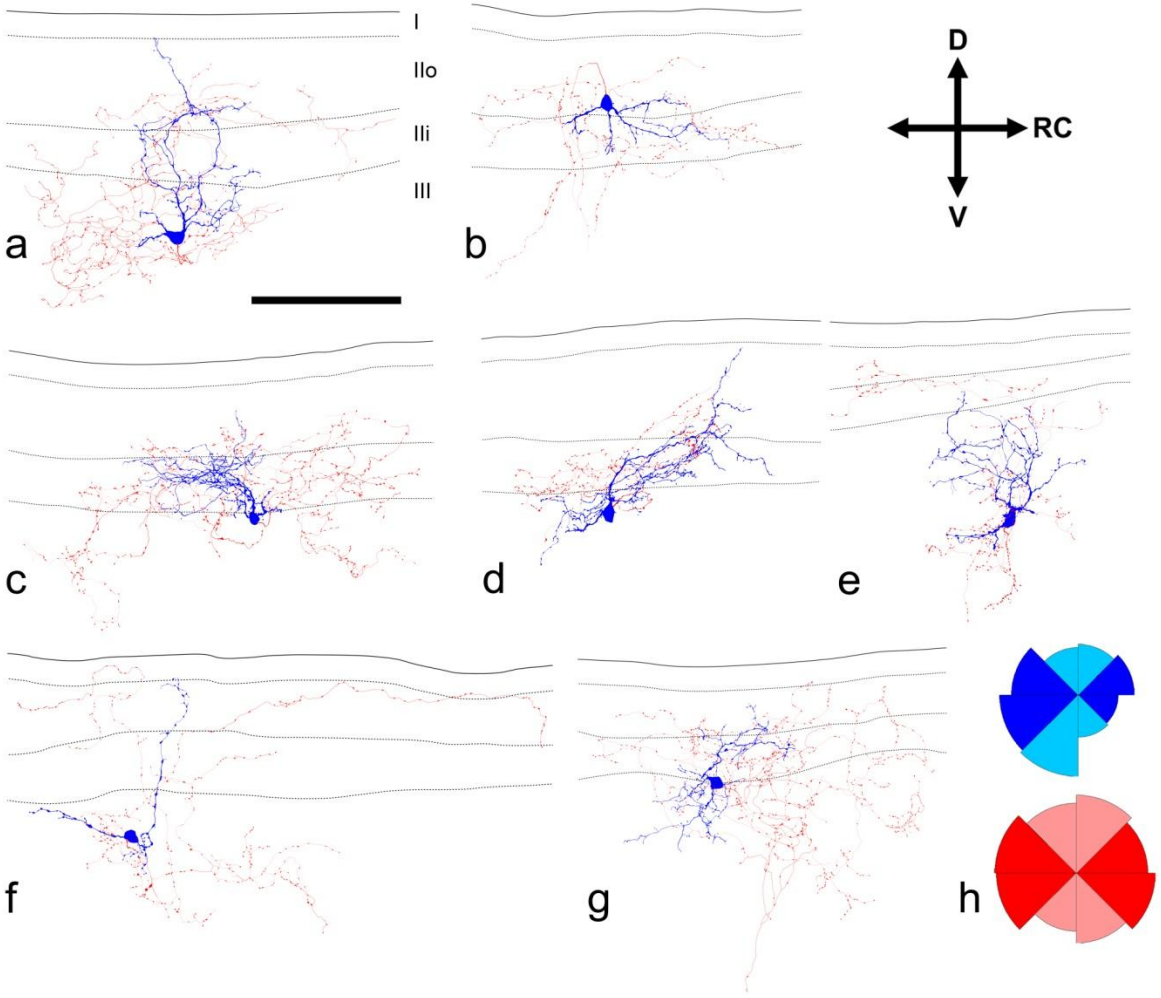
I
IIo
IIi
III
a
b
D
RC
V
c
d
e
f
g
h

Figure 4-14 Examples of NPY-GFP cells with a notable spread in the dorsoventral axis.

a-g, Examples of NPY-GFP cell reconstructions that appear to have a more dorsoventral orientation than other NPY-GFP cells. Dendrites and cell bodies of all cells are blue, and the axons are red. Laminar boundaries between lamina I, IIo, IIi, and III are indicated with dashed lines and the border between the white and grey matter is indicated with a solid line. **h** polar histograms for the cell reconstruction shown in **g** (not to scale), dendritic trees and axonal arbors are shown in blue and red respectively. Note the greater length given to the dorsoventral components for both dendrites and axon, shown in the lighter shades of blue and red. Scale bar = 100µm, D = dorsal, V = ventral, RC = rostrocaudal.

Table 4-7 Summary of NPY-GFP cell morphometric properties and comparison between lamina II and III cells

	Measure	All cells	LII cells	LIII cells	*p* value
Dendrites	RC spread (µm)	166 ± 67	171 ± 55	164 ± 73	0.647
	DV spread (µm)	90 ± 44	68 ± 25	101 ± 48	0.001**
	ML spread (µm)	50 ± 23	48 ± 23	51 ± 23	0.564
	Total length (µm)	1305 ± 804	1296 ± 899	1311 ± 762	0.950
	RC length (µm)	820 ± 535	859 ± 592	799 ± 509	0.704
	DV length (µm)	486 ± 299	437 ± 320	512 ± 289	0.389
	Spine density	4.9 ± 3.9	4.9 ± 4.1	4.9 ± 3.8	0.956
Axon	RC spread (µm)	390 ± 270	411 ± 342	378 ± 225	0.686
	DV spread (µm)	145 ± 57	127 ± 40	156 ± 62	0.025*
	ML spread (µm)	69 ± 33	71 ± 41	69 ±27	0.838
	Total length (µm)	4967 ± 2117	5327 ± 2179	4770 ± 2083	0.323
	RC length (µm)	3299 ± 1618	3639 ± 1776	3114 ± 1514	0.238
	DV length (µm)	1668 ± 667	1688 ± 617	1656 ± 700	0.851
	Bouton density	11.2 ± 4.1	11 ± 3.7	11.2 ± 4.3	0.995

A table summarising morphometric parameters measured from NPY-GFP cells. This group is also divided into those with somata located in lamina II or lamina III for statistical comparison (Student's unpaired t-test), and significant differences between groups are highlighted in yellow. For dendrites n = 57 (21 in lamina II and 36 in lamina III) and for axon n = 65 (25 in lamina II and 40 or lamina III) * $p < 0.05$, ** $p < 0.01$.

4.2.2 Populations of NPY-GFP cells with dorsoventrally elongated axons

Although it was difficult to identify patterns within the morphologically heterogeneous dataset of NPY-GFP cells, a subset of these cells had a notably greater spread in the dorsoventral axis for axon, and many of these cells were found in lamina III (examples in Figure 4-14 and see above). It had been previously reported that NPY-expressing interneurons pre-synaptic to lamina III projection neurons are likely to belong to a distinct populations of NPY-expressing interneurons (Polgár et al., 2011). This population is predicted to have larger axonal boutons that were more brightly immunoreactive for NPY, and contain intervaricose portions elongated in the same dorsoventral orientation as the dendrites of lamina III projection neurons. As the axons from some of these cells were orientated dorsoventrally it was possible that they were a population that target the lamina III projection neurons.

To test whether there was a separate population of dorsoventrally elongated cells, polar histograms were generated for the axon of each cell, and the length of axon projecting in dorsoventral and rostrocaudal axes were plotted for all recorded NPY-GFP cells that had a filled axon (Figure 4-15). The scatterplot did not show a distinct group with greater dorsoventral axonal length. To further test whether there was a distinct group of NPY-GFP cells with dorsoventrally elongated axons, the ratio of dorsoventral axonal length to rostrocaudal axonal length was plotted, and a frequency histogram of these data was plotted (Figure 4-15 b). This plot displayed a unimodal distribution and further suggests that there is no separate population of cells with dorsoventrally elongated axonal arbors. It is therefore unlikely the NPY-GFP cells that innervate the lamina III projection neurons can be identified based on the shape of their axonal arbors.

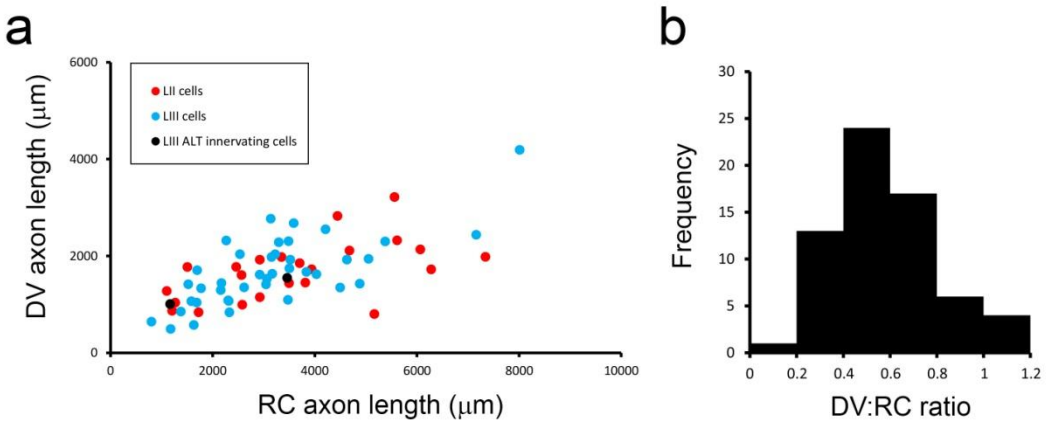
a
b
LII cells
LIII cells
LIII ALT innervating cells
DV axon length (μm)
RC axon length (μm)
Frequency
DV:RC ratio
0
2000
4000
6000
8000
10000
0
5
10
15
20
25
30
0.2
0.4
0.6
0.8
1
1.2

Figure 4-15 Lack of evidence for a separate population of NPY-GFP cells with greater dorsoventrally orientated axon

a, scatterplot of length of axon projecting in the rostrocaudal axis against length of axon projecting in the dorsoventral axis, for lamina II and lamina III located cells. Cells that were found to innervate purported lamina III ALT cells are also shown, to see whether they have differences in their axonal length in the different axes. These two cells do not appear to have a longer dorsoventral length for axon than the other NPY-GFP cells **b**, frequency histogram of dorsoventral:rostrocaudal (DV:RC) ratios for axonal length for all NPY-GFP cells. Note the unimodal distribution of DV:RC ratios, indicating there is no distinct group of cells with a larger DV:RC ratio.

4.2.3 **Post-synaptic targets of NPY-GFP cells**

Previous reports demonstrated that NPY-IR axonal boutons in the rat dorsal horn provide input to PKCγ-expressing interneurons and projection neurons in lamina III (Polgár et al., 2011). In both the rat and mouse spinal cord, the somata and proximal dendrites of lamina III projection neurons are densely innervated by axonal boutons containing NPY, and peptidergic C-fibres terminals containing CGRP (Cameron et al., 2015; Polgár et al., 2011). This input from NPY-expressing boutons is presumably from local inhibitory interneurons, and therefore it was likely that at least some axon from the Neurobiotin-labelled NPY-GFP cells would target these cells. To test whether PKCγ-expressing interneurons or ALT neurons in lamina III were innervated by NPY-GFP cells, axon containing sections from some of the recorded cells were immunoreacted for PKCγ and gephyrin, or CGRP and NPY.

In total, sections containing axons from 18 different cells were immunoreacted for PKCγ and gephyrin. Antibodies raised against gephyrin were included in the reaction to confirm that contacts from axonal boutons were synaptic, since gephyrin is a scaffold protein associated with the post-synaptic density of inhibitory synapses (Todd et al., 1995, 1996). In 7/18 cells axonal boutons were occasionally seen to contact PKCγ-immunoreactive processes. However, no more than 5 contacts from filled axonal boutons were seen in each example and none of these were associated with a post-synaptic gephyrin punctum. These observations suggest that some NPY-GFP cells may provide incidental contacts with PKCγ expressing interneurons, but they are unlikely to be a major output from the NPY-GFP cells. Furthermore gephyrin staining may be sub-optimal in tissue immersion fixed with formaldehyde following whole-cell recording, and this could result in fewer gephyrin puncta being detected by the antibodies. For these reasons this approach was not pursued further.

Axon containing sections from 38 different recorded cells were immunoreacted for CGRP and NPY, which delineate the proximal dendrites and cell bodies of lamina III projection neurons (Cameron et al., 2015). Unlike the lamina III projection neurons in the rat the lamina III projection neurons in the mouse do not express NK1r, and therefore immunostaining for this receptor cannot be used to reveal these cells (Cameron et al., 2015). Immunostaining for CGRP and NPY is the most convenient way to visualise these projection neurons as they are densely innervated by CGRP- and NPY-containing boutons.

This also prevents the need to retrogradely label projection neurons by brain injection prior to cell recording experiments, which is a more labour intensive process. The vast majority of cells (36/38) showed no sign of contributing to clusters of CGRP- and NPY-immunoreactive boutons. However, in 2 cases the axons of filled cells contributed to bundles of NPY that were intermingled with CGRP boutons, and in one of these instances the axon contributed to 3 separate bundles, which were each over 100 μm apart and likely belonged to several different projection neurons (Figure 4-16). The first cell contributed 21/326 of its axonal boutons to one of these bundles, and the other contributed 104/340 of its axonal boutons to multiple bundles. These were counts of axonal boutons tested and did not include all axonal boutons from each cell. For both of the cells that innervated bundles of CGRP and NPY, the dendrites were not recovered and it could not be determined whether these cells had different somatodendritic morphology when compared to other NPY-GFP cells. Both of these cells expressed high levels of NPY in their axonal boutons, and had segments of axons that did not appear to be associated with bundles of NPY and CGRP boutons. The axonal boutons of all 38 filled cells were tested for the presence of NPY, and only 11/38 expressed detectable levels of NPY in their axonal boutons. Similarly to the PrP-GFP cells, this is likely due to the loss of peptide during the whole cell recording to levels that are undetectable for the NPY antibody used.

4.2.4 Input to NPY-GFP cells from low threshold mechanosensory fibres

Evidence of monosynaptic input to NPY-GFP cells from myelinated afferents was only found for one cell in dorsal root stimulation experiments, but this may have been due to the severing of myelinated afferent fibres during the slice preparation. To investigate whether this input could be seen anatomically the dendritic trees of 4 cells were reacted with antibodies against VGluT1 to reveal the terminals of LTMRs. Similar to experiments for the PrP-GFP cells only contacts onto dendritic spines were assessed and only boutons ventral to and including lamina IIi were counted, since these are highly likely to originate from LTMRs (Todd et al., 2003). Between 20 and 111 dendritic spines (mean = 48) were counted from the 4 Neurobiotin filled NPY-GFP cells, and these were assessed for VGluT1 contacts. Between 2 and 16 spines received a VGluT1 contact and this accounted for 7 – 21% of the spines counted for each cell (mean = 14%). An example of a cell receiving contacts from VGluT1-expressing boutons is shown in Figure 4-17.

4.2.5 Responses of NPY-IR cells to noxious mechanical stimulation

Noxious mechanical stimulation experiments were performed by Dr David Hughes and were also used in a recent study (Smith et al., 2015).

Taken together, the results of the dorsal root stimulation experiments, mEPSC analysis in response to capsaicin, and the location of the dendritic trees of NPY-GFP suggest that these cells receive input from C-fibres that do not express TRPV1 receptors (see electrophysiology data chapter section 3.2.3 and 3.2.4 for details). These cells receive input from TRPV1-lacking unmyelinated afferents, which suggests that peptidergic C-fibres do not provide this input (Cavanaugh et al., 2011). Since the NPY-GFP cells did not receive input from TRPM8 expressing primary afferents (see electrophysiology chapter, section 3.2.4), this C fibre input would not include innocuous cooling fibres (Dhaka et al., 2008). Therefore this monosynaptic C fibre input could include non-peptidergic nociceptive fibres or C-LTMRs. Currently there is no way to specifically activate the C-LTMRs to test whether they are providing input to the NPY-GFP cells, and it was seen that many of the recorded cells that received C fibre input were located in the medial dorsal horn where the C-LTMR are not present (Li et al., 2011; Seal et al., 2009). For these reasons input to NPY-GFP from non peptidergic nociceptors was tested. These fibres could be activated by noxious mechanical stimuli as many non-peptidergic nociceptive fibres are known to transmit mechanonociceptive information (Cavanaugh et al., 2009). To test this, 3 wild type mice were stimulated by pinch to the plantar surface of the hindpaw with watchmaker's forceps, and were perfusion fixed 5 minutes after the stimulation. These were the same stimulated animals that were used in a recent study of calretinin-expressing cells (D.I. Hughes unpublished data and Smith et al., 2015). Transverse sections were cut at 60 μm and were immunoreacted for pERK, NPY and PKCγ. For this analysis only lamina III neurons were counted as the majority of the NPY-GFP cells in the present report were found in deeper laminae, and previous studies in the rat had already quantified phosphorylation of ERK in NPY-expressing cells of the superficial dorsal horn (Polgár et al., 2013b). Lamina III was defined as the area 100 μm ventral to the PKCγ plexus and the number of pERK positive cells in lamina III was counted. From this, the number of NPY-expressing pERK positive cells was counted, and this was expressed as a percentage of responsive lamina III cells. Between 40-68 pERK positive cells in lamina III from 3 or 4 sections for each animal were counted. Between 4-9 pERK positive cells were

immunoreactive for NPY, and this corresponded to 10-13% of the cells counted for each animal (mean = 11.7%). These data are summarised in Table 4-8, and give the cell counts for individual animals. The proportion of all NPY-expressing cells in lamina III that were pERK positive was not quantified because activation of neurons by pinch stimulation resulted in punctuate activation of cells that was not continuous throughout the mediolateral extent of the dorsal horn. The stimulation also labelled fewer cells in lamina III than dorsal laminae, probably because this is not the principal central termination site of nociceptive fibres. The number of NPY-IR cells that were activated by pinch would therefore be underestimated, since only a small area in the dorsal horn is activated by the stimulus. It was noted that many of the projection neurons in the deeper laminae were also pERK positive, indicating that these are also responsive to pinch stimulation (Polgár et al., 2007)(Figure 4-18). These results show that several NPY-expressing cells in the deeper laminae can be activated by noxious pinch stimulation, and also their post-synaptic targets.

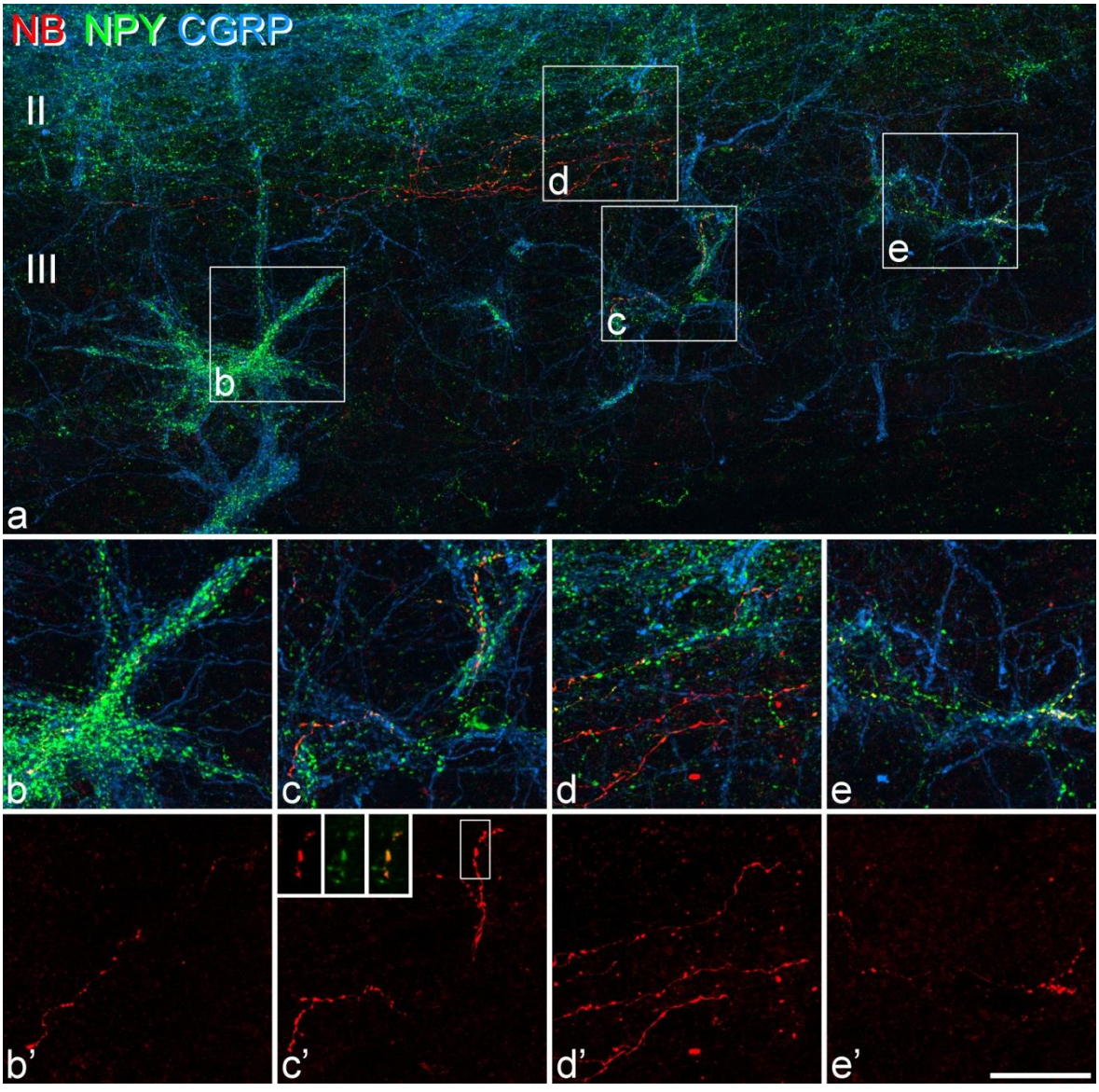
NB NPY CGRP
II
III
a
b
c
d
e
b
c
d
e
b'
c'
d'
e'

Figure 4-16 Example of a filled NPY-GFP axon that innervates multiple bundles of NPY and CGRP boutons that outline lamina III ALT neurons

a, shows the region innervated by the filled NPY-GFP axon, bundles of NPY and CGRP can be seen outlining large cell bodies and dendrites in lamina III. Lamina II and III can be distinguished by the dense CGRP and NPY plexus in lamina II. **b - e**, show enlargements of boxed areas shown in **a**. **b' – e'** show the same areas only displaying the filled axon. Note that **b, c,** and **e** show the filled axon contributing to dense bundles of CGRP and NPY boutons, whereas the filled axon in d is not associated with such bundles. Inset in c' shows axonal boutons that are strongly immunoreactive for NPY. **a** and **b – e** and **b' – e'** are projections of 79 optical sections at 0.5 µm z-spacing, and the inset in fig **c'** is a projection of 9 optical sections at 0.5 µm z-spacing. Scale bar is 100 µm for **a** and 50 µm for **b-e**.

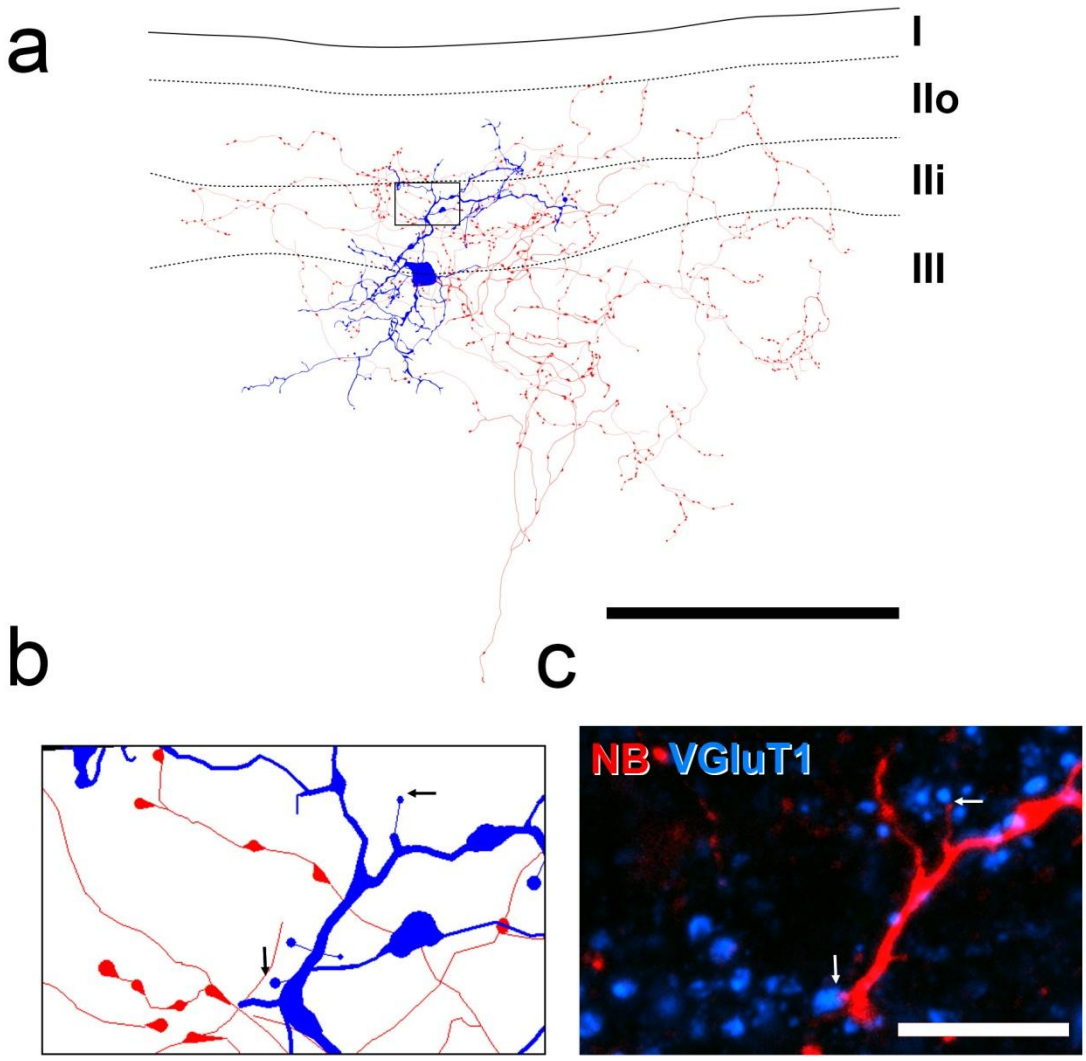
a
I
IIo
IIi
III
b
c
NB VGluT1

Figure 4-17 Example of a reconstructed NPY-GFP cell that receives VGluT1 input onto dendritic spines

a, cell reconstruction of the filled cell reacted for VGluT1. **b**, Enlargement of the boxed region in a to show the dendritic spines of the reconstruction in more detail. **c**, Immunostaining a dendrite containing section of the cell for VGluT1 reveals contacts onto dendritic spines, which likely originate from LTMRs. Spines receiving contacts are indicated by arrows in **b** and **c**, scale bars in **a** and **c** are 100 µm and 20 µm respectively, and c is a projection of 6 optical slices at 0.5 µm z-spacing.

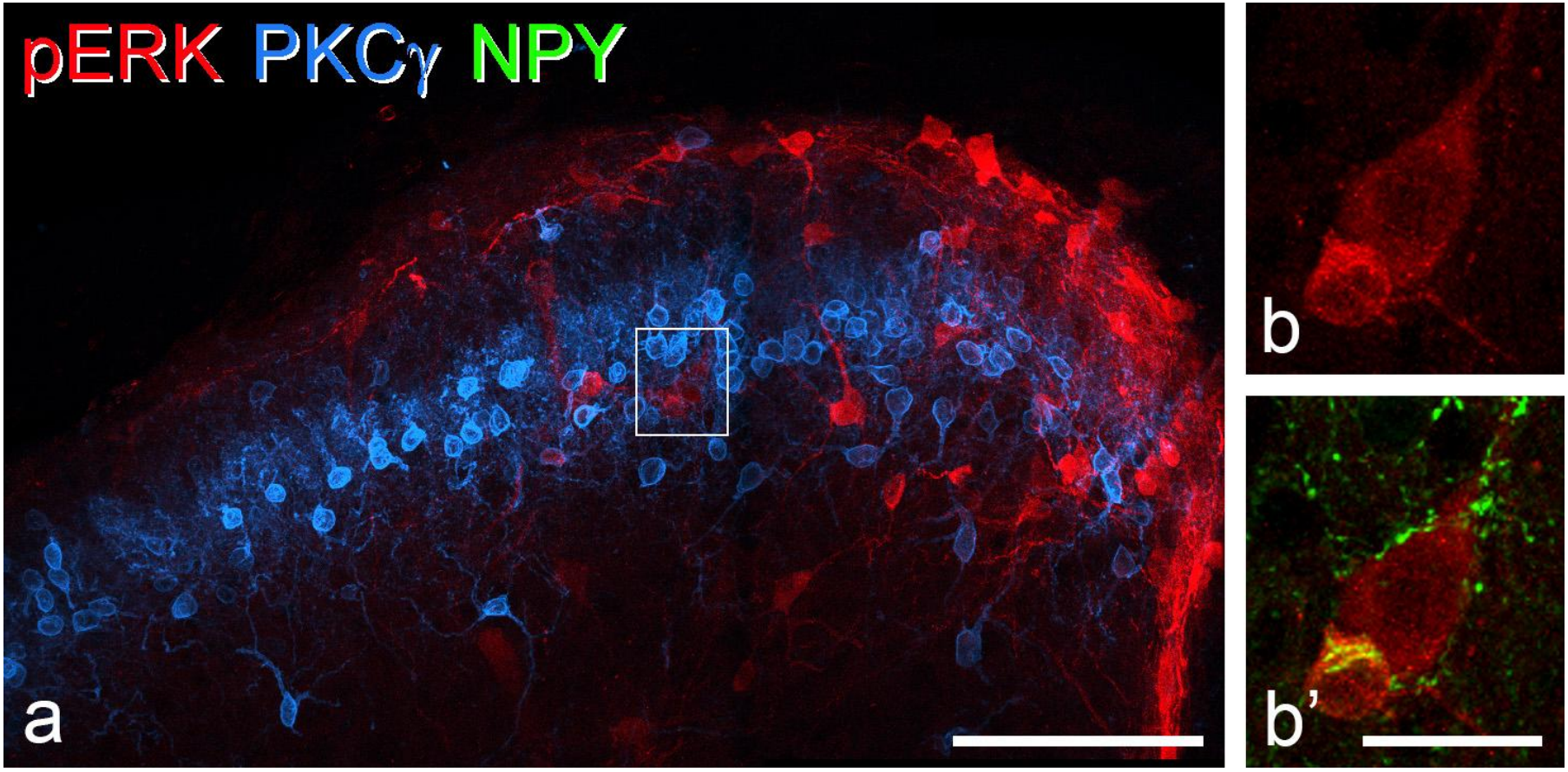
pERK PKCγ NPY
a
b
b’

Figure 4-18 Phosphorylation of ERK in response to pinch stimulation in NPY expressing and NPY innervated neurons by pinch stimulation

a, Example of a transverse section from a pinch stimulated animal showing phosphorylation of ERK in the ipsilateral dorsal horn **b**, enlargement of the boxed area in **a**, showing two neurons activated by pinch stimulation including one that contains NPY and another that is innervated by multiple NPY expressing axonal boutons. **a**, is a projection of 24 optical sections at 1 µm z-spacing and **b** is a projection of 6 optical sections at 1 µm z-spacing. The scale bar in **a** is 100 µm and is 20 µm in **b**.

Table 4-8 Number of cells that respond to noxious mechanical stimulation and express NPY

Animal	Number of pERK cells	Number of pERK+/NPY+	Percentage of pERK+ that are NPY+
A	63	7	11.1
B	68	9	13.2
C	40	4	10.0
Total	**171**	**20**	**11.6**

4.3 NPY-GFP and PrP-GFP cells cannot be distinguished based on measures of cell morphology but have differing physiological properties

4.3.1 Morphological parameters of cell soma and dendrites

Measures of somatodendritic morphology are the most commonly used criteria for defining interneuron populations of the dorsal horn (Grudt and Perl, 2002; Yasaka et al., 2007, 2010). Since the PrP-GFP and the NPY-GFP populations are completely separate groups of dorsal horn interneuron, it was tested whether they could be distinguished based on measures of somatodendritic morphology. To allow a fair comparison, only lamina II NPY-GFP (20) and PrP-GFP (70) neurons were chosen as the classification scheme only includes cells in lamina II, and there are likely differences between these groups due to their laminar location (Grudt and Perl, 2002). In total 55 measures were used for somatodendritic morphology, including 6 measures of the cell soma and 49 measures of dendritic trees. This data was reduced to a lower number of dimensions by PCA, whilst maintaining most of the variance in the dataset. The number of components to be retained was decided based on a scree plot at the point where a plateau was reached; this approach retained 5 principal components that accounted for 61% of the variance in the dataset (Figure 4-19 a). Hierarchical cluster analysis was performed on a transformed dataset using Ward's method as the linkage rule. This approach failed to separate NPY-GFP cells into different clusters, and the cells appeared to be distributed throughout the dendrogram (Figure 4-19 b). This indicates that these distinct cell types cannot be identified solely based on these morphometric measures.

4.3.2 Physiological parameters

These same two populations of cells were also compared for their physiological parameters. This dataset only included 10 NPY-GFP cells and 36 PrP-GFP cells located in lamina II, as many cells were excluded because they were either recorded at a higher bath temperature or were treated with bath-applied TTX, which prevented action potential properties from being measured. Hierarchical cluster analysis was performed on a standardised dataset of physiological parameters, which were rescaled according to 4 principal components (scree plot shown in Figure 4-20 a). Although perfect separation was

not achieved, most NPY-GFP cells appeared to be clustered in the same or closely related groups (Figure 4-20 b). However, these groups also contained some PrP-GFP cells, although the majority of PrP-GFP cells were found in separate clusters. This suggests that based on physiological parameters the NPY-GFP cells are different from the majority of the PrP-GFP cells, although some PrP-GFP cells are indistinguishable from NPY-GFP cells based on these parameters.

To further investigate which physiological parameters differed between these two populations of cells, each of the physiological parameters was compared between NPY-GFP (10) and PrP-GFP cells (36) in lamina II. Parameters related to action potential properties were generally the same, although spike frequency adaptation (0.72 ± 0.11 for NPY-GFP and 0.53 ± 0.15 for PrP-GFP cells) and mV drop (20.9 ± 12.9 mV for NPY-GFP cells and 9.1 ± 9.3 mV for PrP-GFP cells) differed significantly ($p < 0.001$ for spike frequency adaptation; $p < 0.05$ for mV drop; Student's unpaired t-test). This difference can be seen in the examples illustrated in the electrophysiology data chapter (Figure 3-1 a and Figure 3-4 a). These are the change in frequency in a tonic firing cell at its maximum firing frequency, and the difference in action potential height between the first and the last action potential (see Appendix for further details). Other properties that differed between these groups of cells were input resistance (1496 ± 708 MΩ for NPY-GFP cells and 893 ± 473 MΩ for PrP-GFP cells) and rheobase current (12.2 ± 4.7 pA for NPY-GFP cells and 27.6 ± 14.7 pA for PrP-GFP cells), which are both related to the excitability of the cells ($p < 0.05$ for input resistance, and $p < 0.001$ for rheobase current; unpaired t-test). These comparisons indicate that there are some physiological measures that differ between the PrP-GFP and the NPY-GFP cells but these cells are indistinguishable based on morphological parameters of the soma and dendrites. This further suggests that although functional properties are different this is not related to the measures of somatodendritic morphology.

a

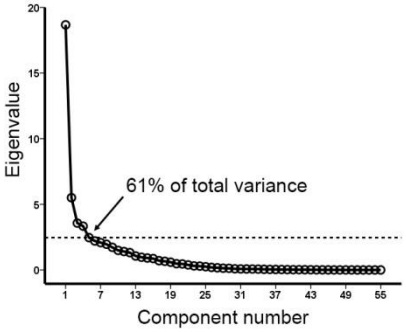
Eigenvalue
20
15
10
5
0
61% of total variance
1
7
13
19
25
31
37
43
49
55
Component number

b

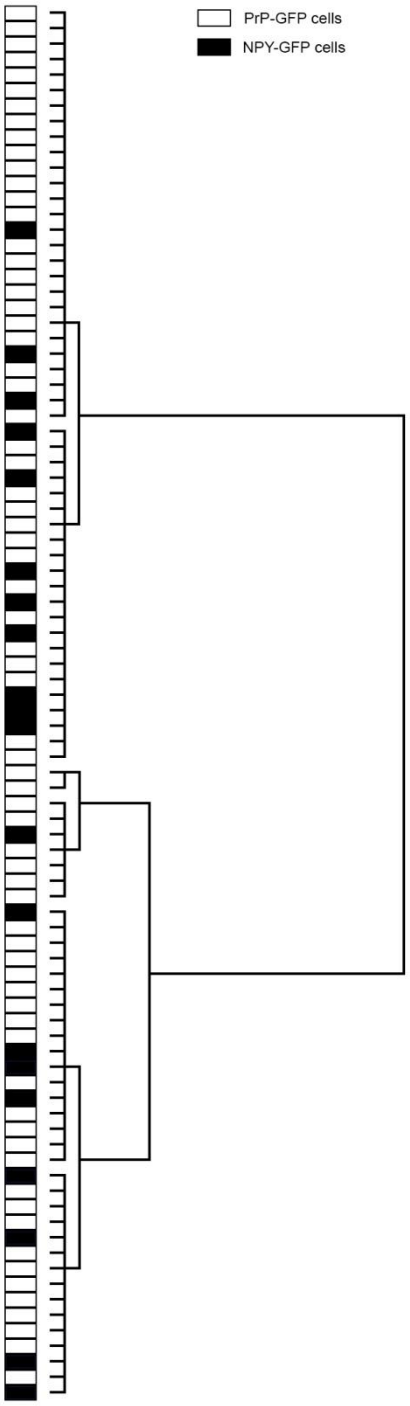
PrP-GFP cells
NPY-GFP cells

Figure 4-19 Hierarchical cluster analysis cannot distinguish NPY-GFP from PrP-GFP cells in lamina II using measures of somatodendritic morphology

a, Scree plot of the principal components and their corresponding eigenvalues produced from a dataset of measures of somatodendritic morphology from NPY-GFP and PrP-GFP cells located in lamina II. Five principal components were retained for hierarchical cluster analysis based on the point at which the plot reached a plateau, and this retained 61% of the total variance of the original dataset. **b,** Dendrogram generated by hierarchical cluster analysis of the lamina II NPY-GFP and PrP-GFP cells using the first 5 principal components. NPY-GFP and PrP-GFP cells are not grouped into separate clusters using this method, and indicate that these cells are not notably different in terms of their somatodendritic morphology.

a

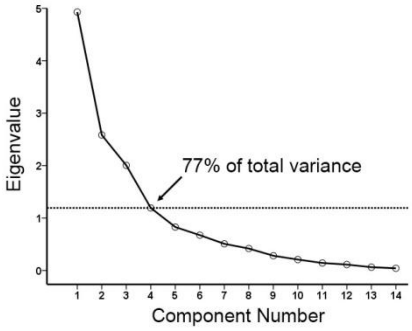
Eigenvalue
77% of total variance
Component Number
0
1
2
3
4
5
1 2 3 4 5 6 7 8 9 10 11 12 13 14

b

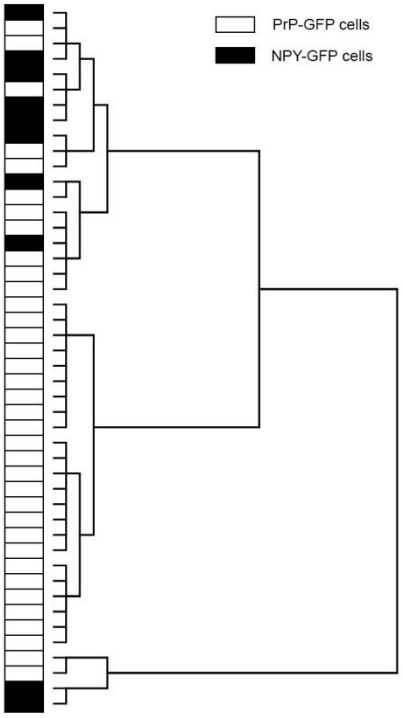
PrP-GFP cells
NPY-GFP cells

Figure 4-20 Physiological parameters differ between NPY-GFP and PrP-GFP cells in lamina II and can be partly distinguished from each other using hierarchical cluster analysis

a, Principal component analysis of a dataset of passive and active membrane properties from NPY-GFP cells and PrP-GFP cells located in lamina II generated the scree plot. Four principal components were retained due to the point at which the plot appeared to reach a plateau. **b**, Hierarchical cluster analysis based on the four principal components retained from the principal component analysis. Although there are NPY-GFP and PrP-GFP cells clustered together, the analysis appears to group most PrP-GFP cells together. Most NPY-GFP cells are present in closely related clusters but this also includes other PrP-GFP cells.

Table 4-9 Comparison of physiological parameters between NPY-GFP cells and PrP-GFP cells located in lamina II

Physiological parameter	NPY-GFP	PrP-GFP	P-value (t-test)
IV slope (nS)	0.77 ± 0.29	1.42 ± 0.66	< 0.001***
Input resistance (MΩ)	1496 ± 708	893 ± 473	0.027*
Resting membrane potential (mV)	-55.3 ± 7.1	-56.6 ± 8.8	0.631
Rheobase current (pA)	12.2 ± 4.7	27.6 ± 14.7	< 0.001***
Latency to first action potential (ms)	402 ± 249	294 ± 148	0.217
Action potential threshold (mV)	-33.2 ± 4.4	-32.1 ± 5.2	0.527
Action potential height (mV)	55.9 ± 13.3	54.4 ± 10.8	0.370
Afterhyperpolarisation (mV)	19.8 ± 29.5	22.0 ± 16.7	0.826
Action potential width (ms)	3.8 ± 1.8	3.5 ± 1.0	0.671
Action potential rise (mV/ms)	76 ± 35	70 ± 32	0.622
Action potential fall (mV/ms)	-40 ± 24	-37 ± 16	0.703
Maximum firing frequency (Hz)	21.9 ± 10.6	24.5 ± 6.6	0.491
Spike frequency adaptation	0.72 ± 0.11	0.53 ± 0.15	< 0.001***
Drop in action potential height (mV)	20.9 ± 12.9	9.1 ± 9.3	0.020*

Comparison of active and passive membrane properties for cells in lamina II. NPY-GFP cells, n = 10; PrP-GFP cells, n = 36. Measures that show a significant difference are highlighted in yellow and significance is taken as $p < 0.05$ (*), <0.01(**) and <0.001(***) (Student's unpaired t-test assuming equal variance)

5 Discussion

5.1 PrP-GFP cells

The main findings from this part of the study were that 1) PrP-GFP cells have greater morphologically diversity than previously reported and rarely display central cell morphology. 2) They receive input from several types of primary afferent that transmit different sensory modalities. 3) The nNOS- and galanin-expressing PrP-GFP cells exhibit slight morphological differences. 4) Subsets of these cells project their axons into lamina I where they are likely to contact projection neurons.

5.1.1 Inputs to PrP-GFP cells

The PrP-GFP cells were shown to receive synaptic input from several different types of primary afferent. They received monosynaptic input from TRPV1- and TRPM8-expressing primary afferent fibres, and dorsal root stimulation experiments confirm that these cells receive monosynaptic input from C-fibres. In one case there was also monosynaptic input from Aδ fibres. VGluT1 is expressed in the boutons of A-LTMRs, and by immunostaining sections that contained the filled dendritic trees of PrP-GFP cells for VGluT1 it was shown that these cells are highly likely to receive synaptic input from A-LTMRs. The axonal boutons of A-LTMRs contacted the dendritic spines, which are sites of excitatory synaptic input to neurons and are therefore highly likely to be synaptic. At least some of these VGluT1-containing boutons form synapses with dendritic spines, and this was demonstrated using a combined method of confocal and electron microscopy (Ganley et al., 2015). This confirms that contacts from these boutons to dendritic spines of PrP-GFP cells were synaptic. The finding of VGluT1 contacts onto dendritic spines of cells that responded to capsaicin suggests that A-LTMRs and TRPV1-expressing C-fibres can converge onto the same cell. The majority of cells tested for VGluT1-expressing contacts possessed an axon that innervated lamina I, and these could provide feed forward inhibition from LTMRs to lamina I projection neurons.

Although there was a significant increase in the frequency of mEPSCs in response to bath application of capsaicin and icilin, this was relatively small when compared to the responses seen in other studies (Baccei et al., 2003; Dickie and Torsney, 2014). On average the increase in mEPSC frequency was from 0.2 Hz to 3.6 Hz in response to 2 μM capsaicin, whereas in studies of NK1r-expressing projection neurons in lamina I, 1 μM capsaicin increased mEPSC frequency by over 20 Hz (Dickie and Torsney, 2014). In a

study of superficial dorsal horn neurons in postnatal rats, 2 μM capsaicin increased the frequency of mEPSCs by over 40 Hz in 9-10 day old animals, and this would almost certainly have included interneurons as these vastly outnumber projection neurons in the superficial dorsal horn (Baccei et al., 2003; Todd, 2010). In addition, the PrP-GFP cells that express nNOS did not express c-fos in response to hindpaw injection of capsaicin, which is consistent with the finding in rat that inhibitory interneurons expressing nNOS rarely respond to intraplantar capsaicin injection (Ganley et al., 2015; Polgár et al., 2013b). Therefore, it is likely there is a relatively weak input to PrP-GFP cells from C-fibres that express TRPV1, and this low level of input may not be sufficient to activate these cells.

TRPM8 is found on a distinct population of C-fibres that are responsible for transmitting stimuli perceived as innocuous cool (Dhaka et al., 2008). These afferents terminate in lamina I, and cells that receive input from TRPM8 expressing fibres are located in laminae I and IIo (Dhaka et al., 2008; Wrigley et al., 2009). The source of TRPM8 input to the PrP-GFP cells is likely to originate from these cool responsive fibres, although it is possible it is also derived from a small population of cells that express both the TRPM8 and TRPV1 channels, since 12% of TRPM8 expressing neurons in the mouse DRG also express TRPV1 (Dhaka et al., 2008). Two PrP-GFP cells responded to both icilin and capsaicin in a subset of cells tested, showing that either there is convergence of TRPV1- and TRPM8-expressing C-fibres onto the same cell, or the C-fibres providing this input expressed both channels. However, this second possibility is unlikely since fibres expressing both TRPV1 and TRPM8 are relatively rare, comprising approximately 1% of all C-fibres (Dhaka et al., 2008). In perfusion fixed tissue from PrP-GFP mice, it was observed that the dendritic spines of PrP-GFP cells frequently received contacts from IB4-binding and CGRP-containing boutons, which supports the suggestion that both peptidergic and non-peptidergic nociceptive C-fibres provide input to these cells (Ganley et al., 2015). Taken together, these results suggest that the PrP-GFP cells receive input from most known types of unmyelinated fibre.

Dorsal root stimulation experiments showed that PrP-GFP cells receive input mainly from monosynaptic C-fibres, as well as polysynaptic input from Aβ, Aδ and C-fibres. This is at odds with the anatomical finding that these cells receive synapses from A-LTMRs expressing VGluT1, because dorsal root stimulation rarely generated monosynaptic eEPSCs from myelinated fibres to these cells (Ganley et al., 2015). However, the preparation of parasagittal spinal cord slices for dorsal root stimulation experiments may

have severed many of the Aβ fibres that provide direct input to PrP-GFP cells. Alternatively, A- LTMRs could form silent synapses. These may be unmasked during altered pain states, as has been suggested for synaptic input to NK1r-expressing projection neurons in lamina I, which receive a higher incidence and magnitude of monosynaptic eEPSCs from Aδ afferents in response to CFA inflammation (Torsney, 2011). These silent synapses would be purely mediated by NMDA receptors that are only active at depolarised membrane potentials, and their activation could recruit AMPA receptors to the synapse. However, the frequency of these silent synapses in the superficial dorsal horn has been debated, with some groups finding a very low incidence of cells with pure NMDA synapses (<5%), and others finding a much higher incidence with over 20% of cells having them (Bardoni, 2004; Yasaka et al., 2009). These findings are likely to be due to differences in the stimulation protocol used, the method of slice preparation and recording, and possibly the recruitment of AMPA receptors to pure NMDA synapses during an experiment. As these experiments on silent synapse were performed in the rat, there may also be a species difference in their frequency for mice. Therefore, it is difficult to determine the reason for this inconsistency between anatomical and physiological findings for A-LTMR input to PrP-GFP cells.

Since VGluT1 is expressed in virtually all the central terminals of A-LTMRs, it cannot be determined whether these are from RA or SA Aβ fibres, or thinly myelinated Aδ fibres (Todd et al., 2003). However, based on the distribution of the central terminals of SA A-LTMRs in the mouse, which terminate ventral to where the PrP-GFP neurons and their dendritic arbors are located, these are unlikely to provide input to PrP-GFP cells (Woodbury and Koerber, 2007). The central branches of RA fibres terminate in the same region as the dendritic trees of PrP-GFP cells, and it is likely that these are the source of VGluT1 inputs to these cells (Woodbury et al., 2001). Moreover, inhibitory cells that were strongly nNOS immunoreactive, and are therefore highly likely to be labelled in the PrP-GFP mouse (A.J. Todd and F. Garzillo unpublished data), received input directly from "early Ret +" RA fibres (Ganley et al., 2015). These "early Ret" RA fibres were labelled in a cross between Ret^{CreER} mice, which express cre from the Ret promoter, and Ai34 tdTomato reporter mice (Ganley et al., 2015; Luo et al., 2009). The Ai34 tdTomato reporter mouse expresses a synaptophysin-tdTomato fusion protein, which is targeted to the axonal terminals (Luo et al., 2009). These mice were injected prenatally with tamoxifen, since Ret^{CreER} is an inducible cre line, which requires tamoxifen for the fusion protein of cre and the oestrogen receptor (ER) to enter the nucleus. This is required for

DNA recombination, which allows the reporter to be expressed. The cells that express Ret early in development need to be labelled, in order to label the “early Ret +” cells, which include the RA fibres, with the tdTomato reporter. This indicates that nNOS-expressing PrP-GFP cells receive input from RA mechanoreceptors, which includes fibres that innervate Meissner and Pacinian corpuscles, and lanceolate endings that innervate hair follicles (Luo et al., 2009).

The PrP-GFP cells almost certainly receive synaptic input from local excitatory interneurons as they frequently show polysynaptic input in response to dorsal root stimulation. However, although we saw polysynaptic input to these cells, the original study of PrP-GFP cells did not report polysynaptic input to these cells (Hantman et al., 2004). Furthermore paired recording experiments did not find excitatory connections from any morphological class of interneurons to PrP-GFP cells (Zheng et al., 2010). While Zheng *et al* (2010) did not detect input from excitatory interneurons to the PrP-GFP cells, these cells were frequently seen include vertical cells, which are predominantly excitatory interneurons, among their post-synaptic targets. Other synaptic connections were found between PrP-GFP and islet cells, and these were reciprocal inhibitory synapses. Taken together with the results of the present study this suggests that the PrP-GFP cells receive synaptic input from many types of primary afferent fibre and other interneurons, and can provide inputs to other types of neuron, including projection neurons and other interneurons. This suggests a much more complex involvement in the dorsal horn microcircuitry than the simple arrangement suggested previously (Hantman et al., 2004).

5.1.2 Morphological and neurochemical features of recorded PrP-GFP cells

Morphologically these cells are more variable than originally reported, with very few cells displaying the morphological properties of central cells. Many of the PrP-GFP cells in the present study cannot be classified according to the scheme devised by Grudt and Perl, although none of them had the morphological characteristics of islet cells. This would be expected if the morphological properties of these cells were entirely random. Therefore it is possible that although not all cells in the dorsal horn can be categorised based on morphology, some morphological cell types do exist and these include islet cells. This is supported by the observation that islet cells are invariably found to be inhibitory interneurons, and that they are found in certain neurochemically defined groups, such as

those that express parvalbumin or calretinin (Hughes et al., 2012; Maxwell et al., 2007; Smith et al., 2015; Yasaka et al., 2010).

Unexpectedly nNOS and/or galanin could not be detected in all of the filled cells, although a subset did contain detectable levels of either nNOS or galanin. This is surprising since in a previous study nNOS and/or galanin was detected in 98% of GFP-expressing cells, and immunoreactivity for both nNOS and galanin was seen in 35% of the PrP-GFP cells (Iwagaki et al., 2013). This is likely to be due to the neurochemical content of the cell being reduced to an undetectable level during the whole-cell recording. Although a subset of PrP-GFP cells did contain detectable nNOS or galanin following recording, these recorded cells could not unequivocally be assigned to the nNOS- or the galanin-expressing population, since they may have initially contained both neurochemicals with one being diluted to an undetectable level during the whole-cell recording. Despite this possibility, it is likely that the PrP-GFP cells that initially contained high levels of each neurochemical retained a detectable level following recordings. In addition, PrP-GFP cells that express high levels of neurochemical are usually only immunoreactive for galanin or nNOS (Iwagaki et al., 2013). Conversely, PrP-GFP cells that express both nNOS and galanin generally only express a low level of each neurochemical, and are perhaps more prone to having their neurochemical content reduced to undetectable levels. Furthermore, nNOS may be more easily lost from the cell, because it is a cytoplasmic protein that is free to diffuse between the cytoplasm and the intracellular solution of the electrode, whereas galanin may be more easily retained in cells because it is contained in dense core vesicles (Valtschanoff et al., 1992b; Zhang et al., 1995). There are several other factors that could influence the loss of neurochemicals during the recordings; such as the duration of recording, the application of drugs, or the health and activity of the cell during a recording. Since these factors vary between experiments it cannot be determined whether the cells with undetectable levels of nNOS or galanin were those cells that initially expressed both. There were slight morphological differences between the cells that contained nNOS or galanin, and this finding is consistent with previous reports that galanin-expressing cells were located more dorsally than the cells that were nNOS-expressing (Iwagaki et al., 2013).

Other morphological differences between cells that contained detectable nNOS and galanin following recordings included somata, the extent of dendrites in all axes (rostrocaudal dorsoventral and mediolateral), and the extent of axons in the dorsoventral and

mediolateral axes. These findings suggest a scaling difference between cells in which nNOS or galanin could be detected, as opposed to a difference in the overall shape of their dendritic trees and axonal arbors. Despite this, the two groups were largely distinguishable using PCA followed by hierarchical cluster analysis. The lengths of dendritic trees and axonal arbors in different laminae were also different between groups, and these would influence the clustering procedure during cluster analysis. These differences are important in terms of functional properties as they affect the primary afferent inputs these cells can receive, and influence their likely post-synaptic targets. Therefore, although these cells had some statistically significant differences and could be distinguished by cluster analysis with some accuracy, it is unlikely that these groups would be identified as morphologically different using the Grudt and Perl (2002) classification scheme.

5.1.3 PrP-GFP cells that innervate lamina I

From reconstructions of PrP-GFP neurons, a subset of cells that innervated lamina I was identified. Although the majority of cells had an axon that was present in lamina I (53/87), only those with over 20 axonal boutons in this lamina were defined as innervating lamina I (30/87). Due to internalisation and degradation of NK1r during electrophysiology experiments it was not possible to identify NK1r-expressing projection neurons by immunocytochemistry on sections taken from slices. Furthermore it is difficult to identify giant lamina I cells in parasagittal sections of spinal cord (Polgár et al., 2008; Puskár et al., 2001). It was therefore not possible to test directly whether the axons from recorded cells innervated these projection neurons in lamina I. However, many of the GFP-expressing boutons present in lamina I in PrP-GFP mice contacted NK1r-expressing cells or giant cells, and these contacts were confirmed as synaptic by the post-synaptic expression of gephyrin (Ganley et al., 2015). The giant cells in particular are densely innervated by nNOS and GFP-containing boutons with most giant cells receiving between 62 and 82% of their inhibitory input from these boutons. NK1r-expressing neurons in lamina I and the giant cells are found to include projection neurons, which is shown by retrograde labelling from the LPb and the CVLM in the rat (Al-Ghamdi et al., 2009; Spike et al., 2003). Thus, although it is not certain that the PrP-GFP cells are innervating projection neurons, it is highly likely that at least some of their output will be onto these cells.

Apart from having an axon with over 20 boutons in lamina I, this subset was indistinguishable from other PrP-GFP cells in terms of morphological and physiological parameters. Despite this feature, the axon and axonal boutons from lamina I-innervating

cells was mostly present in lamina II, indicating that cells in this lamina are the major output of these cells. Since the lamina I projection neurons or their dendrites are not present in lamina II, it is likely that they are only a minor output of the PrP-GFP cells. Nevertheless this still represents a subset that is highly likely to have a distinct function, since they are innervating lamina I projection neurons and most GFP-expressing cells in the PrP-GFP mouse do not have this axonal distribution.

5.1.4 **Possible roles of PrP-GFP cells**

The heterogeneity in cell shape, synaptic inputs, neurochemistry and post-synaptic targets of PrP-GFP cells suggest that they are not a homogeneous functional population. Those cells that project their axon into lamina I also have considerable axon and axonal boutons present in other laminae, which indicates that their function is not solely to inhibit projection neurons. Cells that project their axon into lamina I were also seen to receive contacts from A-LTMRs in all cells tested. This is a potential disynaptic link between low threshold fibres to projection neurons, which would allow the activation of LTMRs to inhibit projection neurons in the ALT. These cells may in part form a basis for pain suppression by innocuous stimuli as hypothesised in the Gate Control Theory of pain, where activation of low threshold fibres suppresses pain transmission to the brain through the activation of inhibitory interneurons (Melzack and Wall, 1965).

A recent study implicated glycinergic dorsal horn interneurons in gating pain in the spinal cord, since inhibition of this population resulted in spontaneous pain behaviour and heightened pain sensitivity, and the input to these cells was predominantly from A-LTMRs (Foster et al., 2015). Other anatomical studies have shown that at least some dorsal horn neurons with NADPH diaphorase activity (a marker for nNOS expressing cells) are enriched with glycine as well as GABA (Spike et al., 1993). Therefore it is possible that some PrP-GFP cells are glycinergic neurons responsible for suppressing projection neurons that transmit pain signals. Furthermore, it was shown in the GlyT2-cre mouse that 80% of inhibitory nNOS cells in the superficial dorsal horn were cre-expressing, which further supports this hypothesis (Foster et al., 2015). It is also possible that the nNOS-containing PrP-GFP cells could perform this role without inhibiting projection neurons, and may achieve this by controlling network excitability in the dorsal horn. This is in agreement with the finding that only around one third of cells could inhibit projection neurons (i.e. have an axon in lamina I), and these could only provide a minority of their output to projection neurons. Sections from the 2 cells that responded to capsaicin that were

immunoreacted for VGluT1 were also seen to receive contacts from A-LTMRs. The convergence of TRPV1-expressing C-fibres and A-LTMRs onto the same cell suggests that the same cell may respond to a range of different modalities, and have a wide dynamic range (WDR). WDR neurons respond to a range of stimulus intensities, and their responses increase with the stimulus intensity (Dado et al., 1994).

The finding that PrP-GFP cells receive input from a variety of primary afferent fibres and have multiple post-synaptic targets makes it difficult to predict their role. However, recent work on the bhlhb5 knockout mouse has shown that a population of inhibitory interneurons is lost that have similar neurochemical features to the PrP-GFP cells (Ross et al., 2010). This mouse displays a heightened response to itch inducing stimuli, and the cause of this elevated itch is thought to be the loss of the B5-I neurons, which require the expression of bhlhb5 for development. It was shown that these inhibitory interneurons express the sst_{2A} receptor as well as galanin and/or nNOS (Kardon et al., 2014). Like the PrP-GFP cells, the B5-I neurons were also shown to receive monosynaptic input from TRPV1- and TRPM8-expressing sensory fibres, and this could be a basis for itch suppression by counter-stimulation. These shared features suggest that the PrP-GFP cells could represent a functionally similar population of cells to the B5-I neurons, and function to inhibit itch. However, the PrP-GFP cells only represent a subset of the B5-I neurons, since B5-I neurons account for all nNOS- and/or galanin-expressing inhibitory neurons, whereas the PrP-GFP mouse labels 57% of nNOS-, 23% of galanin-, and 83% of nNOS and galanin-expressing inhibitory neurons (Iwagaki et al., 2013; Kardon et al., 2014). Therefore the PrP-GFP cells may not include the B5-I neurons that are responsible for inhibiting itch. The finding that these cells also receive input from LTMRs does not agree with this theory, as innocuous mechanical stimulation does not apparently suppress itch. It is possible however, that the input from LTMRs is not strong enough to activate these cells, and that they are more tuned to respond to C fibre input. This is in agreement with the scarcity of functional input from LTMRs seen in dorsal root stimulation experiments. It is also possible that only a subset of PrP-GFP is involved in the inhibition of itch. The findings of Kardon et al (2014) suggests that the galanin-expressing cells are responsible for this inhibition of itch, since these cells all express the kappa opioid dynorphin, which is seen to inhibit itch when delivered intrathecally (Sardella et al., 2011b). Furthermore, the intrathecal injection of kappa opioid antagonists increased itch behaviours in response to pruritogens, and together these findings suggest that kappa opioids are required for normal response to itch. As a source of kappa opioids, the galanin-expressing cells are well placed

to inhibit itch though release of dynorphin. Moreover, the more dorsal location of the galanin-expressing cells means they are more likely to be within the termination zone of the nociceptive Aδ and C-fibres, which are thought to inhibit itch by scratching and other counter stimulation (Akiyama et al., 2011). The finding that kappa opioids are able to inhibit itch does not exclude the possibility that nNOS-expressing inhibitory interneurons are also involved in itch suppression. Ablation of glycinergic cells in the GlyT2-cre mouse, which included 80% of the nNOS-expressing inhibitory interneurons in the superficial dorsal horn, also showed deficits in itch behaviour, suggesting that glycine-enriched nNOS cells could also be involved in itch suppression (Foster et al., 2015).

In summary, the functions of the PrP-GFP cells are difficult to determine from the present study. However, it is likely that this group contain cells that are involved in a number of different processes due to their heterogeneity and varied inputs and outputs. Although a definitive role of these cells cannot be determined, it is certain that they play much more varied roles in the dorsal horn circuitry than previously anticipated. A circuit diagram summarising the known connectivity of the PrP-GFP cells is shown in Figure 5-1

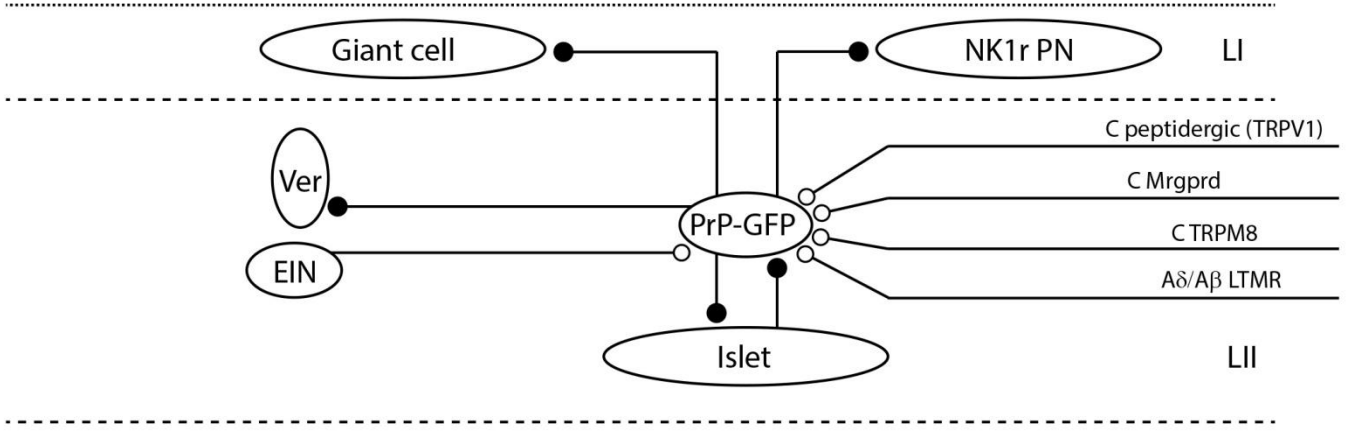
Giant cell
NK1r PN
LI
C peptidergic (TRPV1)
Ver
C Mrgprd
PrP-GFP
C TRPM8
EIN
Aδ/Aβ LTMR
Islet
LII

Figure 5-1 Circuit diagram illustrating the synaptic inputs and outputs of PrP-GFP cells

Inhibitory connections are shown in black and excitatory connections are shown in white. Elements in this diagram are not weighted or to scale, and each PrP-GFP cell may not receive/provide all of the connections illustrated. This diagram is to highlight all the possible known connections of these cells, although there is likely variability within the PrP-GFP population with some cells making certain connections and not others. However, it is seen that some cells receive input from both low-threshold A and nociceptive C-fibres, and all cell that innervate lamina I also have considerable axon present in lamina II. Black boutons indicate inhibitory connections and while boutons indicate excitatory connections. Reciprocal connections between PrP-GFP and islet cells, and connections from PrP-GFP to vertical cells was shown in (Zheng et al., 2010), and input from non-peptidergic C-nociceptors and further evidence for Aδ/Aβ input was shown in Ganley et al 2015.

5.2 NPY-GFP cells

The main findings from the study of NPY-GFP cells are that 1) these cells, like the PrP-GFP neurons, are a morphologically heterogeneous group that does not include islet cells. 2) NPY-GFP cells located in lamina III are preferentially labelled in the NPY-GFP mouse line 3) The lamina III NPY-GFP cells can receive input from C-fibres, and this is likely to be due to the presence of dorsally directed dendrites that project into lamina II. 4) Few of these cells appear to provide input to the lamina III ALT neurons, and those that do can innervate several bundles, presumably surrounding more than one cell. 5) The NPY-expressing boutons that innervate each of these lamina III projection neurons are likely to originate from several NPY-expressing cells.

5.2.1 NPY-GFP mouse line

The NPY-GFP mouse line was developed to label NPY-expressing cells in the central nervous system with GFP, thus allowing targeted whole-cell recordings to be taken from NPY-expressing cells of the hypothalamic arcuate nucleus (van den Pol et al., 2009). The generation of this mouse utilised a large bacterial artificial chromosome (BAC) containing sequences from 114423 bp upstream to 28595 bp downstream of the NPY gene, and included the NPY promoter and a large amount of flanking DNA sequence (van den Pol et al., 2009). This resulted in a pattern of GFP expression that closely resembled the expression of NPY seen in the mouse central nervous system, with several brain regions expressing GFP in nearly every NPY-immunoreactive cell. However, the pattern of GFP expression did not perfectly match the NPY immunoreactivity seen in the dorsal horn, labelling just 33% of lamina II NPY-expressing cells and 82% of NPY-expressing cells in lamina III. This is possibly due to the lack of transcription at the BAC integration site in these cells, or suppression of GFP expression in the NPY-containing cells of the superficial dorsal horn. Epigenetic factors, such as the DNA methylation, can result in regions of the genome being silenced, which may explain the lack of GFP expression in some cells. This pattern of GFP expression resulted in the NPY-expressing cells in lamina II being underrepresented in sample of recorded NPY-GFP cells (23 lamina II cells versus 42 lamina III cells). Since only one third of lamina II cells were labelled, it is unknown whether this was representative of all NPY-expressing cells in this lamina.

Alternative strategies to label NPY-expressing cells in the superficial laminae could be used in order to characterise the cells that are underrepresented in the current report. The

GENSAT project has also produced a mouse line that labels cells with GFP under the control of the NPY promoter, and this appears to label cells in the superficial dorsal horn. There are also two mouse lines available that express cre from the NPY promoter, the RH26 and the RH28 mice lines. Crossing these cre-expressing mouse lines with a reporter mouse should label NPY-expressing cells with a reporter protein. However, when the RH26-cre mouse is crossed with a reporter line approximately 80% of the Pax2 positive neurons in the superficial dorsal horn are labelled, whereas only 18% of lamina I and II inhibitory neurons are NPY immunoreactive in the rat (E. Polgár and A.J. Todd unpublished observations) A recent study that associates these NPY-cre cells labelled in the RH26 mouse with suppressing mechanical-evoked itch estimates that only 35% of these cells at P30 are immunoreactive for NPY (Bourane et al., 2015). This is likely to be due to the transient expression of NPY during development, with crosses with reporter mice permanently labelling these transient NPY-expressing cells with reporter protein. An alternative strategy is to inject an adeno-associated virus (AAV), which contains a reporter gene that is expressed in a cre-dependent manner, directly into the spinal cord of adult RH26-cre animals. This strategy would avoid labelling the transient NPY-expressing cells during development.

5.2.2 **Morphological properties of NPY-GFP cells**

This is apparently the first study to investigate the morphological properties of dorsal horn interneurons that express NPY. The somatodendritic morphology of NPY-GFP cells varied greatly in terms of shape and size, with some cells having simple unbranching dendrites and others displaying complex highly branched dendritic trees. One feature that was often seen in these cells was the presence of a dorsally directed dendritic tree. This characteristic was not shown by all cells, but was commonly seen in the NPY-GFP cells with somata in lamina III. Despite their heterogeneity none of these cells displayed the morphological properties of islet cells, and most would be unclassified according to the Grudt and Perl (2002) scheme. Axonal arborisation patterns also varied greatly between cells, and the 2 NPY-GFP neurons that innervated the lamina III ALT neurons did not have a distinct axonal arborisation pattern that would allow them to be distinguished from other NPY-expressing cells. In summary, the NPY-GFP cells did not show any consistent morphological features except for never having islet cell morphology.

5.2.3 Comparison of NPY-GFP cells with other neurochemically distinct populations of interneurons in the dorsal horn

Since the NPY-GFP cells represent a neurochemically distinct population from other cells that have been described in this region, comparisons could be made between the morphological features of these cells and other neurons in the dorsal horn. The inhibitory neurons that express parvalbumin are found to have islet and central-like morphology (Hughes et al., 2012). Since NPY-GFP cells are never islet morphology they could be distinguished from the parvalbumin-expressing cells that displayed islet morphology, but they would not appear to be different from other parvalbumin-expressing cells. The cholinergic neurons are a subset of the nNOS-expressing population, and are unlikely to overlap with NPY-expressing cells, which never express nNOS in the rat (Laing et al., 1994; Spike et al., 1993). Cholinergic cells in lamina III have also been characterised in terms of their morphology, and were described as having rostrocaudally orientated dendritic trees that frequently extended dorsally (Mesnage et al., 2011). This is very similar to what is seen in the present report, especially for those cells with somata in lamina III. However, Mesnage *et al* (2011) also suggested these cholinergic neurons were a comparable size to the lamina II islet cells seen in Yasaka *et al* (2007), which would allow these cells to be distinguished from NPY-GFP cells in terms of the size of their dendritic trees. Indeed, the average rostrocaudal extent of a small sample of Neurobiotin-filled cholinergic cells was 485.6 ± 33.3 μm, whereas this same measure for NPY-GFP cells in lamina III was 162.6 ± 2.08 μm (values are mean ± SEM)(Mesnage et al., 2011). Therefore rostrocaudal extent of the dendritic tree would allow NPY-GFP and cholinergic interneurons in lamina III to be distinguished from each other. Recently, two populations of calretinin-expressing cells were described in the mouse dorsal horn, which were either excitatory and had variable morphology, or were inhibitory cells and had islet morphology (Smith et al., 2015). The inhibitory population of calretinin-expressing cells had different morphological properties to the NPY-GFP cells, and these two groups would be easily distinguished. However, the morphological heterogeneity of the excitatory calretinin-expressing cells would prevent this group from being distinguished from the similarly heterogeneous NPY-GFP cells. A combination of morphology and neurotransmitter phenotype would allow both excitatory and inhibitory calretinin-expressing neurons to be distinguished from the NPY-GFP cells. Comparisons were also made between the NPY- and PrP-GFP cells, which are completely non-overlapping populations in terms of neurochemistry, and these will be discussed later (see section 5.3 below). Taken together

these comparisons suggest that neurochemically distinct populations in the dorsal horn cannot be distinguished from each other by somatodendritic morphology except for groups that include cell with islet morphology.

5.2.4 **Primary afferent input to NPY-GFP cells**

From dorsal root stimulation experiments the most common type of response seen for NPY-GFP cells was monosynaptic C-fibre input (11/14 responsive cells). The 6 monosynaptic eEPSCs from C-fibres that were tested for capsaicin sensitivity were not affected by bath application of capsaicin. Furthermore, very few NPY-GFP cells tested responded to bath application of capsaicin in the mEPSC analysis. This is possibly due to the lack of dorsal NPY-GFP cells with dendrites present in laminae I and IIo, where TRPV1-expressing peptidergic C-fibres terminate. It is also unsurprising that no cells responded to TRPM8 agonists, because the central terminals of fibres that express TRPM8 are found in lamina I, where effectively none of the dendrites from the NPY-GFP cells were located (Dhaka et al., 2008). The response to TRPM8 was still tested since cells in lamina IIo of the dorsal horn were identified that responded to TRPM8 agonists (Wrigley et al., 2009). This indicates that the C-fibres that innervated NPY-GFP cells did not express TRPV1 or TRPM8 (Nakatsuka et al., 2002; Yang et al., 1999).

Since TRPV1 is restricted to the peptidergic C-fibres, the monosynaptic input to these cells is likely to be from C^{Mrgprd} fibres or C-LTMRs, as these are non-peptidergic C afferents (Cavanaugh et al., 2009; Seal et al., 2009). Since none of the NPY-GFP cells responded to bath application of TRPM8 in the mEPSC analysis, this C-fibre input would not be from those fibres responsible for innocuous cooling sensation (Dhaka et al., 2007, 2008; Hensel, 1981). It was observed that many of the recorded cells were located in the medial part of the dorsal horn, determined by the presence of vertical myelin bundles in the slice and the large amount of white matter from the dorsal columns above the grey matter. Therefore at least some of this C-fibre input was probably from C^{Mrgprd} fibres, since C-LTMRs are only found in hairy skin and terminate in the lateral two thirds of the dorsal horn (Seal et al., 2009). C^{Mrgprd} fibres have been associated with mechanonociception, and if the NPY-GFP cells received monosynaptic input from this group of C-fibres, they may also be involved in a circuit to regulate the perception of noxious mechanical stimuli (Cavanaugh et al., 2009). C-LTMRs were previously associated with the development of mechanical pain hypersensitivity, but recently the contribution of C-LTMRs to mechanical allodynia was reassessed and it was found that peripheral VGluT3 expressing cells (i.e. C-LTMRs) were

not involved in the development of mechanical hypersensitivity following injury (Peirs et al., 2015; Seal et al., 2009). Rather, intrinsic dorsal horn neurons that transiently express VGluT3 during development are required for this development of mechanical hypersensitivity.

Although it was likely that NPY-GFP cells received monosynaptic input from C^{Mrgprd} fibres, it could not be confirmed from dorsal root stimulation experiments whether C-LTMRs or C^{Mrgprd} fibres provided this input. Despite the fact that many of the NPY-GFP cells were located in lamina III, monosynaptic C fibre input was still observed in six of these cells (see results chapter, section 4.2.1). Furthermore, previous studies have seen cells in lamina III that are activated by noxious mechanical stimuli (Polgár et al., 2007, 2013b). To test whether the NPY-GFP cells could respond to noxious mechanical stimulation, animals were pinch stimulated and the number of activated cells was assessed. These experiments counted the NPY-expressing cells as opposed to cells labelled in the NPY-GFP mouse. Therefore, analysis was limited to NPY-expressing cells in lamina III, because this is where the somata of most NPY-GFP cells are located. This analysis showed that around 10% of the cells in lamina III activated by noxious pinch expressed NPY, and therefore these cells are activated *in vivo* by noxious mechanical stimulation. This further suggests that the monosynaptic C fibre input to these cells is likely to be from C^{Mrgprd} fibres. However, this is not definitive as the NPY-expressing cells may not be directly innervated by mechanonociceptive primary afferents, but form part of a circuit that responds to mechanical noxious stimuli.

Monosynaptic input to NPY-GFP cells from TRPV1-expressing C-fibres was rarely observed. Nevertheless, the sample of NPY-GFP cells in this report show a population that often received input from C-fibres that lacked TRP channels, and rarely from peptidergic C-fibres. It is possible that there are a population of heat-sensitive NPY-expressing cells that were not frequently labelled with the NPY-GFP mouse, and these were not sampled in the present report. Using another mouse line that labels a higher proportion of the dorsal NPY-expressing cells could be used to test this (see section 5.2.1 above).

Dorsal root stimulation experiments showed these cells rarely received monosynaptic input from myelinated fibres, with only one example of monosynaptic Aδ fibre input being recorded from NPY-GFP cells. This may be due to the severing of myelinated fibres during the preparation of spinal cord slices, as mentioned previously (see section 5.1.1

above). However, the dendritic spines of these NPY-GFP cells often received contacts from VGluT1-expressing boutons, which are likely to originate from A-LTMRs (Todd et al., 2003). Although VGluT1-expressing boutons contact the dendritic spines of NPY-GFP cells, the present study could not confirm these contacts as synaptic. It is also possible that this source of VGluT1 is from the corticospinal tract, since 96% of the axons from this tract express VGluT1, and their terminals are found in laminae I-VI (Du Beau et al., 2012). Therefore it is uncertain whether the NPY-GFP cells frequently receive synapses directly from mylelinated afferents.

In the present report it was not possible to reliably test for post-synaptic markers in filled cells (e.g. PSD95 or ionotropic Glutamate receptors). The presence of synapses could be tested directly on recorded cells if the Neurobiotin was revealed using avidin-conjugated HRP, followed by a diaminobenzidine (DAB) reaction to label the cells. If slices were processed for electron microscopy it would be possible to detect VGluT1 in axonal boutons using an immunogold reaction (Alvarez et al., 2004). Synapses could then be confirmed between gold-containing boutons and DAB-filled dendrites by the presence of vesicle clustering at the pre-synaptic site, and the presence of pre- and post-synaptic densities. The dorsal root stimulation experiments also showed many polysynaptic responses (10/14 responsive cells) to NPY-GFP cells, demonstrating that these cells received input from excitatory interneurons.

5.2.5 Cells that innervate lamina III ALT neurons

Two NPY-GFP cells were found to contribute to the dense bundles of NPY-containing axons and peptidergic C-fibres that are associated with lamina III ALT neurons (Cameron et al., 2015; Polgár et al., 2011). These were a rare occurrence, as only 2/38 cells tested showed this axonal arrangement. Unfortunately, neither of these cells had their dendritic trees recovered for analysis, and therefore a comparison between the somatodendritic morphology of these cells and those that did not innervate lamina III ALT neurons was not possible. In both cases a high level of NPY-immunoreactivity was detected in some of their axonal boutons, which was predicted in an earlier study of NPY immunoreactivity in the rat (Polgár et al., 2011). Both of these cells were located in lamina III and were not seen to have a different axonal arborisation pattern when compared to the other NPY-GFP cells.

There are a number of possible reasons why these ALT neuron-innervating cells were rarely observed; for example they may lack GFP in the NPY-GFP mouse, as is the case for NPY-expressing cells in laminae I and II. Secondly, it is possible that these cells make up a very small population of NPY-expressing neurons. A third possibility is that they are relatively difficult to record from in the *in vitro* slice preparation used in this report. An argument against the first possibility is the fact that the NPY-GFP mouse labels approximately 80% of NPY-expressing cells in lamina III, and this was where the somata for both examples of NPY-GFP cells that innervated lamina III ALT neurons were found. Nevertheless, it is still conceivable that many of the NPY-expressing cells that innervate LIII ALT neurons are included in the 20% of lamina III NPY-expressing cells that are not labelled in this mouse line, or that they are more commonly found in NPY-expressing cells in lamina II. At present it is not known what proportion of NPY-expressing cells have an axon that contributes to this arrangement surrounding purported ALT neurons, and therefore it is difficult to assess how frequently these cells would be seen in the NPY-GFP mouse. The third possibility may also be true, since both examples of cells that innervated the bundles of NPY-expressing axons and CGRP-expressing boutons had truncated dendrites, which is a sign of poor health following whole-cell recording. This present study could not clarify why NPY-GFP cells that innervated purported ALT neurons were rarely seen, and it is possible that more than one of the factors discussed was involved in this finding.

In the two examples of NPY-GFP cells that contributed to the bundles of NPY axons, the majority of the NPY-expressing boutons were not labelled with Neurobiotin. This indicates that the NPY-expressing axons that provide output to ALT neurons originate from multiple cells. Furthermore, in one of these examples a single axon from a filled NPY-GFP cell was seen to innervate three bundles of CGRP-expressing and NPY-expressing boutons, which are presumably surrounding different ALT neurons. This suggests that the axon of a single cell will innervate multiple ALT neurons. In both examples the majority of the axon did not contribute to these bundles of NPY-containing boutons, and therefore this only represents a minority of their output. Taken together, this suggests that NPY-expressing cells that innervate the lamina III ALT neurons are likely to have a complex role in the dorsal horn circuitry, with multiple cells innervating several ALT neurons as well as other cells in the dorsal horn.

ALT neurons in lamina III are surrounded by numerous NPY-expressing boutons, although many of these boutons are not directly in contact with the dendrites and somata of these cells (Polgár et al., 2011). These boutons also apparently express a higher level of NPY than other NPY-expressing boutons that are not associated with these cells. In the two examples of NPY-GFP cells that were seen to contribute their axon to these NPY bundles, there was a high level of NPY expressed in their boutons, which was detectable by immunocytochemistry. Only 11/38 recorded NPY-GFP cells contained detectable levels of NPY following recordings, implying that in most cases NPY is diluted to an undetectable level during whole-cell recording, similar to the loss of detectable neuropeptides seen in PrP-GFP cells. Taken together, this is consistent with the suggestion that the NPY-GFP cells that innervate lamina III ALT neurons express higher levels of NPY than other NPY-GFP cells.

The fact that NPY was expressed at higher levels in these NPY-GFP cells that innervated lamina III ALT neurons, raises the question of what the role of NPY is in these cells. The effects of NPY in the dorsal horn are mediated through the Y1 receptor and the Y2 receptor (Y1R and Y2R) (Brumovsky et al., 2007). Although five types of NPY receptor exist, Y1R and Y2R are most commonly found in the dorsal horn, with Y2R being expressed on primary afferent fibres and Y1R being expressed on both dorsal horn neurons and primary afferents (Brumovsky et al., 2005, 2006, 2002). The neurons in the spinal cord that express Y1R have been divided into seven distinct populations, and those defined as being type-4 Y1R-expressing cells appear similar in several features to the lamina III ALT neurons (Brumovsky et al., 2007). These features include a large multipolar dendritic tree and dorsally directed dendrites that enter laminae I-II (Naim et al., 1997, 1998). If the type 4 Y1R-expressing neurons are the same population as the lamina III ALT neurons, then the release of NPY from lamina III ALT-innervating NPY-GFP cells should influence them. The effects of NPY can be inhibitory or excitatory, although many studies suggest that the action mediated through Y1R receptors is inhibitory (Naveilhan et al., 2001; Smith et al., 2007). This would enable the ALT/type-4 Y1R-expressing neurons to be inhibited through both fast GABA neurotransmission and slower NPY-mediated effects. The effects of NPY would presumably be mediated through volume transmission rather than synapses, and therefore the bundles of NPY that surround lamina III ALT/type-4 Y1R-expressing neurons could still influence this cell without necessarily having to form contacts.

NPY is generally thought to have an antinociceptive role, and increased expression of NPY in DRG neurons is observed following nerve injury and peripheral inflammation (Wakisaka et al., 1991; Zhang et al., 1994). It has been suggested that this response to nerve injury and inflammation is a compensatory mechanism to reduce excitatory signalling, which is enhanced by the injury. This possibility has recently been tested, using mice expressing an allele in which transcription of NPY is inhibited by doxycycline (Solway et al., 2011; Ste Marie et al., 2005). Using mice heterozygous for this allele ($NPY^{tet/tet}$), NPY could be conditionally depleted by introducing doxycycline to the drinking water. It was reported that following nerve injury or injection of CFA (models of neuropathic and inflammatory pain respectively), the depletion of NPY caused an increase in hypersensitivity to both thermal and mechanical stimuli. Furthermore, this hypersensitivity was reversible following removal of doxycycline from the drinking water, and could be reinstated when doxycycline was reintroduced (Solway et al., 2011). This indicates that during neuropathic or inflammatory pain, increased expression of NPY can limit the development of hypersensitivity. Since NPY is increased in primary afferent fibres during these pain states (Wakisaka et al., 1991; Zhang et al., 1994), it is difficult to assess the role of NPY in normal sensory processing. It is therefore uncertain what the function of NPY is in the NPY-GFP neurons.

5.2.6 **Possible functions of NPY-GFP cells**

The results in this report indicate that some NPY-GFP cells receive monosynaptic input from C-fibres, and these cells are not responsive to capsaicin or icilin in pharmacological experiments. Since TRPV1 is mainly restricted to peptidergic C-fibres in the mouse, this suggests that the input to these cells could be from non-peptidergic C-fibres, such as the C^{Mrgprd} fibres or C-LTMRs (Seal et al., 2009; Zylka et al., 2005). Due to the medial location of some of the recorded cells that received C fibre input, it is likely that some of these inputs are from C^{Mrgprd} fibres that can respond to noxious mechanical stimuli (Cavanaugh et al., 2009). Since C-LTMRs are only found in the hairy skin and terminate in the lateral dorsal horn, it is unlikely that these would provide input to the medially located NPY-GFP cells (Li et al., 2011; Seal et al., 2009). Many of the NPY-GFP cells that received monosynaptic C fibre input had their somata located in lamina III (n = 6), as well as dendrites that projected dorsally. Phosphorylation of ERK was therefore used to test whether the NPY-expressing cells in lamina III could respond to noxious mechanical stimulation. Approximately 10% of the pERK-containing cells in lamina III were NPY-immunoreactive following noxious pinch stimulation. Furthermore, many lamina III

neurons that were densely innervated by NPY-containing axonal boutons, and therefore highly likely to be ALT neurons, were also activated by pinch stimulation. This is in agreement with observations made in studies of the rat dorsal horn, in which NPY-expressing lamina III cells and lamina III ALT neurons were activated by noxious mechanical stimuli (Polgar et al., 2007, 2013). Taken together, these results suggest that NPY-GFP cells could respond to nociceptive mechanical signals.

Although activation of NPY-GFP cells in response to noxious heat or capsaicin injection was not tested, some of the recorded NPY-GFP cells were seen to receive monosynaptic input from TRPV1-lacking C-fibres, which was assessed by dorsal root simulation and pharmacological experiments. This finding may be due to the recorded NPY-GFP cells being underrepresented in superficial laminae, where most of these TRPV1-expressing fibres terminate (Cavanaugh et al., 2009)This is also where the NPY-expressing cells that responded to heat and capsaicin were located in the rat (Polgár et al., 2013b). However, there is also a species difference between the rat and the mouse in terms of TRPV1 expression in primary afferents. In the rat IB4 binding afferents commonly express TRPV1 (Guo et al., 1999), whereas in the mouse co-localisation of TRPV1 and IB4 binding is rarely seen (Zwick et al., 2002). Furthermore, the correlation between activation of cells by heat and capsaicin is not straightforward, and there is often a mismatch between the activation of cells in response to capsaicin and heat application. For example, nNOS-expressing cells can be activated by heat stimulation but not by capsaicin injection in the rat (Polgár et al., 2013b). Similarly, the PrP-GFP cells in the PrP-GFP mouse receive monosynaptic input from TRPV1-expressing C-fibres, but do not respond to noxious heat based on c-fos expression (Ganley et al., 2015) . There are also reports of TRPV1-lacking/IB4 binding C-fibres that respond to heat in mice, indicating that not all heat-sensitive fibres are TRPV1-expressing (Woodbury et al., 2004). On the other hand, TRPV1 is thought to be the principal heat transducer in sensory fibres, since it is gated by noxious heat and capsaicin (Caterina et al., 1997). Therefore it is not certain whether the NPY-GFP cells respond to heat stimuli from the results of the present report.

Although a previous study quantified phosphorylation of ERK in NPY-expressing cells following pinch stimulation, this study was performed in the rat and only included cells in laminae I and II (Polgár et al., 2013b). In contrast, the present study only analysed cells in lamina III of the mouse, because NPY-GFP cells in lamina III were observed that had dorsally directed dendrites and received monosynaptic C-fibre input. A comparison

between the results of the present study and the findings of Polgár *et al* (2013b) was not possible, since the present study only quantified the proportion of pERK cells that expressed NPY. This was because neurons in lamina III that phosphorylated ERK were far more diffuse than in superficial laminae. Moreover, it would be difficult to define the region of ERK phosphorylation in lamina III due to the discontinuous pattern of cell activation produced by pinch stimulation. For these reasons a quantification of lamina III NPY-expressing cells that phosphorylated ERK was not performed.
Some of the NPY-GFP cells can provide input to ALT neurons in lamina III, and these putative ALT neurons and NPY-expressing cells are both seen to respond to pinch stimulation. Therefore one possible function of these cells could be to limit the intensity of mechanical pain and its spread to other somatotopic areas, to ensure that the response to a noxious insult is the appropriate intensity and perceived in the correct area (Sandkühler, 2009). The NPY-GFP cells are well placed for this as they can receive input from nociceptive afferents. A very small subset of the NPY-GFP cells could inhibit projection neurons that contribute to the ALT, and these cells could reduce the pain signals that are sent to the brain. This function was previously described as attenuation, which is required for the correct response to noxious stimulation (Sandkühler, 2009).

5.3 Similarities and differences between PrP-GFP and NPY-GFP neurons

From the cell reconstructions of recorded PrP- and NPY-GFP cells it was possible to assess morphological similarities and differences between these populations. It was found that cells in both groups had heterogeneous somatodendritic morphology, and cells with islet morphology were never found in either of these groups. Since islet cells are the only morphological cell type in the dorsal horn that consistently have an inhibitory phenotype, the finding that two separate populations of inhibitory interneurons are never this shape suggests that islet cells may represent a distinct population of inhibitory interneurons (Grudt and Perl, 2002; Maxwell et al., 2007; Yasaka et al., 2007, 2010).

Differences were found in the axonal distribution of PrP- and NPY-GFP cells. A subset of PrP-GFP cells projected their axons into lamina I and provided over 20 axonal boutons to this lamina (30/87). In contrast, only one NPY-GFP cell in lamina II was found to contribute this number of boutons to lamina I (1/23). This demonstrates that virtually no NPY-GFP cells provide synaptic output to lamina I, whereas approximately one third of

the PrP-GFP cells do, and highlights a major difference in the post-synaptic targets of these neurons. Further analysis of GFP-expressing boutons in the PrP-GFP mouse have shown that many of these are pre-synaptic to various projection neurons (Ganley et al., 2015). Similarly, a small subset (2/38) of NPY-GFP cells possesses axons that contact a different population of projection neurons. These projection neurons contribute to the ALT in the mouse, and can be readily identified by their dense innervation by bundles of CGRP-expressing and NPY-expressing axonal boutons (Cameron et al., 2015). For both PrP- and NPY-GFP classes that are purported to innervate projection neurons, the majority of their axonal boutons are not associated with these targets. This suggests that these neurons must have multiple post-synaptic targets within the dorsal horn, and individual cells could therefore perform multiple functions within the dorsal horn microcircuitry. Nevertheless, these neurons do show selectivity in their post-synaptic targets, as only certain cells from each group showed these patterns of innervation.

NPY- and PrP-GFP cells in lamina II also exhibited differences in their active and passive membrane properties, with NPY-GFP cells having a higher input resistance than PrP-GFP cells. Input resistance is related to the size of the cell, because bigger cells have a larger surface area with more ion channels and hence display less resistance to current flow. Although both groups frequently showed tonic firing of action potentials, the tonic firing properties varied between NPY- and PrP-GFP cells. The PrP-GFP neurons showed a greater slowing in their action potential firing frequency towards the end of current steps than the NPY-GFP cells, a phenomenon known as spike frequency adaptation. The height of these action potentials decreased more between the first and the last action potential of firing for the NPY-GFP cells, when compared to the PrP-GFP cells, measured as mV drop (see Appendix). These findings are difficult to interpret, but suggests that there are slight differences in the biophysical properties of the membranes between these groups of cells.

5.4 The use of cluster analysis to distinguish different cell types

Unlike the aims of most research that uses hierarchical cluster analysis, the purpose of this study was not to identify different populations of neurons based on morphological or physiological parameters. The aim was to take groups of cells that were already known to be different in some way, and then to test whether they could be distinguished objectively by using morphological and physiological parameters. This would then indicate whether

certain features were useful in identifying genuinely different populations. This was an important question to address since many studies rely on morphological properties of cell somata and dendrites to classify dorsal horn neurons (Grudt and Perl, 2002; Wang and Zylka, 2009; Yasaka et al., 2007, 2010).

Due to the high likelihood that LI-innervating and non-LI-innervating PrP-GFP cells have different functional roles, hierarchical cluster analysis was used to test whether there were discernible morphological features for these two groups. This analysis showed that there was little difference between the PrP-GFP cells that give rise to over 20 boutons in lamina I and other PrP-GFP cells, in terms of their somatodendritic morphology. This indicates that morphological properties, except for having an axon with over 20 boutons in lamina I, are not useful for distinguishing these groups. Likewise physiological properties could not reliably separate PrP-GFP cells that innervated lamina I from those that did not, suggesting that these two groups may not be different from each other except in terms of their axonal laminar location.

Previous reports indicate that interneurons with different functions may be distinguishable in part by their expression of different neuropeptides and various proteins, due to the non-overlapping distribution of certain neurochemical markers, and the different responses of these neurochemically groups to various stimuli (Polgár et al., 2013b; Todd, 2010). In this report a subset of PrP-GFP cells were identified as containing galanin or nNOS, and these were found to be different in some morphometric measurements. These could also be distinguished by hierarchical cluster analysis with some accuracy, using morphological properties. The main differences between these groups were the dorsoventral location of their cell bodies and processes, and the spread of their dendritic trees and axonal arbors in the different axes. However, these two groups could not always be distinguished and the hierarchical cluster analysis failed to completely separate these groups into discrete clusters. Furthermore these cells were not apparently different in terms of somatodendritic morphology, and were different only in terms of their scale and laminar location, which would not be distinguished using the Grudt and Perl (2002) classification scheme.

The NPY- and PrP-GFP cells are non-overlapping populations, as indicated by their distinct neurochemical profiles (Iwagaki et al., 2013). However, when these two populations in lamina II were compared by a cluster analysis using morphological parameters, there was no separation of these two groups. Three possible conclusions that

may be taken from this finding are 1) These two groups of cells are not distinct populations of cells, and the expression of neurochemicals in these groups is random 2) Certain morphological parameters are important but these were not included in this analysis, or 3) Somatodendritic morphological parameters are not important criteria for classifying these interneurons. The first conclusion is unlikely to be true, since these cells are seen to differ in many ways, such as their axonal targets, the synaptic inputs they receive from primary afferents. To make this clustering procedure as objective as possible, 55 parameters were chosen to measure as many potential features that could differ between these cells. It is very unlikely that there was a measure not included in this analysis that would differ significantly between these two groups, and these cells were indistinguishable from visual inspection. Therefore the second conclusion also seems unlikely. Taken together, these observations would suggest that somatodendritic parameters are not useful in distinguishing these cells. Studies of the mouse neocortex demonstrated that it was possible to use morphological and physiological parameters of somatostatin expressing interneurons independently and produce the same groups (McGarry et al., 2010). This indicates that when genuine morphological differences are present between groups, they can be distinguished using this method of PCA followed by hierarchical cluster analysis. For this reason, similar morphological and physiological parameters to this study were used for cluster analysis in the present report. It also showed that morphology and physiology of neurons can be correlated, since the same groups could be identified separately by using either morphological or physiological properties.

5.5 **Conclusions and future direction**

The present study, and reports from others groups, have demonstrated that identifying functional cell types in the dorsal horn is a complicated and challenging endeavour, and it is unlikely that any one method of cell classification will be of use on its own. On the other hand, it is likely that each method has its advantages. For example, although morphology is not a useful way to distinguish the NPY- and PrP-GFP cells, as shown in this study, certain morphological patterns do exist, since islet cells are always inhibitory, while radial and most vertical cells are excitatory (Grudt and Perl, 2002; Maxwell et al., 2007; Yasaka et al., 2007, 2010). Furthermore the cells in this study were never seen to have the appearance of islet or radial cells, suggesting cell morphology is not entirely random and certain morphological types do exist in the dorsal horn. There may be several groups within these morphological populations, for example, islet cells can contain GABA only or both GABA

and glycine (Spike and Todd, 1992), and islet cells can express various calcium-binding proteins such as parvalbumin and calretinin (Hughes et al., 2012; Smith et al., 2015). Similarly, action potential firing patterns can indicate whether a cell is excitatory or inhibitory, with tonic and initial bursting firing patterns associated with inhibitory cells, and delayed and gap firing patterns associated with excitatory neurons (Yasaka et al., 2010). Although firing pattern is related to fast transmitter content, it does not identify cells that perform specific functions in the dorsal horn, and firing pattern can be affected by the polarisation of the neuronal membrane (Ruscheweyh et al., 2004; Yasaka et al., 2010). Equally, while expression of certain markers such as calcium-binding proteins and peptides can identify non-overlapping cell populations in the dorsal horn, these groups are likely to include multiple populations that are involved in different processes. For example, the present report showed that the NPY-GFP cells included a population that innervated ALT neurons in lamina III, but the vast majority of cells tested did not show this pattern of innervation. Similarly, a subset of PrP-GFP cells that included lamina I among their synaptic outputs was identified, and this group is likely to serve a different function to the PrP-GFP cells that do not show this feature.

Although neurochemically defined groups appear to have distinct functions, these groups are likely to include more than one functional population of cells. For example, although nNOS is expressed in inhibitory interneurons, it is also expressed in some excitatory interneurons (Sardella et al., 2011a). Intersectional approaches can be used to more precisely determine neurochemical populations of neurons, such as interneurons expressing both nNOS and sst2A being inhibitory interneurons (Iwagaki et al., 2013). A recent report used an intersectional genetic strategy to specifically label and ablate neurochemical populations of cells in the spinal cord (Duan et al., 2014). In this approach, mouse reporter lines were used that contained either the diphtheria toxin receptor, for diphtheria mediated cell ablation, or tdTomato to label cells. Two STOP cassettes flanked by different recombination sites were upstream of the reporter genes, meaning that the gene would only be expressed in the presence of two different DNA recombinases. These recombination sites were loxP sites, recognised by cre-recombinase, and FRT sites, recognised by flippase. Lbx1-Flpo mice were generated in this report, and were used to specifically express flippase in most neurons of the spinal cord (Duan et al., 2014). These included all inhibitory interneurons and most of the excitatory neurons, including those located in superficial laminae (Xu et al., 2013). Various cre-expressing lines of mice were used to specify several neurochemical groups. When triple transgenic mice were generated, with

Lbx1-Flpo, $Tau^{DTR/+}$ (a conditional allele requiring cre-recombinase and flippase for expression), and cre alleles, a specific neurochemical population of spinal cord neurons would express the diphtheria receptor, enabling specific cells in adult mice to be eliminated by injection of diphtheria toxin. By generating triple transgenic Lbx1-Flpo; $Tau^{DTR/+}$; Som-cre mice, Duan *et al* (2014) were able to selectively ablate somatostatin-expressing neurons in the dorsal horn, and suggested that they were a population that included cells required for transmitting noxious mechanical stimuli. Using the same approach they generated Lbx1-Flpo, $Tau^{DTR/+}$; dyn-cre triple transgenic mice, and indicated that they included a group required for the gating of mechanical pain. The intersectional approach can be used to label the atypical calretinin-expressing inhibitory cells, recently reported by Smith *et al* (2015). Using another GFP-expressing mouse line to label inhibitory interneurons, the nociceptin-GFP mouse, we have observed that the GFP-expressing cells include a group of calretinin-expressing cells (A.J. Todd, D.I. Hughes, and H.U. Zeilhofer unpublished observations). Furthermore, these cells seem to have the morphological properties of islet cells, and a dendritic tree that is restricted to lamina IIi. These examples demonstrate the usefulness of the intersectional approach to more precisely define populations of neurons in the dorsal horn.

Measures of gene expression in neurons can be used to identify neuronal populations, and group them based on their similarity in terms of their transcriptional profile (Usoskin et al., 2015). This is an attractive and unbiased method of identifying groups of cells that may have similar functions, as the transcriptional state will undoubtedly affect the functional properties of neurons. This method was used recently to identify different DRG populations in an objective manner (Usoskin et al., 2015). However, this method would not take into account the connectivity and laminar location of neurons in the dorsal horn, which would determine the neuronal circuits in which they are involved. Nevertheless, this method will undoubtedly provide important information about the organisation of the dorsal horn and could potentially identify new markers for cells in this region.

The ultimate aim of these studies is to identify cell types that are involved in specific functions, and to determine how these are arranged into circuits that process sensory information. Therefore functional studies of dorsal horn neuronal populations are important to assess the contribution of particular groups of cells to different behaviours. With the advent of advanced techniques such as optogenetics (Wang et al., 2007), designer receptors exclusively activated by designer drugs (DREADD)(Armbruster et al., 2007)),

and the selective expression of diphtheria toxin receptor in specific neuronal populations (Duan et al., 2014), it is now possible to manipulate specific populations of neurons in the central nervous system. Cre-mediated recombination can be used to restrict the expression of these channels and receptors to specific populations of cells, which are engineered to express cre-recombinase under the control of various promoters. Viruses that contain the genes for channelrhodopsins and DREADDs can be injected into specific areas of the nervous system, to allow populations of neurons to be manipulated in particular anatomical regions. For example, this approach was used to ablate, activate, and inhibit the synapses of glycinergic neurons in the dorsal horn (Foster et al., 2015). However, these techniques first require the identification of genetically defined neuronal populations or anatomical regions to investigate. Despite this they can be used to investigate the role of neurons that have been implicated in a specific function or behaviour.

Understanding the connectivity between different neurons and neuronal populations is also required to determine their function in the dorsal horn. The results from this report suggest that this is likely to be more complicated than anticipated, since it is clear that even if particular neurons are selectively targeted by individual interneurons, these may still only represent a fraction of their total synaptic output. Nevertheless, definite patterns of connectivity are seen in the dorsal horn, for example, giant cells receive approximately 80% of their inhibitory input from nNOS-expressing interneurons, and such patterns of connectivity are found between neurons in paired recording experiments (Ganley et al., 2015; Lu and Perl, 2003, 2005; Lu et al., 2013; Zheng et al., 2010).

Virus-based transsynaptic tracing methods have been used successfully to determine the cells that are pre-synaptic to specific neuronal populations (Foster et al., 2015; Stepien et al., 2010). This strategy requires a modified rabies virus, in which the gene encoding the viral glycoprotein is replaced by the gene for a fluorescent protein. This prevents the rabies virus from infecting cells in a non-specific manner, and causes infected cells to express a fluorescent protein. The virus was also pseudotyped with the EnvA glycoprotein, meaning that it expresses the EnvA glycoprotein in the viral capsid instead of the rabies glycoprotein, which enables the virus to infect cells specifically that express the receptor TVA (Wickersham et al., 2007). This approach was used to determine the primary afferent fibres pre-synaptic to glycinergic cells, by using $GlyT2^{cre}$ mice crossed with a TVA reporter line to express TVA in glycinergic cells in a cre –dependent manner (Foster et al., 2015). Retrograde labelling of cells pre-synaptic to the glycinergic neurons was enabled by

the co-injection of an AAV that contained a different fluorescent protein and the gene for a rabies glycoprotein (B19.G), which is also expressed in a cre-dependent manner. Since the rabies glycoprotein could be only expressed in cre-expressing cells, only cells that were monosynaptic to these could be labelled. The retrograde transsynaptic labelling approach has also been used to label motoneurons and premotor interneurons in the ventral horn, by injecting the rabies virus and the helper virus into muscles where motoneurons terminate (Stepien et al., 2010). This approach could be applied to various other neuronal populations in the dorsal horn to determine their connectivity between cells within and beyond the dorsal horn.

These advanced techniques discussed above provide many potential lines of research to be explored. The main questions that arise from the present study are:

- What are the morphological and physiological properties of the superficial NPY-expressing cells, and do these differ from those found in lamina III?
- What functional differences exist between the galanin-, nNOS- and NPY-expressing neurons in the dorsal horn?
- What are the synaptic outputs of the NPY- and PrP-GFP cells, other than the projection neurons?

These questions could be addressed using mice that express cre from the nNOS, galanin and NPY promoters, which would then be crossed with different reporter animals. As mentioned above, there are already mice available from the GENSAT project that express cre under the control of the NPY and galanin promoters, and mice expressing cre from the nNOS promoter could also be generated. However, galanin is also found in primary afferent fibres, and an intersectional approach would be required in order to specifically target the dorsal horn neurons (Hökfelt et al., 1987). For instance, using a reporter mouse that requires the expression of two recombinases, and another mouse that expresses a recombinase other than cre specifically in the spinal cord, such as the Lbx1-Flpo mouse line used by Duan *et al* (2014). Alternatively, a dynorphin-cre mouse could be used, since dynorphin expressing cells include virtually all inhibitory galanin-expressing cells in the dorsal horn, as well as some excitatory interneurons (Sardella et al., 2011b).

The RH26 NPY-cre line from the GENSAT project is seen to reliably label the NPY-expressing cells in the superficial laminae, and could be used to address the first question.

These cells would be labelled by direct spinal injection of an AAV that expresses tdTomato in a cre-dependent manner, to avoid permanently labelling the cells that express NPY transiently during development (Bourane et al., 2015). The NPY-cre cells could be characterised in a similar manner to the NPY-GFP cells in this report. In particular, it would be interesting to see whether the NPY-cre cells received input from TRPV1-expressing C-fibres, because NPY-expressing cells in the rat respond to noxious heat and the NPY-GFP cells in this report did not receive monosynaptic input from TRPV1-expressing afferents. To determine the synaptic outputs of these cells, an AAV that expresses channelrhodopsin 2 (ChR2) in a cre-dependent manner could be used to enable light-activation of the RH26-cre cells. Visualised whole-cell recordings could be taken from a random sample of dorsal horn neurons, and light evoked IPSCs in these cells would demonstrate that they receive input from NPY-cre cells. The recorded cells could then be characterised in terms of their laminar location, expression of peptides and neurochemicals, and whether they have a distinct morphological appearance. This would address the second question of what are the other post-synaptic targets of NPY-expressing cells.

The PrP-GFP cells are a group of cells that are randomly labelled using a PrP-GFP construct, and it is not possible to generate a mouse that specifically expresses cre in this same population of cells. However, mice are available that express cre in galanin/dynorphin and nNOS expressing cells, which are included among the PrP-GFP cells. This would allow these two groups to be distinguished, and galanin- and nNOS-expressing cells could be assessed more reliably than by confirming the presence of nNOS or galanin in the cell following recording experiments. As both galanin and nNOS-expressing interneurons are lost in the dorsal horn of bhlhb5 knockout mice, it is unclear whether one or both of these groups is involved in the suppression of itch (Kardon et al., 2014). By selectively ablating these populations in the adult, it would be possible to see whether normal itch behaviours are affected by one or both of these groups.

In the present study there were very few recorded monosynaptic eEPSCs from A fibres in dorsal root stimulation experiments, possibly due to the severing of primary afferents during the preparation of slices. It would be advantageous to use a retrograde virus-based approach to label the DRG neurons pre-synaptic to these neuronal populations, as used by Foster *et al* (2015). This would allow the DRG neurons providing monosynaptic input to these cells to be determined from multiple dorsal roots, and would highlight the relative

contribution of different molecularly defined primary afferent types to cre-expressing cells. This would also allow the contribution of TRP channel expressing DRG neurons to be assessed for nNOS- and galanin/dynorphin-expressing cells. This would be of interest as the present study identified weak input from TRP channel expressing afferent fibres to PrP-GFP neurons, which include nNOS- and galanin-expressing cells.

The findings of this study indicate that the structure of cells in the dorsal horn is far more complicated than previously anticipated. This is shown by the morphological heterogeneity of the cell populations assessed, and the failure to distinguish these based on morphological parameters. The neuronal circuits in which these cells are involved are likely to be highly complex. For example, even cells that have known post-synaptic targets such as projection neurons also innervate other cells. Future studies of dorsal horn neurons require more refined methods to identify functional populations of interneurons, and should consider the findings of this study when interpreting the morphological properties of these populations.

6 References

Abraira, V.E., and Ginty, D.D. (2013). The Sensory Neurons of Touch. Neuron *79*, 618–639.

Akiyama, T., Iodi Carstens, M., and Carstens, E. (2011). Transmitters and Pathways Mediating Inhibition of Spinal Itch-Signaling Neurons by Scratching and Other Counterstimuli. PLoS ONE *6*, e22665.

Al-Ghamdi, K.S., Polgar, E., and Todd, A.J. (2009). Soma size distinguishes projection neurons from neurokinin 1 receptor-expressing interneurons in lamina I of the rat lumbar spinal dorsal horn. Neuroscience *164*, 1794–1804.

Alvarez, F.J., Villalba, R.M., Zerda, R., and Schneider, S.P. (2004). Vesicular glutamate transporters in the spinal cord, with special reference to sensory primary afferent synapses. J. Comp. Neurol. *472*, 257–280.

Armbruster, B.N., Li, X., Pausch, M.H., Herlitze, S., and Roth, B.L. (2007). Evolving the lock to fit the key to create a family of G protein-coupled receptors potently activated by an inert ligand. Proc. Natl. Acad. Sci. U. S. A. *104*, 5163–5168.

Baccei, M.L., Bardoni, R., and Fitzgerald, M. (2003). Development of nociceptive synaptic inputs to the neonatal rat dorsal horn: glutamate release by capsaicin and menthol. J. Physiol. *549*, 231–242.

Bailey, A.L., and Ribeiro-da-Silva, A. (2006). Transient loss of terminals from non-peptidergic nociceptive fibers in the substantia gelatinosa of spinal cord following chronic constriction injury of the sciatic nerve. Neuroscience *138*, 675–690.

Bardoni, R. (2004). Presynaptic NMDA Receptors Modulate Glutamate Release from Primary Sensory Neurons in Rat Spinal Cord Dorsal Horn. J. Neurosci. *24*, 2774–2781.

Baseer, N. (2014). Spinal cord neuronal circuitry involving dorsal horn projection cells. PhD. University of Glasgow.

Baseer, N., Al-Baloushi, A.S., Watanabe, M., Shehab, S.A.S., and Todd, A.J. (2014). Selective innervation of NK1 receptor–lacking lamina I spinoparabrachial neurons by presumed nonpeptidergic Aδ nociceptors in the rat: Pain *155*, 2291–2300.

Bernardi, P.S., Valtschanoff, J.G., Weinberg, R.J., Schmidt, H.H., and Rustioni, A. (1995). Synaptic interactions between primary afferent terminals and GABA and nitric oxide-synthesizing neurons in superficial laminae of the rat spinal cord. J. Neurosci. *15*, 1363–1371.

Bourane, S., Duan, B., Koch, S.C., Dalet, A., Britz, O., Garcia-Campmany, L., Kim, E., Cheng, L., Ghosh, A., Ma, Q., et al. (2015). Gate control of mechanical itch by a subpopulation of spinal cord interneurons. Science *350*, 550–554.

Bröhl, D., Strehle, M., Wende, H., Hori, K., Bormuth, I., Nave, K.-A., Müller, T., and Birchmeier, C. (2008). A transcriptional network coordinately determines transmitter and peptidergic fate in the dorsal spinal cord. Dev. Biol. *322*, 381–393.

Brown, A.G., and Fyffe, R.E. (1981). Form and function of dorsal horn neurones with axons ascending the dorsal columns in cat. J. Physiol. *321*, 31–47.

Brown, P.B., Gladfelter, W.E., Culberson, J.C., Covalt-Dunning, D., Sonty, R.V., Pubols, L.M., and Millecchia, R.J. (1991). Somatotopic organization of single primary afferent axon projections to cat spinal cord dorsal horn. J. Neurosci. *11*, 298–309.

Brumovsky, P., Stanic, D., Shuster, S., Herzog, H., Villar, M., and Hökfelt, T. (2005). Neuropeptide Y2 receptor protein is present in peptidergic and nonpeptidergic primary sensory neurons of the mouse. J. Comp. Neurol. *489*, 328–348.

Brumovsky, P., Hofstetter, C., Olson, L., Ohning, G., Villar, M., and Hökfelt, T. (2006). The neuropeptide tyrosine Y1R is expressed in interneurons and projection neurons in the dorsal horn and area X of the rat spinal cord. Neuroscience *138*, 1361–1376.

Brumovsky, P., Shi, T.S., Landry, M., Villar, M.J., and Hökfelt, T. (2007). Neuropeptide tyrosine and pain. Trends Pharmacol. Sci. *28*, 93–102.

Brumovsky, P.R., Shi, T.J., Matsuda, H., Kopp, J., Villar, M.J., and Hökfelt, T. (2002). NPY Y1 receptors are present in axonal processes of DRG neurons. Exp. Neurol. *174*, 1–10.

Cameron, A.A., Leah, J.D., and Snow, P.J. (1986). The electrophysiological and morphological characteristics of feline dorsal root ganglion cells. Brain Res. *362*, 1–6.

Cameron, D., Polgár, E., Gutierrez-Mecinas, M., Gomez-Lima, M., Watanabe, M., and Todd, A.J. (2015). The organisation of spinoparabrachial neurons in the mouse. Pain *156*, 2061–2071.

Caterina, M.J., Schumacher, M.A., Tominaga, M., Rosen, T.A., Levine, J.D., and Julius, D. (1997). The capsaicin receptor: a heat-activated ion channel in the pain pathway. Nature *389*, 816–824.

Cattell, R.B. (1966). The scree test for the number of factors. Multivar. Behav Res *1*, 245–276.

Cavanaugh, D.J., Lee, H., Lo, L., Shields, S.D., Zylka, M.J., Basbaum, A.I., and Anderson, D.J. (2009). Distinct subsets of unmyelinated primary sensory fibers mediate behavioral responses to noxious thermal and mechanical stimuli. Proc. Natl. Acad. Sci. *106*, 9075–9080.

Cavanaugh, D.J., Chesler, A.T., Bráz, J.M., Shah, N.M., Julius, D., and Basbaum, A.I. (2011). Restriction of Transient Receptor Potential Vanilloid-1 to the Peptidergic Subset of Primary Afferent Neurons Follows Its Developmental Downregulation in Nonpeptidergic Neurons. J. Neurosci. *31*, 10119–10127.

Cheng, L., Arata, A., Mizuguchi, R., Qian, Y., Karunaratne, A., Gray, P.A., Arata, S., Shirasawa, S., Bouchard, M., Luo, P., et al. (2004). Tlx3 and Tlx1 are post-mitotic selector genes determining glutamatergic over GABAergic cell fates. Nat. Neurosci. *7*, 510–517.

Dado, R.J., Katter, J.T., and Giesler, G.J., Jr (1994). Spinothalamic and spinohypothalamic tract neurons in the cervical enlargement of rats. II. Responses to innocuous and noxious mechanical and thermal stimuli. J. Neurophysiol. *71*, 981–1002.

Del Barrio, M.G., Bourane, S., Grossmann, K., Schüle, R., Britsch, S., O'Leary, D.D.M., and Goulding, M. (2013). A Transcription Factor Code Defines Nine Sensory Interneuron Subtypes in the Mechanosensory Area of the Spinal Cord. PLoS ONE *8*, e77928.

Dhaka, A., Murray, A.N., Mathur, J., Earley, T.J., Petrus, M.J., and Patapoutian, A. (2007). TRPM8 is required for cold sensation in mice. Neuron *54*, 371–378.

Dhaka, A., Earley, T.J., Watson, J., and Patapoutian, A. (2008). Visualizing cold spots: TRPM8-expressing sensory neurons and their projections. J. Neurosci. Off. J. Soc. Neurosci. *28*, 566–575.

Dickenson, A.H., and Sullivan, A.F. (1987). Evidence for a role of the NMDA receptor in the frequency dependent potentiation of deep rat dorsal horn nociceptive neurones following C fibre stimulation. Neuropharmacology *26*, 1235–1238.

Dickie, A.C., and Torsney, C. (2014). The chemerin receptor 23 agonist, chemerin, attenuates monosynaptic C-fibre input to lamina I neurokinin 1 receptor expressing rat spinal cord neurons in inflammatory pain. Mol. Pain *10*, 24.

Djouhri, L., and Lawson, S.N. (2004). Aβ-fiber nociceptive primary afferent neurons: a review of incidence and properties in relation to other afferent A-fiber neurons in mammals. Brain Res. Rev. *46*, 131–145.

Djouhri, L., Bleazard, L., and Lawson, S.N. (1998). Association of somatic action potential shape with sensory receptive properties in guinea-pig dorsal root ganglion neurones. J. Physiol. *513 (Pt 3)*, 857–872.

Duan, B., Cheng, L., Bourane, S., Britz, O., Padilla, C., Garcia-Campmany, L., Krashes, M., Knowlton, W., Velasquez, T., Ren, X., et al. (2014). Identification of Spinal Circuits Transmitting and Gating Mechanical Pain. Cell *159*, 1417–1432.

Du Beau, A., Shakya Shrestha, S., Bannatyne, B.A., Jalicy, S.M., Linnen, S., and Maxwell, D.J. (2012). Neurotransmitter phenotypes of descending systems in the rat lumbar spinal cord. Neuroscience *227*, 67–79.

Fleming, M.S., Ramos, D., Han, S.B., Zhao, J., Son, Y.-J., and Luo, W. (2012). The majority of dorsal spinal cord gastrin releasing peptide is synthesized locally whereas neuromedin B is highly expressed in pain-and itch-sensing somatosensory neurons. Mol Pain *8*, 52.

Foster, E., Wildner, H., Tudeau, L., Haueter, S., Ralvenius, W.T., Jegen, M., Johannssen, H., Hösli, L., Haenraets, K., Ghanem, A., et al. (2015). Targeted Ablation, Silencing, and Activation Establish Glycinergic Dorsal Horn Neurons as Key Components of a Spinal Gate for Pain and Itch. Neuron *85*, 1289–1304.

Ganley, R.P., Iwagaki, N., del Rio, P., Baseer, N., Dickie, A.C., Boyle, K.A., Polgar, E., Watanabe, M., Abraira, V.E., Zimmerman, A., et al. (2015). Inhibitory Interneurons That Express GFP in the PrP-GFP Mouse Spinal Cord Are Morphologically Heterogeneous, Innervated by Several Classes of Primary Afferent and Include Lamina I Projection Neurons among Their Postsynaptic Targets. J. Neurosci. *35*, 7626–7642.

Gerke, M.B., and Plenderleith, M.B. (2004). Ultrastructural analysis of the central terminals of primary sensory neurones labelled by transganglionic transport of bandeiraea simplicifolia I-isolectin B4. Neuroscience *127*, 165–175.

Gibson, S.J., Polak, J.M., Bloom, S.R., Sabate, I.M., Mulderry, P.M., Ghatei, M.A., McGregor, G.P., Morrison, J.F., Kelly, J.S., and Evans, R.M. (1984). Calcitonin gene-

related peptide immunoreactivity in the spinal cord of man and of eight other species. J. Neurosci. Off. J. Soc. Neurosci. *4*, 3101–3111.

Glasgow, S.M., Henke, R.M., Macdonald, R.J., Wright, C.V.E., and Johnson, J.E. (2005). Ptf1a determines GABAergic over glutamatergic neuronal cell fate in the spinal cord dorsal horn. Dev. Camb. Engl. *132*, 5461–5469.

Gobel, S. (1975). Golgi studies in the substantia gelatinosa neurons in the spinal trigeminal nucleus. J. Comp. Neurol. *162*, 397–415.

Gobel, S., Falls, W.M., Bennett, G.J., Abdelmoumene, M., Hayashi, H., and Humphrey, E. (1980). An EM analysis of the synaptic connections of horseradish peroxidase-filled stalked cells and islet cells in the substantia gelatinosa of adult cat spinal cord. J. Comp. Neurol. *194*, 781–807.

Graham, B.A., Brichta, A.M., and Callister, R.J. (2008). Recording temperature affects the excitability of mouse superficial dorsal horn neurons, in vitro. J. Neurophysiol. *99*, 2048–2059.

Gross, M.K., Dottori, M., and Goulding, M. (2002). Lbx1 specifies somatosensory association interneurons in the dorsal spinal cord. Neuron *34*, 535–549.

Grudt, T.J., and Perl, E.R. (2002). Correlations between neuronal morphology and electrophysiological features in the rodent superficial dorsal horn. J. Physiol. *540*, 189–207.

Guo, A., Vulchanova, L., Wang, J., Li, X., and Elde, R. (1999). Immunocytochemical localization of the vanilloid receptor 1 (VR1): relationship to neuropeptides, the P2X3 purinoceptor and IB4 binding sites. Eur. J. Neurosci. *11*, 946–958.

Gutierrez-Mecinas, M., Watanabe, M., and Todd, A.J. (2014). Expression of gastrin-releasing peptide by excitatory interneurons in the mouse superficial dorsal horn. Mol. Pain *10*, 79.

Han, L., Ma, C., Liu, Q., Weng, H.-J., Cui, Y., Tang, Z., Kim, Y., Nie, H., Qu, L., Patel, K.N., et al. (2012). A subpopulation of nociceptors specifically linked to itch. Nat. Neurosci. *16*, 174–182.

Han, Z.S., Zhang, E.T., and Craig, A.D. (1998). Nociceptive and thermoreceptive lamina I neurons are anatomically distinct. Nat. Neurosci. *1*, 218–225.

Hantman, A.W., and Perl, E.R. (2005). Molecular and genetic features of a labeled class of spinal substantia gelatinosa neurons in a transgenic mouse. J. Comp. Neurol. *492*, 90–100.

Hantman, A.W., van den Pol, A.N., and Perl, E.R. (2004). Morphological and physiological features of a set of spinal substantia gelatinosa neurons defined by green fluorescent protein expression. J. Neurosci. *24*, 836–842.

Heinke, B., Ruscheweyh, R., Forsthuber, L., Wunderbaldinger, G., and Sandkuhler, J. (2004). Physiological, neurochemical and morphological properties of a subgroup of GABAergic spinal lamina II neurones identified by expression of green fluorescent protein in mice. J. Physiol.-Lond. *560*, 249–266.

Hensel, H. (1981). Thermoreception and temperature regulation. Monogr. Physiol. Soc. *38*, 1–321.

Herbison, A.E., Simonian, S.X., Norris, P.J., and Emson, P.C. (1996). Relationship of neuronal nitric oxide synthase immunoreactivity to GnRH neurons in the ovariectomized and intact female rat. J. Neuroendocrinol. *8*, 73–82.

Hökfelt, T., Kellerth, J.O., Nilsson, G., and Pernow, B. (1975). Substance p: localization in the central nervous system and in some primary sensory neurons. Science *190*, 889–890.

Hökfelt, T., Elde, R., Johansson, O., Luft, R., Nilsson, G., and Arimura, A. (1976). Immunohistochemical evidence for separate populations of somatostatin-containing and substance P-containing primary afferent neurons in the rat. Neuroscience *1*, 131–136.

Hökfelt, T., Wiesenfeld-Hallin, Z., Villar, M., and Melander, T. (1987). Increase of galanin-like immunoreactivity in rat dorsal root ganglion cells after peripheral axotomy. Neurosci. Lett. *83*, 217–220.

Hughes, D.I., Sikander, S., Kinnon, C.M., Boyle, K.A., Watanabe, M., Callister, R.J., and Graham, B.A. (2012). Morphological, neurochemical and electrophysiological features of parvalbumin-expressing cells: a likely source of axo-axonic inputs in the mouse spinal dorsal horn. J. Physiol. *590*, 3927–3951.

Ikeda, H., Heinke, B., Ruscheweyh, R., and Sandkuhler, J. (2003). Synaptic plasticity in spinal lamina I projection neurons that mediate hyperalgesia. Science *299*, 1237–1240.

Ikeda, H., Stark, J., Fischer, H., Wagner, M., Drdla, R., Jager, T., and Sandkuhler, J. (2006). Synaptic Amplifier of Inflammatory Pain in the Spinal Dorsal Horn. Science *312*, 1659–1662.

Iwagaki, N., Garzillo, F., Polgár, E., Riddell, J.S., and Todd, A.J. (2013). Neurochemical characterisation of lamina II inhibitory interneurons that express GFP in the PrP-GFP mouse. Mol Pain *9*, 56.

Kardon, A.P., Polgár, E., Hachisuka, J., Snyder, L.M., Cameron, D., Savage, S., Cai, X., Karnup, S., Fan, C.R., Hemenway, G.M., et al. (2014). Dynorphin Acts as a Neuromodulator to Inhibit Itch in the Dorsal Horn of the Spinal Cord. Neuron *82*, 573–586.

Kim, Y.S., Park, J.H., Choi, S.J., Bae, J.Y., Ahn, D.K., McKemy, D.D., and Bae, Y.C. (2014). Central Connectivity of Transient Receptor Potential Melastatin 8-Expressing Axons in the Brain Stem and Spinal Dorsal Horn. PLoS ONE *9*, e94080.

Kirsch, P., Hafner, M., Zentgraf, H., and Schilling, L. (2003). Time Course of Fluorescence Intensity and Protein Expression in HeLa Cells Stably Transfected with hrGFP. Mol. Cells *15*, 341–348.

Kobayashi, K., Fukuoka, T., Obata, K., Yamanaka, H., Dai, Y., Tokunaga, A., and Noguchi, K. (2005). Distinct expression of TRPM8, TRPA1, and TRPV1 mRNAs in rat primary afferent neurons with aδ/c-fibers and colocalization with trk receptors. J. Comp. Neurol. *493*, 596–606.

Koerber, H.R., and Mendell, L.M. (1988). Functional specialization of central projections from identified primary afferent fibers. J. Neurophysiol. *60*, 1597–1614.

Koerber, H.R., Druzinsky, R.E., and Mendell, L.M. (1988). Properties of somata of spinal dorsal root ganglion cells differ according to peripheral receptor innervated. J. Neurophysiol. *60*, 1584–1596.

Koltzenburg, M., Stucky, C.L., and Lewin, G.R. (1997). Receptive properties of mouse sensory neurons innervating hairy skin. J. Neurophysiol. *78*, 1841–1850.

Laing, I., Todd, A.J., Heizmann, C.W., and Schmidt, H. (1994). Subpopulations of GABAergic neurons in laminae I–III of rat spinal dorsal horn defined by coexistence with classical transmitters, peptides, nitric oxide synthase or parvalbumin. Neuroscience *61*, 123–132.

Landry, M., Bouali-Benazzouz, R., El Mestikawy, S., Ravassard, P., and Nagy, F. (2004). Expression of vesicular glutamate transporters in rat lumbar spinal cord, with a note on dorsal root ganglia. J. Comp. Neurol. *468*, 380–394.

Lawson, S.N., and Nickels, S. (1980). The Use of Morphometric Techniques to Analyze the Effect of Neonatal Capsaicin Treatment on Rat Dorsal Root-Ganglia and Dorsal Roots. J. Physiol.-Lond. *303*, 12.

Li, L., Rutlin, M., Abraira, V.E., Cassidy, C., Kus, L., Gong, S., Jankowski, M.P., Luo, W., Heintz, N., Koerber, H.R., et al. (2011). The Functional Organization of Cutaneous Low-Threshold Mechanosensory Neurons. Cell *147*, 1615–1627.

Light, A.R., and Perl, E.R. (1979). Spinal termination of functionally identified primary afferent neurons with slowly conducting myelinated fibers. J. Comp. Neurol. *186*, 133–150.

Liu, Q., Sikand, P., Ma, C., Tang, Z., Han, L., Li, Z., Sun, S., LaMotte, R.H., and Dong, X. (2012a). Mechanisms of Itch Evoked by -Alanine. J. Neurosci. *32*, 14532–14537.

Liu, T., Berta, T., Xu, Z.-Z., Park, C.-K., Zhang, L., Lü, N., Liu, Q., Liu, Y., Gao, Y.-J., Liu, Y.-C., et al. (2012b). TLR3 deficiency impairs spinal cord synaptic transmission, central sensitization, and pruritus in mice. J. Clin. Invest. *122*, 2195–2207.

Löken, L.S., Wessberg, J., Morrison, I., McGlone, F., and Olausson, H. (2009). Coding of pleasant touch by unmyelinated afferents in humans. Nat. Neurosci. *12*, 547–548.

Lu, Y., and Perl, E.R. (2003). A specific inhibitory pathway between substantia gelatinosa neurons receiving direct C-fiber input. J. Neurosci. *23*, 8752–8758.

Lu, Y., and Perl, E.R. (2005). Modular organization of excitatory circuits between neurons of the spinal superficial dorsal horn (laminae I and II). J. Neurosci. *25*, 3900–3907.

Lu, Y., Dong, H., Gao, Y., Gong, Y., Ren, Y., Gu, N., Zhou, S., Xia, N., Sun, Y.-Y., Ji, R.-R., et al. (2013). A feed-forward spinal cord glycinergic neural circuit gates mechanical allodynia. J. Clin. Invest. *123*, 4050–4062.

Luo, W., Enomoto, H., Rice, F.L., Milbrandt, J., and Ginty, D.D. (2009). Molecular identification of rapidly adapting mechanoreceptors and their developmental dependence on ret signaling. Neuron *64*, 841–856.

Lynn, B. (1984). Effect of neonatal treatment with capsaicin on the numbers and properties of cutaneous afferent units from the hairy skin of the rat. Brain Res. *322*, 255–260.

Mantyh, P.W., Rogers, S.D., Honore, P., Allen, B.J., Ghilardi, J.R., Li, J., Daughters, R.S., Lappi, D.A., Wiley, R.G., and Simone, D.A. (1997). Inhibition of hyperalgesia by ablation of lamina I spinal neurons expressing the substance P receptor. Science *278*, 275–279.

Marshall, G.E., Shehab, S.A., Spike, R.C., and Todd, A.J. (1996). Neurokinin-1 receptors on lumbar spinothalamic neurons in the rat. Neuroscience *72*, 255–263.

Marvizón, J.C.G., Chen, W., and Murphy, N. (2009). Enkephalins, dynorphins, and β-endorphin in the rat dorsal horn: An immunofluorescence colocalization study. J. Comp. Neurol. *517*, 51–68.

Maxwell, D.J., Belle, M.D., Cheunsuang, O., Stewart, A., and Morris, R. (2007). Morphology of inhibitory and excitatory interneurons in superficial laminae of the rat dorsal horn. J. Physiol. *584*, 521–533.

McGarry, L.M., Packer, A.M., Fino, E., Nikolenko, V., Sippy, T., and Yuste, R. (2010). Quantitative classification of somatostatin-positive neocortical interneurons identifies three interneuron subtypes. Front. Neural Circuits *4*, 12.

McKemy, D.D., Neuhausser, W.M., and Julius, D. (2002). Identification of a cold receptor reveals a general role for TRP channels in thermosensation. Nature *416*, 52–58.

Melzack, R., and Wall, P.D. (1965). Pain mechanisms: a new theory. Science *150*, 971–979.

Mesnage, B., Gaillard, S., Godin, A.G., Rodeau, J.-L., Hammer, M., Von Engelhardt, J., Wiseman, P.W., De Koninck, Y., Schlichter, R., and Cordero-Erausquin, M. (2011). Morphological and functional characterization of cholinergic interneurons in the dorsal horn of the mouse spinal cord. J. Comp. Neurol. *519*, 3139–3158.

Miraucourt, L.S., Dallel, R., and Voisin, D.L. (2007). Glycine Inhibitory Dysfunction Turns Touch into Pain through PKCgamma Interneurons. PLoS ONE *2*, e1116.

Mishra, S.K., and Hoon, M.A. (2013). The cells and circuitry for itch responses in mice. Science *340*, 968–971.

Molander, C., Xu, Q., and Grant, G. (1984). The cytoarchitectonic organization of the spinal cord in the rat. I. The lower thoracic and lumbosacral cord. J. Comp. Neurol. *230*, 133–141.

Molander, C., Xu, Q., Rivero-Melian, C., and Grant, G. (1989). Cytoarchitectonic organization of the spinal cord in the rat: II. The cervical and upper thoracic cord. J. Comp. Neurol. *289*, 375–385.

Naim, M., Spike, R.C., Watt, C., Shehab, S.A., and Todd, A.J. (1997). Cells in laminae III and IV of the rat spinal cord that possess the neurokinin-1 receptor and have dorsally directed dendrites receive a major synaptic input from tachykinin-containing primary afferents. J. Neurosci. Off. J. Soc. Neurosci. *17*, 5536–5548.

Naim, M.M., Shehab, S.A., and Todd, A.J. (1998). Cells in laminae III and IV of the rat spinal cord which possess the neurokinin-1 receptor receive monosynaptic input from myelinated primary afferents. Eur. J. Neurosci. *10*, 3012–3019.

Nakatsuka, T., Ataka, T., Kumamoto, E., Tamaki, T., and Yoshimura, M. (2000). Alteration in synaptic inputs through C-afferent fibers to substantia gelatinosa neurons of the rat spinal dorsal horn during postnatal development. Neuroscience *99*, 549–556.

Nakatsuka, T., Furue, H., Yoshimura, M., and Gu, J.G. (2002). Activation of central terminal vanilloid receptor-1 receptors and αβ-methylene-ATP-sensitive P2X receptors reveals a converged synaptic activity onto the deep dorsal horn neurons of the spinal cord. J. Neurosci. *22*, 1228–1237.

Naveilhan, P., Hassani, H., Lucas, G., Blakeman, K.H., Hao, J.X., Xu, X.J., Wiesenfeld-Hallin, Z., Thorén, P., and Ernfors, P. (2001). Reduced antinociception and plasma extravasation in mice lacking a neuropeptide Y receptor. Nature *409*, 513–517.

Nichols, M.L., Allen, B.J., Rogers, S.D., Ghilardi, J.R., Honore, P., Luger, N.M., Finke, M.P., Li, J., Lappi, D.A., Simone, D.A., et al. (1999). Transmission of chronic nociception by spinal neurons expressing the substance P receptor. Science *286*, 1558–1561.

Oliva, A.A., Jr, Jiang, M., Lam, T., Smith, K.L., and Swann, J.W. (2000). Novel hippocampal interneuronal subtypes identified using transgenic mice that express green fluorescent protein in GABAergic interneurons. J. Neurosci. *20*, 3354–3368.

Oliveira, A.L.R., Hydling, F., Olsson, E., Shi, T., Edwards, R.H., Fujiyama, F., Kaneko, T., Hökfelt, T., Cullheim, S., and Meister, B. (2003). Cellular localization of three vesicular glutamate transporter mRNAs and proteins in rat spinal cord and dorsal root ganglia. Synap. N. Y. N *50*, 117–129.

Peirs, C., Williams, S.-P.G., Zhao, X., Walsh, C.E., Gedeon, J.Y., Cagle, N.E., Goldring, A.C., Hioki, H., Liu, Z., Marell, P.S., et al. (2015). Dorsal Horn Circuits for Persistent Mechanical Pain. Neuron *87*, 797–812.

Polgár, E., Shehab, S.A., Watt, C., and Todd, A.J. (1999a). GABAergic neurons that contain neuropeptide Y selectively target cells with the neurokinin 1 receptor in laminae III and IV of the rat spinal cord. J. Neurosci. *19*, 2637–2646.

Polgár, E., Fowler, J.H., McGill, M.M., and Todd, A.J. (1999b). The types of neuron which contain protein kinase C gamma in rat spinal cord. Brain Res. *833*, 71–80.

Polgár, E., Furuta, T., Kaneko, T., and Todd, A. (2006). Characterization of neurons that express preprotachykinin B in the dorsal horn of the rat spinal cord. Neuroscience *139*, 687–697.

Polgár, E., Campbell, A.D., MacIntyre, L.M., Watanabe, M., and Todd, A.J. (2007). Phosphorylation of ERK in neurokinin 1 receptor-expressing neurons in laminae III and IV of the rat spinal dorsal horn following noxious stimulation. Mol. Pain *3*.

Polgár, E., Al-Khater, K.M., Shehab, S., Watanabe, M., and Todd, A.J. (2008). Large projection neurons in lamina I of the rat spinal cord that lack the neurokinin 1 receptor are densely innervated by VGLUT2-containing axons and possess GluR4-containing AMPA receptors. J. Neurosci. Off. J. Soc. Neurosci. *28*, 13150–13160.

Polgár, E., Sardella, T.C.P., Watanabe, M., and Todd, A.J. (2011). Quantitative Study of NPY-Expressing GABAergic Neurons and Axons in Rat Spinal Dorsal Horn. J. Comp. Neurol. *519*, 1007–1023.

Polgár, E., Durrieux, C., Hughes, D.I., and Todd, A.J. (2013a). A Quantitative Study of Inhibitory Interneurons in Laminae I-III of the Mouse Spinal Dorsal Horn. PLoS ONE *8*, e78309.

Polgár, E., Sardella, T.C.P., Tiong, S.Y.X., Locke, S., Watanabe, M., and Todd, A.J. (2013b). Functional differences between neurochemically defined populations of inhibitory interneurons in the rat spinal dorsal horn. PAIN 2606–2615.

Pow, D.V., and Crook, D.K. (1993). Extremely high titre polyclonal antisera against small neurotransmitter molecules: rapid production, characterisation and use in light- and electron-microscopic immunocytochemistry. J. Neurosci. Methods *48*, 51–63.

Prescott, S.A., and De Koninck, Y.D. (2002). Four cell types with distinctive membrane properties and morphologies in lamina I of the spinal dorsal horn of the adult rat. J. Physiol. *539*, 817–836.

Proudlock, F., Spike, R.C., and Todd, A.J. (1993). Immunocytochemical study of somatostatin, neurotensin, GABA, and glycine in rat spinal dorsal horn. J. Comp. Neurol. *327*, 289–297.

Punnakkal, P., von Schoultz, C., Haenraets, K., Wildner, H., and Zeilhofer, H.U. (2014). Morphological, biophysical and synaptic properties of glutamatergic neurons of the mouse spinal dorsal horn. J. Physiol. *592*, 759–776.

Puskár, Z., Polgár, E., and Todd, A.J. (2001). A population of large lamina I projection neurons with selective inhibitory input in rat spinal cord. Neuroscience *102*, 167–176.

Ralston, H.J., 3rd (1979). The fine structure of laminae I, II and III of the macaque spinal cord. J. Comp. Neurol. *184*, 619–642.

Ralston, H.J., 3rd (1982). The fine structure of laminae IV, V, and VI of the Macaque spinal cord. J. Comp. Neurol. *212*, 425–434.

Ramón y Cajal, S. (1909). Histologie du système nerveux de l'homme & des vertébrés (Paris : Maloine).

Rau, K.K., McIlwrath, S.L., Wang, H., Lawson, J.J., Jankowski, M.P., Zylka, M.J., Anderson, D.J., and Koerber, H.R. (2009). Mrgprd enhances excitability in specific populations of cutaneous murine polymodal nociceptors. J. Neurosci. *29*, 8612–8619.

Rexed, B. (1952). The cytoarchitectonic organization of the spinal cord in the cat. J. Comp. Neurol. *96*, 414–495.

Ribeiro-da-Silva, A., and Coimbra, A. (1982). Two types of synaptic glomeruli and their distribution in laminae I-III of the rat spinal cord. J. Comp. Neurol. *209*, 176–186.

Ribeiro-da-Silva, A., and Coimbra, A. (1984). Capsaicin causes selective damage to type I synaptic glomeruli in rat substantia gelatinosa. Brain Res. *290*, 380–383.

Ribeiro-Da-Silva, A., Castro-Lopes, J.M., and Coimbra, A. (1986). Distribution of glomeruli with fluoride-resistant acid phosphatase (FRAP)-containing terminals in the substantia gelatinosa of the rat. Brain Res. *377*, 323–329.

Romesburg, C. (2004). Cluster Analysis for Researchers (Lulu.com).

Ross, S.E. (2011). Pain and itch: insights into the neural circuits of aversive somatosensation in health and disease. Curr. Opin. Neurobiol. *21*, 880–887.

Ross, S.E., Mardinly, A.R., McCord, A.E., Zurawski, J., Cohen, S., Jung, C., Hu, L., Mok, S.I., Shah, A., Savner, E.M., et al. (2010). Loss of Inhibitory Interneurons in the Dorsal Spinal Cord and Elevated Itch in Bhlhb5 Mutant Mice. Neuron *65*, 886–898.

Rowan, S., Todd, A.J., and Spike, R.C. (1993). Evidence that neuropeptide Y is present in GABAergic neurons in the superficial dorsal horn of the rat spinal cord. Neuroscience *53*, 537–545.

Ruscheweyh, R., and Sandkühler, J. (2002). Lamina-specific membrane and discharge properties of rat spinal dorsal horn neurones in vitro. J. Physiol. *541*, 231–244.

Ruscheweyh, R., Ikeda, H., Heinke, B., and Sandkühler, J. (2004). Distinctive membrane and discharge properties of rat spinal lamina I projection neurones in vitro. J. Physiol. *555*, 527–543.

Sandkühler, J. (2009). Models and Mechanisms of Hyperalgesia and Allodynia. Physiol. Rev. *89*, 707–758.

Sardella, T.C.P., Polgar, E., Watanabe, M., and Todd, A.J. (2011a). A quantitative study of neuronal nitric oxide synthase expression in laminae I-III of the rat spinal dorsal horn. Neuroscience *192*, 708–720.

Sardella, T.C.P., Polgar, E., Garzillo, F., Furuta, T., Kaneko, T., Watanabe, M., and Todd, A.J. (2011b). Dynorphin is expressed primarily by GABAergic neurons that contain galanin in the rat dorsal horn. Mol. Pain *7*.

Scheibel, M.E., and Scheibel, A.B. (1968). Terminal axonal patterns in cat spinal cord. II. The dorsal horn. Brain Res. *9*, 32–58.

Seal, R.P., Wang, X., Guan, Y., Raja, S.N., Woodbury, C.J., Basbaum, A.I., and Edwards, R.H. (2009). Injury-induced mechanical hypersensitivity requires C-low threshold mechanoreceptors. Nature *462*, 651–655.

Shehab, S.A.S., and Hughes, D.I. (2011). Simultaneous identification of unmyelinated and myelinated primary somatic afferents by co-injection of isolectin B4 and Cholera toxin subunit B into the sciatic nerve of the rat. J. Neurosci. Methods *198*, 213–221.

Sherman, S.E., and Loomis, C.W. (1994). Morphine insensitive allodynia is produced by intrathecal strychnine in the lightly anesthetized rat. Pain *56*, 17–29.

Shinohara, T., Harada, M., Ogi, K., Maruyama, M., Fujii, R., Tanaka, H., Fukusumi, S., Komatsu, H., Hosoya, M., Noguchi, Y., et al. (2004). Identification of a G Protein-coupled Receptor Specifically Responsive to β-Alanine. J. Biol. Chem. *279*, 23559–23564.

Simmons, D.R., Spike, R.C., and Todd, A.J. (1995). Galanin is contained in GABAergic neurons in the rat spinal dorsal horn. Neurosci. Lett. *187*, 119–122.

Smith, K.M., Boyle, K.A., Madden, J.F., Dickinson, S.A., Jobling, P., Callister, R.J., Hughes, D.I., and Graham, B.A. (2015). Functional heterogeneity of calretinin-expressing neurons in the mouse superficial dorsal horn: implications for spinal pain processing. J. Physiol. *593*, 4319–4339.

Smith, P.A., Moran, T.D., Abdulla, F., Tumber, K.K., and Taylor, B.K. (2007). Spinal mechanisms of NPY analgesia. Peptides *28*, 464–474.

Snider, W.D., and McMahon, S.B. (1998). Tackling pain at the source: new ideas about nociceptors. Neuron *20*, 629–632.

Solorzano, C., Villafuerte, D., Meda, K., Cevikbas, F., Bráz, J., Sharif-Naeini, R., Juarez-Salinas, D., Llewellyn-Smith, I.J., Guan, Z., and Basbaum, A.I. (2015). Primary afferent and spinal cord expression of gastrin-releasing peptide: message, protein, and antibody concerns. J. Neurosci. Off. J. Soc. Neurosci. *35*, 648–657.

Solway, B., Bose, S.C., Corder, G., Donahue, R.R., and Taylor, B.K. (2011). Tonic inhibition of chronic pain by neuropeptide Y. Proc. Natl. Acad. Sci. U. S. A. *108*, 7224–7229.

Spike, R.C., and Todd, A.J. (1992). Ultrastructural and immunocytochemical study of lamina II islet cells in rat spinal dorsal horn. J. Comp. Neurol. *323*, 359–369.

Spike, R.C., Todd, A.J., and Johnston, H.M. (1993). Coexistence of NADPH diaphorase with GABA, glycine, and acetylcholine in rat spinal cord. J. Comp. Neurol. *335*, 320–333.

Spike, R.C., Puskar, Z., Andrew, D., and Todd, A.J. (2003). A quantitative and morphological study of projection neurons in lamina I of the rat lumbar spinal cord. Eur. J. Neurosci. *18*, 2433–2448.

Standaert, D.G., Watson, S.J., Houghten, R.A., and Saper, C.B. (1986). Opioid peptide immunoreactivity in spinal and trigeminal dorsal horn neurons projecting to the parabrachial nucleus in the rat. J. Neurosci. Off. J. Soc. Neurosci. *6*, 1220–1226.

Ste Marie, L., Luquet, S., Cole, T.B., and Palmiter, R.D. (2005). Modulation of neuropeptide Y expression in adult mice does not affect feeding. Proc. Natl. Acad. Sci. U. S. A. *102*, 18632–18637.

Stepien, A.E., Tripodi, M., and Arber, S. (2010). Monosynaptic rabies virus reveals premotor network organization and synaptic specificity of cholinergic partition cells. Neuron *68*, 456–472.

Sun, Y.-G., and Chen, Z.-F. (2007). A gastrin-releasing peptide receptor mediates the itch sensation in the spinal cord. Nature *448*, 700–703.

Sun, Y.-G., Zhao, Z.-Q., Meng, X.-L., Yin, J., Liu, X.-Y., and Chen, Z.-F. (2009). Cellular Basis of Itch Sensation. Science *325*, 1531–1534.

Takamori, S., Rhee, J.S., Rosenmund, C., and Jahn, R. (2001). Identification of Differentiation-Associated Brain-Specific Phosphate Transporter as a Second Vesicular Glutamate Transporter (VGLUT2). J. Neurosci. *21*, RC182 (1–6).

Taylor, A.M.W., Peleshok, J.C., and Ribeiro-da-Silva, A. (2009). Distribution of P2X(3)-immunoreactive fibers in hairy and glabrous skin of the rat. J. Comp. Neurol. *514*, 555–566.

Todd, A.J. (2010). Neuronal circuitry for pain processing in the dorsal horn. Nat. Rev. Neurosci. *11*, 823–836.

Todd, A.J., and McKenzie, J. (1989). GABA-immunoreactive neurons in the dorsal horn of the rat spinal cord. Neuroscience *31*, 799–806.

Todd, A.J., and Spike, R.C. (1992). Co-localization of Met-enkephalin and somatostatin in the spinal cord of the rat. Neurosci. Lett. *145*, 71–74.

Todd, A.J., and Sullivan, A.C. (1990). Light microscope study of the coexistence of GABA-like and glycine-like immunoreactivities in the spinal cord of the rat. J. Comp. Neurol. *296*, 496–505.

Todd, A.J., Spike, R.C., Chong, D., and Neilson, M. (1995). The relationship between glycine and gephyrin in synapses of the rat spinal cord. Eur. J. Neurosci. *7*, 1–11.

Todd, A.J., Watt, C., Spike, R.C., and Sieghart, W. (1996). Colocalization of GABA, glycine, and their receptors at synapses in the rat spinal cord. J. Neurosci. *16*, 974–982.

Todd, A.J., Spike, R.C., and Polgar, E. (1998). A quantitiative study of neurons which express neurokinin-1 or somatostatin sst2a receptor in rat spinal dorsal horn. Neuroscience *85*, 459–473.

Todd, A.J., McGill, M.M., and Shehab, S.A. (2000). Neurokinin 1 receptor expression by neurons in laminae I, III and IV of the rat spinal dorsal horn that project to the brainstem. Eur. J. Neurosci. *12*, 689–700.

Todd, A.J., Puskar, Z., Spike, R.C., Hughes, C., Watt, C., and Forrest, L. (2002). Projection neurons in lamina I of rat spinal cord with the neurokinin 1 receptor are selectively innervated by substance p-containing afferents and respond to noxious stimulation. J. Neurosci. Off. J. Soc. Neurosci. *22*, 4103–4113.

Todd, A.J., Hughes, D.I., Polgar, E., Nagy, G.G., Mackie, M., Ottersen, O.P., and Maxwell, D.J. (2003). The expression of vesicular glutamate transporters VGLUT1 and VGLUT2 in neurochemically defined axonal populations in the rat spinal cord with emphasis on the dorsal horn. Eur. J. Neurosci. *17*, 13–27.

Todd, A.J., Spike, R.C., Young, S., and Puskar, Z. (2005). Fos induction in lamina I projection neurons in response to noxious thermal stimuli. Neuroscience *131*, 209–217.

Torsney, C. (2011). Inflammatory Pain Unmasks Heterosynaptic Facilitation in Lamina I Neurokinin 1 Receptor-Expressing Neurons in Rat Spinal Cord. J. Neurosci. *31*, 5158–5168.

Torsney, C., and MacDermott, A.B. (2006). Disinhibition Opens the Gate to Pathological Pain Signaling in Superficial Neurokinin 1 Receptor-Expressing Neurons in Rat Spinal Cord. J. Neurosci. *26*, 1833–1843.

Traub, R.J., and Mendell, L.M. (1988). The spinal projection of individual identified A-delta-and C-fibers. J. Neurophysiol. *59*, 41–55.

Usoskin, D., Furlan, A., Islam, S., Abdo, H., Lönnerberg, P., Lou, D., Hjerling-Leffler, J., Haeggström, J., Kharchenko, O., Kharchenko, P.V., et al. (2015). Unbiased classification of sensory neuron types by large-scale single-cell RNA sequencing. Nat. Neurosci. *18*, 145–153.

Valtschanoff, J.G., Weinberg, R.J., and Rustioni, A. (1992a). NADPH diaphorase in the spinal cord of rats. J. Comp. Neurol. *321*, 209–222.

Valtschanoff, J.G., Weinberg, R.J., Rustioni, A., and Schmidt, H.H. (1992b). Nitric oxide synthase and GABA colocalize in lamina II of rat spinal cord. Neurosci. Lett. *148*, 6–10.

van den Pol, A.N., Ghosh, P.K., Liu, R. -j., Li, Y., Aghajanian, G.K., and Gao, X.-B. (2002). Hypocretin (orexin) enhances neuron activity and cell synchrony in developing mouse GFP-expressing locus coeruleus. J. Physiol. *541*, 169–185.

van den Pol, A.N., Yao, Y., Fu, L.-Y., Foo, K., Huang, H., Coppari, R., Lowell, B.B., and Broberger, C. (2009). Neuromedin B and gastrin-releasing peptide excite arcuate nucleus neuropeptide Y neurons in a novel transgenic mouse expressing strong Renilla green fluorescent protein in NPY neurons. J. Neurosci. Off. J. Soc. Neurosci. *29*, 4622–4639.

Wakisaka, S., Kajander, K.C., and Bennett, G.J. (1991). Increased neuropeptide Y (NPY)-like immunoreactivity in rat sensory neurons following peripheral axotomy. Neurosci. Lett. *124*, 200–203.

Wang, H., and Zylka, M.J. (2009). Mrgprd-expressing polymodal nociceptive neurons innervate most known classes of substantia gelatinosa neurons. J. Neurosci. *29*, 13202–13209.

Wang, H., Peca, J., Matsuzaki, M., Matsuzaki, K., Noguchi, J., Qiu, L., Wang, D., Zhang, F., Boyden, E., Deisseroth, K., et al. (2007). High-speed mapping of synaptic connectivity using photostimulation in Channelrhodopsin-2 transgenic mice. Proc. Natl. Acad. Sci. U. S. A. *104*, 8143–8148.

Ward, J. (1963). Hierarchical Grouping to Optimize an Objective Function. J. Am. Stat. Assoc. *58*, 236–244.

West, S.J., Bannister, K., Dickenson, A.H., and Bennett, D.L. (2015). Circuitry and plasticity of the dorsal horn--toward a better understanding of neuropathic pain. Neuroscience *300*, 254–275.

Wickersham, I.R., Lyon, D.C., Barnard, R.J.O., Mori, T., Finke, S., Conzelmann, K.-K., Young, J.A.T., and Callaway, E.M. (2007). Monosynaptic Restriction of Transsynaptic Tracing from Single, Genetically Targeted Neurons. Neuron *53*, 639–647.

Wildner, H., Müller, T., Cho, S.-H., Bröhl, D., Cepko, C.L., Guillemot, F., and Birchmeier, C. (2006). dILA neurons in the dorsal spinal cord are the product of terminal and non-terminal asymmetric progenitor cell divisions, and require Mash1 for their development. Dev. Camb. Engl. *133*, 2105–2113.

Wildner, H., Das Gupta, R., Brohl, D., Heppenstall, P.A., Zeilhofer, H.U., and Birchmeier, C. (2013). Genome-Wide Expression Analysis of Ptf1a- and Ascl1-Deficient Mice Reveals New Markers for Distinct Dorsal Horn Interneuron Populations Contributing to Nociceptive Reflex Plasticity. J. Neurosci. *33*, 7299–7307.

Woodbury, C.J., and Koerber, H.R. (2007). Central and peripheral anatomy of slowly adapting type I low-threshold mechanoreceptors innervating trunk skin of neonatal mice. J. Comp. Neurol. *505*, 547–561.

Woodbury, C.J., Ritter, A.M., and Koerber, H.R. (2001). Central anatomy of individual rapidly adapting low-threshold mechanoreceptors innervating the “hairy” skin of newborn mice: Early maturation of hair follicle afferents. J. Comp. Neurol. *436*, 304–323.

Woodbury, C.J., Zwick, M., Wang, S., Lawson, J.J., Caterina, M.J., Koltzenburg, M., Albers, K.M., Koerber, H.R., and Davis, B.M. (2004). Nociceptors lacking TRPV1 and TRPV2 have normal heat responses. J. Neurosci. Off. J. Soc. Neurosci. *24*, 6410–6415.

Woodbury, C.J., Kullmann, F.A., McIlwrath, S.L., and Koerber, H.R. (2008). Identity of myelinated cutaneous sensory neurons projecting to nocireceptive laminae following nerve injury in adult mice. J. Comp. Neurol. *508*, 500–509.

Wrigley, P.J., Jeong, H.-J., and Vaughan, C.W. (2009). Primary afferents with TRPM8 and TRPA1 profiles target distinct subpopulations of rat superficial dorsal horn neurones. Br. J. Pharmacol. *157*, 371–380.

Xu, Y., Lopes, C., Wende, H., Guo, Z., Cheng, L., Birchmeier, C., and Ma, Q. (2013). Ontogeny of Excitatory Spinal Neurons Processing Distinct Somatic Sensory Modalities. J. Neurosci. *33*, 14738–14748.

Yaksh, T.L. (1989). Behavioral and autonomic correlates of the tactile evoked allodynia produced by spinal glycine inhibition: effects of modulatory receptor systems and excitatory amino acid antagonists. Pain *37*, 111–123.

Yang, K., Kumamoto, E., Furue, H., Li, Y.Q., and Yoshimura, M. (1999). Action of capsaicin on dorsal root-evoked synaptic transmission to substantia gelatinosa neurons in adult rat spinal cord slices. Brain Res. *830*, 268–273.

Yasaka, T., Kato, G., Furue, H., Rashid, M.H., Sonohata, M., Tamae, A., Murata, Y., Masuko, S., and Yoshimura, M. (2007). Cell-type-specific excitatory and inhibitory circuits involving primary afferents in the substantia gelatinosa of the rat spinal dorsal horn in vitro. J. Physiol. *581*, 603–618.

Yasaka, T., Hughes, D.I., Polgar, E., Nagy, G.G., Watanabe, M., Riddell, J.S., and Todd, A.J. (2009). Evidence against AMPA Receptor-Lacking Glutamatergic Synapses in the Superficial Dorsal Horn of the Rat Spinal Cord. J. Neurosci. *29*, 13401–13409.

Yasaka, T., Tiong, S.Y.X., Hughes, D.I., Riddell, J.S., and Todd, A.J. (2010). Populations of inhibitory and excitatory interneurons in lamina II of the adult rat spinal dorsal horn revealed by a combined electrophysiological and anatomical approach. Pain *151*.

Yasaka, T., Tiong, S.Y., Polgár, E., Watanabe, M., Kumamoto, E., Riddell, J.S., and Todd, A.J. (2014). A putative relay circuit providing low-threshold mechanoreceptive input to lamina I projection neurons via vertical cells in lamina II of the rat dorsal horn. Mol. Pain *10*, 1–11.

Yoshida, T., Fukaya, M., Uchigashima, M., Miura, E., Kamiya, H., Kano, M., and Watanabe, M. (2006). Localization of Diacylglycerol Lipase-α around Postsynaptic Spine Suggests Close Proximity between Production Site of an Endocannabinoid, 2-Arachidonoyl-glycerol, and Presynaptic Cannabinoid CB1 Receptor. J. Neurosci. *26*, 4740–4751.

Zeilhofer, H.U., Studler, B., Arabadzisz, D., Schweizer, C., Ahmadi, S., Layh, B., Bösl, M.R., and Fritschy, J.-M. (2005). Glycinergic neurons expressing enhanced green

fluorescent protein in bacterial artificial chromosome transgenic mice. J. Comp. Neurol. *482*, 123–141.

Zhang, E.T., Han, Z.S., and Craig, A.D. (1996). Morphological classes of spinothalamic lamina I neurons in the cat. J. Comp. Neurol. *367*, 537–549.

Zhang, X., Wiesenfeld-Hallin, Z., and Hökfelt, T. (1994). Effect of peripheral axotomy on expression of neuropeptide Y receptor mRNA in rat lumbar dorsal root ganglia. Eur. J. Neurosci. *6*, 43–57.

Zhang, X., Nicholas, A.P., and Hökfelt, T. (1995). Ultrastructural studies on peptides in the dorsal horn of the rat spinal cord—II. Co-existence of galanin with other peptides in local neurons. Neuroscience *64*, 875–891.

Zheng, J., Lu, Y., and Perl, E.R. (2010). Inhibitory neurones of the spinal substantia gelatinosa mediate interaction of signals from primary afferents. J. Physiol.-Lond. *588*, 2065–2075.

Zotterman, Y. (1939). Touch, pain and tickling: an electro-physiological investigation on cutaneous sensory nerves. J. Physiol. *95*, 1–28.

Zwick, M., Davis, B.M., Woodbury, C.J., Burkett, J.N., Koerber, H.R., Simpson, J.F., and Albers, K.M. (2002). Glial cell line-derived neurotrophic factor is a survival factor for isolectin B4-positive, but not vanilloid receptor 1-positive, neurons in the mouse. J. Neurosci. Off. J. Soc. Neurosci. *22*, 4057–4065.

Zylka, M.J., Rice, F.L., and Anderson, D.J. (2005). Topographically Distinct Epidermal Nociceptive Circuits Revealed by Axonal Tracers Targeted to Mrgprd. Neuron *45*, 17–25.

7 Publication

Ganley, R.P., Iwagaki, N., del Rio, P., Baseer, N., Dickie, A.C., Boyle, K.A., Polgar, E., Watanabe, M., Abraira, V.E., Zimmerman, A., Riddell, J. S., and Todd, A. J. (2015). Inhibitory Interneurons That Express GFP in the PrP-GFP Mouse Spinal Cord Are Morphologically Heterogeneous, Innervated by Several Classes of Primary Afferent and Include Lamina I Projection Neurons among Their Post-synaptic Targets. J. Neurosci. *35*, 7626–7642.

8 Appendix

8.1 Morphological parameters measured for cluster analysis

8.1.1 Soma measures

The soma is reconstructed using a series of contours spaced 1μm apart in the z-axis. The two-dimensional measurements of the soma use the contour with the largest area.

Somatic area (μm^2) = the area of the contour with the largest area of the 2D contours used to outline the soma
Somatic perimeter (μm) = the perimeter of the contour with the largest area used to outline the soma
Somatic aspect ratio = the maximum diameter of the soma / the minimum diameter of the soma
Somatic compactness = a measure of how compact the soma is based on the soma contour with the largest area. $[((4/\pi)*\text{Area}))]^{1/2}$/max diameter
Somatic roundness = $(4*\text{Area})/(\pi*\text{maxdiameter}^2)$
Soma lamina location = the lamina in which the cell soma is present

8.1.2 Dendritic measurements

Dendrites are reconstructed using Neurolucida Neuron tracing

Dendrite number = the number of dendrites the cell contains
Total dendritic length (μm) = the total length of dendrite
Average dendritic length (μm) = total dendritic length / dendrite number
Total number of branches = the total number of branch points (nodes) that are present on the dendrites of the cell
Spine number = the number of spines present on the cells' dendritic trees
Spine density = total spine number / total dendritic length
Rostrocaudal spread (μm) = the distance between the most distal co-ordinates in the x axis of the dendrites

Dorsoventral spread (µm) = the distance between the most distal co-ordinates in the y-axis of the dendrites

Mediolateral spread (µm) = the distance between the most distal co-ordinates in the z-axis of the dendrites

Rostrocaudal spread / Dorsoventral spread = the ratio of the rostrocaudal to dorsoventral spread

K dimension = A measure of how the dendritic tree fills space using the nested cubes method.

Number of dendritic Scholl sections = the number of concentric spheres originating from the soma increasing by 50µm that contain the total dendritic tree

Sholl length 50µm = the length of dendrite contained in the first 50µm Sholl

Sholl length 100µm = the length of dendrite contained in the second Sholl

Sholl length 150µm = the length of dendrite contained in the third Sholl

Sholl length 200µm = the length of dendrite contained in the fourth Sholl

Sholl length 250µm = the length of dendrite contained in the fifth Sholl

Sholl length 300µm = the length of dendrite contained in the sixth Sholl

Dendritic Sholl density = total dendritic length / Number of dendritic Sholl sections

Dendritic Sholl node density = the total number of nodes / Number of dendritic Sholl sections

Sholl node count 50µm = the number of branch points contained in the first 50µm Sholl

Sholl node count 100µm = the number of branch points contained in the second Sholl

Sholl node count 150µm = the number of branch points contained in the third Sholl

Sholl node count 200µm = the number of branch points contained in the fourth Sholl

Sholl node count 250µm = the number of branch points contained in the fifth Sholl

Sholl node count 300µm = the number of branch points contained in the sixth Sholl

Node distance along process 50µm (dendrite) = number of nodes appearing along a process between 0 and 50µm

Node distance along process 100µm (dendrite) = number of nodes appearing along a process between 50 and 100µm from the soma

Node distance along process 150µm (dendrite) = number of nodes appearing along a process between 100 and 150µm from the soma

Node distance along process 200µm (dendrite) = number of nodes appearing along a process between 150 and 200µm from the soma

Node distance along process 250µm (dendrite) = number of nodes appearing along a process between 200 and 250µm from the soma

Node distance along process 300µm (dendrite) = number of nodes appearing along a process between 250 and 300µm from the soma
Dendritic torsion ratio = total dendrite length / total dendrite length in a fan in diagram
Convex hull dendritic area = the area of a convex hull on a 2 dimensional projection of the dendritic tree
Convex hull dendritic perimeter = the perimeter of the 2 dimensional convex hull
Convex hull dendritic volume = the volume of a 3 dimensional convex hull around the dendritic tree
Convex hull dendritic surface area = the surface area of a 3 dimensional convex hull around the dendritic tree
Planar angle average = the average angle of the planar angles of a dendritic tree
Planar angle standard deviation = a measure of variation of planar angles
Local angle average = the average angle of the local angles of a dendritic tree
Local angle standard deviation = a measure of variation of local angles
Spline angle average = the average angle of the spline angles of a dendritic tree
Spline angle standard deviation = a measure of variation of spline angles
Layer length lamina I = the length of dendrite contained in lamina I
Layer length lamina IIo = the length of dendrite contained in lamina IIo
Layer length lamina IIi = the length of dendrite contained in lamina IIi
Layer length lamina III = the length of dendrite contained in lamina III

8.1.3 Axonal measurements

Axons are reconstructed using Neurolucida Neuron tracing

Total axonal length (µm) = the total length of axon the cell contains
Total number of branches = the number of branch points (nodes) the axon contains
Varicosity number = the total number of varicosities on the axon
Varicosity density = Varicosity number / total axonal length
Average varicosity diameter (µm) = the mean diameter of the varicosities on the axon
Standard deviation of varicosity diameter = the variability in varicosity size
Rostrocaudal spread (µm) = see dendrite measurements
Dorsoventral spread = see dendrite measurements
Mediolateral spread = see dendrite measurements
Rostrocaudal spread / Dorsoventral spread = see dendrite measurements
K-dimension = see dendrite measurements

Number of dendritic Sholl sections = the number of concentric spheres centred on the cell soma increasing by 100µm each time that contain the axonal plexus

Sholl length (100µm) = the length of axon contained in the first 100µm Sholl

Sholl length (200µm) = the length of axon contained in the second Sholl

Sholl length (300µm) = the length of axon contained in the third Sholl

Sholl length (400µm) = the length of axon contained in the fourth Sholl

Sholl length (500µm) = the length of axon contained in the fifth Sholl

Sholl length (>500µm) = the total length of axon contained in larger Sholl sections

Axonal Sholl length density = see dendritic measurements

Axonal Sholl node density = see dendritic measurements

Sholl node count 100µm = the number of branch points contained in the first 100µm Sholl

Sholl node count 200µm = the number of branch points contained in the second Sholl

Sholl node count 300µm = the number of branch points contained in the third Sholl

Sholl node count 400µm = the number of branch points contained in the fourth Sholl

Sholl node count 500µm = the number of branch points contained in the fifth Sholl

Sholl node count >500µm = the number of branch points contained in the sixth Sholl

Node distance along process 200µm (axon) = the number of branch points appearing along the axon between 0 and 200µm from the soma

Node distance along process 400µm (axon) = the number of branch points appearing along the axon between 200 and 400µm from the soma

Node distance along process 600µm (axon) = the number of branch points appearing along the axon between 400 and 600µm from the soma

Node distance along process 800µm (axon) = the number of branch points appearing along the axon between 600 and 800µm from the soma

Node distance along process 1000µm (axon) = the number of branch points appearing along the axon between 800 and 1000µm from the soma

Node distance along process >1000µm (axon) = the number of branch points appearing along the axon >1000µm from the soma

Axonal torsion ratio = see dendritic measurements

Convex hull axonal area = see dendritic measurements

Convex hull axonal perimeter = see dendritic measurements

Convex hull axonal volume = see dendritic measurements

Planar angle average = see dendritic measurements

Planar angle standard deviation = see dendritic measurements

Local angle average = see dendritic measurements

Local angle standard deviation = see dendritic measurements
Spline angle average = see dendritic measurements
Spline angle standard deviation = see dendritic measurements
Boutons in lamina I = number of boutons present in lamina I
Boutons in lamina IIo = number of boutons present in lamina IIo
Boutons in lamina IIi = number of boutons present in lamina IIi
Boutons in lamina III = number of boutons present in lamina III
Layer length lamina I = see dendritic measurements
Layer length lamina IIo = see dendritic measurements
Layer length lamina IIi = see dendritic measurements
Layer length lamina III = see dendritic measurements

8.2 Further details of measurements

8.2.1 K-dimension

The K-dimension is measured using the nested cube method of fractal analysis. A cube containing the dendritic tree is divided into 8 cubes, and the number of cubes and the number of cubes containing part of the tree is counted. This process is repeated and the number of cubes is counted at each stage. The log base 8 of the number of cubes and the number of cubes containing a process is taken and these are plotted against each other. The gradient of this plot is taken to be the K-dimension

8.2.2 Torsion ratio

Torsion ratio is based on the fan in diagram, which is a 2-dimensional projection of the cells 3-dimensional structure. An axis is placed on the cell centre and this is rotated 360^{o} through the cell. The length of process collected on this plane will be less than the original length, as some depth of the projection will be lost. The torsion ratio is the total process length divided by the length in the fan in projection.

8.2.3 Convex hull

Convex hull analysis places a convex polygon around the distal points of a given process or set of processes. This polygon is then used to calculate measurements of surface area and volume providing a measure of the space influenced by the processes. In the 2

dimensional measures, a projection of the tree is used and a two-dimensional convex polygon is placed around the distal points of that projection.

8.2.4 Angle measurements

Planar angle = the angle between the two end points of a segment, which include origins nodes and endpoints. This gives an overall structure of the tree and disregards local information.
Local angle = measures the change in direction using local information about the first line segment after a node.
Spline angle = each segment is represented by a cubic curve between the endpoints. The spline angle is the change in direction between a tangent taken at the first and second endpoint angle.

8.2.5 Laminar boundaries

In cell reconstructions the laminar boundaries are added to determine the length of each process and soma location. The laminar I boundary is taken to be 20μm below the start of the grey matter, as this is seen as an area that contains lamina I NK1r positive projection cells in the mouse. Unlike the case in the rat, lamina I thickness appears uniform throughout the mediolateral extent of the dorsal horns in mouse transverse sections. The border between lamina II inner and II outer is determined by PKCγ immunoreactivity, as the axonal plexus of PKCγ positive excitatory interneurons is a determinant of lamina IIi. The ventral border of this plexus is taken to be the lamina III border.

8.2.6 Varicosities

In cell reconstructions, varicosities are represented as single points along the axon. This represents each axonal bouton as a circle regardless of the shape of the bouton. During the reconstruction, the point thickness that most accurately represents the area of the bouton is used. The circle diameter is used as a measure of the size of each varicosity.

8.3 Physiological parameters measured for cluster analysis

Physiological measurements were taken using PClamp 10 software (Molecular Devices). Action potential parameters were measured from the first action potential from the Rheobase current. Fmax, SFA and mV drop were calculated using the trace from the maximum current injection that induced stable repetitive action potential generation

IV slope (nS) = the gradient of the line of a graph of voltage against current, generated from current response to subthreshold voltage steps.
Rm (MΩ) = input resistance, calculated as the reciprocal of IV slope (1/IV slope)
Vm (mV) = the resting membrane potential, calculated as the point where the line of voltage against current intercepts the x axis (voltage when current is 0)
Rheobase current (pA) = the minimum injected current required to generate an action potential
Latency (ms) = time taken to generate the first action potential in response to injection of the Rheobase current
Vth (mV) = voltage threshold, the membrane potential at which the cell will fire an action potential. This is calculated from a differentiated trace of an action potential, and is define as when the voltage increase with time exceeds 10mV/ms
AP (mV) = action potential height, the voltage difference in voltage between the voltage threshold and the peak of the action potential
AHP (mV) = after hyperpolarisation, the difference between the voltage threshold and the most negative potential on the following the action potential.
AP width (ms) = action potential width, the time taken for the action potential to reach voltage threshold again during action potential decay.
Rise (V/s) = the maximum change in voltage with time on the rising phase of the action potential
Fall (V/s) = the maximum decay in voltage with time on the decaying phase of the action potential
Fmax (Hz) = the maximum firing rate of action potentials in response to maximum current injection
SFA = spike frequency adaptation, the frequency of the last three action potentials / the frequency of the first three action potentials in response to maximum current injection
mV drop (mV) = Difference in peak values between the first and the last action potential